VALIDATION AND APPLICATION OF AN URBAN TURBULENCE PARAMETERISATION SCHEME FOR MESOSCALE ATMOSPHERIC MODELS

THÈSE N^O 3032 (2004)

PRÉSENTÉE À LA FACULTÉ ENVIRONNEMENT NATUEL, ARCHITECTURAL ET CONSTRUIT

Institut des sciences et technologies de l'environnement

SECTION DES SCIENCES ET INGÉNIERIE DE L'ENVIRONNEMENT

ÉCOLE POLYTECHNIQUE FÉDÉRALE DE LAUSANNE

POUR L'OBTENTION DU GRADE DE DOCTEUR ÈS SCIENCES TECHNIQUES

PAR

Yves-Alain F. ROULET

diplôme en sciences naturelles EPF
de nationalité suisse et originaire de Neuchâtel et Peseux (NE)

acceptée sur proposition du jury:

Dr A. Clappier, directeur de thèse
Prof. H. Davies, rapporteur
Dr A. Martilli, rapporteur
Dr M. Rotach, rapporteur

Lausanne, EPFL
2004

Résumé

Croissance de la population mondiale, utilisation effrénée des ressources naturelles, augmentation des polluants émis dans l'atmosphère: voici quelques obstacles (et non des moindre) auxquels nous sommes confrontés de nos jours afin d'assurer la durabilité de notre planète en général, et de la qualité de l'air en particulier. Dans le cas de la pollution atmosphérique, les processus gouvernant le transport et les transformations chimiques des polluants sont complexes et très fortement non linéaires. L'utilisation de modèles numériques pour la simulation des champs météorologiques, qui eux-mêmes déterminent le transport des polluants dans l'atmosphère, représente de ce fait un outil très adapté pour la description et la compréhension de la pollution de l'air.

Ce travail se concentre sur la simulation météorologique à l'aide d'un modèle à méso-échelle. L'accent est tout particulièrement porté sur la paramétrisation des effets induits par la présence d'une surface urbaine sur les champs météorologiques. Un schéma de paramétrisation urbaine a été développé et implémenté dans un modèle méso-échelle, FVM (Finite Volume Model) lors d'un travail précédent. Ce nouveau schéma représente une surface urbaine d'une manière plus précise que les méthodes traditionnelles de paramétrisation.

Lors de la première partie de ce travail, le module urbain a été validé en off-line pour une simulation unidimensionnelle à l'intérieur d'un canyon urbain dans la ville de Bâle/Suisse. Les résultats de la simulation ont été comparés à des mesures prises dans ce même canyon urbain lors d'une campagne de mesures intensive organisée dans le cadre du projet BUBBLE (Basel UrBan Boundary Layer Experiment). La comparaison avec les mesures, ainsi qu'avec les résultats d'une simulation utilisant la méthode traditionnelle, ont démontré que le schéma détaillé de paramétrisation urbaine améliorait la qualité de la modélisation des flux turbulents et des paramètres météorologiques dans la canopée urbaine.

Dans un deuxième temps, le modèle méso-échelle FVM a été utilisé pour une simulation en trois dimensions sur la ville de Bâle et ses environs. Il a été montré que le modèle est capable de reproduire l'évolution générale des vents régnant lors de l'épisode simulé, et que l'utilisation du module urbain détaillé permet une amélioration de la simulation des températures en ville.

La troisième partie de ce travail présente une étude de qualité de l'air sur le bassin de la ville de Mexico. Le modèle méso-échelle est utilisé pour simuler les conditions météorologiques régnant lors de l'épisode de pollution choisi (1 et 2 Mars 1997). Les champs météorologiques ainsi obtenus sont utilisés par un modèle photochimique Eulérien, le modèle TAPOM, qui calcule la distribution spatiale et temporelle des polluants atmosphériques. Cette simulation sur le bassin de Mexico a montré une distribution des polluants en accord avec les concentrations mesurées. Le modèle ainsi validé a pu être utilisé pour tester des scénarios de réduction des émissions.

L'utilisation de la paramétrisation urbaine détaillée pour la simulation des champs météorologiques et des concentrations de polluants a permis d'améliorer les résultats dans presque toutes les applications de ce travail. Par conséquent, l'outil complet de modélisation utilisé ici peut être employé pour des études de qualité de l'air sur des villes et leurs environs.

Abstract

Growing population, extensive use (and abuse) of the natural resources, increasing pollutants emissions in the atmosphere: these are a few obstacles (and not the least) one has to face with nowadays to ensure the sustainability of our planet in general, and of the air quality in particular. In the case of air pollution, the processes that govern the transport and the chemical transformation of pollutants are highly complex and non-linear. The use of numerical models for simulating meteorological fields, which in turn will determine the transport of pollutants in the atmosphere, is thus a very appropriate tool to describe and understand the air pollution problematic.

This work focuses on the meteorological simulation, using a mesoscale model. The stress is particularly put on the parameterisation of urban induced effects on the meteorological fields above a city. A detailed urban parameterisation scheme has been implemented in a mesoscale model in a previous work. This new scheme takes into account the presence of a city in a more accurate way as the traditional method usually used in mesoscale models.

In the first part of this work, the urban module was validated for a one-dimensional off-line simulation within and above a street canyon in the city of Basel/Switzerland. The simulation results were compared with measurements taken within and above the same street canyon during an intensive observation period in the frame of the BUBBLE project (Basel UrBan Boundary Layer Experiment). The comparison with the measurements and with a simulation using the traditional urban parameterisation showed that the detailed urban scheme improved the quality of the simulation of turbulent fluxes and meteorological parameters (wind, temperature) in the urban canopy.

Further on, the mesoscale was applied for a three-dimensional simulation over the city of Basel and its surroundings. The results showed that the model is able to reproduce the wind pattern

that prevailed during the simulated episode, and that the accuracy of the temperature simulation in the city is improved with the urban module.

In the third part of this work, an air quality study was performed over the Mexico City basin. The mesoscale model simulated the meteorological conditions for the chosen episode (1 and 2 March 1997). The results were then passed to TAPOM, a Eulerian photochemical model that calculates the space and time distribution of air pollutants. The simulated concentrations over the basin showed good agreement with the observed values. The validated model could then be used to test some emissions reduction scenarios for Mexico City.

The use of the detailed urban parameterisation scheme for meteorological fields and air pollutants concentration simulation improved the quality of the results in almost all the applied situations. Consequently, the full modelling tool presented and validated in this work can be used for air quality modelling studies over cities and their surroundings.

Remerciements

Cette thèse a été effectuée dans le laboratoire de pollution de l'air de l'EPFL, dirigé par le Prof. Hubert van den Bergh. Mes premiers remerciements lui sont donc destinés, pour m'avoir donné la possibilité de travailler dans son laboratoire. Je suis également reconnaissant à Alain Clappier, mon directeur de thèse, pour m'avoir appris les bases de la modélisation atmosphérique. Je tiens aussi à remercier les autres membres du jury, présidé par le Prof. H. van den Bergh:

- le Prof. Huw C. Davies, qui, à l'occasion de ses cours de météorologie dynamique, a éveillé mon intérêt pour la compréhension de l'atmosphère par les équations et la modélisation

- Mathias Rotach, avec qui j'ai suivi mes premiers cours de sciences atmosphériques, pour avoir mis à ma disposition sa grande expérience de l'analyse des mesures météorologiques

- Alberto Martilli, le créateur du module urbain, pour m'avoir initié à la modélisation météorologique en milieu urbain et sans qui mon travail n'aurait jamais pris cette forme

Ce travail n'aurait pas pu être mené à terme sans la contribution d'un bon nombre de personnes, que je tiens également à remercier chaleureusement:

- mes collègues de bureau et amis, Martin Junier et Clive Muller, pour la bonne collaboration, les matchs de foot et l'excellente ambiance dans le bureau

- les autres membres du groupe, avec qui j'ai collaboré à un moment ou à un autre de mon travail: Vijay Sathya, Jérôme Kübler, Olivier Couach, Frank Kirchner et Erika Zarate

- Daniel Grandjean, David Meylan et Jean-Daniel Bonjour, les responsables informatique de l'institut, sans qui un travail de modélisation numérique deviendrait très vite un calvaire…

- le Dr. Klaus Müller, pour la correction de l'anglais dans le texte

Finalement, je tiens à remercier mes parents et ma sœur pour leur présence tout au long du chemin parcouru jusqu'ici, et, bien sûr, Chrystèle pour son soutien constant et pour m'avoir permis de vivre et de partager ce moment important de ma vie avec elle.

Acknowledgments

" Everybody talks about the weather,

but nobody does anything about it."

24th August **1897**
Charles Dudley Warner (1829-1900),
American editor and author

"Continued accumulation of

anthropogenic greenhouse gases in the

atmosphere is likely to lead to

measurable climate change"

Intergovernmental Panel on Climate
Change, First Comprehensive Report
on Climate Change, **1990**

TABLE OF CONTENTS

Chapter 1: Introduction

Chapter 2: Description and testing of the models

Chapter 3: Validation of the urban parameterisation
in one dimensional simulation

Chapter 4: Simulation of atmospheric flow fields over the region of Basel

Chapter 5: Meteorological and air-quality modelling over the Mexico City basin

Chapter 6: Conclusions and prospects

Appendix A: Profiles of measured and simulated wind speed and direction

Appendix B: Hourly evolution of simulated NO_2 and O_3 concentration

Chapter 1

Introduction

1.1. Structure and chemical composition of the atmosphere

"La Terre est bleue comme une orange" (Paul Eluard, L'Amour la poésie, 1929). French poet Paul Eluard was neither a scientist nor an astronaut, yet his famous phrase is a fitting statement concerning our topic of atmospheric models. Our atmosphere can indeed be seen as a very thin peel (that is, thin in comparison to the radius of the Earth) wrapping the Earth and making life possible thanks to its gas composition. Nearly 100 % of the atmosphere's mass consists of the four chemical species: nitrogen (N_2, 78 %), oxygen (O_2, 21 %), argon (Ar, 0.93 %), and carbon dioxide (CO_2, 0.03 %), which maintain these constant proportions up to about 80 km above the Earth's surface. The last few hundredths of a percent consist of trace elements, which can have concentrations that are constant in time, as for instance methane (CH_4), carbon monoxide (CO), and hydrogen (H_2), or variable, as ozone (O_3), sulphur dioxide (SO_2), and the nitrogen oxides (NO and NO_2, commonly denoted together as NO_x). In addition, water (H_2O) is present in highly variable proportions and totalling about 1 % of the atmosphere's volume, either as a gas or condensed as clouds.

Among these species, the so-called greenhouse gases (CO_2, CH_4, O_3, etc.) play a significant role for our climate; they trap the long-wave terrestrial radiation and thus counteract the cooling of the Earth's surface caused by reemission of stored energy that comes from the direct short-wave insolation or indirect long-wave cloud backscattering. By analogy to gardening experience, this is called the greenhouse effect. Despite their low concentrations, the greenhouse gases are vital for life, since the average temperature at the Earth's surface would be too low for life as we know it, without this effect. Anthropogenic activities are partly responsible for the formation and emission of greenhouse gases, but water, as the major greenhouse gas, is naturally present in the Earth's atmosphere.
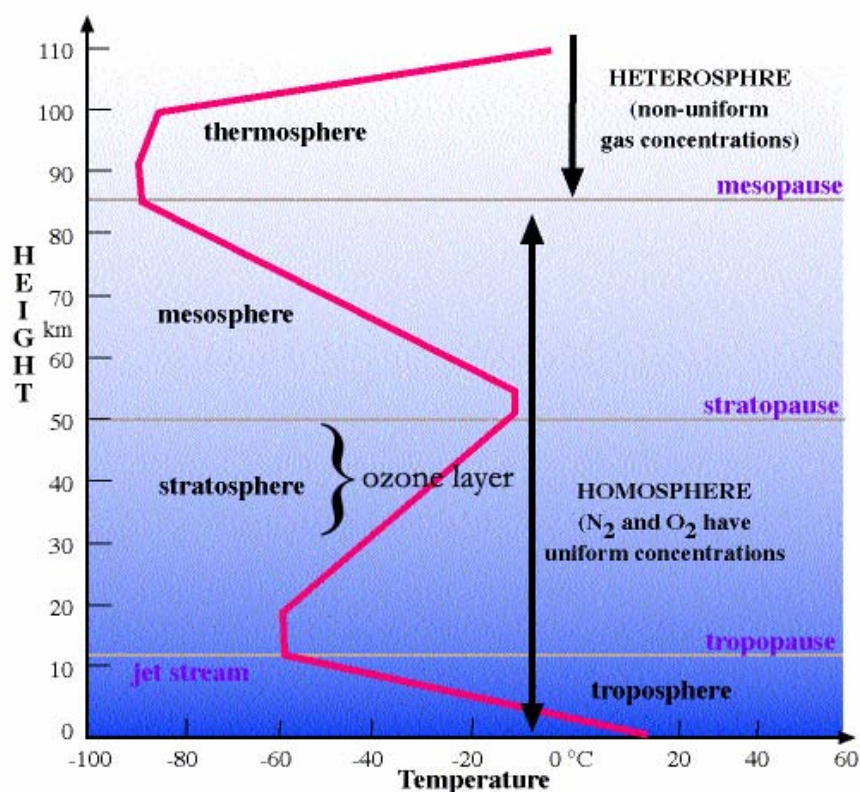

Figure 1.1. Vertical temperature distribution in the atmosphere.

In the vertical direction, the atmosphere can in turn be decomposed in four distinct layers of different thickness, usually associated with a specific vertical temperature distribution and specific

concentrations of its chemical species (Figure 1.1). Imagine for a moment that we are riding on a sunbeam travelling towards the Earth. The first layer we would come across after leaving extraterrestrial space and entering the Earth's atmosphere is the thermosphere (also called ionosphere or heterosphere). At its outer boundary, 500-600 km above the Earth's surface, we find the highest temperature of the entire atmosphere, which depending on solar activity may reach 1000 to 2000 K. As we cross the thermosphere, air temperature decreases very strongly and reaches the lowest values of the entire atmosphere (~193 K) at the mesopause, where the Northern Lights seen in high latitudes have their origin.

The mesosphere is situated between the mesopause (about 80 km above the Earth's surface) and the stratopause (about 50 km above the Earth's surface). In it, there is a constant strong temperature increase from 193 K at the mesopause to 273 K at the stratopause. The local temperature maximum at this height is due to the absorption of UV rays and the resulting stratospheric ozone formation and decomposition. This stratopause marks the upper boundary of the stratosphere, still a very dry layer within which the temperature strongly decreases over the top half of the layer, down to about 20 km above the surface of the Earth. The temperature then remains more or less constant (at 213 to 223 K) between the lower boundary of what is called the ozone layer and the tropopause. The region of the tropopause is characterised by very strong winds (the Jet Stream, also called the Easterly and Westerly Jets, and well known to air pilots). Our journey ends as we cross the troposphere. Its thickness varies from 8 km in high latitudes to 18 km over the Equator. It is characterised by a strong positive temperature gradient (~6 K per km) toward the Earth's surface, and by high (and highly variable) concentrations of water vapour and condensed water.

1.2. Tropospheric meteorology

Major part of all relevant weather processes occurs in the troposphere, hence it is crucial for a wide range of domains of human interest (air pollution, agriculture, outdoor activities, etc.) to have a good understanding of the atmospheric phenomena taking place in this layer. These phenomena can have either a thermal or a mechanical origin.

Daytime solar heating of the Earth's surface generally gives rise to vertical turbulence and mixing of the air. In addition, it induces another thermal process occurring in a diurnal cycle, viz., differential surface heating due to different thermal properties of the soil, shadowed zones, the distribution of land and sea, etc. It produces the local horizontal wind systems, *eg* land and sea breezes arising from the differences in heat uptake between land and water (Figure 1.2).
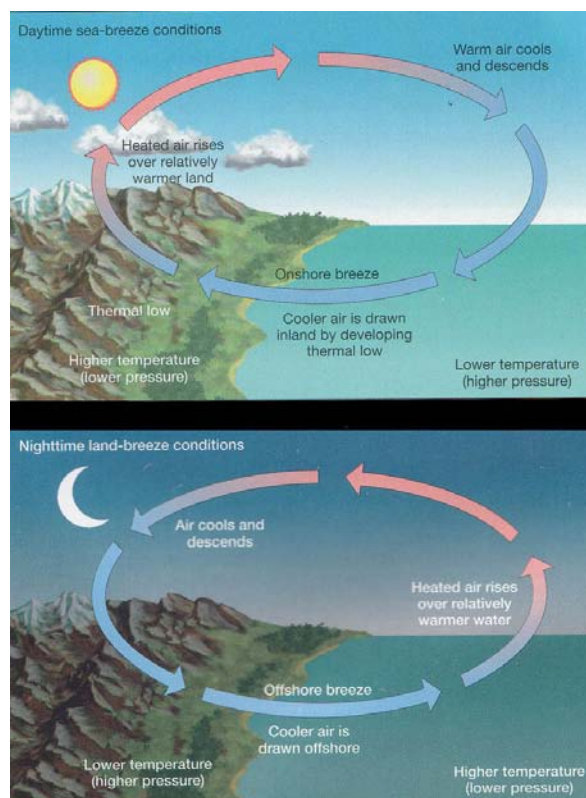
Figure 1.2. Formation of daytime sea breeze (top) and nighttime land breeze (bottom) as consequences of different thermal characteristics of land and water.

During daytime, land because of its lower specific heat is warmer than water (less solar energy is needed to raise its temperature). As a consequence, air above land is warmer, rises up and is transported offshore, where it cools down and sinks. At water level, this air is transported back to land. This transport is driven by the low pressure set up over land, relative to the water surface, when warm air is lifted up from land surfaces. The reverse process takes place during nighttime, when the land surface cools more rapidly than the water. Land and sea breezes are very important for local meteorology including pollutant dispersion in coastal regions (for example, see the study on air quality of the Athens basin by Martilli *et al*, 2003).

On the other hand, mechanical influences arise from the fact that the Earth's topography leads to perturbations of the flow fields near the ground, such as the formation of gravity waves (lee waves) and associated cloud formation downwind of obstacles (mountains, buildings, etc., Figure 1.3), dry and warm wind on the lee side of mountain ranges (Foehn in the Alps or Chinook in the Rocky Mountains), or the deceleration of air flow near the ground due to frictional forces.

Figure 1.3. Gravity (mountain) wave formation on the lee side of an obstacle.

Some phenomena arise from a combination of thermal and mechanical influences, *eg* mountain and valley winds due to a differ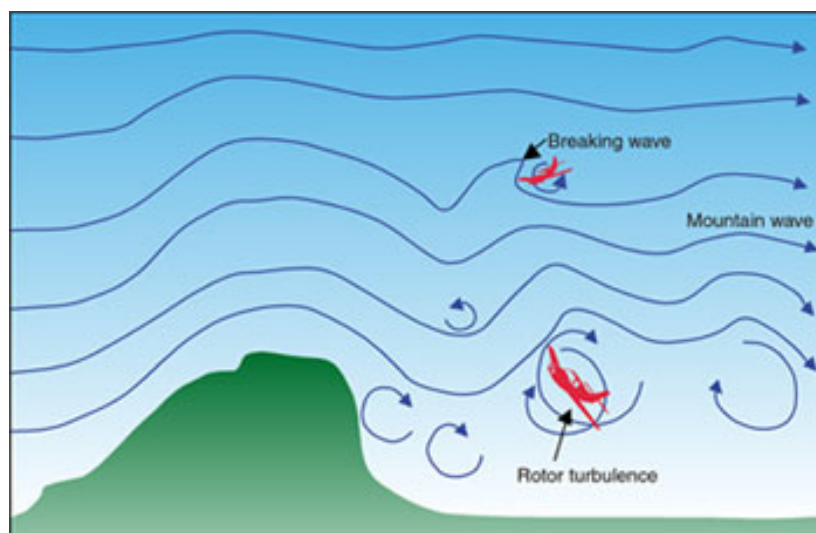ential heating of the valley sides and valley floor (anabatic or upslope wind during daytime, katabatic or downslope winds during nighttime). Barry and Chorley (1992) provided a rather detailed description of flow perturbations caused by thermal and mechanical processes.

All these phenomena are important for the space and time distribution of air pollutant concentrations, and hence must be taken into account for appropriate, efficient air quality management.

1.3. The problems of air pollution in the troposphere

Human activities are confined to the troposphere and vitally depend on it, hence it is crucial to preserve the troposphere from all degradation. Therefore, investigations of all the natural processes taking place in this part of the atmosphere are of great interest and importance. An anthropogenic forcing on global climate has been recognized as a potential threat for more than a decade (*eg* Intergovernmental Panel on Climate Change (IPCC) reports, 1992, 1994) by the scientific community and by policy makers. The Rio Earth Summit, organized by the United Nations in 1992, and the related final document, the Agenda 21, in that sense were the first worldwide events bringing together governments, nongovernmental agencies, and scientists from both developed and developing countries. It is now broadly recognized that the population growth of recent decades puts considerable stress on the environment in general, and on air quality in particular. Ever more people live in concentrated urban areas. Cities grow larger in every part of the world. In 2003, there were 325 cities with more than one million inhabitants, against only 270 just 13 years earlier (Molina and Molina, 2002). Energy consumption and the resulting mass of pollutants released to the atmosphere is a direct function of the intensity of

human activities, which are highest in urbanized zones. Thus, fossil fuel consumption and associated emissions have experienced an exponential growth since 1850 and the industrial revolution (Figure 1.4).

Figure 1.4. Global trend in fossil fuel CO_2 emissions [Giga tons] from 1860 to 1998 (Hengeveld, 1999).

We all know that as a result, air quality has strongly deteriorated, particularly so in large cities and their surroundings, and millions of people are being exposed to harmful levels of air pollutants.

Air pollution originates from two types of pollutants when considering their formation. Primary pollutants are directly emitted into the atmosphere; they include the nitrogen oxides (NO_x) released by road traffic and heating, and the volatile organic compounds (VOC) largely coming from industrial activities. Secondary pollutants are formed in the atmosphere as a result of chemical transformation of the primary pollutants. This is true for low-altitude ozone (not to be confused with the ozone of the ozone layer) that builds up through a reaction cycle involving NO_x and VOC and taking place in the presence of solar energy (Figure 1.5). The process can be

described very generally by Eq. (1.1) (for a complete description of the full ozone production and destruction cycle, see *eg* Seinfeld *et al*, 1998).
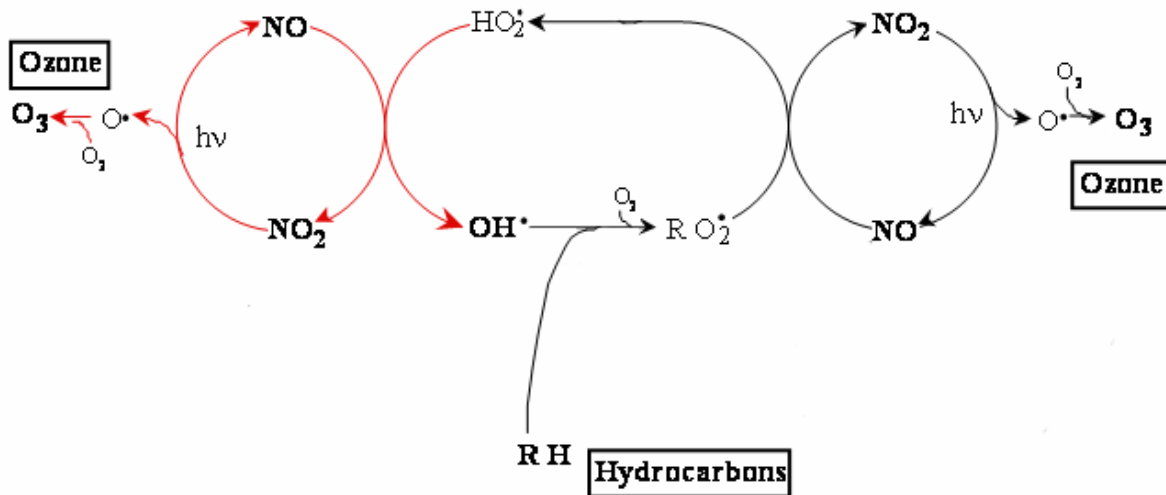
Figure 1.5. Ozone formation cycle (simplified).

$$VOC + NO_x \xrightarrow{\;hv\;} O_3 \tag{1.1}$$

where *hv* represents the solar radiation initiating the reaction. Ozone formation occurs relatively close to the ground in the plume downwind of primary pollutant emission, usually at distances of 10 to 100 km from the sources, when VOC and NO_x both are present in relevant quantities. As a result, effects of primary pollutants on human health, vegetation, and infrastructure (including monuments, buildings, and metallic structures) act *in situ*, i.e., mainly in the cities where traffic and industrial activities are highest, while secondary pollutants often affect human health and vegetation (as in the case of ozone) in rural areas. This situation reveals one of the more difficult problems to solve for policy makers dealing with air quality management, namely, that polluting and polluted areas often are not the same. The problems become even more complex to handle in the instance of transcontinental pollutant transport, which occurs in the stratosphere.

1.4. Definition of the space and time scales

From an environmental point of view, two major space scales are important for an understanding of pollution problems in the troposphere when considering what has been said above.

Microscale processes ranging from a few centimetres to several meters (Stull, 1988) must first be considered for air quality. Microscale phenomena will determine how pollutants are transmitted from their sources to the lower layer of the troposphere, called the Planetary Boundary Layer (PBL). The troposphere can in fact be divided into two parts: the PBL, extending a certain distance upward from the surface and, above it, the free atmosphere. The PBL is directly influenced by the presence of the Earth's surface, as it reacts to such forcings as frictional drag, solar heating, and evapotranspiration. Each of these forcings generates turbulence in the form of eddies of different sizes that can be as high as the boundary layer itself. The thickness of the PBL mainly depends on solar activity at the ground (Figure 1.6).
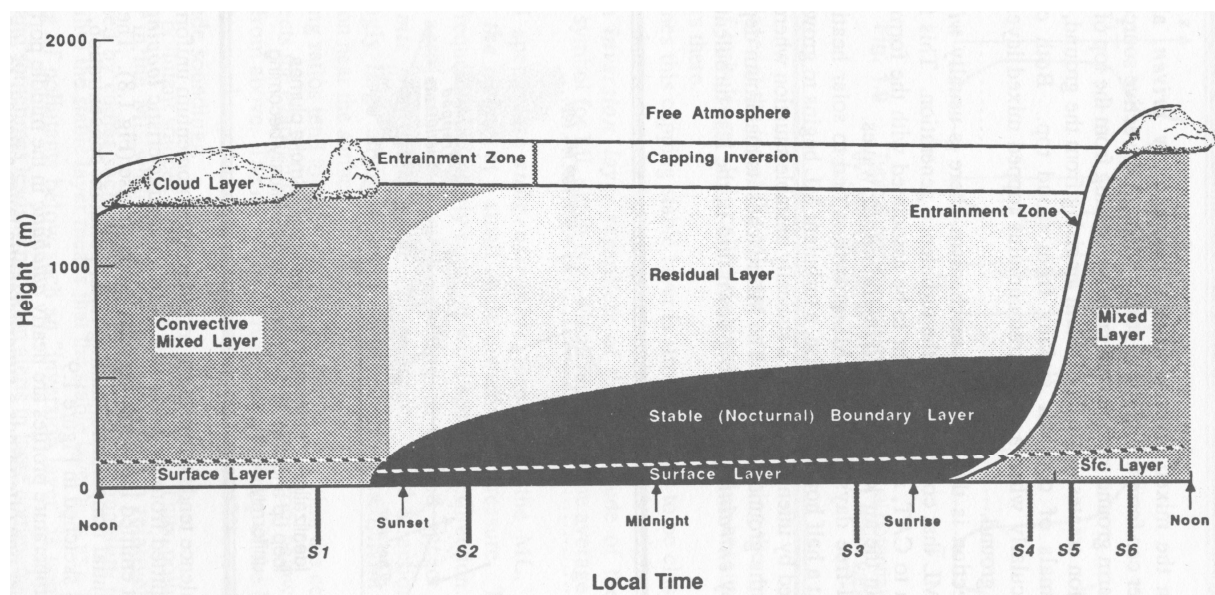

Figure 1.6. Diurnal development of the Planetary Boundary Layer thickness. The daytime convective mixed layer, with a very homogenous vertical distribution (temperature, air pollutants, etc.), is replaced by a stable boundary layer near the ground and a residual layer containing the remainder of daytime turbulence and trapping the air pollutants (Stull, 1988).

It is smallest during night and on cloudy days: stable (nocturnal) boundary layer, a few tenths of a meter thick, and largest during a sunny afternoon: convective mixed layer typically 1500 to 3000 m thick. The stable boundary layer is topped by a residual layer containing the remainder of daytime turbulence and those air pollutants that have been vertically advected by daytime turbulence. This layer is separated from the free atmosphere by a temperature inversion, which prevents upward air movements to the free atmosphere. The mixed layer starts to grow about half an hour after sunrise, and attains its maximum thickness in late afternoon. It grows by entraining, or mixing down into it, the less turbulent air from above, and is separated from the free atmosphere by an entrainment zone.

As already mentioned, major part of the primary pollutants are emitted from urbanized areas, where the presence of buildings has a very strong influence on lower atmospheric flow fields. The alteration of flow fields due to drag from buildings and heat storage in street canyons are typical urban-induced phenomena that must be considered for an accurate air quality understanding (Brown, 2000).

Mesoscale processes are the second variety of phenomena involved in local-level air pollution (Figure 1.7). Pielke (1984) defined these processes as having a time scale and a horizontal space scale smaller than the conventional rawinsonde network[1], but significantly larger than individual cumulus clouds (500 to 1000 m, Rodts *et al*, 2003). Put quantitatively, their characteristic

[1] A radiosonde is a balloon-borne instrument used to simultaneously measure and transmit meteorological data while ascending through the atmosphere. Thus, rawinsonde observations of the atmosphere describe the vertical profile of temperature, humidity, and wind direction and speed as a function of pressure and height from the surface to the altitude where the sounding is terminated. The WMO recommends a minimum upper-air station spacing of about 250 km over large land areas and 1000 km over sparsely populated and oceanic regions and further recommends that observations be taken one-to-four times daily (OFCM, 1997).

horizontal scale amounts to a few kilometres to several hundred kilometres, while the time scale

is between 1 and 12 h. The vertical scale extends from tens of meters to the thickness of the

troposphere. It includes transport and deposition of pollutants through local wind systems that

are thermally or mechanically induced, or that are both thermally and mechanically induced (see

Section 1.3).
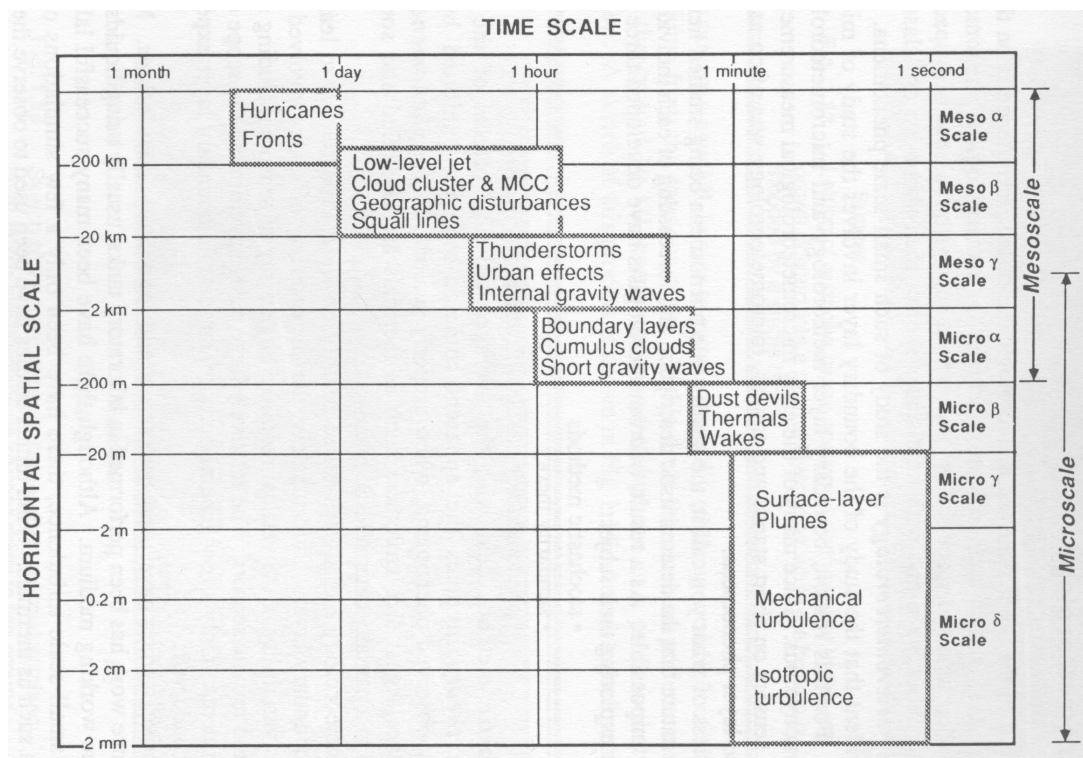
Figure 1.7. Definition of time and space scales for atmospheric phenomena (Stull, 1988).

1.5. The modelling tools

Due to the complexity and nonlinearity of the processes involved on both of the above scales,

numerical modelling will constitute the most appropriate tool for achieving an integrated air

quality management. It will be able to account for microscale phenomena, which describe

pollutant transfer to the atmosphere (mostly in urban areas), as well as for mesoscale phenomena,

which stand for horizontal pollutant transport, and it will also be able to link these processes by

considering various feedback mechanisms between the two scales. A decoupling of the two scales in the model will be required for a more accurate modelling of meteorological flow fields close to ground in urban areas.

In the process of air quality management, the simulated meteorological fields (pressure, temperature, humidity, wind, etc.) are used to feed a Eulerian transport and photochemical model. This type of model calculates transport of pollutants and their chemical transformations in the troposphere, and provides the space and time distribution of pollutant concentrations as its output. Accurate emission inventories (traffic, industries) as well as the topography and the landuse coverage of the domain are the major inputs of a photochemical model, together with the meteorological fields.

Chapter 2 will describe in greater detail the structure of the models used in this work, i.e., the mesoscale atmospheric model, the decoupled urban parameterisation scheme, which has been implemented in the mesoscale model, and the Eulerian photochemical model.

In a first step, the urban module was validated for one-dimensional simulations in a street canyon using *in-situ* measurements in the city of Basel/Switzerland (Chapter 3), which were recorded in the context of the Basel UrBan Boundary Layer Experiment (BUBBLE) measuring campaigns. This large urban PBL experiment was undertaken under the umbrella of the European COST 715 action. Its aim was that of investigating the exchange processes occurring near the urban surface as well as the flows occurring in the upper part of the Urban Boundary Layer (UBL). The tools used were surface and remote sensing instrumentation on one hand, and a mesoscale meteorological model on the other hand.

Based on the one-dimensional validation, the mesoscale model was run with the urban parameterisation in three-dimensional simulations of atmospheric flow fields over the region of Basel (Chapter 4). Results of the model were compared with observations coming from several measuring stations placed in the domain.

In Chapter 5, the mesoscale model with urban parameterisation was applied to a study of air quality over Mexico City, a megacity impacted every day by very high levels of pollution. The simulated meteorological fields were then used as input for the photochemical model. The results demonstrate, on one hand the influence of a city on the atmospheric flow fields close to ground, and on the other hand the utility of a detailed urban parameterisation for the modelling of air-pollutant concentrations.

In Chapter 6, conclusions and the prospects for future developments of the mesoscale model and the urban parameterisation scheme will be presented.

References

Barry, R. G. and Chorley, R. J.: 1992, *Atmosphere, weather and climate, 6th edition,* Routledge, London, pp. 97-139

Brown, M.: 2000, 'Urban parameterisations for mesoscale meteorological models', in Z. Boybeyi (ed.), *Mesoscale Atmospheric Dispersion*, Wessex Press, pp. 193-256

Hengeveld, H.: 1999, 'Climate change and the ocean environment – Understanding the science', *Proceedings, Climate Change and Salmon Stocks Conference*, Vancouver, BC, Canada, October 27 1999

Houghton, J. T., Callander, B. A. and Varney, S. K. (Eds.): 1992, *Climate change 1992*, Intergovernmental Panel on Climate Change (IPCC), Cambridge University Press, 200 pp.

Houghton, J. T., Meira Filho, L. G., Bruce, J., Lee, H., Callander, B. A., Haites, E., Harris, N. and Maskell, K. (Eds.): 1995, *Climate change 1994: Radiative forcing of climate change and an evaluation of the IPCC IS92 emission scenarios*, Intergovernmental Panel on Climate Change (IPCC), Cambridge University Press, 339 pp.

Martilli, A., Roulet, Y.-A., Junier, M., Kirchner, F., Rotach, M. W. and Clappier, A.: 2003, 'On the impact of urban exchange parameterisations on air quality simulations: the Athens case', *Atmos. Environ.* **37**, 4217-4231

Molina, L. T. and Molina, M. J. (Ed.): 2002, *Air quality in the Mexico megacity, an integrated assessment*, Kluwer Academic Publishers, 384 pp.

OFCM (Office of the Federal Coordinator for Meteorology): 1997, 'Federal meteorological handbook No. 3: Rawinsonde and pibal observations', *FCM-H3*, Washington, DC

Pielke, R. A.: 1984, *Mesoscale meteorological modeling,* Academic Press, Orlando, Florida, 612 pp.

Rodts, S. M. A., Duynkerke, P. G. and Jonker, H. J. J.: 2003, 'Size distribution and dynamical properties of shallow cumulus clouds from aircraft observations and satellite data', *J. Atmos. Sci.* **60**, 1895-1912

Seinfeld, J. H. and Pandis, S. N.: 1998, *Atmospheric chemistry and physics, from air pollution to climate change*, John Wiley and Sons, Inc., 1326 pp.

Stull, R. B.: 1988, *An introduction to boundary layer meteorology*, Kluwer Academic Publishers, 670 pp.

Chapter 2

Description and testing of the models

Abstract

Efficient air quality modelling requires considering a wide range of atmospheric processes spread out over various time and space scales. These processes are complex and nonlinear, and linked together by numerous feedbacks; therefore, a reasonable approach when taking into account all the elements concerned is that of using numerical atmospheric models. In local air pollution (on the scale of a city and its surroundings), one must describe processes occurring on two main scales, namely, microscale processes on the scale of a few meters in size, and mesoscale processes on the scale of a few kilometers to several hundreds of kilometers in size. The latter are simulated by atmospheric mesoscale models.

Microscale processes in urban areas are widely influenced by the presence of buildings, and therefore require a separate treatment. For this purpose, an urban parameterisation scheme has been inserted into the mesoscale model used here. The mesoscale model and the urban scheme are described in this chapter, together with the Eulerian photochemical model used for the modelling of air pollutant concentrations. A sensitivity analysis is performed with the main input parameters in order to test and validate the model and enhance the understanding of its working.

2.1. Mesoscale modelling

2.1.1. Introduction

In recent decades, a computer technology offering rapidly growing calculation speed and memory size has greatly contributed to the development of different types of mesoscale models which use different parameterisation schemes and simulate atmospheric flow fields in the troposphere. Among them, RAMS (Pielke *et al*, 1992), MM5 (Grell *et al*, 1994), MEMO (Flassak 1988), TVM (Thunis 1994), Berphomod (Perego 1996), and ADREA (Bartzis *et al*, 1991) should be mentioned. For air quality studies, the results obtained with such models are then put into a Eulerian photochemical model which solves equations for the transport and chemical transformations of air pollutants, and deduces space and time-dependent concentrations of pollutants in the simulated domain. In some cases the two models can be run separately, as for instance the mesoscale model used here, so that meteorological fields produced by the mesoscale model will be used as input for the photochemical model. In other cases, as in Berphomod, the two models are coupled and the meteorological fields thus calculated are immediately used for the photochemical simulation.

2.1.2. Governing equations of the mesoscale atmospheric model

The model selected here (Clappier *et al*, 1996) was partly developed at the Air Pollution Laboratory of the Swiss Federal Institute of Technology in Lausanne. It uses a finite-volume method for space discretisation. The resulting mesh is terrain-following (deformable), and is thus able to take into account the topography of the domain. The model is typically applied over areas of 200 by 200 km in the horizontal, and reaches up to heights of 10 km above the Earth's surface so as to cover the entire troposphere. The volume thus defined is discretised to provide a horizontal resolution with cells of 1 to 5 km and a vertical resolution of typically 10 m close to

the ground, where high accuracy is needed, to 1000 m at the top of the domain, near the tropopause.

In the model, the following conservation equations (Eqs (2.1) to (2.4)) are solved in each cell of the domain:

► Conservation of mass:

$$\frac{\partial \rho}{\partial t} + \frac{\partial \rho U_i}{\partial x_i} = 0$$

$$\qquad I \qquad II$$

(2.1)

where U_i is the wind component in the three space directions (index i thus runs from 1 to 3 in Eqs (2.1) to (2.5)), and ρ the air density. On typical scales of velocity and length for the motions in the mesoscale range, term I is much smaller than term II, and can therefore be neglected (incompressibility approximation).

► Conservation of momentum:

$$\frac{\partial \rho U_i}{\partial t} = -\frac{\partial P}{\partial x_i} - \frac{\partial \rho U_i U_j}{\partial x_j} - \frac{\partial \rho \overline{u_i w}}{\partial z} - \rho \frac{\theta'}{\theta_0} g \delta_{i3} - 2\varepsilon_{ijk}\Omega_j \left(U_k - U_k^G \right) + D_{ui}$$

$$\quad I \qquad\quad II \qquad\quad III \qquad\qquad IV \qquad\quad V \qquad\qquad VI \qquad\qquad VII$$

(2.2)

where term I describes the storage of momentum, term II the pressure-gradient force, term III advection (mean transport), term IV the turbulent transport (the fluctuations around mean transport), term V the vertical action of gravity, term VI the influence of the Earth's rotation (Coriolis effects), and term VII the forces induced by interactions between solid surfaces and airflow (*eg* drag forces and frictional forces).

► Conservation of energy:

$$\frac{\partial \rho \theta}{\partial t} = -\frac{\partial \rho \theta U_i}{\partial x_i} - \frac{\partial \rho \overline{w\theta}}{\partial z} - \frac{1}{C_p}\left(\frac{P_0}{P}\right)^{R/C_p} \frac{\partial R_{lw}}{\partial z} + D_\theta$$

$$\quad I \qquad\qquad II \qquad\quad III \qquad\qquad\qquad IV \qquad\quad V$$

(2.3)

where term *I* represents the storage of heat (potential temperature), term *II* advection, term *III* the turbulent transport, term *IV* the loss through long-wave emissions, and term *V* the impact of sensible heat fluxes from solid surfaces on the potential-temperature budget.

► Conservation of moisture:

$$\frac{\partial \rho H}{\partial t} = -\frac{\partial \rho H U_i}{\partial x_i} - \frac{\partial \rho \overline{wh}}{\partial z} + D_h$$

$$\quad I \qquad\qquad II \qquad\quad III \quad IV$$

(2.4)

where term *I* represents the storage of moisture, term *II* advection, term *III* the turbulent transport, and term *IV* the impact of the latent-heat fluxes from the ground on the humidity budget. Condensation and cloud formation are not taken into account in the model. The *D*-terms in Eqs (2.2) to (2.4) arise from the consideration of urban elements, and are solved by the urban module presented below.

The conservation equations (2.1) to (2.4) are solved explicitly for a discretised time step. This step must fulfil the Courant-Friedrich-Levy (CFL) condition in order to insure stability of the calculation, and hence depends on cell size as well as on the wind speeds prevailing in the cells (the larger a cell and the smaller the wind speed, the longer will be the time step). This in turn has an impact on CPU calculation time, since at longer discretisation times, fewer time steps are needed to cover the entire episode simulated.

Air pressure is solved implicitly with a Poisson differential equation, obtained from a combination of (2.1) and (2.2):

$$\frac{\partial}{\partial x_i}\left(\frac{\partial P}{\partial x_i}\right) = \frac{\partial F_i}{\partial x_i}$$

(2.5)

where in F_i, terms *III* to *VII* of Eq (2.2) are grouped together.

The algorithm used for the transport of scalar variables (temperature, wind, etc.) is based on a third-order Parabolic Piecewise Method (PPM, Collella and Woodward, 1984), which has been extended for multidimensional applications (Clappier, 1998).

The vertical turbulent fluxes above the ground surface are computed with common K-theory (or gradient-transport theory). This theory is a first-order closure approximation for solving the description of turbulent flow[1]. It retains prognostic equations for only the zero-order mean variables such as temperature, wind, and humidity:

$$\overline{u_i^{'}\xi^{'}} = - K \frac{\partial \overline{\xi}}{\partial x_i} \tag{2.6}$$

where K is the turbulent-transfer coefficient (eddy diffusivity), $\overline{u_i^{'}\xi^{'}}$ is the flux of variable i (turbulent part of the variable) in the three directions of space, and ξ is any variable (here, the mean part of the variable concerned). For positive K the fluxes occur in a direction down the local gradients of the variables.

The vertical turbulent-transfer coefficient K_z (for $i = 3$) is parameterized with a $k - l$ closure from Bougeault and Lacarrère (1989). For that purpose, a prognostic equation is solved to compute the turbulent kinetic energy (TKE), which in turn is used to calculate the vertical diffusion coefficients K_z:

---

[1] The closure problem of turbulence is one still unsolved problems of classical physics: it is demonstrated that the number of unknowns in the set of equations for turbulent flow is larger than the number of equations, no matter how much equations are used. This statement is called the closure problem, and was first pointed out by Keller and Friedmann in 1924. It is attributed to the non-linearity of turbulence (Stull, 1988). Turbulence closure thus simplifies the resolution by neglecting higher order variables. The higher the order, the more unknowns are considered, and the more complex will be the set of equations.

$$K_z = C_k * l_k * E^{\frac{1}{2}} \tag{2.7}$$

where C_k is a numerical constant, l_k is a characteristic length, and E is the turbulent kinetic energy. Close to ground, in the so-called surface layer defined as the lower part of the boundary layer, where fluxes vary with height by less than 10 % of their magnitude, the resolution of the conservation equations is not high enough. Therefore, turbulent fluxes of momentum, heat, and water vapour in this layer are computed with an adaptation of the Monin-Obukhov Similarity Theory (MOST)[2] reported by Louis (1979). Inputs needed for this parameterisation are the roughness length, surface temperature, and moisture. Roughness lengths can be obtained from GIS data bases. Surface temperature and moisture can be calculated with a soil module (Tremback and Kessler, 1985), which solves two prognostic equations for temperature and for water content of the soil. Impacts on the simulation results produced by soil module input parameters such as the soil moisture at saturation, the hydraulic conductivity for a soil at saturation, the initial-to-saturation soil moisture ratio, the moisture potential for a soil at saturation, or the specific heat of dry soil, will be evaluated via a sensitivity analysis in the last section of this chapter.

As mentioned above, the model disregards the transport and chemical transformations of pollutants in the atmosphere. However, it includes the possibility of transporting passive tracers, in the same way as it admits the transport of other meteorological scalars such as temperature or humidity. Point-source locations and emissions must then be provided as functions of time as the

[2] Similarity theory is used when the usual governing equations of atmospheric physics fail to describe the behaviour of the PBL. The Monin-Obukhov Similarity Theory (MOST) is a first-order approximation usually applied to the surface layer that holds when the fluxes are constants. The PBL description can then be simplified by utilizing the flux at just a single height, usually at zero height, i.e., at the surface (Stull, 1988).

inputs to the model. Tracer concentrations as functions of time in each cell of the domain are obtained as the output.

2.1.3. Forcing technique

Users must provide the model with a vertical profile of temperature, wind (speed and direction), and humidity as the initial conditions in order to run the model in its basic state. For better adaptation to the local weather situation (regional wind systems) prevailing during the entire simulation period, the model can be forced by meteorological data from a large-scale model using a Four-Dimensional Data Analysis (FDDA) technique (Fast, 1995), which was implemented in the code of the mesoscale model in the frame of this work. This technique allows results from a large-scale model to be combined with the mesoscale model results. For this purpose, a Newtonian (nudging) technique can be incorporated into the model so as to bring the prognostic variables into closer agreement with the meteorological situation given by a large-scale model. The forcing can be realised for wind and temperature at the boundaries of the simulated domain, by adding a tendency term from the large-scale value to the value calculated by the model at the same location. For that purpose, a preprocessor has been developed that transforms large-scale model outputs to the format of the mesoscale grid. The weight given to forcing data, as well as the spatial zone of influence of the forcing in the domain, are user-defined, so that the impact of the forcing in the mesoscale-model calculations is more readily controlled and verified. Large-scale forcing and model-calculated scalars (wind, temperature) are combined by using the equation:

$$\frac{\partial \Phi_M}{\partial t} = \frac{\Phi_L - \Phi_M}{\tau} \tag{2.8}$$

where Φ_M is the scalar of the mesoscale model, Φ_L is the scalar of the large-scale model, ∂t is the model-calculation time step, and τ is the "relaxation time", which represents the weight given to

the large-scale model in each mesoscale grid cell at every time step. The solution of Eq (2.8) after

discretisation that is obtained under the assumption that $\Delta t << \tau$, is:

$$\Phi_M^{t+1} = \frac{\Delta t}{\tau}\Phi_L^t + \left(1 - \frac{\Delta t}{\tau}\right)\Phi_M^t \tag{2.9}$$

Since the observations of large-scale model data are provided at time intervals much longer than

the model time step, a time weighted average is calculated for Φ_L by using the two values that

bracket the current model time:

$$\Phi_L^t = (1 - \alpha)\Phi_L^T + \alpha\Phi_L^{T+1} \tag{2.10}$$

where t is the mesoscale model time, T is the large-scale or observation time, and α is a weighting

factor having values between 0 and 1 and representing the model time positions t relative to T

and T + 1. This forcing technique is applied in the present work for simulations of the

atmosphere over Basel and its surroundings (Chapter 4), and for model simulations over the

Mexico City basin in the frame of an air quality study (Chapter 5).

2.1.4. Solar radiation forcing

The mesoscale model, as already mentioned, does not consider any condensation or cloud-

formation processes. Therefore, no feedback to the solar-radiation calculation (attenuation

through cloud episodes) is taken into account in the model. Since this phenomenon plays an

important role for the amount of energy available for turbulence generation near the ground, and

should therefore be included, solar radiation can be prescribed to the model by data input, rather

than calculating it by the model itself. This constitutes an "indirect" consideration of cloud

formation in the model and will improve the fit to local meteorological conditions prevailing

during the episode simulated.

2.2. Urban modelling

2.2.1. Review of existing urban parameterisation techniques

A city, by its characteristic surface roughness and thermal exchanges with the lower atmosphere, has a strong impact on the structure of the Planetary Boundary Layer (PBL). The processes involved can be induced, both mechanically (turbulence due to the presence of buildings, with a roughness higher than for rural landscapes) and thermally (radiation trapping and shadowing in the street canyon). In the traditional approach to accounting for the presence of an urban area in mesoscale models, MOST is used, just as it is for rural areas, but in doing so, larger surface roughness lengths (z_0) and different soil thermal characteristics are employed. This approach, however, cannot provide an accurate representation of the vertical structure of turbulent fluxes, as it considers sinks of momentum only at ground (first cell of the model), rather than over the entire height of buildings. Measurements performed over different cities throughout the world (Zurich: Rotach, 1993; Sapporo: Oikawa and Meng, 1995; and Vancouver: Roth and Oke, 1993) as well as wind tunnel studies (Kastner-Klein *et al*, 2001) have shown that turbulent fluxes are height-dependent in the Roughness Sublayer (lower part of the Urban Surface Layer, usually having a thickness of some tens of meters). This then means that MOST cannot really be applied. Instead, it was suggested by Rotach (2001) that a local scaling approach should be adopted in this layer. Another weakness of the traditional method is that of neglecting shadowing and radiation trapping in the street canyon, which have real impacts on net radiation and heat balance, and hence on the generation of the Urban Heat Island (UHI) effect.

The energy balance over urban surfaces has been thoroughly studied for several years. Oke (1988) provided a good overview of the earlier findings, while Grimmond and Oke (1995) investigated a number of North American cities under different climatic conditions. For reasons related to limitations in the data collection conditions, these studies were largely restricted to the

suburban situation. In Oke *et al*'s pioneering study of 1998, energy balance measurements were reported for the first time for an extended urbanized area (Mexico City). By now, a large number of energy and radiation balance measurements are available for several urban areas in Central and North America (Mexico City, Vancouver, Tucson, Miami, Chicago, Los Angeles) (Grimond and Oke, 2002) and in Switzerland (Basel) (Rotach, 2002).

In view of these urban data, several methods for urban parameterisation other than the traditional one described above have been developed in recent decades. Most of them focus on improvements of either the dynamical or the thermal part. In many of the methods involving dynamic improvements, the parameterisation retains its MOST basis, but adds urban-induced drag and turbulence production terms (Williams *et al*, 1995, Sorbjan and Uliasz, 1982). More recently, some models were developed where urban-induced drag terms were included, both into the turbulent kinetic energy (TKE) and into the turbulent dissipation rate (Maruyama, 1999, Ca, 1999). In accounting for thermal effects, (anthropogenic) heat sources of a city are often supposed to directly release their heat to the air (Ca, 1999). The surface energy balance can also be modified so as to account for shadowing and radiative-trapping effects of buildings (Masson, 2000). Brown (2000) gave an exhaustive picture of urban parameterisation attempts.

2.2.2. Description of the urban module

In the parameterisation used here, modifications were made in the dynamic as well as in the thermal part of the model. This detailed urban surface exchange parameterisation (see Martilli *et al*, 2002 for a complete description of the module) represents the city as at least one (user-defined) urban class that is characterised by the following parameters:

- shape of the street canyon, expressed in terms of the distance between building rows, and shape of the buildings, expressed in terms of roof width and wall height (see Figure 2.1)

- building height distribution, expressed in terms of the probability γ of having buildings with a certain height z and a density Γ of buildings higher than given values of z (see Figure 2.1); γ and Γ are linked by the equation:

$$\Gamma\left(z_{iu}\right) = \sum_{ju=iu}^{nu} \gamma\left(z_{ju}\right) \tag{2.11}$$

where *nu* is the highest level in the urban grid.

- street orientation (several orientations per class are possible)

- properties of the materials (thermal diffusivity, heat capacity, albedo, and emissivity for the three urban element types, *ie,* street, wall, and roof)
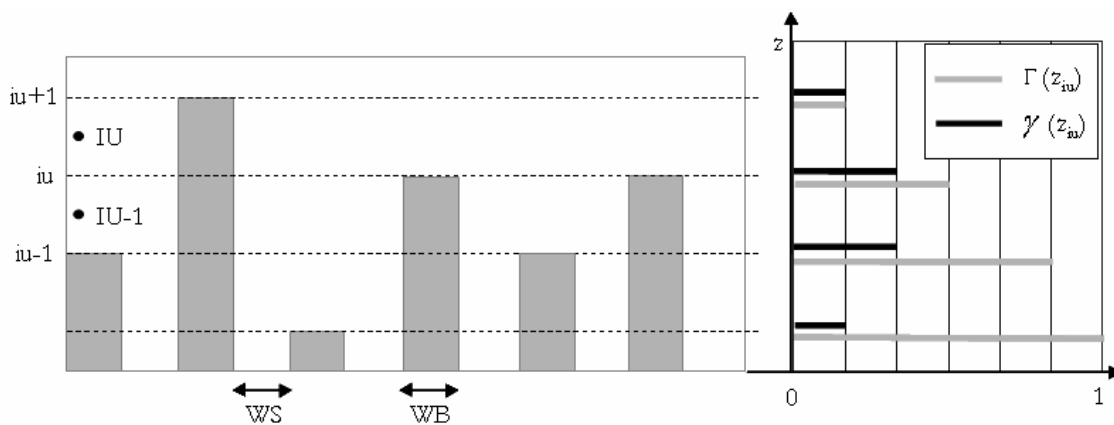

Figure 2.1. Illustration of geometrical urban parameters: street canyon width (WS), building width (WB), and building height distribution in terms of γ and Γ (after Martilli, 2002).

The module calculates turbulent fluxes and meteorological scalars for any given street direction while allowing for the specified building height distribution, and then averages over all defined street directions. This urban parameterisation scheme is implemented as a subgrid of the mesoscale grid in the mesoscale model described above. The horizontal resolution is identical with the resolution of the mesoscale grid, while the vertical resolution must be finer than the mesoscale resolution, and is usually selected to be of the order of 2 to 5 meters (the subgrid

extends vertically only up to the highest building). After their calculation in the urban grid, the fluxes and meteorological variables must then be vertically interpolated in the mesoscale grid.

2.2.3. Calculation of urban effects

The principal impacts of buildings on airflow close to ground are:

- drag forces induced by vertical surfaces of the buildings (walls), with an associated loss of momentum,

- friction forces from horizontal surfaces (canyon floors and roofs), with an associated loss of momentum,

- shadowing and radiation trapping in the street canyon, causing modifications of the heat flux, and

- a more intense generation of TKE from mean kinetic energy.

The module is set up so that the impacts of these effects which are induced by each urban surface type (street, wall, roof) are calculated separately, and are accounted for in proportion to the corresponding surface fraction at each level of the urban grid. Thus, momentum loss due to friction at horizontal surfaces is calculated with MOST and the classical surface layer theory (just as it is for a rural ground surface in the mesoscale model), but the loss is distributed between ground level and the level of the highest building in proportion to the horizontal surface areas at each level. On the other hand, vertical surfaces (walls) induce drag forces, which again are distributed in the vertical direction according to the proportion of walls at each grid level. In this way the urban module is able to account for sinks of momentum due to horizontal and vertical building surfaces over the entire height of the urban canopy.

2.14
Chapter 2 : Description and testing of the models

Horizontal and vertical urban surfaces are treated separately as well for the purposes of heat-flux modification. As the temperature gradient between surface and air depends on the temperature difference between these two media, heat diffusion through the materials is calculated with a constant (user-defined) temperature at the lowest layer (soil temperature for canyon floors, building indoor temperature for roofs and walls).

For the purposes of accounting for shadowing and radiation trapping in the street canyon, view factors are computed for each urban grid layer while multiple reflections of the incident solar radiation and long-wave reemission between walls and canyon floors are considered at each urban grid level (Figure 2.2).
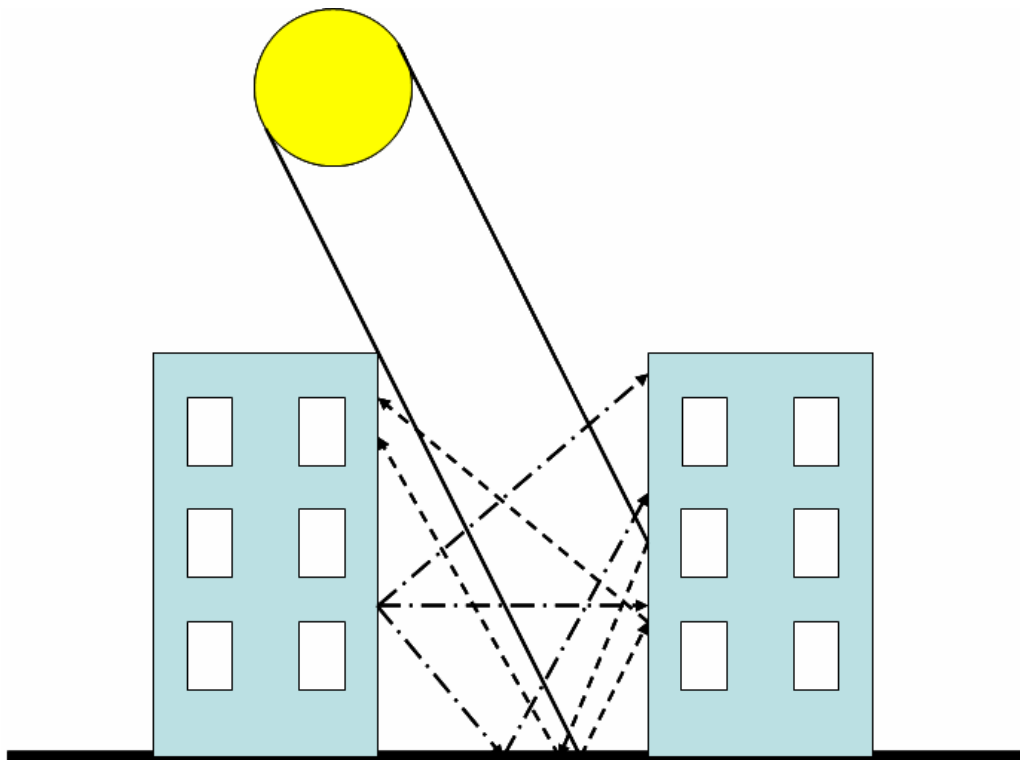

Figure 2.2. Schematic representation of the effects of radiation trapping in the urban module, including the directly incident solar radiation (solid lines), reflected solar radiation (dashed lines), and long-wave reemission from surfaces (dash-dotted lines).

In the computation of the urban terms, the fact must be taken into account that both the original air volume of a grid cell and the horizontal air interfaces separating two neighboring superposed cells are reduced by the presence of buildings. The D terms in the conservation equations (2.2) to (2.4) of the mesoscale model will therefore be equal to the sum of fluxes arising from horizontal and vertical urban surfaces (which are calculated by the urban module), divided by the volume of air of the grid cell (where the building volume is subtracted from the total cell volume):

$$D_I = \frac{F_I^H + F_I^V}{V_I} \tag{2.12}$$

where D_I is the "urban term" of each governing equation of the mesoscale model in the grid cell I, F_I^H and F_I^V are the horizontal (street and roof) and vertical (wall) flux, respectively, which are computed in the urban grid and interpolated in the mesoscale grid, and V_I is the volume of air in the urban grid cell (total volume less volume occupied by buildings).

Concerning the areas of the horizontal air interfaces between any two cells, their reduction due to the presence of buildings has an impact on vertical turbulent transport. As less air surface area is available for vertical exchange between two cells, the turbulent transport is modified as follows:

$$\frac{\partial \rho \overline{wA}}{\partial z} = \frac{1}{V_I} \left(\rho \overline{wA_i} S_i - \rho \overline{wA_{i+1}} S_{i+1} \right) \tag{2.13}$$

where S_i is the area of the air interface between the grid cells I and $I-1$ (total surface area less the surface area occupied by buildings), ρ is the air density, and $\overline{wA}$ is the vertical turbulent transport of a scalar A (temperature, wind speed, humidity, etc.).

2.2.4. Vegetation in urban zones

Vegetation areas present within urban zones (such as parks and gardens) are responsible for latent heat fluxes within these zones. It is very important to consider such vegetation areas in the

calculations, since in the urban module, dry soils are assumed by default. The model needs land-use data as input, in order to determine whether a cell is urban or rural, and, thus, to calculate the corresponding fluxes. A modification in the model has been developed in the frame of this work, in order to be able to consider mixed land-use within one cell. For a calculation of the associated heat fluxes, each cell at ground is defined in terms of an urban class, a rural class, and a ratio of rural to urban soil coverage. For the mixed cells containing both urban and rural soil coverage, fluxes are first calculated separately for the two types of surface (with urban parameterisation for the urban part, and through the soil module of the mesoscale model for the rural part), and are then weighted according to the percentages of each soil coverage type:

$$\Phi = \alpha \phi_{rur} + (1 - \alpha) \phi_{urb} \tag{2.14}$$

where Φ represents a meteorological variable or flux in the mesoscale model, α is the percentage of rural soil coverage in the cell, ϕ_{rur} is the rural contribution, and ϕ_{urb} is the urban contribution to the scalar or flux considered.

2.3. The Eulerian photochemical model

The Eulerian photochemical model selected for this work (Chapter 5), was TAPOM, the "Transport and Air POllution Model" developed jointly at the Air Pollution Laboratory of the Swiss Federal Institute of Technology in Lausanne and the Joint Research Centre in Ispra (Italy). It descretises the simulated domain into cells by the same principles as followed in the mesoscale atmospheric model described above, and solves the equations of transport and of the chemical mechanism in each cell. For the chemical mechanism, that of Stockwell *et al* (1997) called RACM was selected, which considers 76 chemical species linked via 236 reactions. This chemical mechanism has already been used and validated in several air quality studies over various cities using TAPOM (Athens: Martilli *et al*, 2003, Milano: Martilli *et al*, 2002, The Swiss Plateau:

Kuebler, 2001) or other photochemcial models (Grenoble: Couach *et al*, 2004). For the transport

solver, that of Collella and Woodward (1984) was selected in its corrected form for

multidimensional time-splitting applications (Clappier, 1998). The solar radiation module from

Madronich (1998), TUV, was used to calculate the photolysis rate constants for the chemical
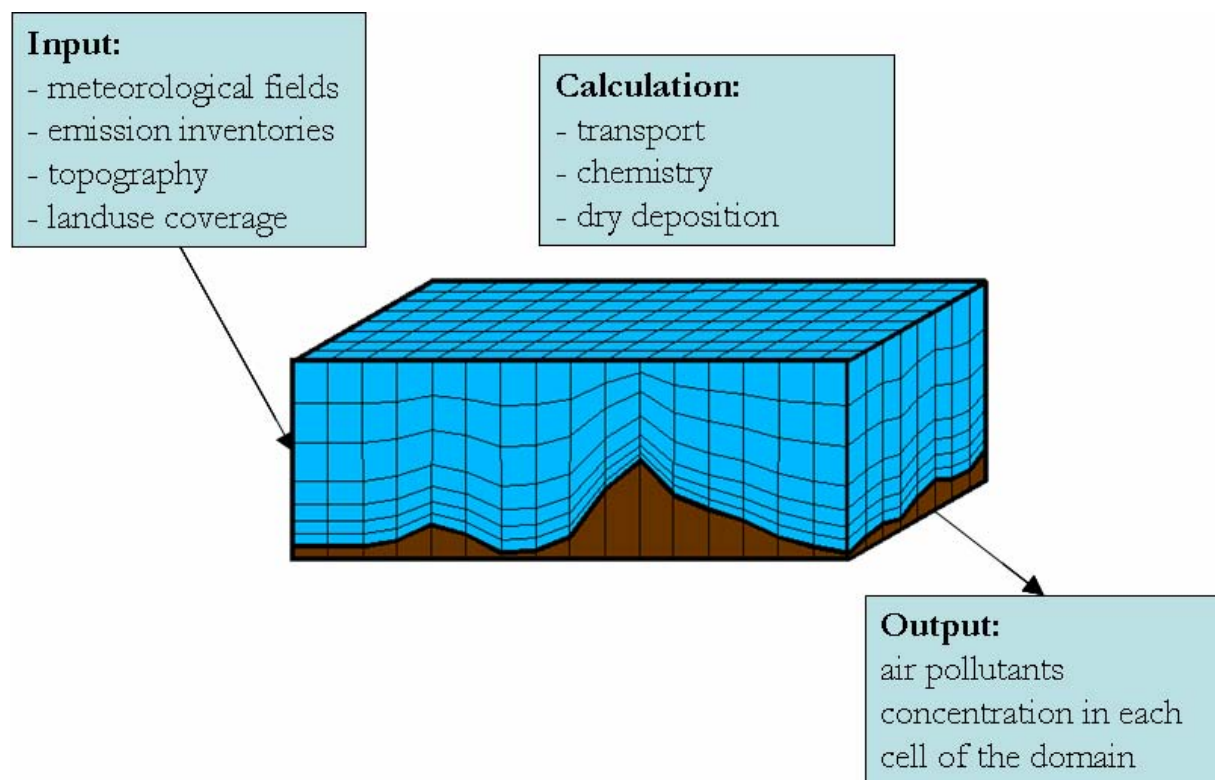
reactions.

Figure 2.3. Inputs and outputs of the Transport and Air POllution Model (TAPOM) used in this work (after Junier, 2004).

As inputs to TAPOM, meteorological flow fields (calculated by the mesoscale atmospheric

model), accurate emission inventories (in their distribution over time and space), topography and

land-use coverage are needed. As outputs, the air-pollutant mass balance in each cell of the

domain and at each discretised time step is calculated via Eq (2.15) (Figure 2.3; see Junier, 2004,

for a complete description of TAPOM).

$$\frac{\partial \rho C_s}{\partial t} + \vec{\nabla} \vec{u} \rho C_s = \vec{\nabla}\left(K \vec{\nabla} C_s \right) + v \frac{S * C_s}{V} + CH + EMI$$

$$\quad I \qquad\quad II \qquad\qquad III \qquad\quad IV \qquad V \qquad VI$$

$$(2.15)$$

where term *I* represents the mass balance derivative, with ρ being the air density and C_s being the mixing ratio of any species within the air, term *II* represents the advection by the mean wind *u*, term *III* accounts for diffusion, with *K* being the diffusion coefficient, term *IV* accounts for dry deposition, with *v* being the dry-deposition velocity, *S* being the horizontal cell surface area at ground, and *V* being the cell volume, term *V* represents is the chemical transformation of C_s, and term *VI* represents the emission contribution of C_s.

2.4. Sensitivity analysis

2.4.1. Introduction

One-dimensional test simulations with 50 % each of urban and rural coverage were performed in order to improve the understanding, determine the impact of each input parameter of the urban scheme as well as of the soil module, and validate these two parameterisations. The qualitative influence of each parameter on the results of the simulation was tested separately. It is important to keep in mind, therefore, that the influence of each urban and rural parameter will be weighted starting from the unchanged rural and urban flux calculation, respectively. The period of simulation lasted from 00 LT 25 June to 00 LT 28 June 2002.

2.4.2. Sensitivity to urban parameters

Each surface type (street, wall, roof) has specific materials properties. These are described in Table 2.1 for the standard setup (base-case simulation). The values selected here are those used originally for theoretical application (Martilli *et al*, 2002) and for the Athens case (Martilli *et al*, 2003). The other input parameters defined for the urban module are:

- two streets orientations: 45° and 135°,

- street and building width: 15 m for both,

- building-height distribution: 5 m, 5 % of the total; 10 m, 25 %; 15 m, 40 %; 20 m, 25 %; and

  25 m, 5 % of the total.

Table 2.1. Standard urban parameters for the 1D test simulations: thermal diffusivity K, heat capacity C_s, emissivity ε, albedo α, and roughness length z_0 (Martilli *et al*, 2002).

Surface	$K \, [10^6 m^2 s^{-1}]$	$C_s \, [MJm^{-3}K^{-1}]$	$\varepsilon \, [-]$	$\alpha \, [-]$	$z_0 \, [m]$
Street	0.286	1.4	0.95	0.2	0.01
Wall	0.67	1.0	0.90	0.2	0.01
Roof	0.67	1.0	0.90	0.2	-

The thermal diffusivity

The first parameter to be tested is the thermal diffusivity. This parameter has an impact on the material's temperature, and hence on the temperature at the air/material interface.
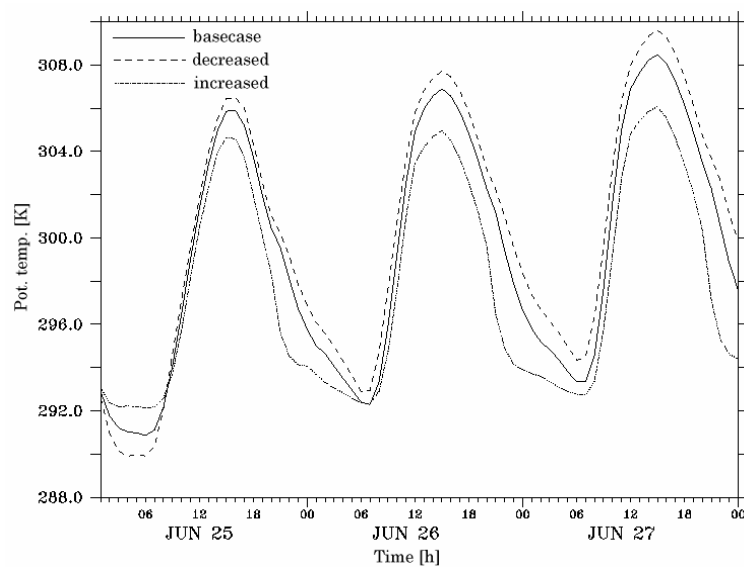

Figure 2.4. The potential temperature at 2.5 m above ground as a function of time from 01 LT 25 June to 00 LT 28 June for the base-case simulation (solid line), for K_{wall} lowered by a factor of 10 (dashed line), and for K_{wall} raised by a factor of 10 (dash-dotted line).

Increasing the thermal diffusivity should result in a decrease of the material's temperature, and *vice versa*. For wall surfaces, a decrease of thermal diffusivity by a factor 10 produces an increase in the potential temperature near the ground (i.e., in the street canyon) of the order of 0.5 to 1.0 K (Figure 2.4). Increasing K_{wall} by the same factor results in a strong temperature decrease close to ground, especially during daytime.

Changes in K_{roof} by the same factor have a similar qualitative impact on the temperature as the changes in K_{wall}, but the differences relative to the base-case simulation are smaller (Figure 2.5). This is to be expected, since the impact of roof surfaces should appear above roof level. It is interesting to note, however, that changes in the thermal characteristics of roofs actually do influence the meteorological parameters within the street canyon, that is, below roof level.
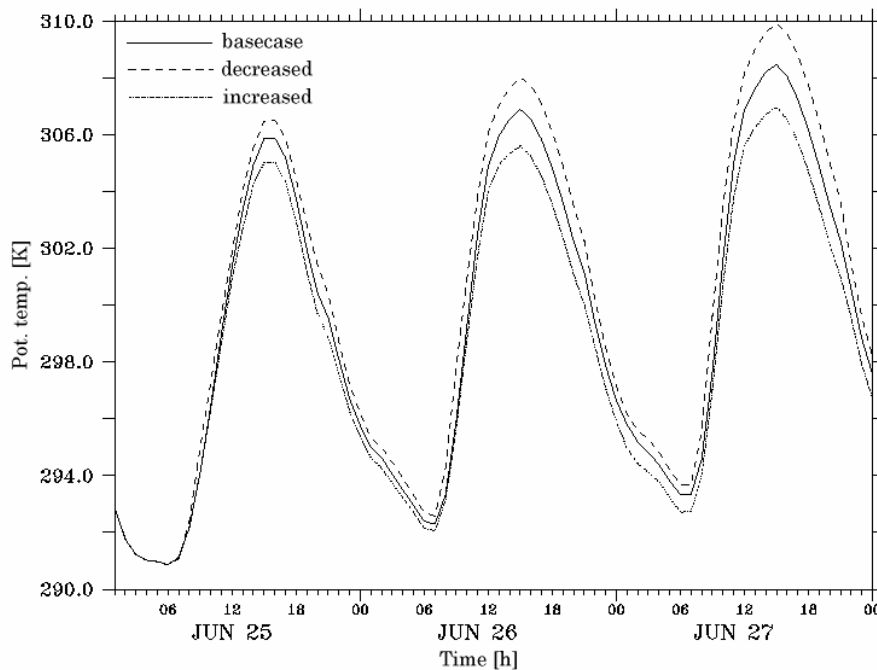

Figure 2.5. The potential temperature at 2.5 m above ground as a function of time from 01 LT 25 June to 00 LT 28 June for the base-case simulation (solid line), for K_{roof} lowered by a factor of 10 (dashed line), and for K_{roof} raised by a factor of 10 (dash-dotted line).

Changes in thermal diffusivity of the street material (K_{street}) produce a time-dependent impact, as the reactions of the model to an increase or decrease of this parameter will vary with the time of day (Figure 2.6). A decrease in thermal diffusivity by a factor of 10 results in an increase of temperature in the street canyon during daytime, and a decrease during nighttime (the daily minimum drops by 1 K, and the daily maximum rises by 1 K). An increase of K_{street} by a factor of 10 produces exactly the opposite (the daily minimum rises by 1 K, and the daily maximum drops by 1 K). In other words, the amplitude of the daily temperature cycle increases (decreases) as the thermal diffusivity decreases (increases).
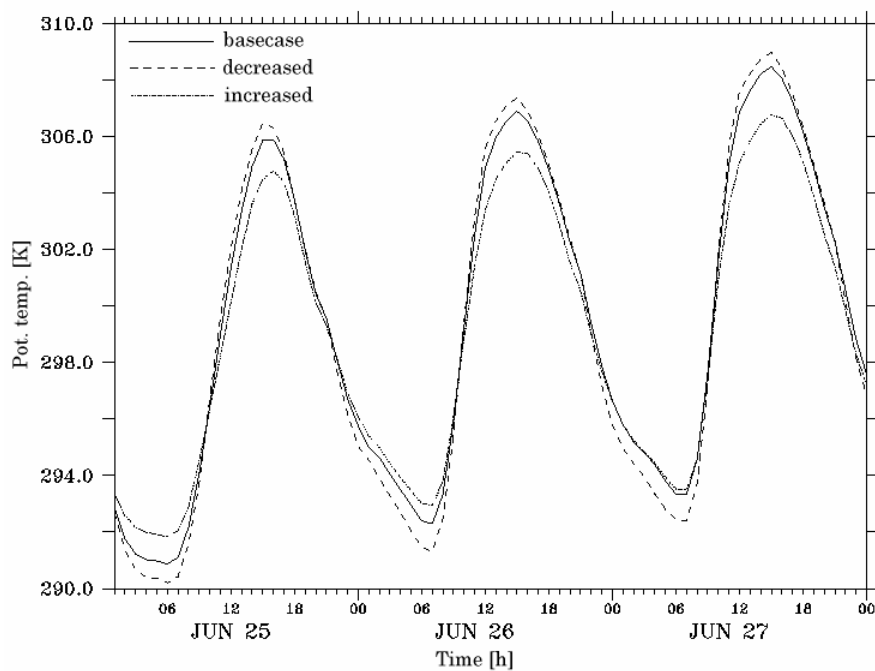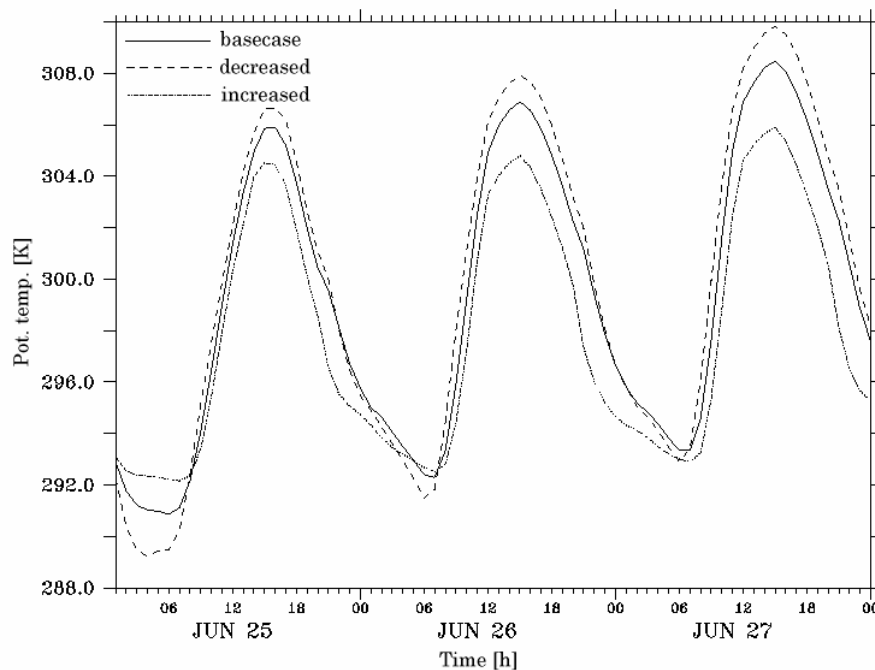

Figure 2.6. The potential temperature at 2.5 m above ground as a function of time from 01 LT 25 June to 00 LT 28 June for the base-case simulation (solid line), for K_{street} lowered by a factor of 10 (dashed line), and for K_{street} raised by a factor of 10 (dash-dotted line).

The heat capacity

Changes in heat capacity (C_s) of the material will have an impact on the temperature in the material, and thus again on air temperature near the surface. For wall surfaces, an increase in heat capacity results in a decrease of air temperature, which is particularly noticeably in the afternoon (Figure 2.7). An interesting feature of this parameter change is that appearing during the last few hours before sunrise, where both increasing and decreasing C_{wall} results in a decrease of air temperature.

Figure 2.7. The potential temperature at 2.5 m above ground as a function of time from 01 LT 25 June to 00 LT 28 June for the base-case simulation (solid line), for C_{wall} lowerd by a factor of 10 (dashed line), and for C_{wall} raised by a factor of 10 (dash-dotted line).

Higher roof heat capacities will lead to a lower air temperature in the street canyon throughout the 24-h day, and *vice versa*, with a maximum impact occurring during daytime (Figure 2.8).
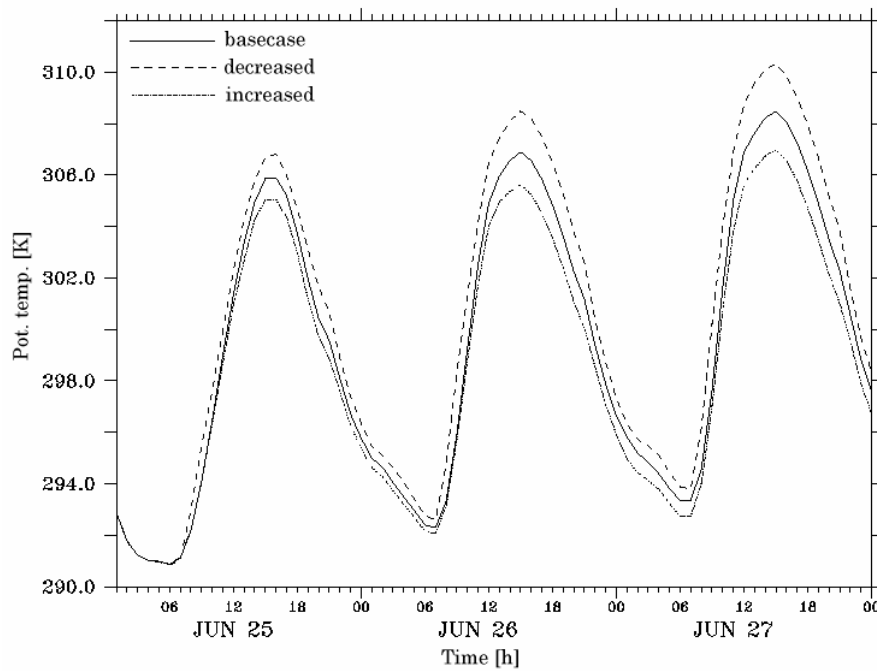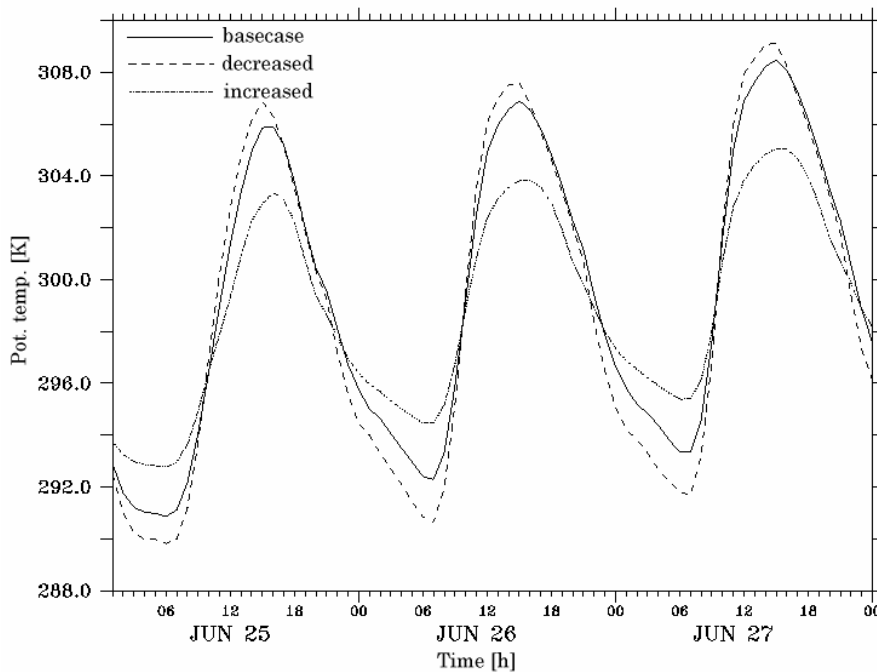
Figure 2.8. The potential temperature at 2.5 m above ground as a function of time from 01 LT 25 June to 00 LT 28 June for the base-case simulation (solid line), for C_{roof} lowered by a factor of 10 (dashed line), and for C_{roof} raised by a factor of 10 (dash-dotted line).

Figure 2.9. The potential temperature at 2.5 m above ground as a function of time from 01 LT 25 June to 00 LT 28 June for the base-case simulation (solid line), for C_{street} lowered by a factor of 10 (dashed line), and for C_{street} raised by a factor of 10 (dash-dotted line).

Changes in C_{street}, by the same factor as tested for the other surfaces produce more important effects on air temperature close to the ground (Figure 2.9). Just as found for the changes in K_{street}, changes in C_{street} produce, not merely an increase or decrease of temperature, but the effect is time-dependant. For lower values of this parameter, the amplitude of the daily temperature cycle is reduced, and *vice versa.*

One can see from the above sensitivity tests that the choice of thermal properties of the materials represented by the thermal diffusivity and the heat capacity in the urban module, have an impact on air temperature in the street canyon, and hence on the heat budget available for turbulence generation. The impact on the daily temperature maxima appears to be cumulative from one day to the next, as the differences relative to the base-case maximum increase each day. The factors of change in K and C used in the sensitivity analysis (that is, an increase or decrease by a factor of 10 in each parameter) were arbitrary chosen, but they are not unrealistic, as can be seen from a summary of the parameter values used in different studies (Table 2.2).

Table 2.2. Values of the thermal properties used in different studies: thermal conductivity λ, heat capacity C, and thermal diffusivity K. The columns contain all the values for each parameter and each surface element collected from the sources (Martilli *et al*, 2002, Masson *et al*, 2002, Dupont, 2004).

	λ [W m^{-1} K^{-1}]			C [MJ m^{-3} K^{-1}]			K [10^{-6}m^2 s^{-1}]		
	Wall	*Roof*	*Street*	*Wall*	*Roof*	*Street*	*Wall*	*Roof*	*Street*
Martilli									
Concrete	0.67	0.67	0.4	1.0	1.0	1.4	0.67	0.67	0.286
Masson, Mexico City									
Asphalt roll		0.2			1.7			0.118	
Concrete (stone)		0.93			1.5			0.62	
Insulation		0.03			0.25			0.12	
Gypsum		0.16			0.87			0.184	
Stone/window	0.88			1.54			0.571		
Insulation/window	0.21			0.32			0.656		
Asphalt/concrete			0.82			1.74			0.471
Stone aggregate			2.1			2.0			1.05
Gravel and soil			0.4			1.4			0.286
Masson, Vancouver									
Gravel		1.4			1.76			0.795	
Insulation		0.03			0.04			0.75	
Concrete		1.51			2.21			0.683	
Dense concrete	1.51			2.11			0.716		
Concrete	0.67			1.0			0.67		
Asphalt/concrete			0.82			1.74			0.471
Stone aggregate			2.1			2.0			1.05
Gravel and soil			0.4			1.4			0.286
Dupont, Philadelphia									
Ceramic tile (city centre)		1.75			2.43			0.72	
Slate tile (residential)		0.84			1.77			0.475	
Sheet metal (indust.-comm.)		53.3			3.9			13.667	
Concrete (high building)		0.8			1.17			0.684	
Concrete				1.17					
Asphalt			0.75			1.94			0.387

The building indoor temperature

Another parameter that must be set by the user in the urban module is the indoor temperature of the buildings. The module calculates temperature changes across the wall with a diffusion equation. Lower indoor temperatures therefore result in lower temperatures at the wall/air interface, and *vice versa* (Figure 2.10).
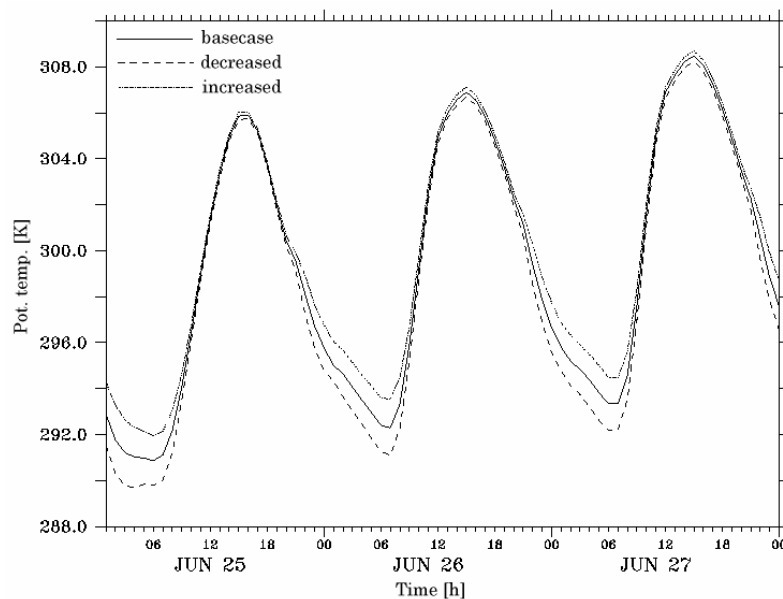

Figure 2.10. The potential temperature at 2.5 m above ground as a function of time from 01 LT 25 June to 00 LT 28 June for the base-case simulation (solid line), for a temperature inside the buildings that is 3 °C lower (dashed line), and for a temperature inside the buildings that is 3 °C higher (dash-dotted line).

The changes in indoor temperature of the buildings have a perceptible impact on air temperature in the street canyon, only when there is no solar radiation input. During daytime, heating of the wall by incoming solar radiation swamps the impact of indoor temperature.

The geometrical parameters of the buildings

It will also be of interest to evaluate the impacts of the geometric parameters (width of buildings and street and the distribution of building heights) used to describe an urban area in the module. The most important airflow effects produced by the presence of buildings are:

- drag induced by obstacles (buildings), which produces a loss of momentum in the street

    canyon,

- enhanced transformation of mean kinetic energy into turbulent kinetic energy, and

- shadowing and radiation trapping, which modify the heat fluxes.

Changes in the geometrical parameters will, therefore, have an impact on heat-related variables (potential temperature, heat flux) as well as on momentum variables (wind, turbulent vertical momentum transport). Tall buildings will favour the formation of channelled flows within the street canyon. As a result, they induce a vertically well mixed air situation in the canyon during nighttime which is due to homogenous conditions of the flows in the canyon. This tends to produce constant vertical profiles of the meteorological parameters within the canyon. Relatively low buildings, of no more than 10 m for instance, are not tall enough to induce such processes, which can be seen from Figure 2.11 where a simulation with 100 % of the buildings reaching 10 m is tested against a simulation with a uniform height of 40 m.
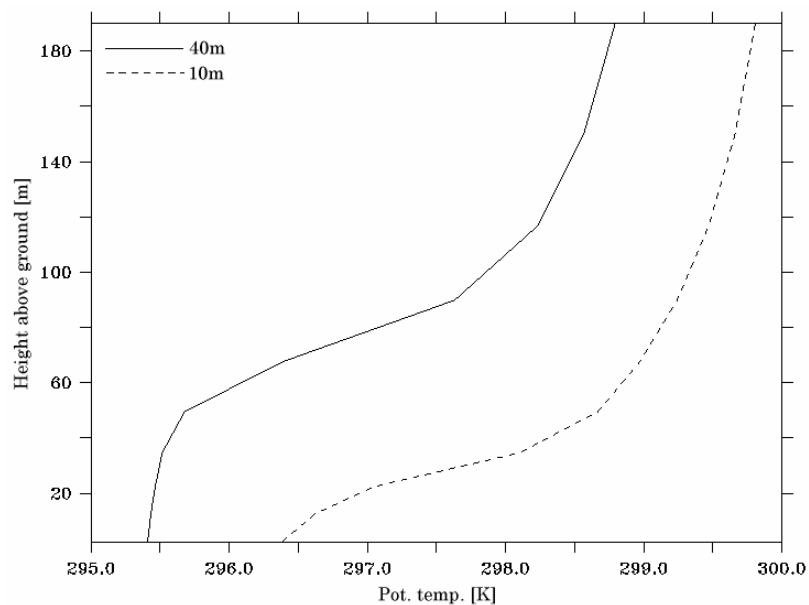

Figure 2.11. Vertical distribution of potential temperature at 00 LT 26 June for uniform building heights of 40 m (solid line) and of 10 m (dashed line).

Turbulent flux variables are also influenced by building height, as can be seen from Figure 2.12 showing a profile of the vertical turbulent kinematic heat flux ($w'\theta'$) over the first 150 m above ground during nighttime, when the maximum value appears at roof height (see the discussion in Chapter 3).
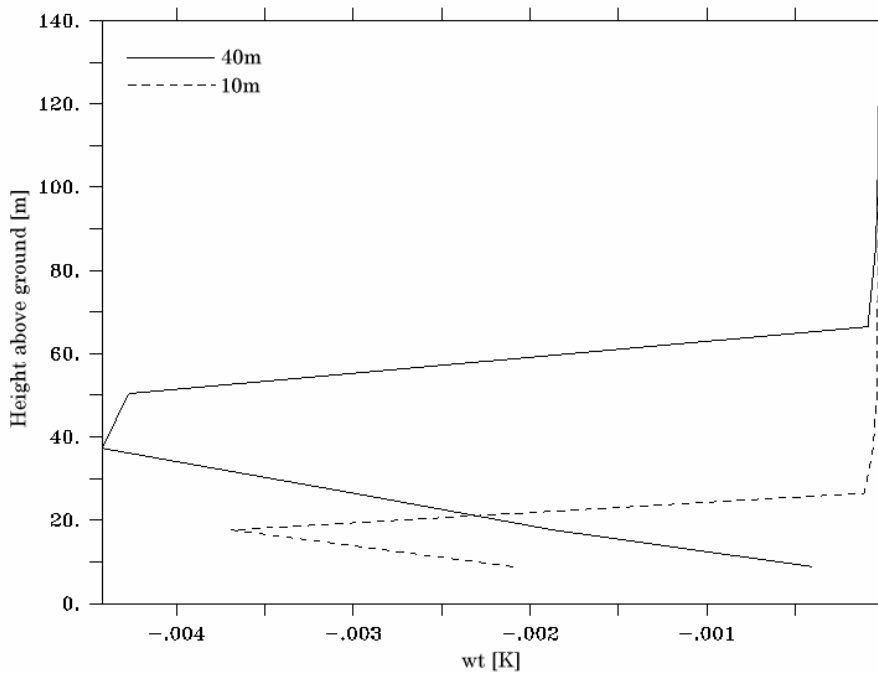

Figure 2.12. Vertical distribution of the vertical turbulent kinematic heat fluxes ($w'\theta'$) at 00 LT 26 June for uniform building heights of 40 m (solid line) and of 10 m (dashed line). No value calculated at ground.

The buildings induce formation of a boundary layer due to shear with a rigid surface at roof height. Hence, the tops of the buildings act as a displaced surface, and the associated logarithmic wind profile appears above the urban canopy (Figure 2.13), just as it would appear directly above ground for a flat homogenous rural surface. In the traditional method of accounting for urban areas in the mesoscale model that was described in Section 2.2, this shift of the roughness surface is accounted for by setting a displacement height equal to the mean building height.
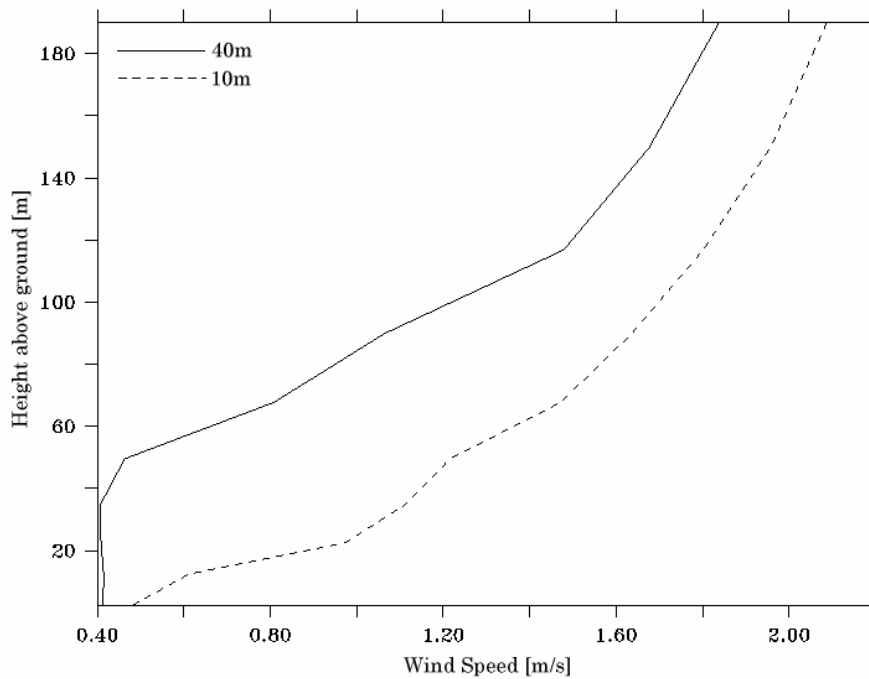
Figure 2.13. Vertical distribution of the wind speeds at 00 LT 26 June for uniform building heights of 40 m (solid line) and of 10 m (dashed line).

The width of the street is important for the size of eddies generated in the street canyon and, hence, for the total amount of turbulent energy production. Simulations were carried out by varying the widths of streets and buildings. Results for the Turbulent Kinetic Energy (TKE) at its maximum (in the afternoon, when the Planetary Boundary Layer is most developed) are shown in Figure 2.14. The production of turbulent energy above the urban canopy is larger for a wide street canyon (*eg*, of 25 m) up to the top of the boundary layer (where TKE falls to zero, which is at about 2500 m in Figure 2.14), no matter what the width of the buildings (the solid and double dash-dotted line are identical), while for narrow streets (*eg*, of 5 m), the building width appears to be important for the amount of turbulent energy production (compare the dashed and dash-dotted line).
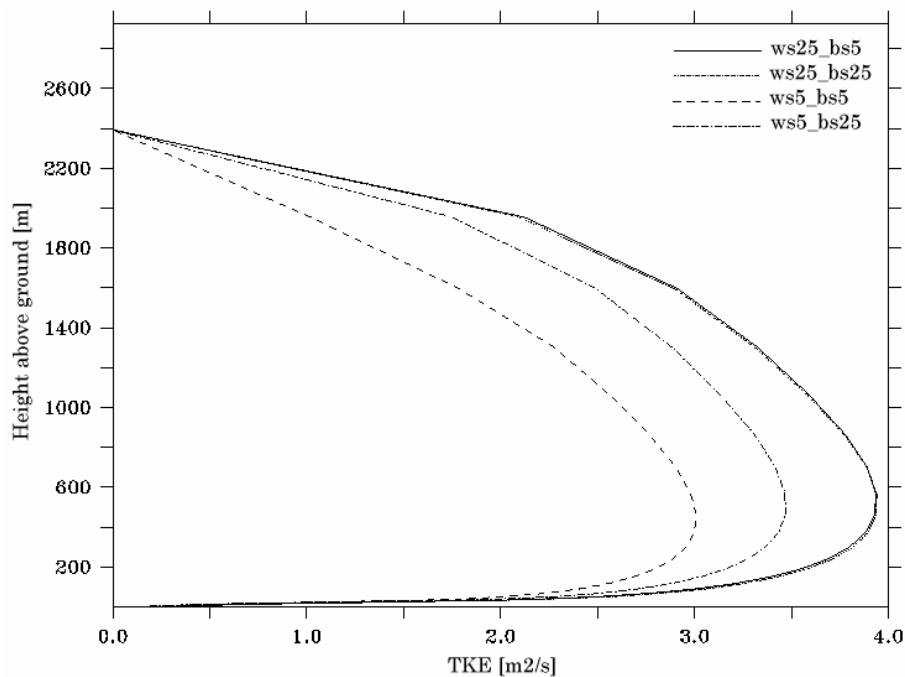
Figure 2.14. Vertical distribution of the turbulent kinetic energy at 15 LT 26 June for the following combinations of the widths of streets and buildings: streets of 25 m and buildings of 5 m (solid line), streets and buildings of 25 m each (double dash-dotted line), streets and buildings of 5 m each (dashed line), and streets of 5 m and buildings of 25 m (dash-dotted line).

Further tests were performed by applying changes within a reasonable range to the remaining parameters (initial temperature of ground and roof, as well as albedo, emissivity, and roughness length for the three surface types), but these changes did not produce any significant impact on the results of the model.

The results and figures presented above are not intended to be exhaustive, but rather to illustrate the impacts of various urban parameters on the values calculated with the mesoscale model. They serve to enhance our understanding of urban parameterisation and of the importance potentially assumed by each parameter of the module. A validation by comparison with measurements is presented in Chapter 3.

2.4.3. Sensitivity to soil parameters

The standard set of soil module parameters for the test simulation is reproduced in Table 2.3. The values selected here for the standard (base-case) simulation are those of Martilli *et al* (2002) used for theoretical application and for the Athens case (Martilli *et al*, 2003). They correspond to a sandy-clay-loam soil according to the USDA (United States Department of Agriculture) Textural classes (Tremback and Kessler, 1985).

Table 2.3. Standard rural parameters for the one-dimensional test simulations: Constant b (depends on soil type), soil moisture η_f at saturation, hydraulic conductivity K_f for a soil at saturation, the initial-to-saturation soil moisture ratio η/η_f, moisture potential ψ_f for a soil at saturation, and specific heat C_d of the dry soil (Martilli *et al*, 2002).

Soil type	b [-]	η_f [$cm^3 cm^{-3}$]	K_f [$cm^2 s^{-2}$]	η/η_f [-]	ψ_f [m]	C_d [$Jm^{-3}K^{-1}$]
Sandy clay loam	7.12	0.42	6.3E-6	0.55	2.99	1.177E6

All parameters listed in Table 2.3 are needed to solve the soil module. For the purposes of model input, the user has to choose among twelve predefined rural classes (the possibility of defining new classes is also available), each of them with specific parameter values for the resolution of the soil module. This allows users to tune the rural parameters so that they will fit the local characteristics. Below, each parameter is tested within a range of possible values covering all twelve predefined classes.

Constant b varies with soil type from 4 (sand) to 10 (sandy clay). When the two extremes were tested against the base-case simulation (b = 7.12), a large impact on air temperature near ground during daytime was observed (Figure 2.15). The daily temperature maximum is lowered by 3 to 4 K when b is lowered from 7.12 to 4. Note that here, both the urban and the rural fluxes are calculated and then weighted by giving them equal importance in the cell, which means that the impact produced by the soil module parameters alone is attenuated by the unchanged urban part.
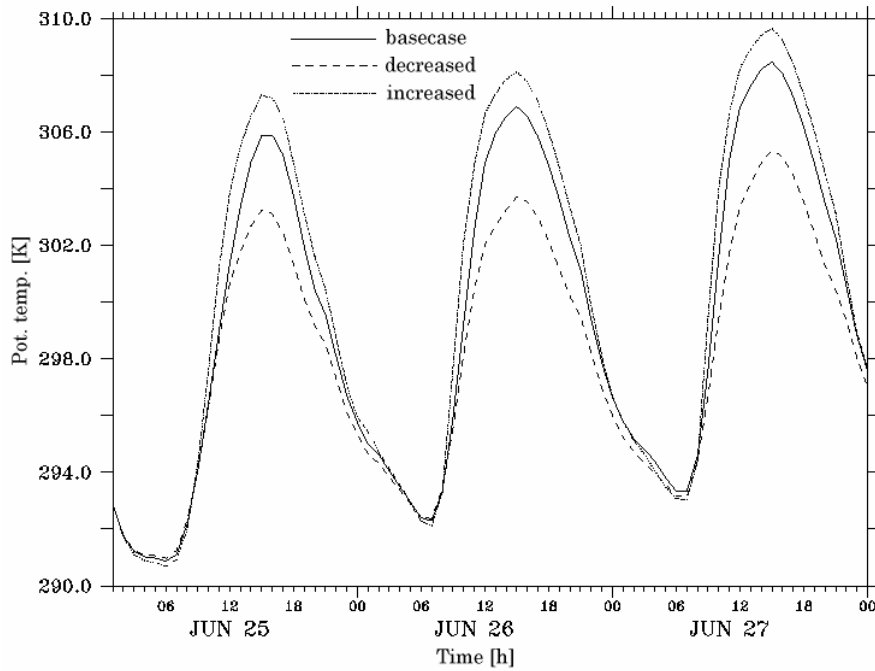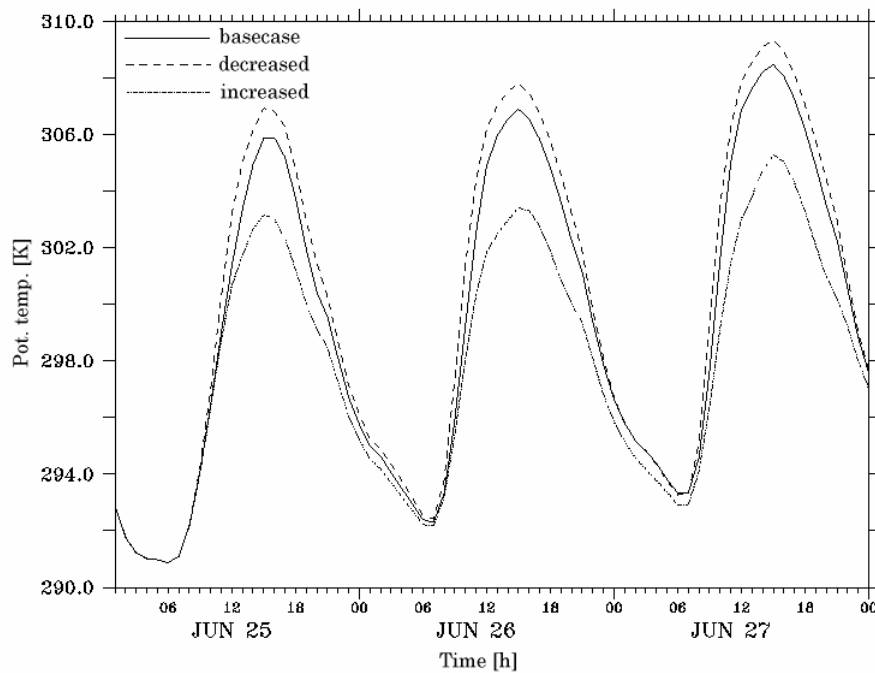
Figure 2.15. The potential temperature at 2.5 m above ground as a function of time from 01 LT 25 June to 00 LT 28 June for the base-case simulation with $b = 7.12$ (solid line), for constant b lowered to a value of 4 (dashed line), and for constant b raised to a value of 10 (dash-dotted line).

The constants b and K_f are linked via Eq (2.16) taken from Tremback and Kessler, which calculates the hydraulic conductivity (K_η). Because of Eq. 2.16, changes in K_f should act in a direction opposite to that of changes in b at constant K_η.

$$K_\eta = K_f \left(\frac{\eta}{\eta_f} \right)^{2b+3}$$
                                                                                      (2.16)

The calculations show that air temperature near ground is indeed increased when K_f is decreased, and *vice versa* (Figure 2.16), and this again only during daytime, as in Figure 2.15 for change in b.

Figure 2.16. The potential temperature at 2.5 m above ground as a function of time from 01 LT 25 June to 00 LT 28 June for the base-case simulation (solid line), for a hydraulic conductivity of the soil at saturation (K_f) lowered by a factor of 10 (dashed line), and for K_f raised by a factor of 10 (dash-dotted line).

Soil moisture at saturation (η_f) has a very low impact on surface temperature (Figure 2.17), as it is a parameter describing a state (saturation) not necessarily reached in the standard case simulated. Moreover, it varies very little between soil types (between 0.39 cm³cm⁻³ for sand and 0.47 cm³cm⁻³ for clay loam). On the other hand, the ratio of initial soil moisture to soil moisture at saturation (η/η_f) has a much stronger effect on air surface temperature (Figure 2.18). One simulation each was carried out with ratios of 0.8 (initially very wet soil type) and 0.3 (initially dry soil type).
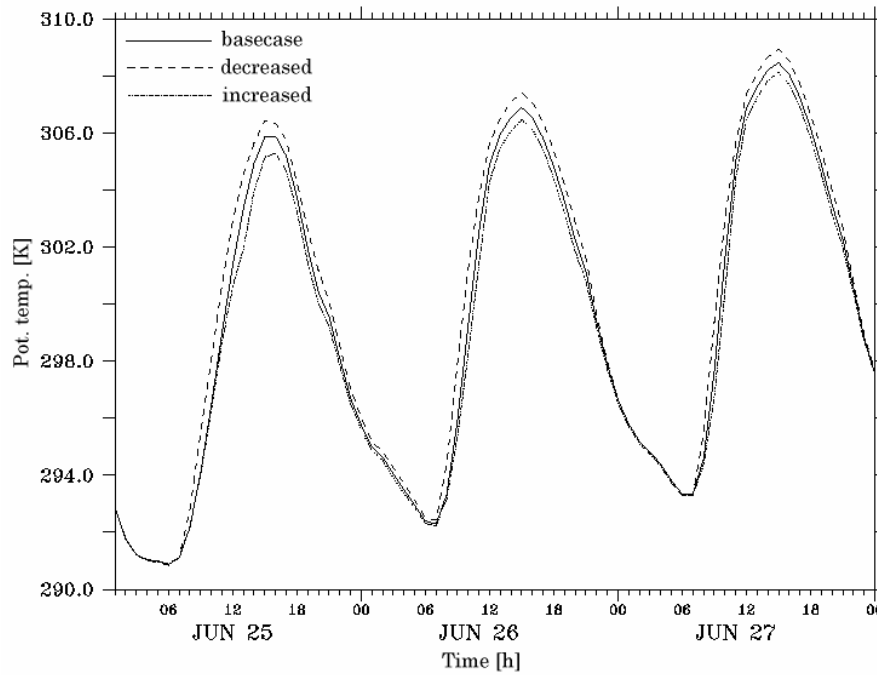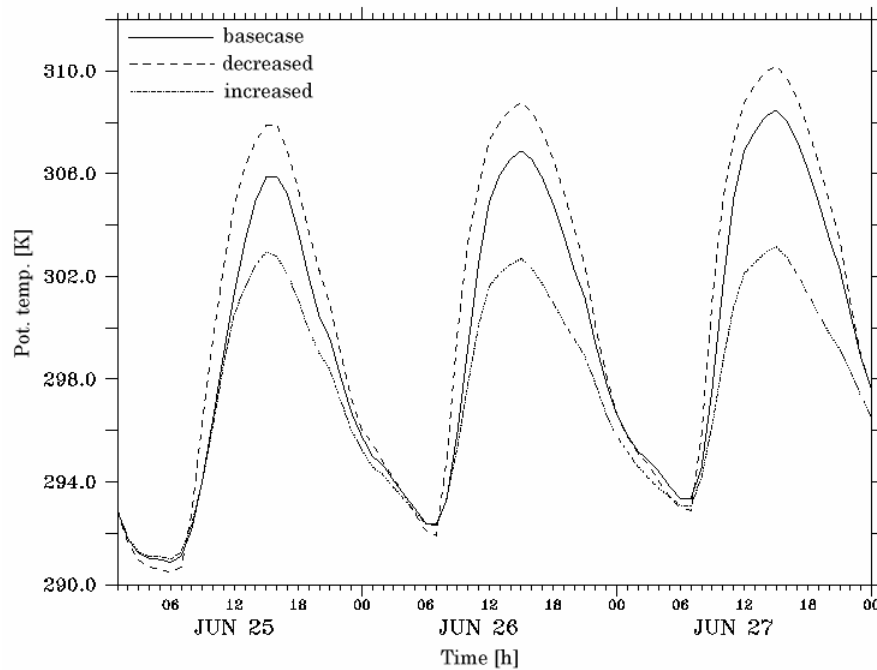
Figure 2.17. The potential temperature at 2.5 m above ground as a function of time from 01 LT 25 June to 00 LT 28 June for the base-case simulation (solid line), a soil moisture at saturation (η_l) lowered by a factor of 2 (dashed line), and a soil moisture at saturation (η_l) raised by a factor of 1.5 (dash-dotted line).

Figure 2.18. The potential temperature at 2.5 m above ground as a function of time from 01 LT 25 June to 00 LT 28 June for the base-case simulation (solid line), a ratio of initial soil moisture to soil moisture at saturation (η/η_l) lowered to a value of 0.3 (dashed line), and a ratio of initial soil moisture to soil moisture at saturation (η/η_l) raised to a value of 0.8 (dash-dotted line).

Tests involving changes within the range of plausible values of specific heat (C_d) and moisture potential at saturation (ψ_j), both needed as well as inputs for the soil module, revealed no significant impacts on air surface temperature.

2.5. Conclusions

The modelling tools used in this work were presented and described. Firstly, the mesoscale meteorological model was introduced, with its governing equations and the different calculation modules included in the model (soil module, turbulence, forcing, etc.). Secondly, the new urban parameterisation scheme was presented, and the main differences with a traditional urban parameterisation were mentioned. Finally, the main features of TAPOM, the Eulerian photochemical model used for the air quality modelling in Chapter 5, were presented.

In a second part, a sensitivity analysis was performed on input parameters to the urban scheme and to the soil module. It revealed how the mesoscale meteorological model reacts to changes in some of these parameters.

Variations in the thermal characteristics of the materials were found to have impacts on air temperature in the street canyon during day and during nighttime. Two different types of impact could be defined: on one hand parameters producing a relatively constant increase (or decrease) in temperature by a decrease (or increase) of the thermal parameter (eg, of K_{wall}), and on the other hand parameters producing a variation in the amplitude of the daily temperature cycle (eg, K_{street}).

Building indoor temperature changes lead to perceptible effects on air temperature, only during nighttime, as solar radiation heating of the walls is determining during daytime. In tests involving

changes in street shape, changes in the vertical temperature and kinematic heat flux profiles within and above the urban canopy could be revealed.

Tests involving changes in the soil module parameters revealed impacts on air temperature that were limited to daytime, if there were any impacts at all.

This sensitivity analysis provides a better understanding of the two parts of the mesoscale model. The reactions of the model to parameter changes are consistent with expectations from the physical properties of building materials (*eg*, an increase in thermal diffusivity will result in a decrease of temperature of the materials). The relative impacts produced by each parameter could be assessed. This is a major prerequisite for any fine tuning of input parameters that would be required in order to fit the model to *in-situ* conditions and measurements, as in Chapters 3, 4, and 5, where the model is run under real one- and three-dimensional conditions.

References

Bartzis, J. G., Venetzanos, A., Varvayanni, M., Catzaros, N. and Megaritou, A.: 1991, 'ADREA-I A transient three dimensional transport code for complex terrain and other applications', *Nuclear Technology,* **94**, 135-148

Brown, M.: 2000, 'Urban parameterisations for mesoscale meteorological models', in Z. Boybeyi (ed.), *Mesoscale Atmospheric Dispersion*, Wessex Press, 448 pp

Ca, V., Asaeda, T. and Ashie, Y.: 1999, 'Development of a numerical model for the evaluation of the urban thermal environment', *J. Wind. Eng. Ind. Aerodyn.* **81**, 181-196

Collella, P. and Woodward, P.: 1984, 'The Piecewise Parabolic Method (PPM) for gas dynamical simulations', *J. Comp. Phys.* **54**, 174-201

Clappier, A., Perrochet, P., Martilli, A., Muller, F. and Krueger, B. C.: 1996, 'A new non-hydrostatic mesoscale model using a CVFE (Control Volume Finite Element) discretisation technique', in P. M. Borell *et al* (eds.), *Proceedings, EUROTRAC Symposium '96*, Computational Mechanics Publications, Southampton, pp. 527-531

Clappier, A.: 1998, 'A correction method for use in multidimensional time-splitting advection algorithms: Application to two- and three-dimensional transport', *Month. Weath. Rev.* **126**, 232-242

Couach, O., Kirchner, F., Jimenez, R., Balin, I., Perego, S. and van den Bergh, H.: 2004, 'A development of ozone abatment strategies for the Grenoble area using modeling and indicators', *Atmos. Environ.* **38**, 1425-1436

Dupont, S, Otte, T. L. and Ching, J. K. S.: 2004, 'Simulation of meteorological fields within and above urban and rural canopies with a mesoscale model (MM5)', *Boundary-Layer Meteorol.,* in press

Fast, J.D.: 1995, 'Mesoscale modeling and Four-Dimensional Data Assimilation in areas of highly complex terrain', *J. Applied. Meteorol.* **34**, 2762-2782

Flassak, Th.: 1988, *Ein nichthydrostatisches mesoskaliges Modell der planetaren Grenzschicht*, PhD Thesis (in German), University of Karlsruhe

Grell, G. A., Duhia, J. and Stauffer, D. R.: 1994, 'A description of the 5th generation of the Penn State/NCAR mesoscale model', *NCAR Technical Note TN 398+STR*

Grimmond, C. S. B. and Oke, T. R.: 1995, 'Comparison of heat fluxes from summertime observations of four North American cities', *J. of Applied Meteorol.* **34**, 873-889

Grimmond, C. S. B. and Oke, T. R.: 2002, 'Turbulent heat fluxes in urban areas: Observations and a local-scale urban meteorological parameterisation scheme (LUMPS)', *J. of Applied Meteorol.* **41**, 792-810

Kastner-Klein, Fedorovich, P. E. and Rotach, M. W.: 2001, 'A wind tunnel study of organized and turbulent air motions in urban street canyons', *J. Wind Engineering Industrial Aerodynamics* **89**, 849-861

Junier M.: 2004, *Gas phase chemistry mechanisms for air quality modelling: generation and application to case studies*, EPFL Thesis n° 2936

Kuebler, J.: 2001, *Integrated assessment of photochemical air pollution control strategies: method development and application to the Swiss Plateau*, EPFL Thesis n° 2412

Louis, J.-F.: 1979, 'A parametric model of vertical eddy fluxes in the atmosphere', *Boundary-Layer Meteorol.* **17**, 187-202

Martilli, A., Clappier, A. and Rotach, M. W.: 2002, 'An urban surface exchange parameterisation for mesoscale models', *Boundary-Layer Meteorol.* **104**, 261-304

Martilli, A., Roulet, Y.-A., Junier, M., Kirchner, F., Rotach, M. W. and Clappier, A.: 2003, 'On the impact of urban exchange parameterisations on air quality simulations: the Athens case', *Atmos. Environ.* **37**, 4217-4231

Martilli, A., Neftel, A., Favaro, G., Kirchner, F., Sillman, S. and Clappier, A.: 2002, 'Simulation of the ozone formation in the northern part of the Po Valley', *J. Geophys. Res.* **107**(D22), 8195

Maruyama, T.: 1999, 'Surface and inlet boundary conditions for the simulation of turbulent boundary layer over complex rough surface', *J. Wind. Eng. Ind. Aerodyn.* **81**, 311-322

Masson, V.: 2000, 'A physically-based scheme for the urban energy budget in atmospheric models', *Boundary-Layer Meteorol.* **94**, 357-397

Masson, V., Grimmond, C. S. B. and Oke, T. R.: 2002, 'Evaluation of the Town Energy Balance (TEB) scheme with direct measurements from dry districts in two cities', *J. Applied Meteorol.* **41**, 1011-1026

Oke, T. R.: 1988, 'The urban energy balance', *Prog. Phys. Geogr.* **12**, 471-508

Oke, T. R., Sponken-Smith, R., Jauregui, E., Grimmond, C. S. B. and Tejada, A.: 1999, 'The energy balance of central Mexico City during the dry season', *Atmos. Env.* **33**, 3919-3930

Oikawa, S. and Meng, Y.: 1995. 'Turbulence characteristics and organized motion in a suburban roughness sublayer', *Boundary-Layer Meteorol.* **74**, 289-312

Perego, S.: 1999, 'A numerical mesoscale model for simulation of regional photosmog in complex terrain: model description and application during POLLUMET 1993 (Switzerland)', *Meteor. Atmos. Phys.* **70**, 43-69.

Pielke, R. A., Cotton, W. R., Walko, R. L., Tremback, C. J., Lyons, W. A., Grasso, L. D., Nicholls, M. E., Moran, M. D., Wesley, D. A., Lee, T. J. and Copeland, J. H.: 1992, 'A comprehensive mesoscale modeling system - RAMS', *Meteorology and Atmospheric Physics* **49**, 69-91

Rotach, M. W.: 1993, 'Turbulence close to a rough urban surface, part I: variances and gradients', *Boundary-Layer Meteorol.* **66**, 75-92

Rotach, M. W.: 2001, 'Urban scale dispersion using lagrangian stochastic dispersion model', *Boundary-Layer Meteorol.* **99**, 379-410

Rotach, M. W.: 2002, 'Overview on the Basel Urban Boundary Layer Experiment – BUBBLE', *Proceedings, AMS 4th Symposium on the Urban Environment*, Norfolk VA., 25-26

Roth, M. and Oke, T. R.: 1993, 'Turbulent transfer Relationships over an Urban Surface I: Spectral characteristics', *Quart. J. Roy Meteorol. Soc.* **119**, 1071-1104

Sorbjan, Z. and Uliasz, M.: 1982, 'Some numerical urban boundary-layer studies', *Boundary-Layer Meteorol.* **22**, 481-502

Stull, R. B.: 1988, *An introduction to boundary layer meteorology*, Kluwer Academic Publishers, 670pp

Thunis, P.: 1994, *Formulation and evaluation of a non-hydrostatic vorticity-mode mesoscale model*, Ph. D. Thesis, Catholic University of Leuven, Belgium

Tremback, C. J. and Kessler, R.: 1985, 'A surface temperature and moisture parameterisation for use in mesoscale numerical models', in *Proceedings of the 7th Conference on Numerical Weather Prediction*, June 17-20, Montreal, Quebec, Canada

Williams, M., Brown, M., Cruz, X., Sosa, G. and Streit, G.: 1995, 'Development and testing of meteorology and air dispersion models for Mexico City', *Atmos. Env.* **29**, 2929-2960

Chapter 3

Validation of the urban parameterisation in one-dimensional simulations

Abstract

The detailed urban parameterisation scheme described in Chapter 2 was used for calculations concerning the air space within and above a street canyon. For a validation of this new scheme, the model was run off-line on a vertical column (one-dimensional simulations) using data from measurements made on top of a 30-m tower as the upper boundary conditions. The data were obtained during the Intensive Observation Period (IOP) of the Basel UrBan Boundary Layer Experiment (BUBBLE). The vertical profiles of meteorological variables were simulated in the street canyon. The parameterisation was validated with data obtained from the tower in the street canyon and directly above roof height. The results of the simulations show that the urban parameterisation scheme is able to capture most of the processes close to ground typically induced by an urban surface. Relative to a model using the traditional approach for urban parameterisation (by a variation of z_0 in order to account for the presence of a city), the current scheme provides improved fitting of measured profiles.

3.1. Introduction

Impacts of a city on the structure of the Planetary Boundary Layer (PBL) which arise from its characteristic surface roughness and thermal exchange must be treated separately in the modelling processes, according to what was explained in Chapter 2. The buildings present in the city induce modifications in the thermal as well as in the dynamic part of the model. The parameterisation used here, which has also been described in Chapter 2, accounts for these two types of modification. It can account for the sinks of momentum present over the entire height of the buildings, as well as for shadowing and radiation trapping effects in the street canyon, which are commonly neglected. This scheme has already been tested in a certain general sense in theoretical one- (Martilli, 2002; Roulet *et al*, 2003) and two-dimensional (Martilli *et al*, 2002), as well as applied two- and three-dimensional cases of the atmosphere over the city of Athens and its surroundings (Martilli, 2003, Martilli *et al*, 2003), but an extended comparison with data obtained by measurements in an urban area is missing. It is the aim of the present chapter, therefore, to validate the urban parameterisation using data from a street canyon. The model is run off-line on a one-dimensional column (which implies that the entire part of the model treating horizontal transport is turned off).

The data used in this work were obtained in the context of BUBBLE (homepage of the project: http://www.unibas.ch/geo/mcr/Projects/BUBBLE/), which was a large urban PBL experiment performed in Basel (Switzerland). The aim of BUBBLE was that of investigating the exchange processes close to the urban surface as well as the flows in the upper part of the Urban Boundary Layer (UBL), on one hand by using surface and remote-sensing instrumentation, and on the other hand by employing a mesoscale meteorological model. During this experiment, detailed observations within and above a street canyon were made more particularly at one site

("Sperrstrasse") from a 30-m tower during an IOP between 15 June and 15 July 2002, and are available in a data base.

Figure 3.1. Map of downtown Basel showing the "Sperrstrasse" measuring point (3) and its surroundings. © GVA Grundbuch- und Vermessungsamt Basel-Stadt.

The wind, temperature, humidity, and radiation were forced by using data obtained at the uppermost observation level. The urban module then calculates the vertical profile of several meteorological variables, the momentum fluxes, and the turbulent fluxes from the forced altitude down to ground. The parameterisation was validated using data obtained from measurements at several heights of the tower in and above the street canyon.

3.2. The 1D off-line model configuration

In this chapter, the model is run on a vertical column with forcing using data from measurements made at 30 m above ground level. The forcing was applied to wind, temperature, solar radiation, long-wave downward radiation, and humidity. The model calculates profiles of meteorological variables from this level down to the ground (see Figure 3.2). In its basic state (see the full description in Chapter 2), the model has a $k - l$ turbulence closure. Hence, above the ground surface the vertical turbulent fluxes are computed using K-theory:

$$\overline{u_j' \xi'} = - K \frac{\partial \overline{\xi}}{\partial x_j} \qquad (3.1)$$

where ξ stands for any of the scalar variables, $\overline{u_j' \xi'}$ represents the fluxes of given variables, and K is the turbulent-transfer coefficient (Stull, 1988). The computation of K in a $k - l$ closure leads to the calculation of a prognostic equation for the turbulent kinetic energy (TKE) (Bougeault and Lacarrère, 1989). Turbulent fluxes at the ground are computed with MOST (Louis, 1979).

Alternatively, the model can be run with the urban parameterisation scheme, where the percentage of urban soil coverage in the cell can be specified as follows: "0 %" will turn off the urban module and consider the cell as a rural area, at percentages between 0 and 100 both rural and urban calculations will be performed and the fluxes weighted, while at "100 %" the cell will be considered as entirely urban.
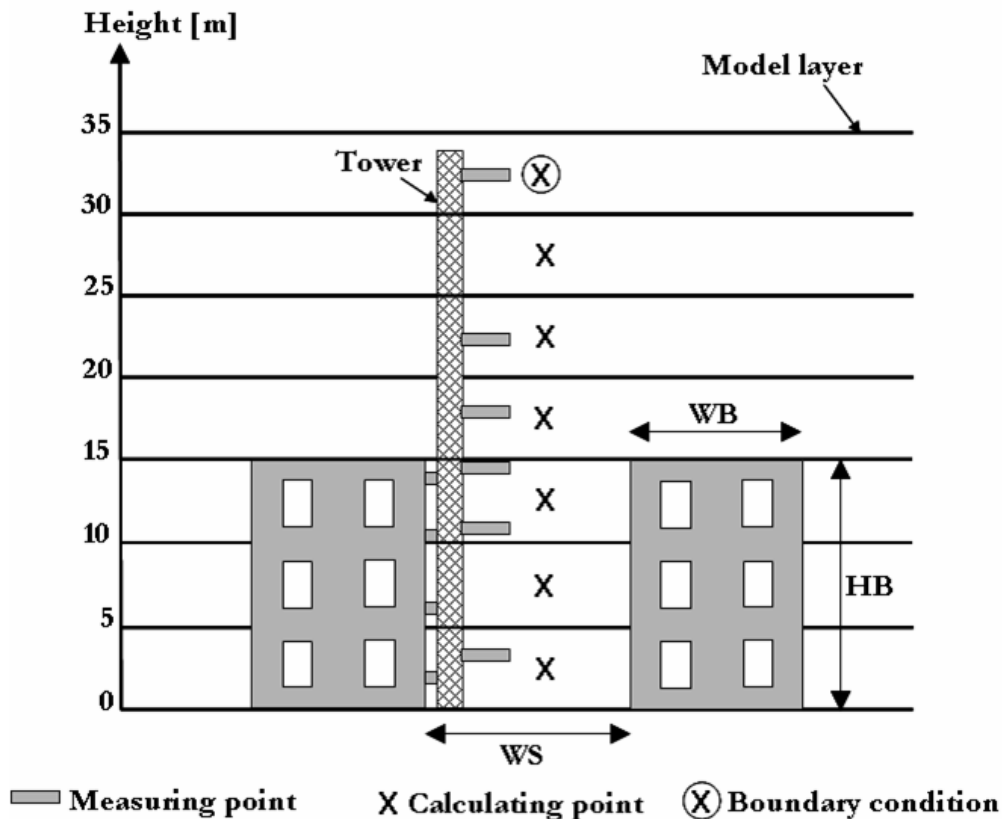
Figure 3.2. Configuration of the 1D offline model with forcing from the top and calculations down to ground in the street canyon, and a schematic representation of the city (street and buildings) in the urban module; HB is the height of the buildings, WB is the width of the buildings, and WS is the width of the street.

The simulation is validated with measurements from the tower above the urban canopy and in the street canyon (Figure 3.2). The vertical resolution was set to 2 m, which produces a 16-layer column up to the top of the model domain corresponding to the highest measuring point on the tower (32 m above ground).

Variations in the building and street characteristics will impact the percentages of vertical (wall) and horizontal (street and roof) surfaces in each layer of the urban grid, and hence the calculations of momentum fluxes, turbulent fluxes, and radiation trapping. It follows that accurate surface data are needed to set these parameters. In the case of Basel, information concerning the building and street parameters in the vicinity of the meteorological tower could be

obtained from a digital three-dimensional building model of the city. For this reason, the results shown hereafter are specific to the Basel site configuration.

3.3. Urban area characteristics and measurements

BUBBLE data were used to force the simulation at the top of the column and validate results of the model at the other levels. The data were collected at the main urban measuring site of the experiment ("Sperrstrasse"). Thus, the urban characteristics needed as inputs for the urban module are described by realistic values valid for this site. It is located in a heavily built-up part of the city ("European urban", dense urban, mainly residential 3 to 4-storey buildings in blocks, flat commercial and light industrial buildings in the backyards). The measuring setup consisted of a 32-m tower inside the street canyon (Figure 3.3). This height represents 2.2 z_H, where z_H is the local height of the buildings. At this height, the flow and turbulence fields as well as energy fluxes were measured. The experimental surface tower was operated for nearly one year. The instrumentation was greatly expanded during the IOP between 15 June and 15 July 2002.

Figure 3.3. The 32-m tower at Sperrstrasse.

Table 3.1 summarises the input parameters used for building and street characterisation (shape and physical properties) in the present study.

Table 3.1. Shape and physical properties of urban elements in the model: Substrate thermal conductivity K_s of the material, specific heat C_s of the material, initial temperature T_{int} of the material, emissivity ε of the surface, albedo α of the surface, and roughness length z_0 of the surface (Martilli *et al,* 2002, adapted in this work for the Basel-Sperrstrasse conditions).

Surface	Size [m]	K_s [$10^6 m^2 s^{-1}$]	C_s [$MJ\,m^{-3}\,K^{-1}$]	T_{int} [°K]	ε [-]	α [-]	Z_0 [m]
Wall	15 m high	0.67	1.0	293	0.90	0.2	---
Roof	30 m wide	0.67	1.0	293	0.90	0.2	0.01
Street	10 m wide	0.28	1.4	290	0.95	0.2	0.01

The orientations of the streets were deduced from a Basel city map (Figure 3.4), and fixed at 70° and 160°, respectively. This input is crucial for the solar radiation incident on the walls, and hence for the energy balance. The values of the parameters describing the physical properties of the urban elements were set so as to fit the Basel site. With the help of Figure 3.4, building height was set to 15 m.

Figure 3.4. Scanned data of building heights including trees around the "Basel Sperrstrasse" site (Keller, 2000), © GVA Grundbuch- und Vermessungsamt Basel-Stadt.

Measurements were taken at six different heights of the tower in and above the street canyon (at 3.6, 11.3, 14.7, 17.9, 22.4 and 31.7 m above ground, Figure 3.2), and are available with a 10-min time resolution. Since model outputs are obtained once every hour, hourly mean values of the measured data were calculated in order to facilitate comparison with simulation results.

3.4. Results

Two different simulations were carried out in order to test the urban module and quantify its impact on meteorological modelling. In the first simulation, denoted '*urban*', the urban surface

exchange parameterisation was used, where the percentage of urban area is set to 100 %. The second simulation, called '*trad*', represents the less detailed, traditional approach used in mesoscale models to account for urban surfaces (modification of roughness length and soil thermal capacity). The period of simulation lasted from 25 to 28 June 2002. Results of the two simulations were compared with data obtained from the tower during the same period.

3.4.1. Wind speed and wind direction

Differences were small between the results of the two simulations directly above roof height (18 m, Figure 3.5), but both overestimated the wind speeds during the day (this effect was more pronounced on 25 and 27 June), and even more strongly so during the night.
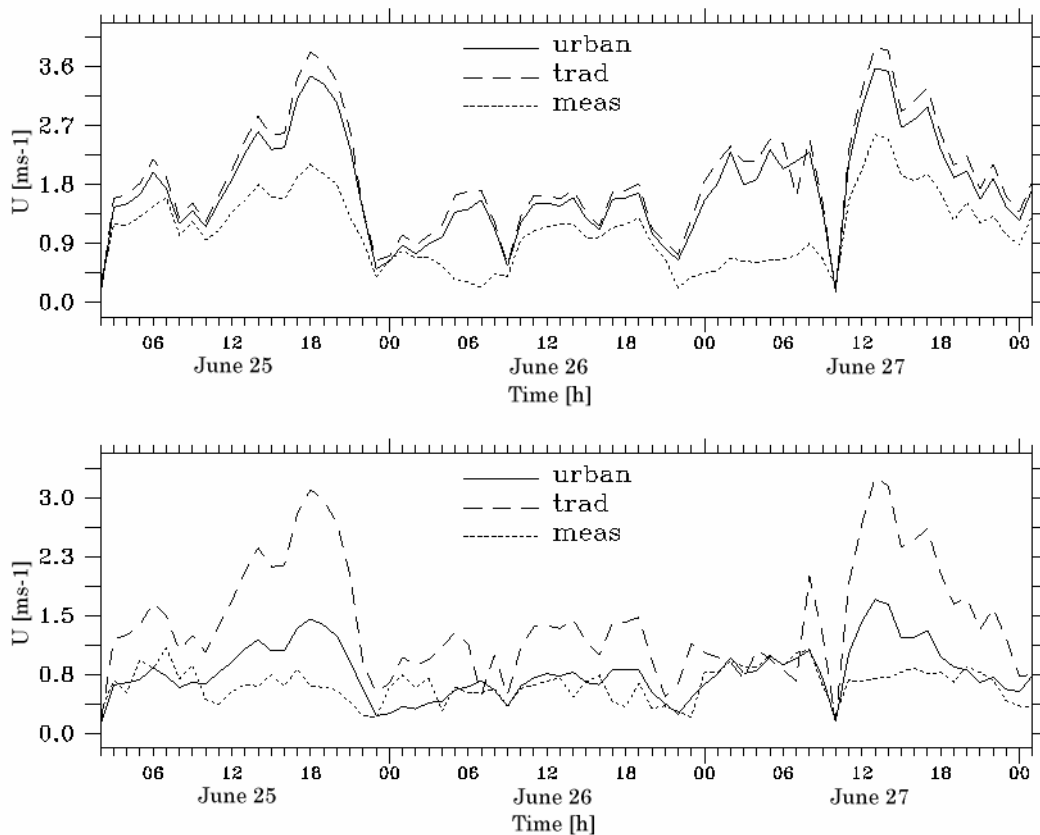
Figure 3.5. Wind speeds as functions of time from 02 LT 25 June to 01 LT 28 June in the street canyon at a height of 3 m (bottom) and, above the urban canopy, at a height of 18 m (top) according to simulations '*urban*' (solid line) and '*trad*' (dashed line) and according to the measurements (dotted line).

In the street canyon, the urban parameterisation is able to represent the deceleration of the flow field caused by obstacles (buildings), while the traditional approach computes larger values in this layer.

The simulation differences arise from the fact that in the urban parameterisation, the distribution of the drag force in the momentum equation is accounted for along the vertical from ground to roof height (Martilli, 2002), while in the traditional scheme the momentum sinks at ground are calculated via a friction velocity, and hence a conventional logarithmic profile is produced for the wind speeds, which is inapplicable in urban areas, according to earlier field measurements (Rotach, 1993a). By extending the momentum sink calculations based on drag forces caused by the buildings in each model layer to the entire height of the buildings, one can shift the boundary layer that is formed because of shear with a rigid surface from the ground level (as in the traditional scheme) to the top of the buildings (in the urban simulation). The associated logarithmic wind profile then appears at heights above the urban canopy. This is well represented by the data obtained during daytime (Figure 3.6).
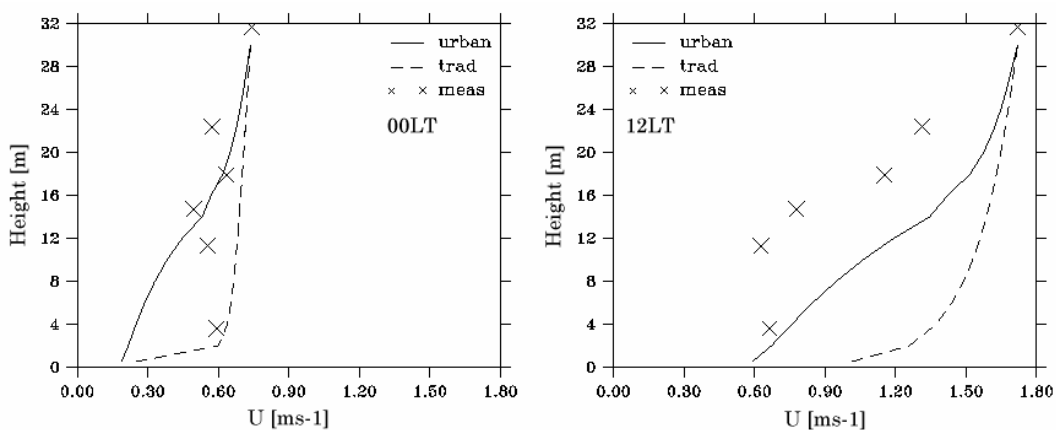
Figure 3.6. Vertical wind profiles in the street canyon obtained at 00 LT (left) and at 12 LT (right) on 26 June from the simulations '*urban*' (solid line) and '*trad*' (dashed line) and from measured data (cross).

In the urban simulation, the overall shape of the profiles observed in daytime can be reproduced. However, it appears that the drag force is underestimated in the simulations above roof level (the gradient is too small at average wind speeds), and overestimated below this level (the gradient is too large at average winds). Above roof level, this might have been caused by the rather homogeneous city structure in the immediate surroundings of the Basel observation site. Thus, in the model which uses local characteristics as an input, the mean building height and its variability is small as compared to that in some sections of the upwind area of influence. The observations, in turn, are influenced by a footprint which varies in size with height, and hence the influence of larger building structures may become more prominent. Below roof level the scheme apparently introduces too little shear. During nighttime, the urban model yields better values in the shear layer, but underestimates wind speeds in the street canyon (Figure 3.6, left) where the traditional method appears to provide a better fit, although wind speeds are very low. Measurements show a well mixed profile in the street canyon.

Apart from the wind speeds, it will be of interest to look at the observed and simulated wind directions in and above the street canyon (Figure 3.7 and Figure 3.8).
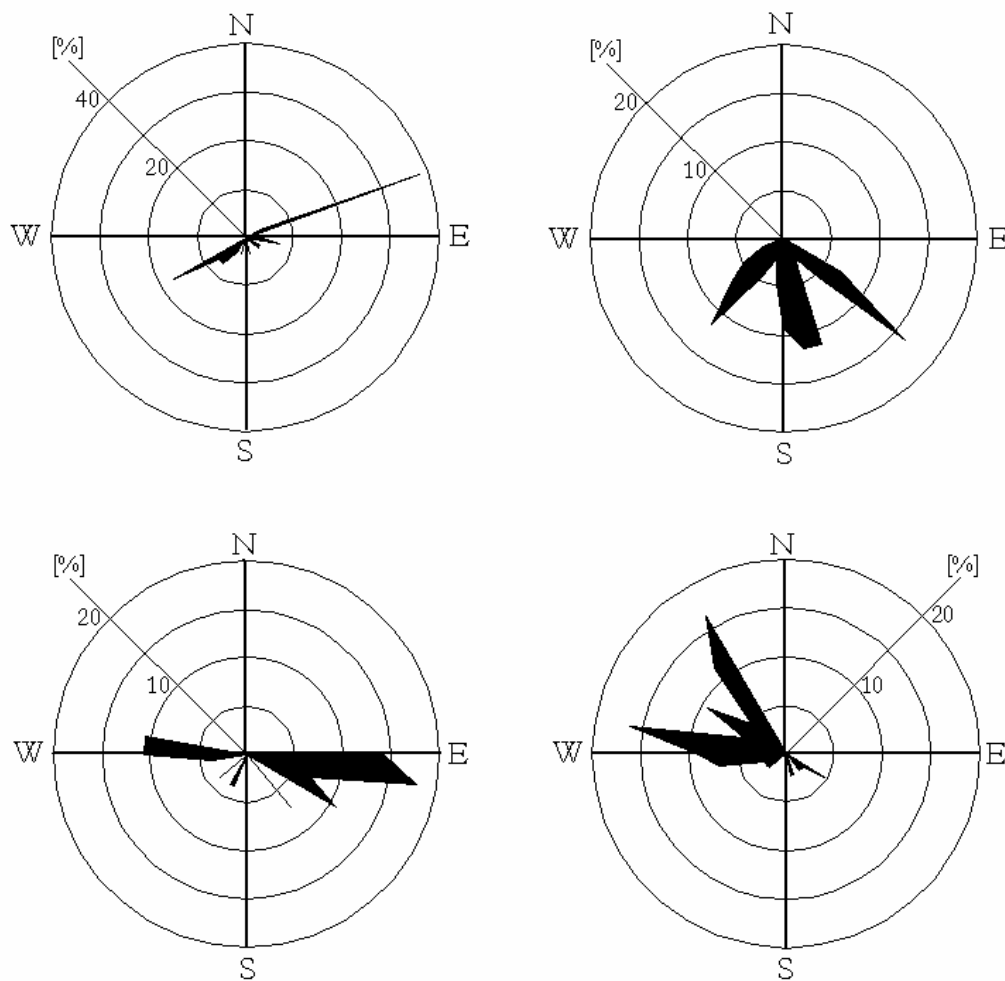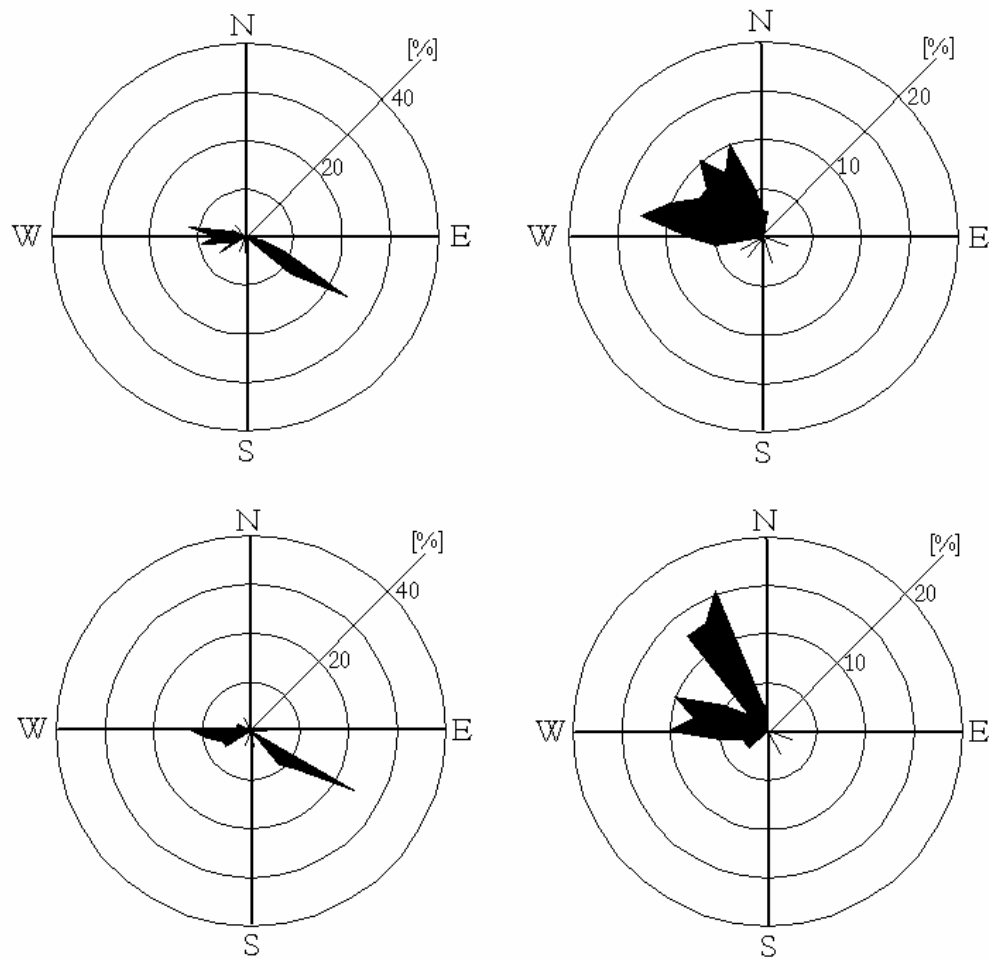
Figure 3.7. Compass roses for the percentages of occurrence of measured wind directions from 02 LT 25 June to 01 LT 28 June in the street canyon at a height of 3 m during nights (top left) and during days (top right) and, above the urban canopy, at a height of 18 m during nights (bottom left) and during days (bottom right).

During this episode, the wind blew mainly from North-West during daytime, and from East during nighttime. Near ground the measurements indicate a direction in the axis of the street during nighttime (70° or 250°, Figure 3.7, top left). During daytime, the direction is mainly perpendicular to the street direction (150° to 200°, Figure 3.7, top right), and opposite to that measured above roof level (Figure 3.7, bottom right). This indicates formation of a vortex in the street canyon perpendicular to the axis of the street.

Figure 3.8. Compass roses for the percentages of occurrence of simulated wind directions from 02 LT 25 June to 01 LT 28 June in the street canyon at a height of 3 m during nights (top left) and during days (top right) and, above the urban canopy, at a height of 18 m during nights (bottom left) and during days (bottom right).

Wind directions above building height obtained with the model (for both the '*trad*' and '*urban*' simulations) are similar to the measured directions (Figure 3.7 and Figure 3.8, bottom). Nevertheless, within the street canyon the model computes a mean direction similar to the direction above the urban canopy (Figure 3.8, top and bottom), and thus is not able to represent the vortex in the street canyon, which is not surprising, inasmuch as the model is not designed to account for such processes.

3.4.2. Temperature

Near the top of the tower, both the urban and the traditional simulations are in good agreement with the data obtained by measurements (Figure 3.9, top), which again is not surprising, since measured data are used as the boundary conditions at the top of the column. By inspecting the results obtained near ground (Figure 3.9, bottom) we can point out some differences appearing between the two simulations, particularly during nighttime.
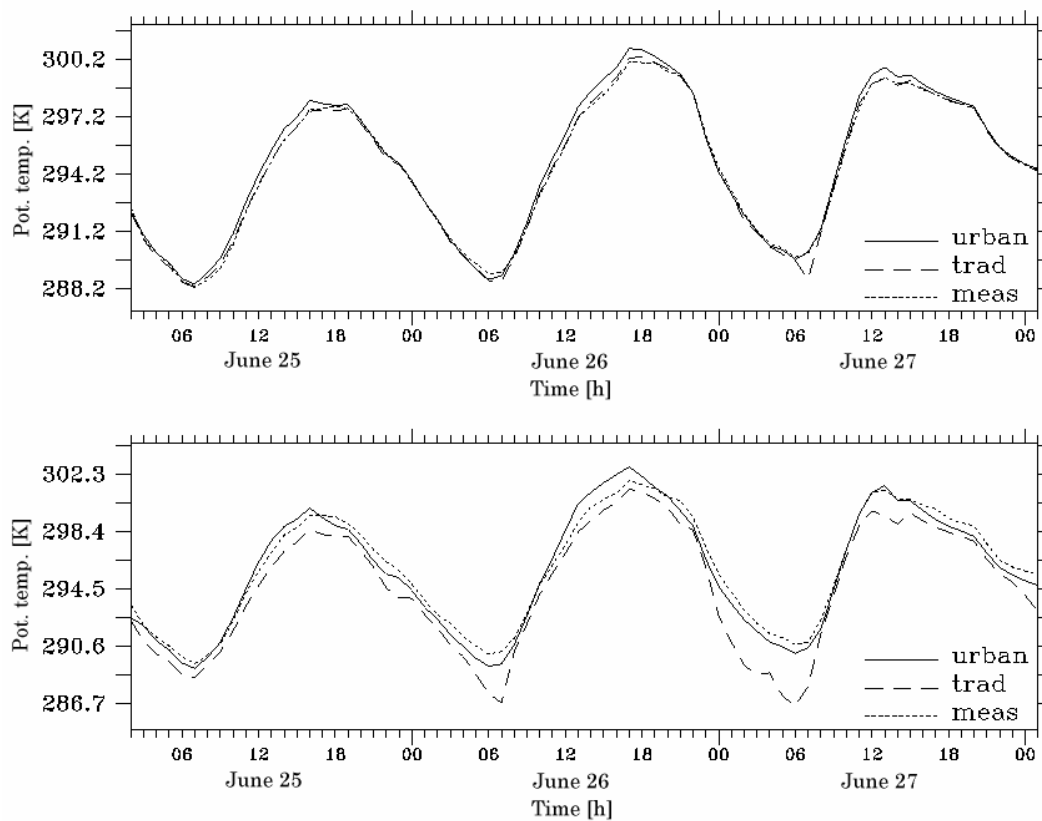
Figure 3.9. The potential temperatures as functions of time from 02 LT 25 June to 01 LT 28 June at a height of 3 m in the street canyon (bottom) and, above the urban canopy, at a height of 18 m (top) according to simulations '*urban*' (solid line) and '*trad*' (dashed line) and according to the measurements (cross).

The urban scheme accounts for radiation-trapping effects in the street canyon, hence the cooling found during nighttime will be less important than that found by the traditional simulation and, hence, better fits the data obtained by the measurements. As a result, '*trad*' may underestimate the

daily minimum by 3 to 4 K. By taking into account the differential heating/cooling of building surfaces while considering radiation trapping, the model is able to simulate generation of the Urban Heat Island (UHI) effect. The urban scheme also calculates heat fluxes coming from the street as well as from the walls. Heat sources then are distributed in the vertical direction up to roof height, while in the traditional parameterisation a single heat source at the ground is employed.

The urban simulation generally yields better results for daytime than the traditional simulation. Nevertheless, it can be seen from Figure 3.9 that daily maximum temperatures may be overestimated in the urban scheme (26 June).
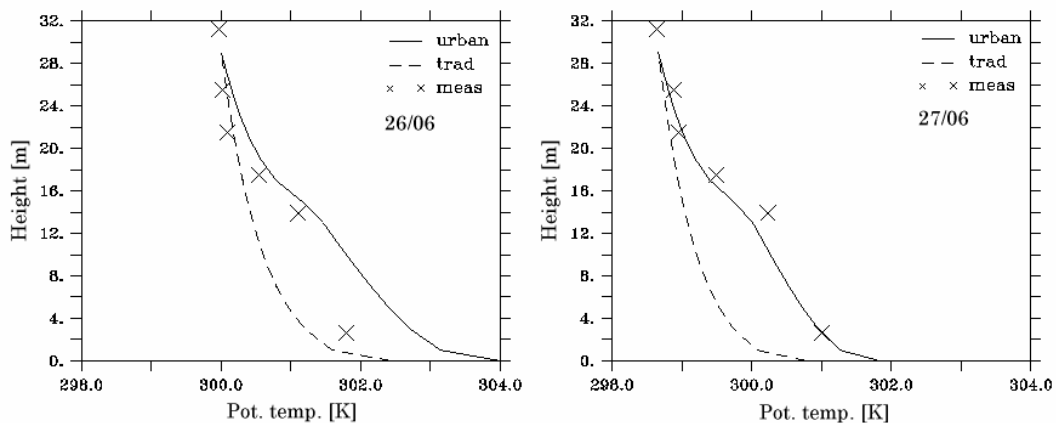
Figure 3.10. Vertical potential temperature profiles in the street canyon during the daily maxima for 26 June (1700 LT) (left) and 27 June (1300 LT) (right) according to simulations *'urban'* (solid line) and *'trad'* (dashed line) and according to the measurements (cross).

The vertical profiles of potential temperature measured at the time of the daily maximum on 26 and 27 June, respectively, are quite similar (Figure 3.10), in that they have a pronounced gradient immediately above roof level and small gradients beneath and above this level. The 'urban' simulation is able to reproduce this shape (between 15 and 20 m above ground), but for both days computes a gradient within the canyon which is high. Moreover, it yields a strong

temperature variation within the first two meters above ground, which may indicate that it overestimates the heat flux from the street surface. This hypothesis cannot be confirmed, since no measurements were made in the bottom three meters of the street canyon. The traditional method is unable to reproduce the measured temperature distribution in the street canyon and in the layer exhibiting the large gradient directly above roof height.

3.4.3. Heat flux

Interesting information as to the ability of the parameterisation scheme to account for turbulence generation can be derived when comparing the heat fluxes calculated with the model, with data obtained by measurements in the street canyon.
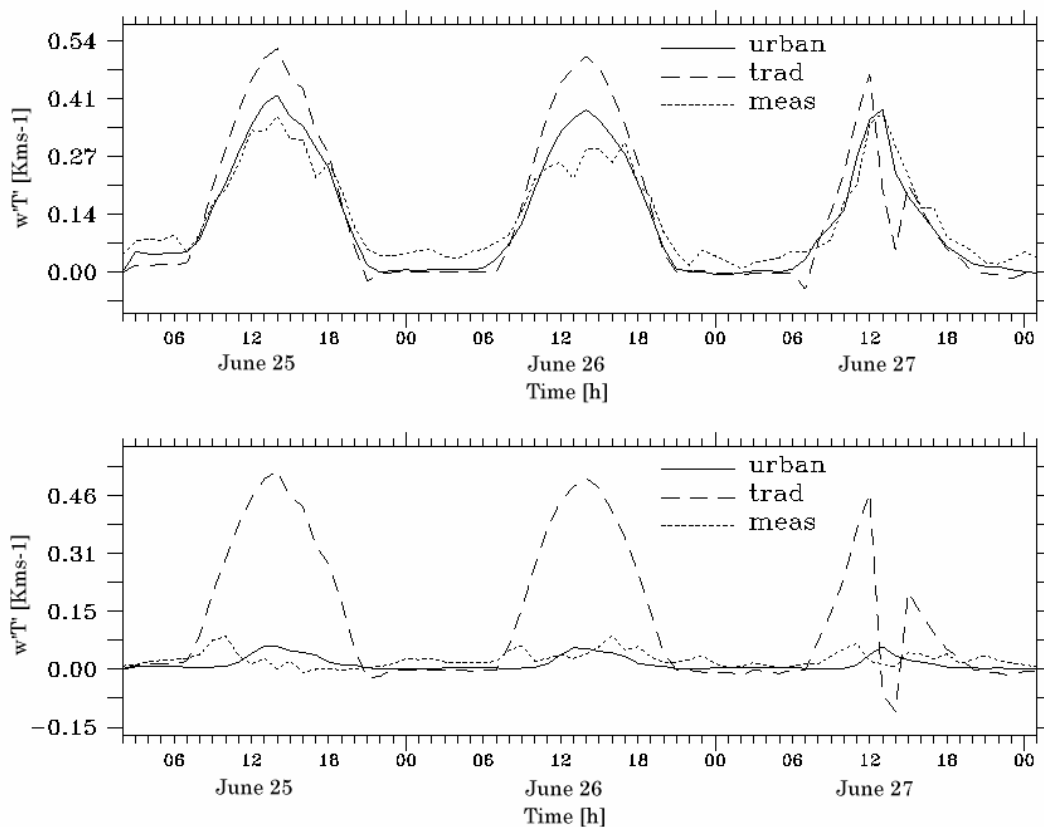
Figure 3.11. Vertical turbulent fluxes of sensible heat ($w'\theta'$) as functions of time from 02 LT 25 June to 01 LT 28 June in the street canyon at a height of 3 m (bottom) and, above the urban canopy, at a height of 18 m (top) according to simulations '*urban*' (solid line) and '*trad*' (dashed line) and according to the measurements (dotted line).

This will be done in terms of the turbulent vertical fluxes of sensible heat ($\overline{w'\theta'}$) above the urban canopy and in the street canyon as functions of time (Figure 3.11).

It can be seen that the traditional parameterisation distinctly overestimates the vertical heat fluxes during daytime. Above roof height, the simulated fluxes are as high as 0.5 to 0.6 Kms^{-1}, while measurements as well as the urban simulation yield values of 0.3 to 0.4 Kms^{-1} at the same time (Figure 3.11, top). Within the street canyon the differences are extremely large, inasmuch as '*trad*' still yields maximum values of 0.4 to 0.5 Kms^{-1}, while the values calculated by '*urban*' are always less than 0.1 Kms^{-1}, both during daytime and during nighttime. Measurements as well as the '*urban*' simulation indicate that the kinematic vertical heat fluxes started decreasing at 13 LT on 27 June, which was due to a cloud episode over the region. The reaction of '*trad*' to this episode is much stronger, inasmuch as the results indicate a very sharp decrease within a one-hour time interval. The vertical profiles found in the street canyon for 26 June confirm these tendencies (Figure 3.12). The profiles for other days of the episode were similar to the ones shown here.
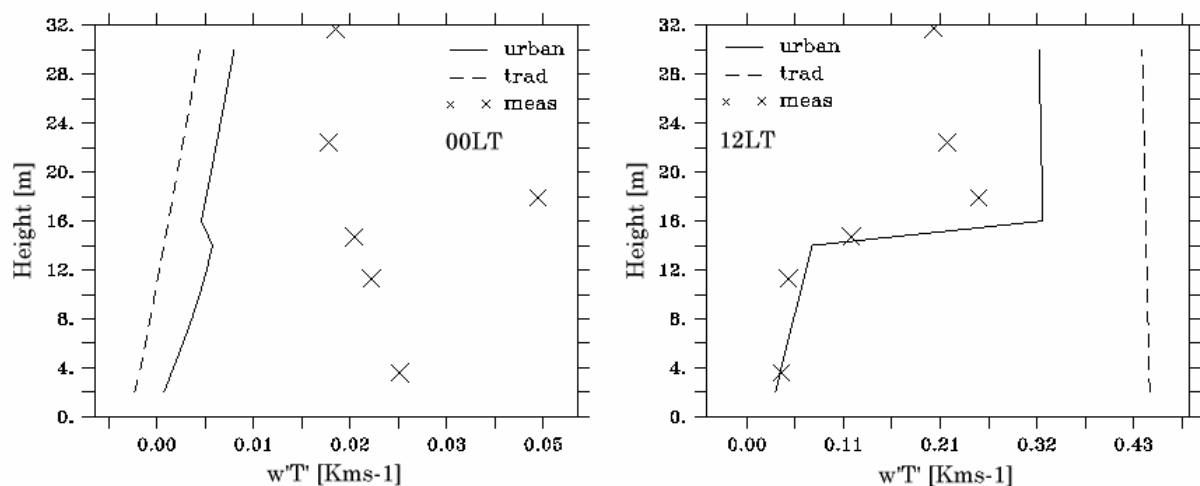

Figure 3.12. Profiles of the vertical turbulent fluxes of sensible heat ($w'\theta'$) in the street canyon at 00 LT (right) and at 12 LT (left) on 26 June according to simulations '*urban*' (solid line) and '*trad*' (dashed line) and according to the measurements (cross).

The relative values obtained by the model during nighttime (Figure 3.12, left) are much smaller than the measured data, but the absolute values of these fluxes are very small. On the other hand, daytime values (Figure 3.12, right) calculated by the urban parameterisation are in very good accord with the measured data. In particular, the homogenous profile within the street canyon and the strong positive gradient at roof height are well captured by '*urban*', whereas '*trad*' computes a profile with a more or less constant value overestimating the observed values.

3.4.4. Momentum

For an assessment of the turbulent exchange of momentum, it will be of interest to look at the local friction velocity defined as:

$$u_{*L} = \sqrt[4]{\left(\overline{u'w'}\right)^2(z) + \left(\overline{v'w'}\right)^2(z)} \tag{3.2}$$

Here, $\overline{u'w'}(z)$ and $\overline{v'w'}(z)$ represent the turbulent vertical momentum transports as functions of height z. These two terms are calculated with the model, and they are also measured in the urban canopy, while the local friction velocity used for the validation is deduced from Eq (3.2). Above roof level, '*trad*' generally shows a somewhat superior ability for reproducing the observations during daytime. During nights, on the other hand, the situation is reversed, *ie*, '*trad*' largely underestimates u_{*L} (Figure 3.13, top).
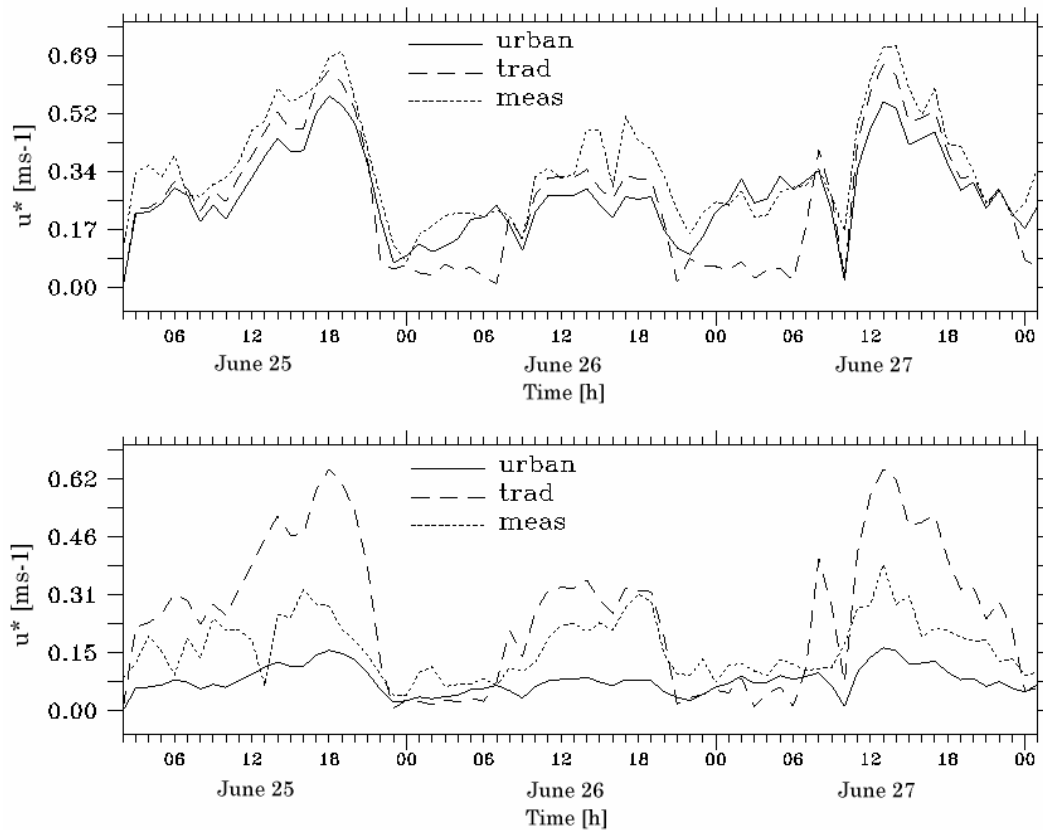
Figure 3.13. The local friction velocities (u_{*L}) as functions of time from 02 LT 25 June to 01 LT 28 June within the street canyon at a height of 3 m (bottom) and, above the urban canopy, at a height of 18 m (top) according to simulations '*urban*' (solid line) and '*trad*' (dashed line) and according to the measurements (dotted line).

Close to the ground (Figure 3.13, bottom), the situation is a little more complex. Although the urban scheme underestimates local friction velocities during daytime, it generally provides a better fit of the measured data than the traditional simulation. This is especially true for 25 and 27 June, when '*trad*' overestimated the daily maximum value by almost 100 %; it performed better for 26 June. After a comparison with Figure 3.5, we can conclude that at moderate wind speeds the '*urban*' simulation is distinctly superior in diagnosing the momentum flux close to the ground, while in the presence of weak flows it has a tendency to strongly underestimate it. This discrepancy arises from the fact that there is directional shear due to flow channelling, which is disregarded in the model, and hence gives rise to an underestimate for the shear term ($\overline{v'w'}$).

The vertical profile of u_{*L} calculated by '*trad*' is more or less constant, and hence in accord with the assumption of MOST underlying this simulation (Figure 3.14).
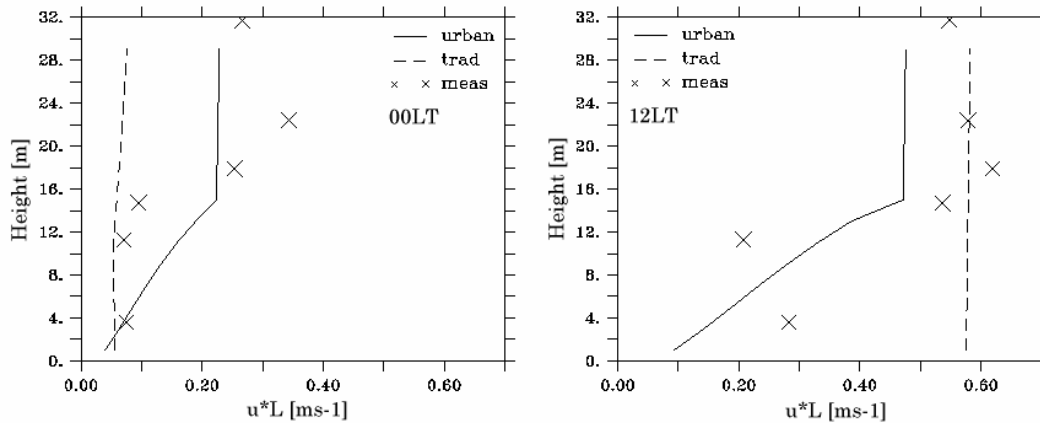

Figure 3.14. Vertical profiles of the local friction velocities (u_{*L}) within the street canyon at 00 LT (right) and at 12 LT (left) on 27 June according to simulations '*urban*' (solid line) and '*trad*' (dashed line) and according to the measurements (cross).

On the other hand, the urban parameterisation is able to represent in broad terms the increase of the local friction velocity occurring with increasing height in the urban canopy, including the maximum occurring at roof height. This is just slightly below the observed maxima at $z/h = 22/14 = 1.5$ and $z/h = 18/14 = 1.25$, respectively, which correspond to the heights of the observed maxima over long periods at the same site (Christen *et al*, 2003) and at other sites (Rotach, 1993b, 2001). The reason for a lower maximum produced by the '*urban*' simulation resides in the specification of height distribution of the buildings on the urban surface. In the present simulations, the local characteristics at the Sperrstrasse site were used, which exhibits a rather small horizontal variability. Martilli *et al* (2002) have demonstrated that the maximum Reynolds stress will occur above mean roof level, and the differences depend on the standard deviation of the height distribution. We conclude, therefore, that the present observations are influenced by a footprint of somewhat larger height variability which is not taken into account in the parameter specification.

The total momentum sink was calculated for both simulations, and compared with data obtained from measurements. For the traditional simulation, it was found as follows:

$$M_{tot} = -u_*^{\,2} \tag{3.3}$$

For the '*urban*' simulation as well as for the measured data, it was calculated as follows:

$$M_{tot} = \left[\sqrt[4]{\left(\overline{u'w'}\right)^2 (z) + \left(\overline{v'w'}\right)^2 (z)} \right]_{max} \tag{3.4}$$

The time variation of the momentum sink over one day is presented in Figure 3.15.
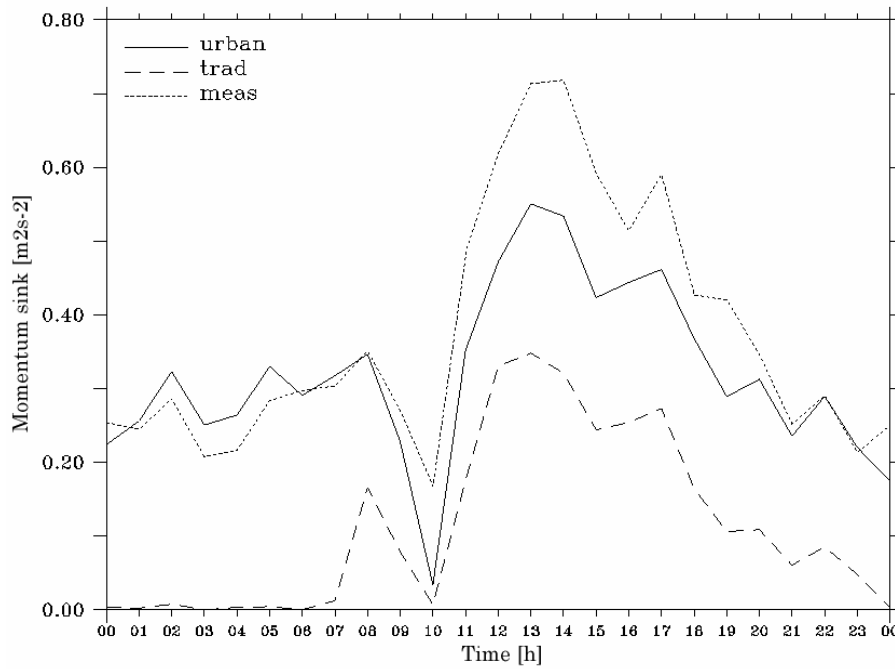
Figure 3.15. Time variation of the total momentum sink according to simulations '*urban*' (solid line) and '*trad*' (dashed line) and according to the measured data (dotted line) from 00 LT 27 June to 00 LT 28 June.

The results obtained by the two simulations are similar during daytime, and in accordance with measured data. The main differences arise during nighttime, when '*trad*' falls to nearly zero. This is probably due to the fact that it computes much more stable nighttime conditions than '*urban*'.

3.4.5. Fluxes vs gradients

It will be of interest at last to compare the relationship between fluxes and gradients of a conserved quantity. For the measured data, this is defined as the ratio of vertical turbulent transport of the quantity to the vertical gradient of the mean quantity (for the wind), and is calculated according to K-theory:

$$K_{m,i} = -\frac{\overline{u'_i w'}}{\dfrac{\partial \overline{U_i}}{\partial z}} \tag{3.5}$$

where index i = 1, 2. In the models, this relationship is expressed in terms of calculated eddy diffusivity using the classical formula (Bougeault and Lacarrère, 1989):

$$K_{m,i} = C_k \, l_k \, E^{1/2} \tag{3.6}$$

where C_k is a numerical constant, l_k is a characteristic length, and E is the TKE.
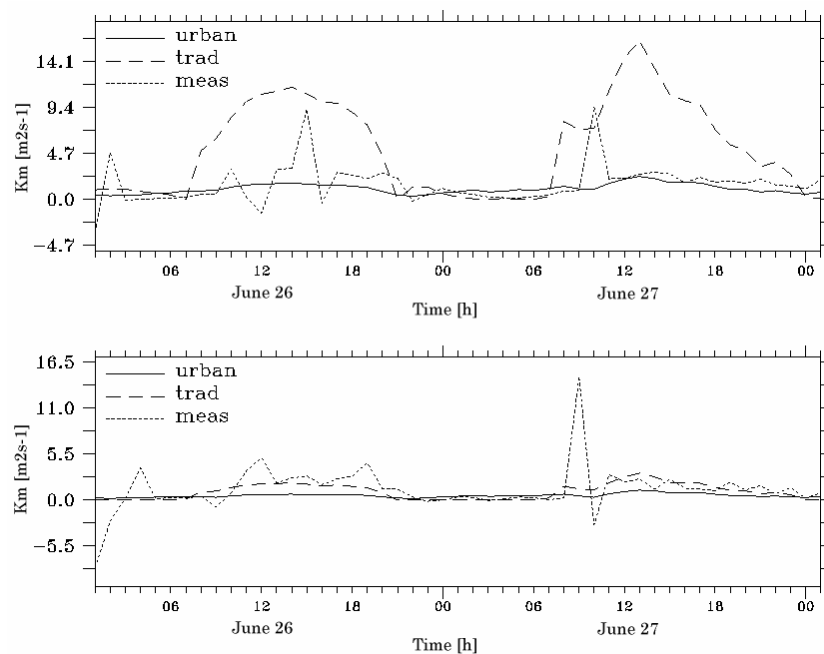
Figure 3.16. Eddy diffusivities for the horizontal wind as functions of time from 01 LT 26 June to 01 LT 28 June within the street canyon at a height of 3 m (bottom) and, above the urban canopy, at a height of 18 m (top) according to simulations '*urban*' (solid line) and '*trad*' (dashed line) and according to the measurements (using data for *u'w'* and *u*, dotted line).

The eddy diffusivities calculated with the traditional method are overestimated relative to the urban simulation and to the measurements during daytime above the urban canopy (Figure 3.16). One can see when looking at vertical profiles in the urban canopy (Figure 3.17) that this overestimation occurs at all levels of the profile.
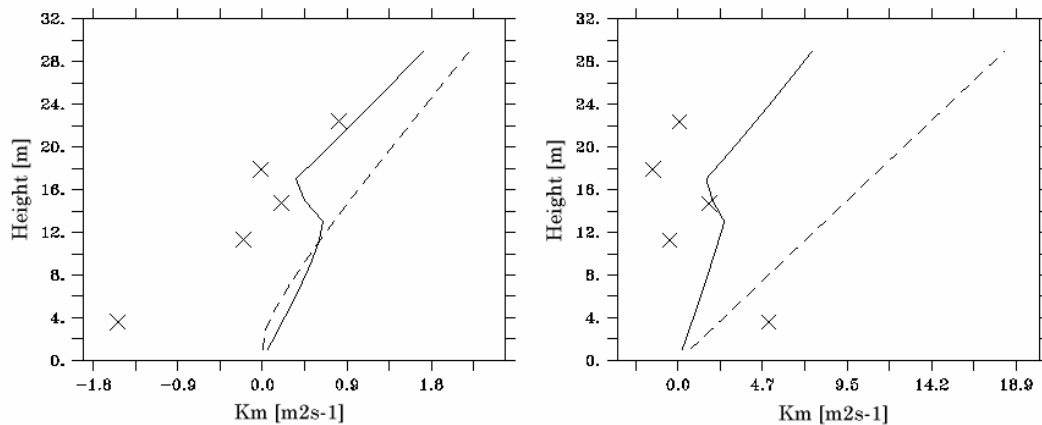

Figure 3.17. Vertical profiles of the diffusion coefficient (K_m) in the street canyon at 00 LT (right) and at 12 LT (left) on 26 June according to simulations '*urban*' (solid line) and '*trad*' (dashed line) and according to the measurements (cross).

Thus, the calculated mixing intensities are larger than those measured, while the profiles of other calculated quantities (U, θ, u_*, etc.) are mostly homogenous within the street canyon (see Figure 3.6, Figure 3.10 or Figure 3.14). On the other hand, the urban scheme is able to reproduce some more details in the vertical profiles, such as the local maximum occurring around roof height and the decrease occurring within the first layer above the roofs, which both appear in the measured data as well.

It can be gathered from Figure 3.16 and Figure 3.17 that the relationship between fluxes and gradients derived from measured data may sometimes be negative, which points to the presence of countergradient fluxes (especially within the canyon). Countergradient transport is a result of nonlocal effects from large eddies (Deardorff, 1966, Holstag, 1991). Evidence for such transport

has for a long time been detected and measured over various surfaces such as grassland (Webb, 1958), agricultural crops (Wilson *et al*, 1982), or forest canopies (Raupach *et al*, 1989). All local turbulence closure schemes using classical mixing-length theory will find the fluxes to be directed down the gradient, which is obviously not in general the case in an urban canopy. Thus, the current parameterisation used in the model, which is based on K-theory, is not able to account for this flux, as this is induced by nonlocal effects (this holds true for '*trad*', and to a smaller extent for '*urban*'). A countergradient contribution which is additive to the vertical gradient of a scalar might therefore be added to the local K-theory equation, as has been suggested, *eg*, for convective boundary layers (Deardorff, 1972, Lüpkes and Heinke-Schlünzen, 1996). Such an extension of the model is regarded as a possible future development for the '*urban*' parameterisation.

3.4.6. Summary of the results

As a tool for summarising the comparison of the urban simulation with the traditional method, Fractional Biases (FB) and Root-Mean-Square Differences (RMSD) have been calculated over the entire episode simulated (25 to 28 June), between '*trad*' and the measured data on the one hand, and between '*urban*' and the measured data on the other hand (Figure 3.18). Both quantities are defined as follow:

$$FB = 2 * \left(\frac{\overline{V_{\mathrm{mod}}} - \overline{V_{meas}}}{V_{\mathrm{mod}} + V_{meas}} \right) \tag{3.7}$$

$$RMSD = \sqrt{\frac{\sum_{i=1}^{n} \left(V_{\mathrm{mod}}^{i} - V_{meas}^{i} \right)}{n}} \tag{3.8}$$

where V_{mod} is the model value, V_{meas} the measured value of a given variable and n the number of occurrence (in this case: number of hour times number of levels).
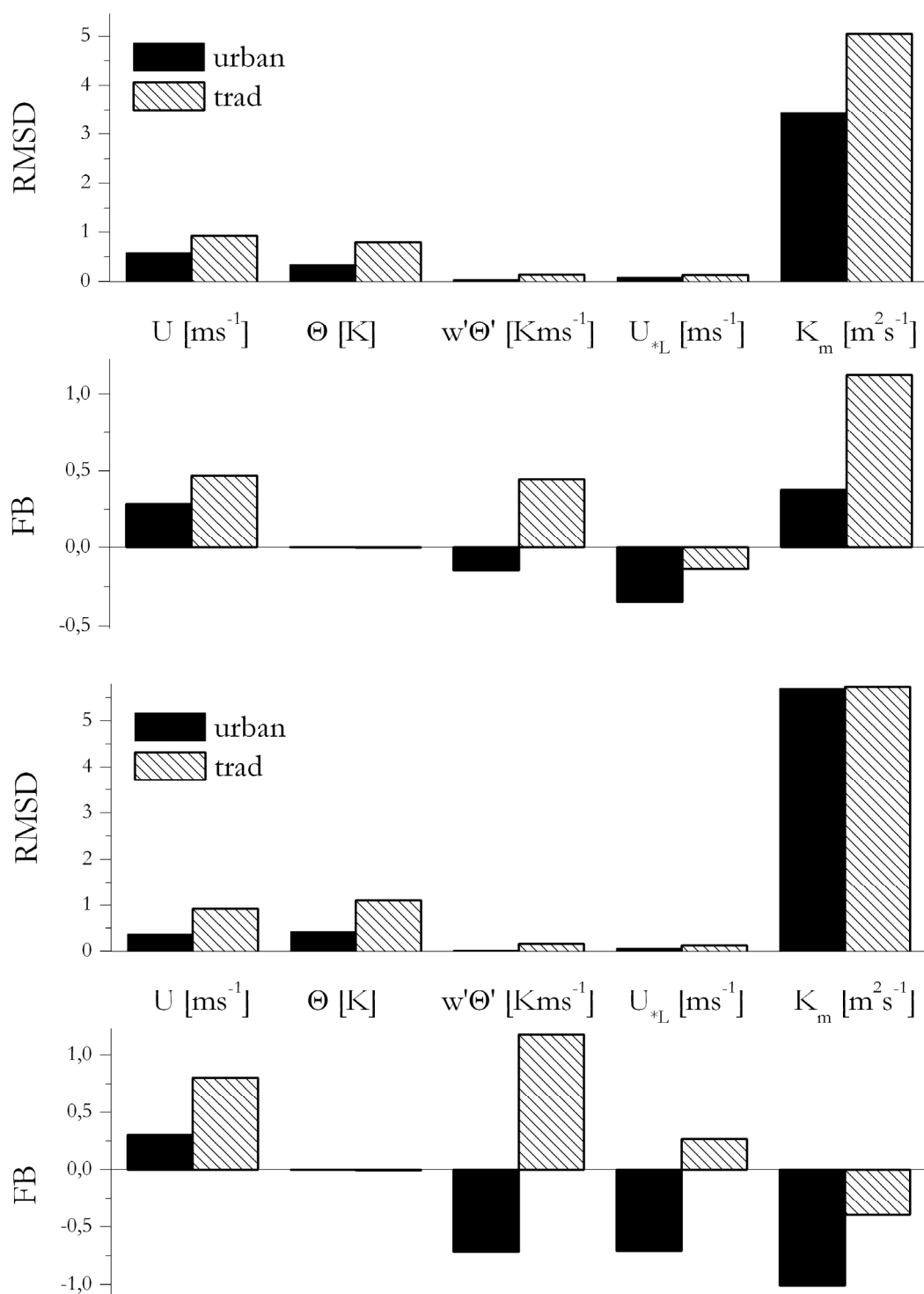
Figure 3.18. Fractional Biases (FB) and Root-Mean-Square Differences (RMSD) for winds (U), potential temperatures (θ), turbulent fluxes of sensible heat ($w'\theta'$), local friction velocities (u_{*L}), and eddy diffusivities (K_m) between '*urban*' and the measured data and also between '*trad*' and the measured data, over the entire episode (25 to 28 June) for all levels together (0-30 m a.g., upper two bar charts), and in the urban canopy alone (0-10 m a.g., lower two bar charts).

The RMSD representing the overall differences between model and observations are distinctly lower for '*urban*' than for '*trad*' for all variables presented in Figure 3.18, a difference which is even more pronounced in the street canyon for U, $w'\theta'$, and u_{*L}. With respect to the quantity θ, the RMSD are higher for both simulations if only the values within the street canyon are considered. This is probably due to the fact that the temperature is forced at the top, and hence should provide a better fit for the measured data in the upper layer. The FB, which represent the absolute mean deviations of the model from the observations, are distinctly lower for '*urban*' than for '*trad*' by factors varying between 1.6 (heat flux in the urban canopy) and 30 (temperature in the urban canopy), except for u_{*L} and K_m in the street canyon.

3.5. Conclusions and future developments

A detailed urban-surface exchange parameterisation implemented in a mesoscale model has been tested off-line in a street canyon, and compared on one hand with simulations using a traditional parameterisation, and on the other hand with data measured in and above a street canyon. The comparison shows that vertical profiles as well as the meteorological variables and turbulent fluxes (sensible heat flux, vertical flux of horizontal momentum, etc.) obtained as functions of time with the urban module yield a better fit of measured data than simulations with a traditional parameterisation. More particularly, typical phenomena due to the presence of an urban area such as the deceleration of the flow field in the urban canopy often are well captured by the new parameterisation. Moreover, the observed vertical profiles often show gradients at roof height (due to the formation of a shear layer) which in general are captured by the urban parameterisation, while the traditional method, because of the assumptions underlying MOST, is not able to reproduce these features. The statistical indicators presented in Figure 3.18 confirm the improvements gained by model results calculated with the urban module. Nevertheless, some weaknesses still exist in this parameterisation, and further development of the scheme is planned.

The possible addition of a countergradient contribution to the calculation of diffusion coefficients is of interest. In the same perspective, a parameterisation for shear stresses arising from flow channelling in the street canyon could also be introduced into the model. The impact of each surface type (street, wall, and roof) on the sensible heat fluxes should also be investigated further, since simulated temperature profiles in the street canyon exhibited a time dependence that differed from that found from the measured data. With a view to future applications, our next step will be that of running the mesoscale model with urban parameterisation in its full three-dimensional configuration over the region of Basel.

References

Bougeault, P. and Lacarrère, P.: 1989, 'Parameterisation of orography-induced turbulence in a mesobeta-scale model', *Mon. Wea. Rev.* **117**, 1872-1890

Christen, A., Vogt, R. and Rotach, M. W.: 2003, 'Profile measurements of selected turbulence characteristics over different urban surfaces', *Proceedings, 4th International Conference on Urban Air Quality, Prague, March 25-27 2003*, 408-411

Deardorff, J.W.: 1966, 'The counter-gradient heat flux in the lower atmosphere and in the laboratory', *J. Atmos. Sci.* **23**, 503-506

Deardorff, J.W.: 1972, 'Theoretical expression for the countergradient vertical heat flux', *J. Geophys. Res.* **77**, 5900-5904

Holstag, A. A. M. and Moeng, C. H.: 1991, 'Eddy diffusivity and countergradient transport in the convective atmospheric boundary layer', *J. Atmos. Sci.* **48**, 1690-1698

Keller, P.: 2000, *Die Bestimmung der Oberflächenrauhigkeit in einer städtischen Umgebung – Eine GIS gestützte Anwendung morphomerischer Methoden*, Diploma Thesis at the Institute of Meteorology, Climatology and Remote Sensing, University of Basel

Louis, J.-F.: 1979, 'A parametric model of vertical eddy fluxes in the atmosphere', *Boundary-Layer Meteorol.* **17**, 187-202

Lüpkes, Ch. and Heinke Schlünzen, K.: 1996, 'Modelling the Arctic convective boundary-layer with different turbulence parameterisations', *Boundary-Layer Meteorol.* **79**, 107-130

Martilli, A., Clappier, A. and Rotach, M. W.: 2002, 'An urban surface exchange parameterisation for mesoscale models', *Boundary-Layer Meteorol.* **104**, 261-304

Martilli, A.: 2002, 'Numerical study of urban impact on Boundary Layer structure: Sensitivity to wind speed, urban morphology, and rural soil moisture', *J. Applied Meteorol.* **41**, 1247-1266

Martilli, A.: 2003, 'A two-dimensional numerical study of the impact of a city on atmospheric circulation and pollutant dispersion in a coastal environment', *Boundary-Layer Meteorol.* **108**, 91-119

Martilli, A., Roulet, Y.-A., Junier, M., Kirchner, F., Rotach, M. W. and Clappier, A.: 2003, 'On the impact of urban exchange parameterisations on air quality simulations: the Athens case', *Atmosph. Env.* **37**, 4217-4231

Raupach, M. R., Finnigan, J. J. and Brunet, Y.: 1989, 'Coherent eddies in vegetation canopies', *Proceedings, 4th Austral. Conf on Heat and Mass Transfer*, 9-12 May 1989, Christchurch, New Zealand, p. 75-90

Rotach, M. W.: 1993a, 'Turbulence close to a rough urban surface. Part I: Reynold stress', *Boundary-Layer Meteorol.* **65**, 1-28

Rotach, M. W.: 1993b, 'Turbulence close to a rough urban surface. Part II: Variances and gradients', *Boundary-Layer Meteorol.* **65**, 1-28

Rotach, M. W.: 2001, 'Simulation of urban-scale dispersion using a lagrangian stochastic dispersion model', *Boundary-Layer Meteorol.* **99**, 379-410

Roulet, Y.-A., Martilli, A., Rotach, M. W. and Clappier, A.: 2003, 'Modelling of urban effects over the city of Basel (Switzerland) as a part of the BUBBLE project', *Proceedings, 5th International Conference on Urban Climate, September 1-5 2003, Lodz, Poland*

Stull, R. B.: 1988, *An introduction to Boundary Layer Meteorology*, Kluwer Academic Publishers, 670 pp.

Webb, E. K.: 1958, 'Vanishing potential temperature gradient in strong convection', *Quart. J. R. Meteor. Soc.* **84**, 118-125

Wilson, J. D., Ward, D. P., Rhurtell, G. W. and Kidd, G. E.: 1982, 'Statistics of atmospheric turbulence within and above a corn canopy', *Boundary-Layer Meteorol.* **24**, 495-519

Chapter 4

Simulation of atmospheric flow fields over the region of Basel

Abstract

The mesoscale meteorological model was applied to the atmosphere over the city of Basel (Switzerland) and its surroundings. The main objective of this chapter is that of validating this model in a realistic three-dimensional domain with the aid of data obtained from measurements made in the city of Basel and at reference rural sites during the BUBBLE measuring campaign. The influence of horizontal resolution on the simulated meteorological fields was evaluated, as was the influence of three different methods used to account for the urban areas (the traditional method, the new urban scheme, and a method without parameterisation).

The results show that the meteorological model is able to represent the meteorological conditions prevailing in the domain during the episode simulated. The technique of fractional land-use coverage within given cells appears to improve the results, particularly so in suburban zones where the heterogeneity of surface coverage is high. It was seen when comparing the results obtained with the model, with experimental results obtained by measurements of the vertical turbulent variables within the urban canopy, that with the new urban scheme a better fit is

obtained than with the traditional method. In the case of cloud formation within the domain, the

radiation forcing technique proved to have utility for simulations of the temperature distribution.

4.1. Introduction

The need for an accurate modelling of the atmospheric flow fields over urban areas has been pointed out in earlier chapters of this work. The urban parameterisation scheme implemented in the mesoscale atmospheric model (Chapter 2) has already been validated for one-dimensional (Roulet *et al*, 2004) and two-dimensional (Martilli, 2002, 2003) cases. For the simulations in three dimensions, the mesoscale model with urban parameterisation has been tested in a case study over Athens (Martilli *et al*, 2003). In the present chapter, this model is applied to the situation over the region of Basel using observations made in the context of the BUBBLE project. The objective was that of running the full three-dimensional mesoscale model including the urban scheme over a realistic domain while considering the topography and land coverage of this domain.

The period of intense observations in Project BUBBLE stretched from 15 June to 15 July 2002. The simulated episode has been defined within this period of time (25 to 29 June 2002) in order to be able to compare results derived from the model with a maximum number of experimental data from different locations.

Section 4.2 describes the specific model setup used in this study, as well as the origin of input data such as topography and land use of the simulated domain.

An overview of the measuring stations available for validation of the model is given in Section 4.3. The validation is performed in different parts of the domain using observation sites situated at the corresponding location. The objective is that of validating the model for the urban, suburban, and rural area.

Just as in the one-dimensional validation (Chapter 3), results calculated by the mesoscale model for turbulent fluxes and meteorological variables are compared with results obtained with a traditional parameterisation method. As a reminder, MOST is assumed in the traditional method, just as for rural areas, but with roughness lengths and thermal properties modified so as to account for the presence of urbanised zones (see the detailed description in Chapter 2).

4.2. Domain definition and the mesoscale-model setup

4.2.1. Domain features

The mesoscale model was applied in two nested grids. The larger grid had a horizontal resolution of 4 km by 4 km (Figure 4.1) and covered a domain of 192 km by 240 km (48 x 60 grid cells). The model extended vertically up to 12 000 m above ground level with a vertical resolution that varied from 10 m close to ground to 1000 m at the top of the domain and led to a total of 32 layers.

Temperature and wind were forced at the boundaries of the domain using NCEP/NCAR Reanalysis data. These data have an original spatial resolution of 2.5° latitude by 2.5° longitude and a time resolution of six hours. They were interpolated on the mesoscale grid to hourly intervals and assimilated to the calculated values using the Four-Dimensional Data-Analysis (FDDA) technique described in Chapter 2.
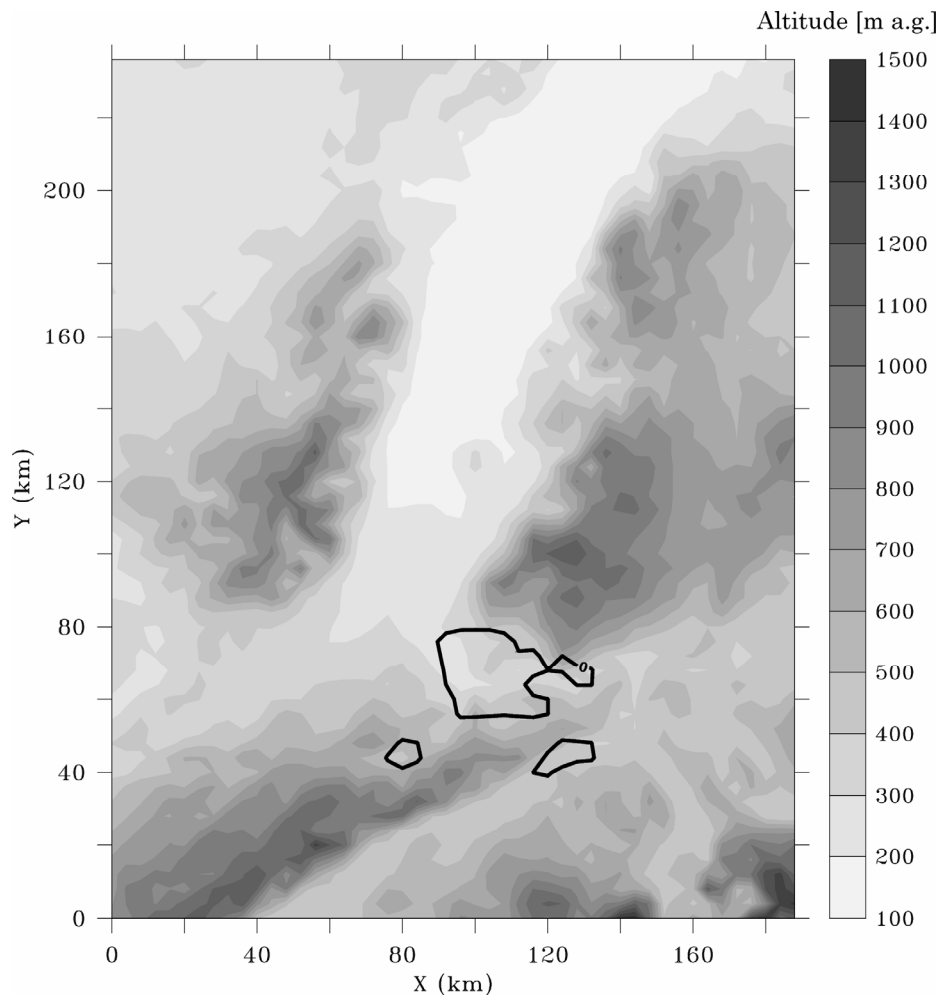
Figure 4.1. Topography of the large domain for the simulation. Black lines delimit the Basel urban area.

Here the forcing parameter τ was set so that the influence of forcing is strongest in cells at the boundaries of the grid, and decreases in steps of 20 % per row of cells toward the interior of the domain (Figure 4.2). The zone of influence will then be limited to the first five cells at each domain boundary (East, West, North, South, and top of the domain).
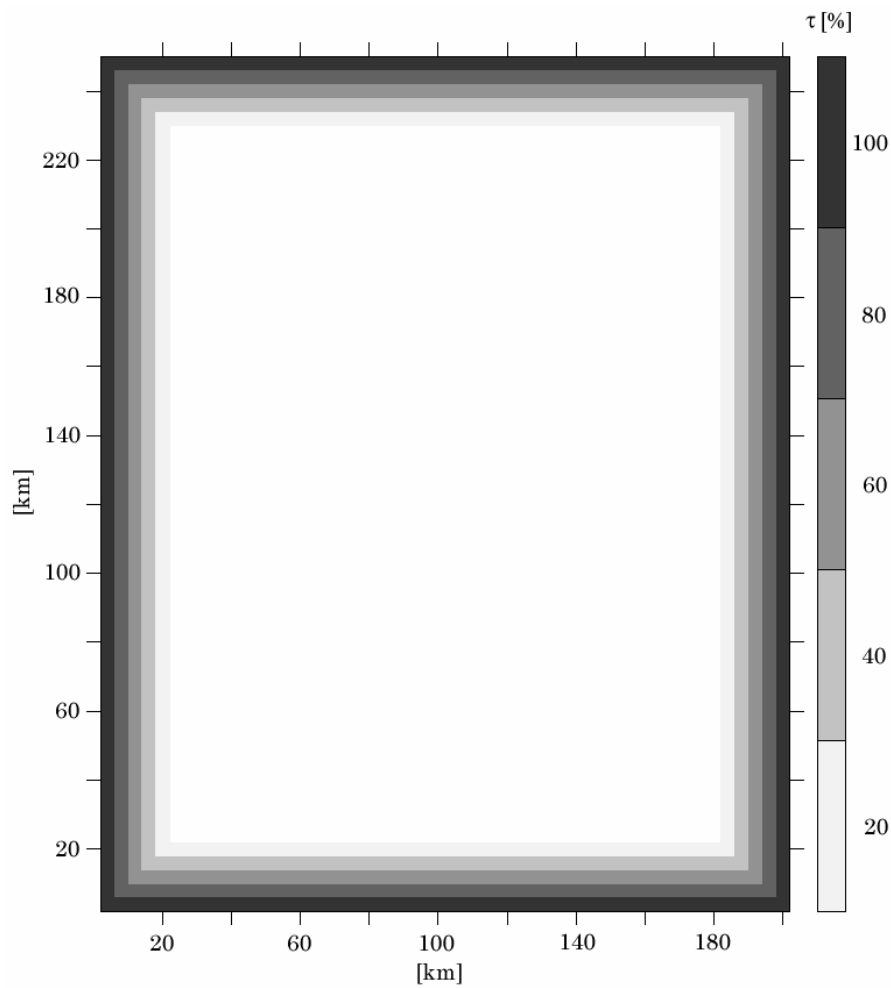
Figure 4.2. Value of the forcing parameter τ in the large domain. The influence of forcing varied in steps of 20 % from 100 % (domain boundary cells) to 0 % in the centre of the domain (white zone).

The results of the large grid were used to force the calculations in the small grid at the boundaries of this grid (using the same technique as in forcing of the large grid by NCEP data). The small grid has a horizontal resolution of 1 km by 1 km (Figure 4.3) and extends over a domain of 52 km by 60 km. The vertical resolution is identical with the resolution in the large grid.
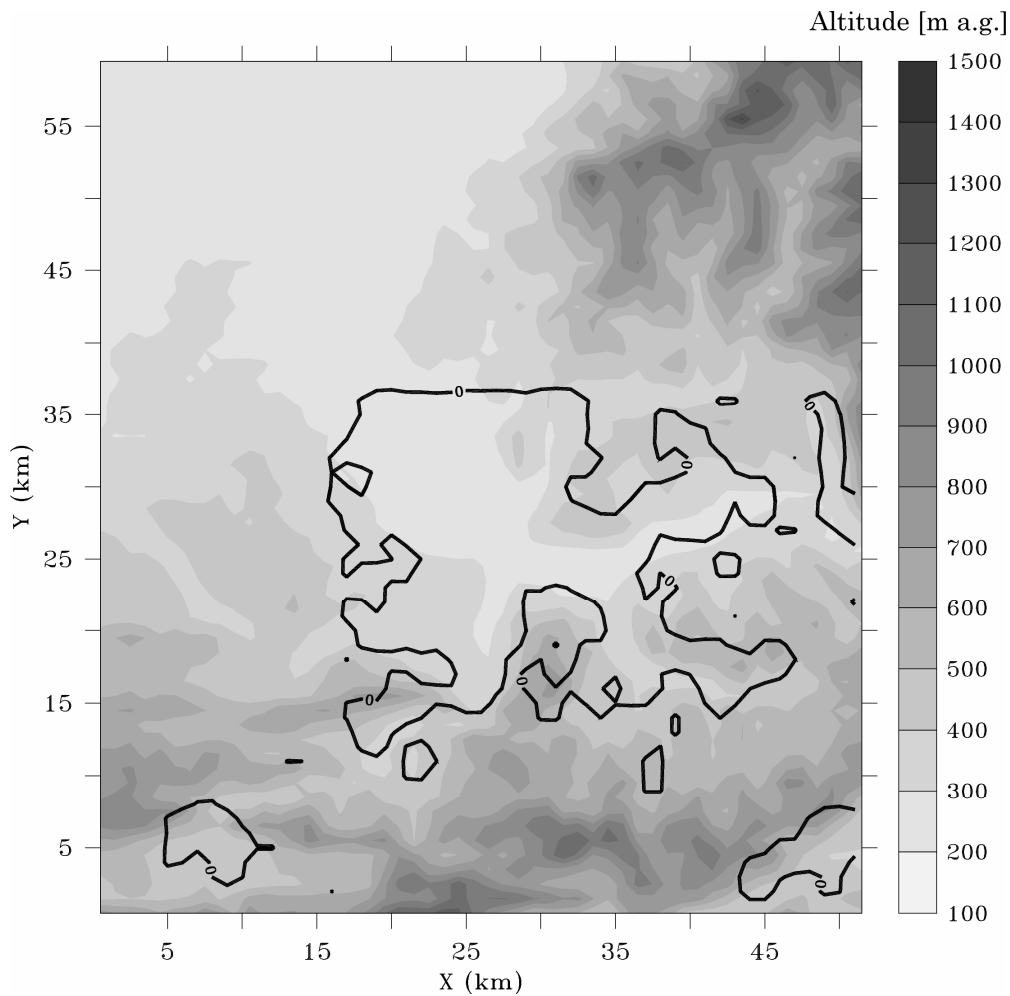
Figure 4.3. Topography of the small domain for the simulation. Black lines delimit the Basel urban area.

The simulated episode stretched from 00 LT 25 June to 12 LT 29 June 2002 and corresponded to a thermally driven meteorological situation included in the BUBBLE intense observation period organised between 15 June and 15 July 2002.

The large domain included part of the Swiss Prealps at the Southern boundary, part of the German Black Forest east of the city (with mountains up to 1000 m a.s.l.), the tail of the Swiss Jura Mountains (south-west of the domain), the French (Alsatian) Vosges mountains in the west, and the Rhine valley east and north of Basel. The city is surrounded by mountains and (geologically speaking) occupies a graben 250-300 m a.s.l. forming the beginning of the Upper

Rhine Valley that extends further north towards Strasbourg. This situation determines the Basel climate, which is one of the warmest of Switzerland. Mountains slow down the winds in the PBL over Basel, and hence favour stationary meteorological situations which in turn enhance heat and pollutant accumulation. Wind flow is influenced by the surrounding mountains acting as a barrier to cloud formation or generating diurnal slope wind systems (as described in Chapter 1).

The small domain included the city of Basel and its more immediate surroundings, as well as a small part of the Black Forest and Jura Mountains. Due to the finer resolution in this grid, altitude now reached 1400 m a.s.l. in the Black Forest, 400 m more than in the large grid.

In this application, domain topography is taken into account for mesh deformation in both domains (the first cell of each column is at the height of the corresponding topographic point). Topographic data were taken from a worldwide Digital Elevation Model (DEM) collected by the U. S. Geological Survey (GTOPO30) and having a resolution of 1 km (http://edcdaac.usgs.gov/gtopo30/gtopo30.asp).

4.2.2. Urban class definition
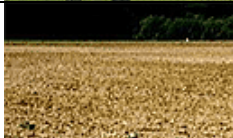
The percentage of rural and urban soil coverage to be specified in each cell and needed for the weighting of urban and rural fluxes was determined from the KABA[1] data base (Fehrenbach, 1999). Among the different maps provided in the data base, a very accurate land coverage description has been recorded having a resolution of 100 m and providing the definition of 15 different land-use classes. The percentage of each class is specified for all ground-level cells

[1] The main objective of Project KABA (Klimanalyse der Region Basel), which was started in 1995, was that of designing physiographic and sociographic maps covering the trinational region of Basel (Switzerland, Germany, and France). (http://www.unibas.ch/geo/mcr/Projects/KABA/index.en.htm).

(Table 4.1). For the purposes of the simulation, all rural and all urban classes have been aggregated to define a rural and an urban land-use percentage. In the present study, only the Basel agglomeration was considered when counting urban soil coverage, although some other cities are present in the domain (Mulhouse or Strasbourg in France). It is questionable whether urban areas several tens of kilometres away from the zone of interest can influence the meteorological situation over the city studied.

Table 4.1. Description of the 15 landuse classes defined in the KABA data base.

No	Land-use class (name)	Sample	z_0 [m]	d [m]	Albedo [%]	Height of roughness element [m]	Soil coverage [%]	Building density [%]
1	Railroad tracks		0.3	0	18	0	10	0
2	Gardens		0.5	0	15	2	20	10
3	High-density buildings		2.5	15	16	20	90	70
4	Village cores		2	10	16	15	80	70
5	Buildings in blocks		2	15	16	20	70	60
6	Buildings in line		1	10	16	15	60	50

7	Building complexes		3	20	17	30	50	40
8	Industrial areas		3	15	19	25	80	40
9	Forest		3	15	13	0	0	0
10	Grassland & orchards		0.1	0	16	0	0	0
11	Farmland		0.1	0	17	0	0	0
12	Water		0.001	0	9	0	0	0
13	Asphalted & concrete areas		0.01	0	18	0	90	0
14	Parks & sports fields		0.5	0	16	10	20	10
15	Single houses		0.6	5	16	10	40	30

Based on the information contained in Table 4.1, three urban classes were defined in terms of specific building parameters (width, height, density):

- dense urbanised areas: mean building height over 11 m, building density higher than 50 % (class 1)

- transition zone (suburban and industrial areas): mean building height between 8 and 11 m, building density between 40 and 50 % (class 2)

- village cores and single houses: mean building height below 8 m, building density lower than 40 % (class 3)

The percentage of urban area within a given cell is weighted with the soil-coverage and building-density data from Table 4.1 (columns 8 and 9). The urban-class definition described above was applied, both to the small and to the large simulation grid.

The thermal characteristics of the building materials were established using data from the literature (Martilli, 2002; Masson, 2002; Dupont, 2004), and refined after tuning of the model (considering the sensitivity analysis presented in Chapter 2). They differ slightly from the parameters used for the one-dimensional validation, inasmuch as they must represent the heterogeneity of the city rather than a single street (Table 4.2).

Table 4.2. Shape and physical properties of urban elements in the model: K_s is the substrate thermal conductivity of the material, C_s is the specific heat of the material, T_{int} is the initial temperature of the material, ε is the emissivity of the surface, α is the albedo of the surface, and z_0 is the roughness length of the surface.

Surface	K_s [$m^2 s^{-1}$]	C_s [$J m^{-3} K^{-1}$]	T_{int} [$°K$]	ε	α	Z_0 [m]
Wall	0.71e-6	2.1e06	293	0.90	0.2	---
Roof	0.79e-6	2.4e06	287	0.90	0.2	0.01
Street	1.05e-6	2.0e06	290	0.95	0.2	0.01

The three urban classes defined above only differ in the distribution of building-height density and in street widths (Table 4.3). Two perpendicular street orientations with angles of 70° and 160° were defined (identical in the three classes).

4.12

Table 4.3. Building-height distribution for the three urban classes defined.

Building height [m]	Percentage of buildings with this height [%]		
	Class 1	Class 2	Class 3
6	-	25	75
8	-	50	25
10	25	25	-
15	50	-	-
20	25	-	-
Building width	15 m	15 m	15 m
Street width	15 m	20 m	30 m

The rural percentages resulting from the KABA data base defined for each cell are shown in Figure 4.4, which is an example for the small domain. The city core of Basel still contains 20 % of rural area. It should be established, therefore, whether the latent heat flux resulting from vegetation areas within urbanized zones should be taken into account for the modelling process (see the results section of this chapter).
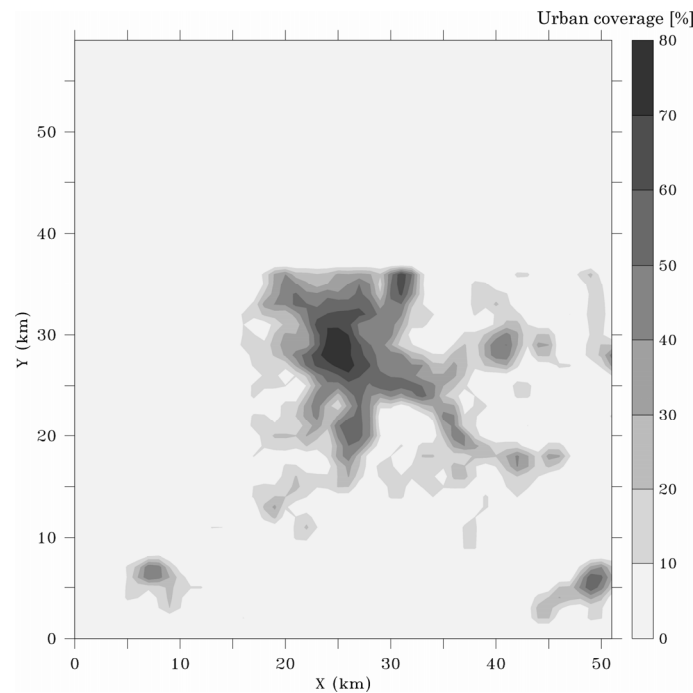
Figure 4.4. Percentage of urban soil coverage in the small domain.

4.3. The measured data

Measured data are available for several urban, suburban, and rural sites of the BUBBLE intense observation period (Figure 4.5). The principal urban site, "Basel-Sperrstrasse", has already been described in Chapter 3, since it was used for validation of the one-dimensional model. The other stations used are listed below (Table 4.4). The time resolution was 10 min for most of the stations and meteorological parameters. A few stations had a resolution of 30 min.
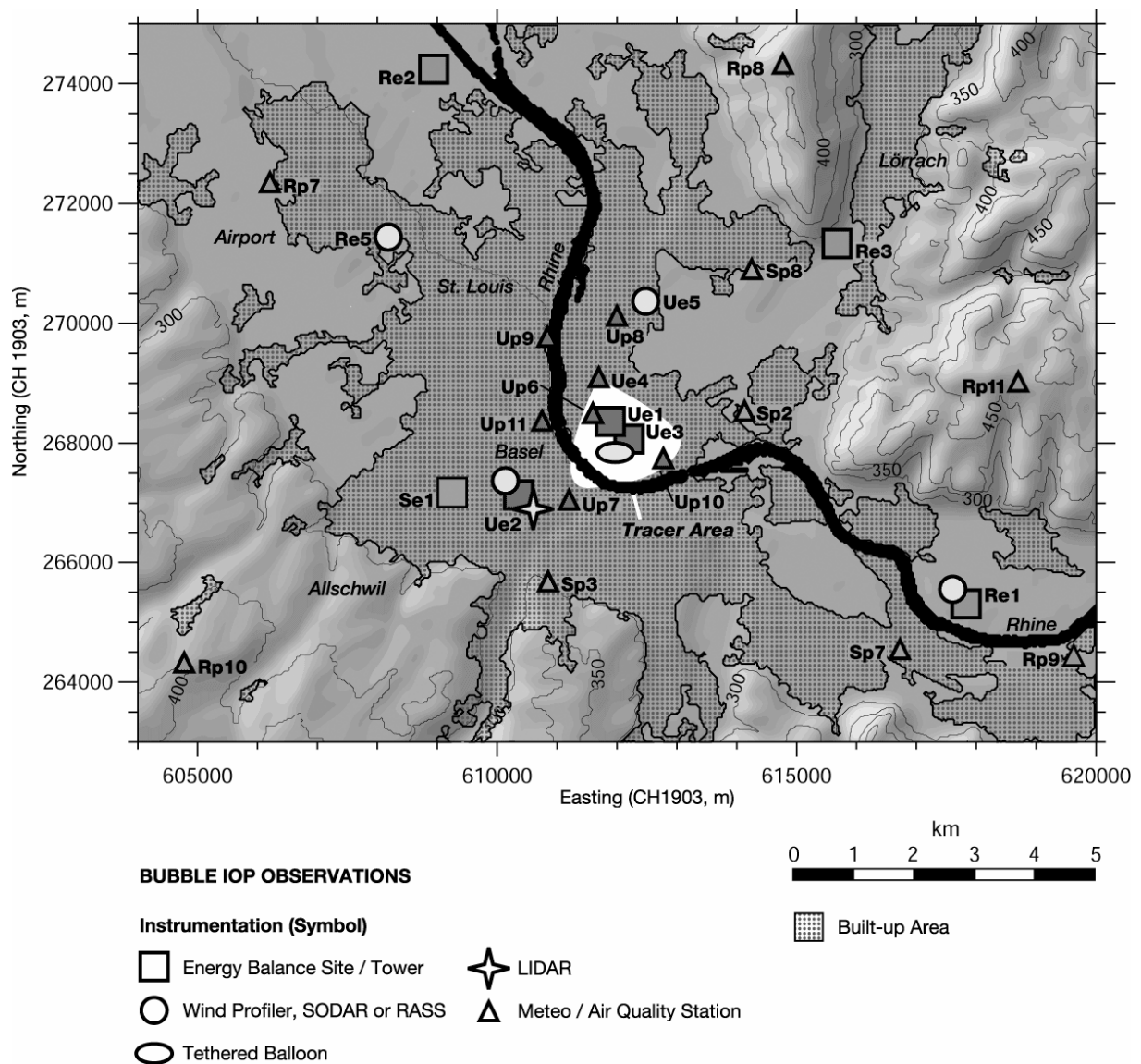

Figure 4.5. Location of the BUBBLE measuring sites (see the list of the stations in Table 4.4).

Data recorded in the context of BUBBLE have already been used and analysed. Christen *et al* (2003) studied turbulence profiles over three different urban and suburban sites. They found very similar behaviour for the three sites. Vogt *et al* (2003) studied vertical profiles of sensible heat flux within and above a street canyon. In connection with a pollutant-dispersion and tracer experiment, Rotach *et al* (2003) studied turbulence profiles in the urban roughness sublayer and showed that the turbulence statistics (such as velocity variances) commonly used in dispersion models may differ from observed values and lead to significant differences between observed and simulated surface concentrations.

Table 4.4. List and description of the measuring stations available for comparison with simulation results (see the location of the stations in Figure 4.5).

Code on map	Station name	Location [Swiss coordinates]	Height [m a.s.l.]	Providers
Rp6	Aesch Schlatthof	610375/258775	353	Lufthygienamt beider Basel
Se1	Allschwil	609250/267180	277	University of Basel
Rp7	Airport Basel-Mulhouse			Meteo France
Sp2	Basel Bäumlihof	614130/268540	289	Gymnasium Bäumlihof
Sp3	Basel-Binnigen (ANETZ)	610850/265620	316	MeteoSwiss, EMPA, BUWAL, University of Basel
Up6	Basel-Feldbergstrasse	611775/268500	255	Lufthygienamt beider Basel
Ue4	Basel-Horburg	611695/269040	254	University of Basel
Re3	Basel-Lange Erlen	615835/271310	275	University of Basel
Up7	Basel-Leonhard	611200/267055	273	Gymnasium Leonhard
Ue5	Basel-Kleinhüningen	612465/270475	265	METEK Gmbh
Up8	Basel-Novartis Klybeck	612000/270125	255	Novartis
Ue3	Basel-Messe	612200/268070	255	TU Dresden, Uni Freiburg
Up9	Basel-Novartis St. Johann	610840/269775	257	Novartis
Up10	Basel-Roche	612775/267750	255	Roche
Ue2	Basel-Spalenring	610360/267140	278	University of Basel, MeteoSwiss
Ue1	Basel-Sperrstrasse	611890/268375	255	University of Basel
Up11	Basel-St. Johann	610750/268375	260	Lufthygienamt beider Basel
Rp10	St. Chrischonaturm	618750/269000	490	MeteoSwiss Lufthygienamt beider Basel

Sp4	Dornach	613080/258930	325	Lufthygienamt beider Basel
Re4	Gempen	617640/257965	710	University of Basel
Re1	Grenzach	617830/265130	265	University of Basel
Sp5	Liestal LHA	621800/259950	320	Lufthygienamt beider Basel
Rp8	Oetlingen	614770/274270	450	University of Basel
Rp9	Pratteln Hardwasser	619625/264500	272	Lufthygienamt beider Basel
Sp6	Rheinfelden	626360/268045	285	UMEG Karlsruhe
Rp10	Schönenbuch	604775/264325	400	Institut für angewandte Pflanzneökologie
Sp7	Schweizerhalle	616725/264550	270	Lufthygienamt beider Basel
Re5	St. Louis	608100/271500	250	University of Freiburg
Re2	Village Neuf	608940/274240	240	University of Basel
Sp8	Weil am Rhein	614250/270905	250	UMEG Karlsruhe

For practical reasons and for reasons of data availability, not all stations listed above were used for the validation. It will be of interest, of course, to compare model results with data from stations representing all three types of land use (urban, suburban, and rural). For this purpose, eight stations were chosen:

- 4 urban stations: Sperrstrasse, Spalenring, Kleinhüningen, and St. Johann

- 2 suburban stations: Liestal and Allschwil

- 2 rural stations: Lange Erlen and Gempen

4.4. Results

Table 4.5 provides a listing of the simulations used for validation of the three-dimensional model. By comparing the results obtained by these different simulations, it will be possible to:

- point out differences between a traditional urban parameterisation and the detailed surface-exchange parameterisation scheme

- measure the influence of the city on PBL meteorological flow

- define the impact of the "flux-weighting" vs. the "rural or urban" method: the method

  implemented recently where urban and rural coverage is considered within each cell can

  be evaluated relative to the method in which a cell can only be urban or rural

- quantify the importance of horizontal resolution

- validate the model by comparing simulation results with measured data

-

Table 4.5. List of the simulations used for validation of the model. "*4-km res*" and "*1-km res*" indicates horizontal resolutions of 1 or 4 km, "*% urb/rur*" indicates that both urban and rural fluxes were calculated and the results weighted with the percentages of urban and rural soil coverage in each cell, "*urb or rur*" indicates that each cell is considered by the model, as either rural or urban, "*rural*" stands for a simulation disregarding urban areas, and "*trad*" denotes a simulation using the traditional method for simulating urban areas.

Simulation name	large	small	4km res	1km res	% urb/rur	urb or rur	rural	trad
urban	X		X		X			
urb_or_rur	X		X			X		
rural	X		X				X	
trad	X		X					X
urban_small_1k		X		X	X			
urb_or_rur_small_1k		X		X		X		
rural_small_1k		X		X			X	
trad_small_1k		X		X				X
urban_small_4k		X	X		X			

With a comparison between the different methods used to simulate urban areas ("*trad*", "*urban*", and "*urb_or_rur*") and from the impact of resolution ("*4-km res*" versus "*1-km res*"), it is intended to define the best compromise between accuracy of the results and CPU time needed for the simulation. With respect to horizontal resolution, a 4 km x 4 km grid simulation will be faster than a 1 km x 1 km grid simulation by a factor 16.

With a comparison of model results with measured data from several sites having different soil coverage (urban, suburban, and rural), it is intended to validate the model for these different

areas. This validation will mainly be performed for temperature and wind, which both are measured at every meteorological observation site. Where possible, turbulence fluxes will also be compared.

4.4.1. *Urban modelling: "urban" vs. "trad" simulation and impact of buildings on airflow*

The new urban parameterisation scheme is tested against the traditional method for simulating urban areas over the large and the small domain defined above. Simulation results for the large grid are compared with ground data from eight sites representing the three defined station types of urban, suburban, and rural (see the locations in Figure 4.5).

The rural and suburban temperature data reveal a greater diurnal amplitude than observed in urban areas, where accumulated daytime heat is released to the urban surface layer at nighttime. The model has a tendency to overestimate the amplitude of the diurnal cycle, and hence to produce higher maxima and lower minima than observed. Still, "*urban*" produces a better data fit than "*trad*", and is able to reproduce some local patterns not detected by "*trad*", *eg*, slope changes between 00 LT and 04 LT on 27 June for most of the stations, where temperatures calculated by "*trad*" continued to fall with a constant slope. The urban scheme overestimates nighttime cooling in the city, but it is able to reproduce the effect of heat release during the night as well as the formation of an associated, milder urban boundary layer (which are not revealed by the "*trad*" simulation).
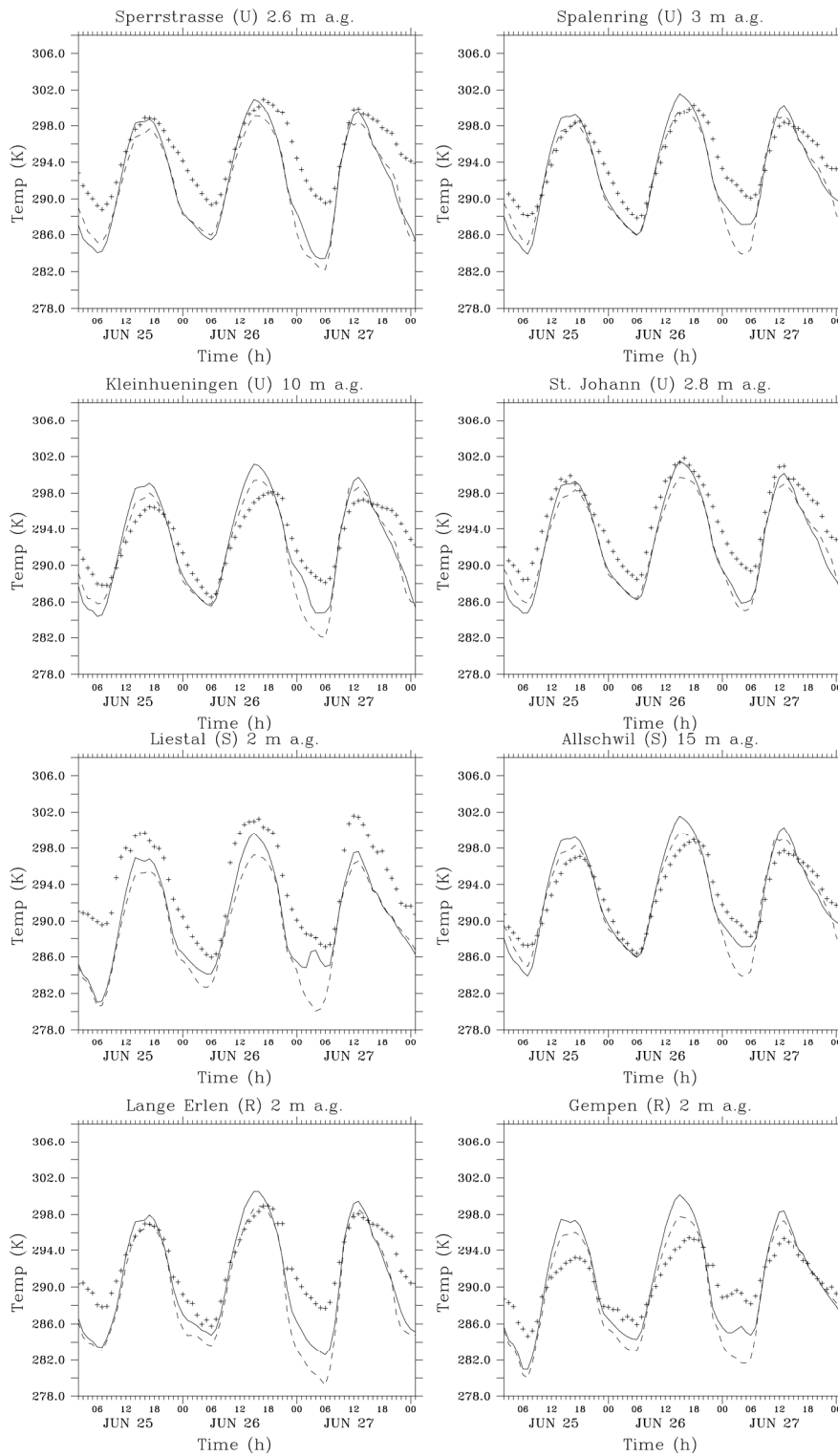
Figure 4.6. Temperatures at the ground as functions of time from 01 LT 25 June to 01 LT 28 June 2002 according to the "*urban*" (solid lines) and the "*trad*" (dashed lines) simulation in the large grid in grid cells corresponding to four urban (U), two suburban (S), and two rural (R) measuring sites; values observed *in situ* (crosses) are reported for comparison.

Fractional bias (which represents the absolute mean error of the model relative to the observations, see the definition given in Chapter 3) and root-mean-square differences (which represent the overall differences between model and observations, see the definition given in Chapter 3) for the temperatures (relative to the observations) are smaller for "*urban*" in all stations shown in Figure 4.6 (Figure 4.7).
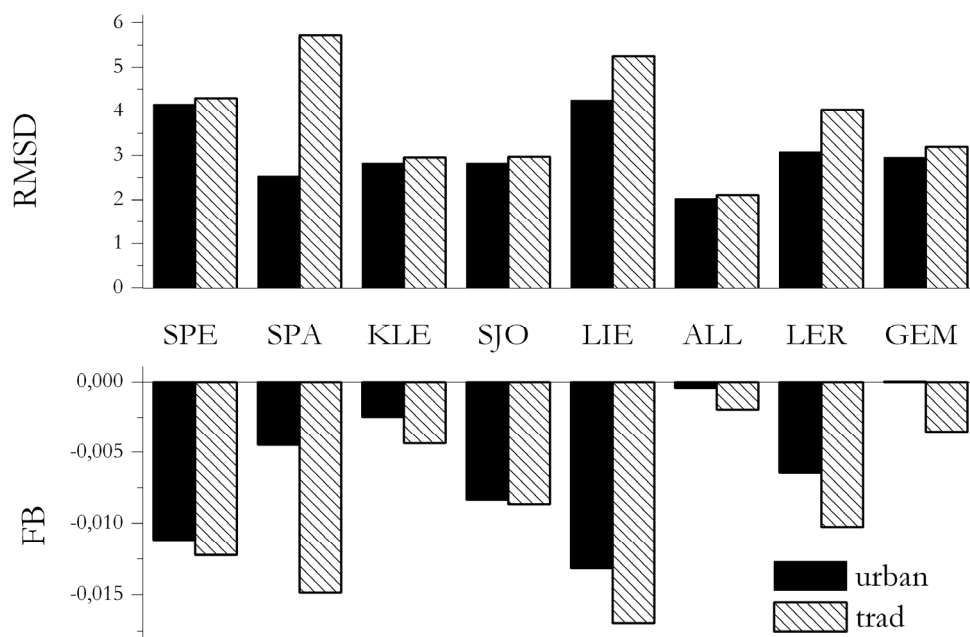

Figure 4.7. Fractional bias (FB) and root mean square difference (RMSD) of "*urban*" resp. "*trad*" temperature simulation on the large domain related to measurements from eight sites for the whole simulation period.

Because of anthropogenic sources of heat and pollution and because of water-proof surfaces (buildings, streets, etc.) that convert incoming radiation to sensible heat and store it more efficiently than the surrounding rural area, the surface layer in a city is generally warmer than that of its surroundings (Oke, 1982; Bornstein, 1987). This leads to formation of the so-called urban heat island. The temperature difference between urban and rural areas is proportional to the size of the city (in terms of inhabitants), and inversely proportional to the regional wind speeds (horizontal mixing between urban and rural zones will be less effective at lower wind speeds,

Oke, 1973). Temperatures at ground in the entire small domain were compared with results of a simulation neglecting urban calculation, denoted "*rural*", in order to see whether the "*urban*" simulation is able to reproduce this phenomenon (Figure 4.8).
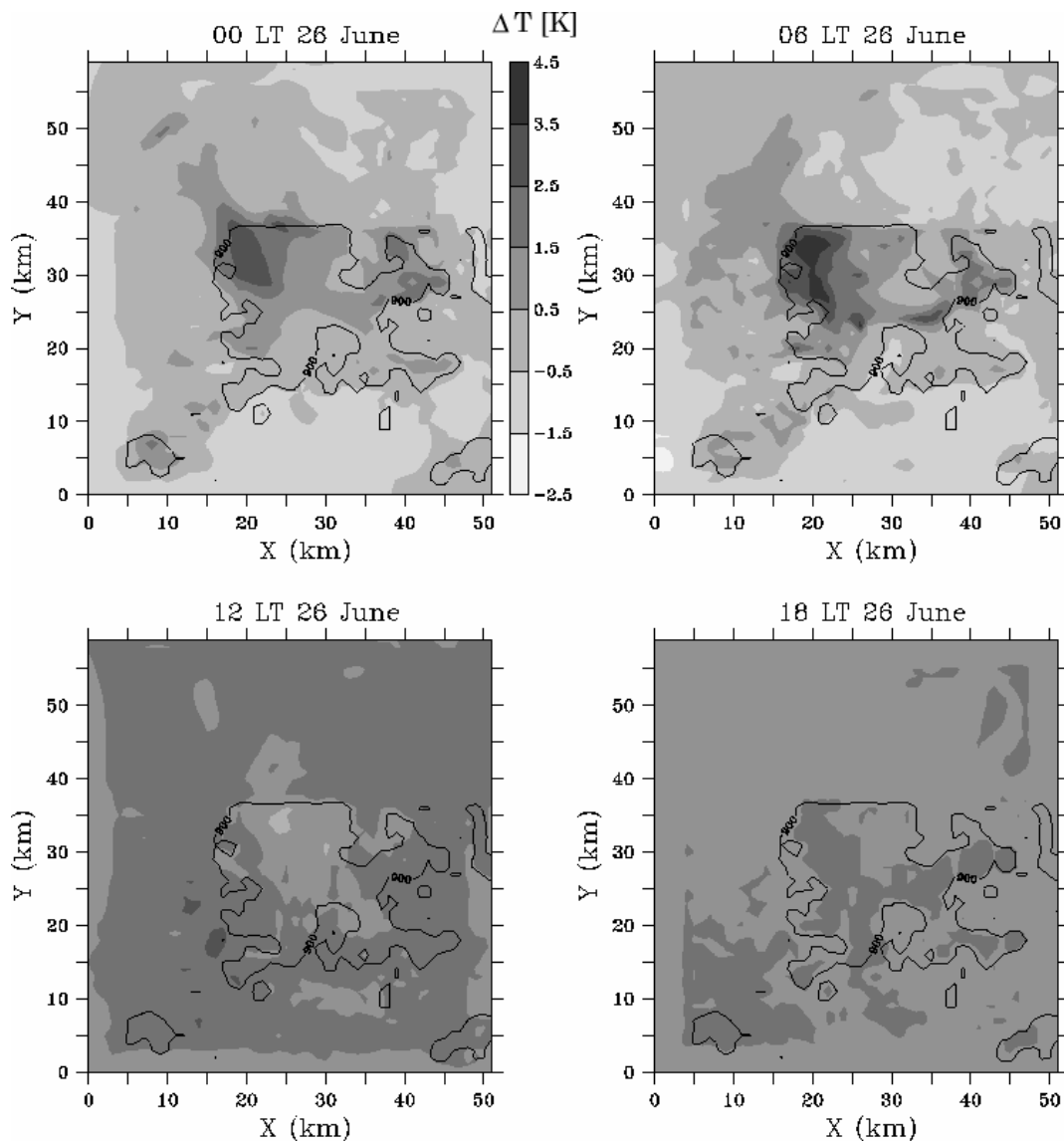

Figure 4.8. Temperature differences (in K) between the "*urban*" and "*rural*" simulation over the small domain at 2.5 m a.g. for 00 LT (top left), 06 LT (top right), 12 LT (bottom left), and 18 LT (bottom right) on 26 June. Positive differences indicate that "*urban*" is warmer.

Concrete and asphalted surfaces are able to store more of the incoming energy than the surrounding countryside, and boost its transformation to sensible heat flux. For this reason the

urban surface layer is warmer than its rural neighbour during the night. Larger temperature differences can indeed be seen in Figure 4.8 at nighttime when surface cooling through longwave radiation releases heat to the surface layer. The temperature differences between the two simulations vanish almost completely around noon, when solar heating overrides the effect of differential thermal properties.

Only two urban stations, Sperrstrasse and Spalenring, measured wind speeds in the street canyon, the other two (Kleinhüningen and St. Johann) measured the wind above roof height. The simulated flow-field deceleration within and directly above the street canyon caused by the presence of buildings can be assessed by comparing it with measured wind speeds and with the *"rural"* simulation (Figure 4.9).

It was confirmed when comparing results obtained in the three different simulations that both the traditional method and the new urban parameterisation are able to reproduce wind deceleration within and directly above the urban canopy. Just as shown by the measured data and by simulation results when validating the one-dimensional model (Chapter 3), a deceleration of the flow fields occurs, not only within the street canyon but also directly above roof height where friction with roof surfaces induces formation of a boundary layer and an associated log-type profile for the wind speeds. Here again, model results obtained within the street canyon (Sperrstrasse and Spalenring) and above roof height (Kleinhüningen and St. Johann) are influenced by buildings (lower wind speeds than according to *"rural"* model results).
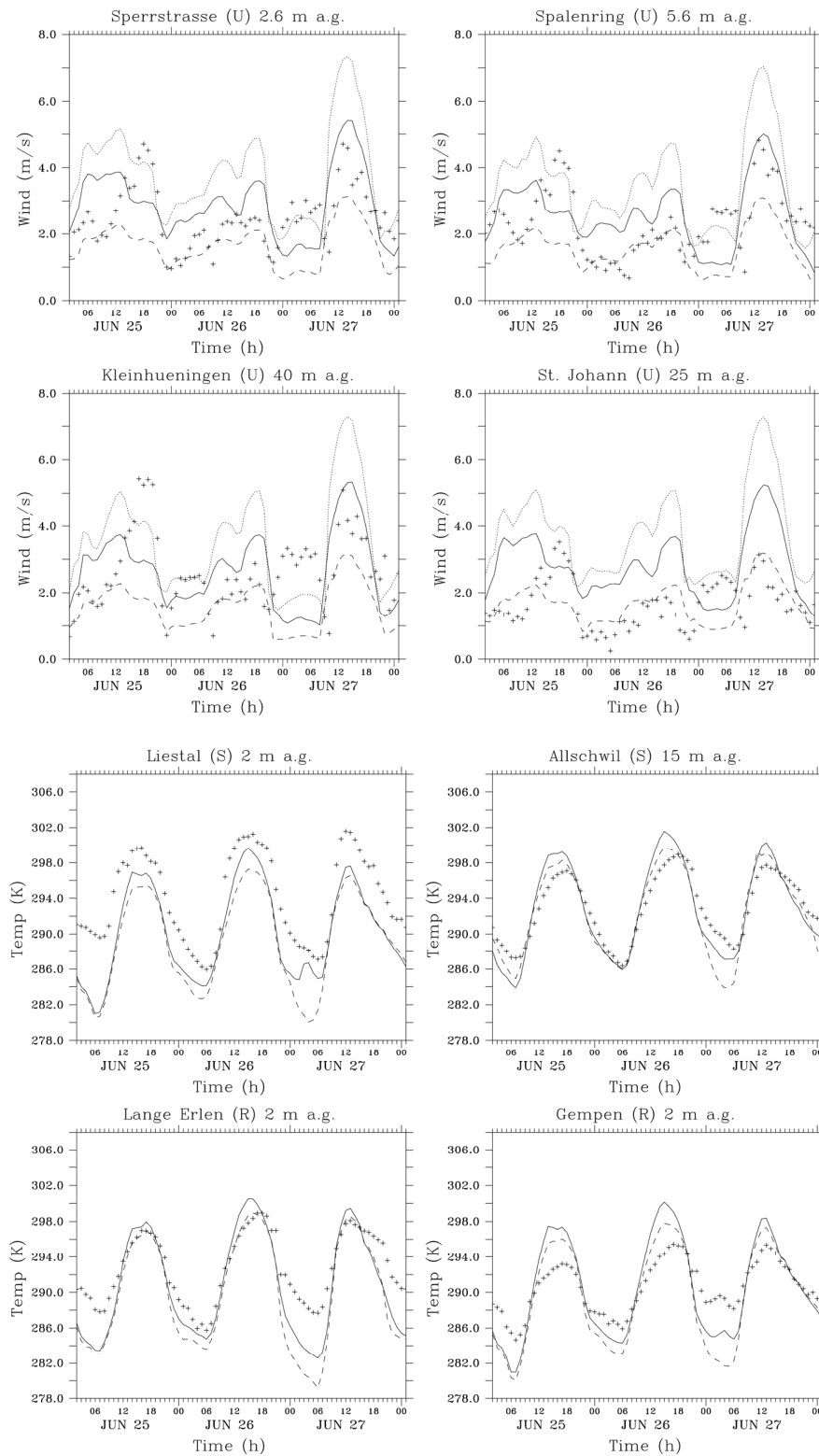
Figure 4.9. Wind speeds over the small domain at four urban (U), two suburban (S), and two rural (R) measuring sites as functions of time from 01 LT 25 June to 01 LT 28 June 2002 according to the "*urban*" (solid lines), "*trad*" (dashed lines), and "*rural*" (dotted lines) simulation and according to observations (crosses).

However, "*trad*" overestimates this effect, inasmuch as simulated wind speeds generally are lower than those measured. On the other hand, "*urban*" yields a better fit of the data, particularly so on 27 June during daytime when higher wind speeds were observed in the domain and the model was able to reproduce this increase (except for the St. Johann station, where lower wind speeds were measured).

The model has a tendency of overestimating wind speeds close to ground (Figure 4.9 and Figure 4.10). This is mainly due to the forcing of wind data. Simulated wind speeds are high close to ground, even though a correction was applied to the NCEP data according to Eq (4.1) for the last 200 m above the surface in order to restore a log-type profile and obtain reasonable wind speed values close to ground:

$$U\left(z_m\right) = U\left(z_f\right)\left(\frac{\ln\left(\frac{z_m}{z_0}\right)}{\ln\left(\frac{z_f}{z_0}\right)}\right) \tag{4.1}$$

where z_m represents the altitude in the mesoscale model, z_f the altitude of the forcing data, and z_0 the roughness length.

The wind directions measured at the eight sites reveal a high degree of conformity (the measuring point above the street canyon was used for Sperrstrasse and Spalenring), confirming the good quality of the BUBBLE data base. The model is not always able to reproduce the measured directions (Figure 4.10), as it is not possible to capture all local features that will influence the wind at a very specific point. The model is able to reproduce the formation of typical wind systems such as the downslope winds in valleys at nighttime (bottom left of Figure 4.10) or the higher wind speeds during daytime (top left) resulting from more important differential heating (the arrows in the four plots represent identical scales).
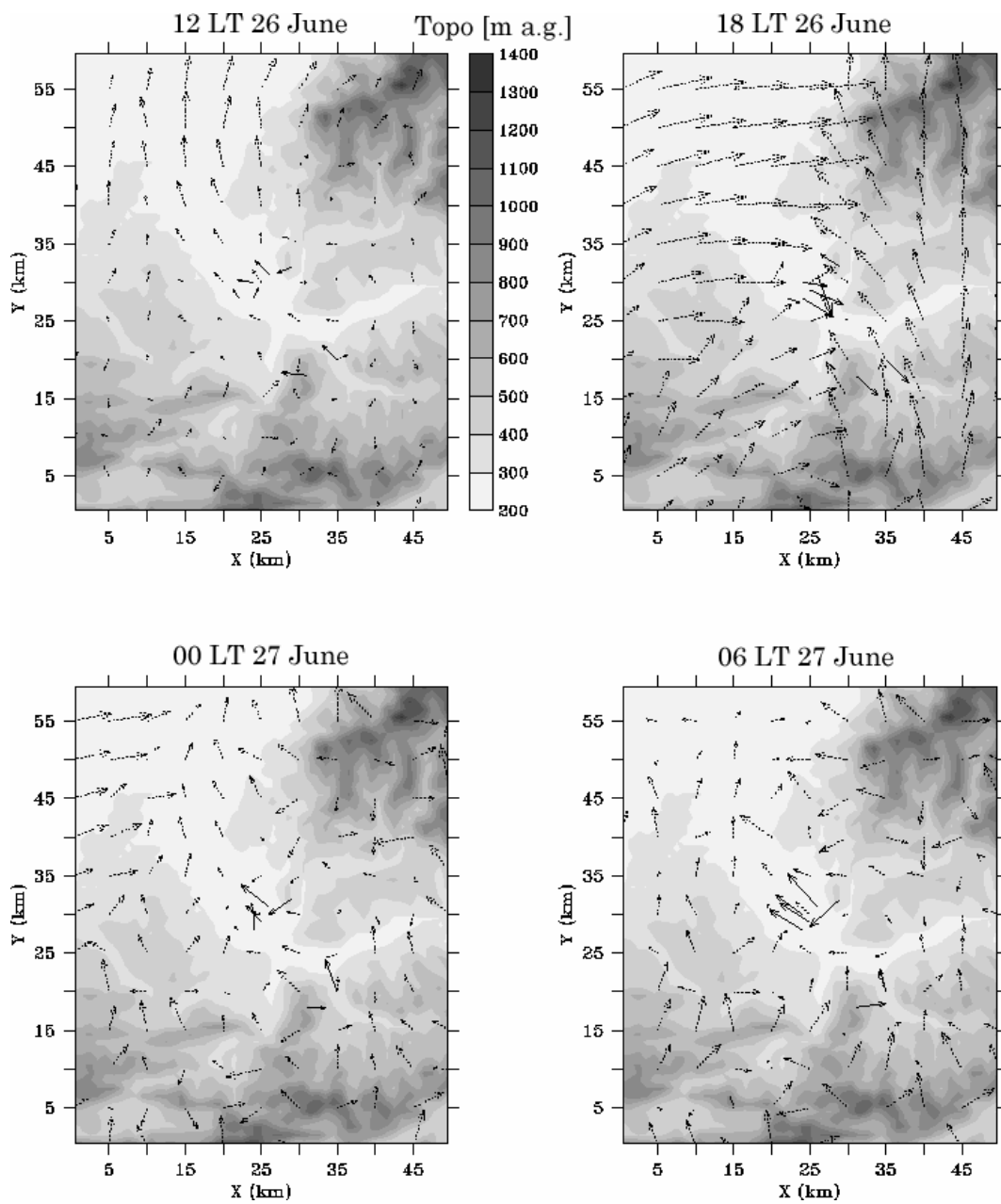
Figure 4.10. Wind directions calculated in the small domain by the "*urban*" simulation (dotted arrows) and measured at eight sites (solid arrows) at 12 LT 26 June (top left), 18 LT 26 June (top right), 00 LT 27 June (bottom left) and 06 LT 27 June 2002 (bottom right).

Values for the turbulent exchange of momentum expressed through the local friction velocity (u^*_L) confirm the results obtained in the one-dimensional validation (Chapter 3). While "*trad*" computes a constant vertical profile within and above the urban canopy (up to 50 m in Figure 4.11), "*urban*" is able to capture the decrease of momentum occurring at roof height (here, at 15 to 20 m) due to friction with the surface, and hence reproduce profile shapes in accordance with

the measured data. Still, the drop in simulated friction velocity occurs at a height (20 to 25 m) that is somewhat larger than the corresponding level in the measured profile (15 m). This is due, on one hand to the model setup, inasmuch as no grid point is available between 12 and 22 m above ground (10 m resolution near the ground), and on the other hand to the defined building-height distribution where the mean height is 20 m, which is representative for the Basel city core but not quite so for the Sperrstrasse site (here the mean height is 15 m, as shown in Chapter 3).
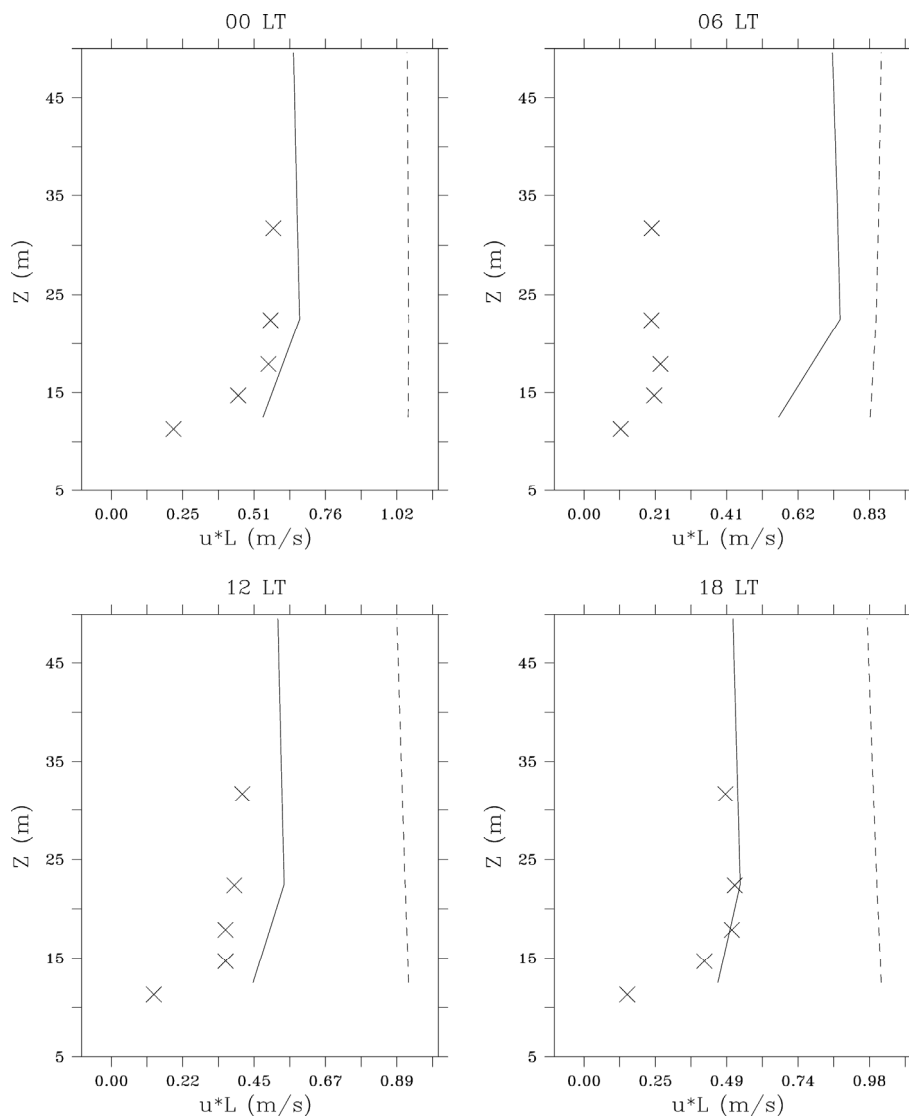

Figure 4.11. Measured vertical profiles (crosses) of local friction velocity ($u*_L$) within the urban canopy at the principal urban observation site (Sperrstrasse) at 00 LT (top left), 06 LT (top right), 12 LT (bottom left), and 18 LT (bottom right) on 26 June 2002, and simulation results according to the "*urban*" (solid lines) and "*trad*" (dashed lines) model for the corresponding cell in the small domain.

The model overestimates local friction velocities in the morning (06 LT in Figure 4.11). This is so because in the model, the onset of vertical diffusion and the development of turbulence occur too abruptly in the morning.

4.4.2. Impact of the "flux-weighting" vs. the "rural or urban" method

As described in Chapter 2, the mesoscale model can consider land-use fractions within given cells (the percentage of rural and urban coverage is determined within each cell). For a mixed cell, both types of fluxes must be calculated by the model (rural with the soil module, and urban with the urban parameterisation scheme). The extra cost in CPU time caused by this double calculation is of the order of 5 % relative to a simulation without fractions (where a cell is defined as rural or urban). It will be important, therefore, to assess the impact of this modification on the quality of the simulation. For this purpose, results of a simulation without land-use fractions ("*urb_or_rur*") were compared with the "*urban*" simulation, where rural and urban calculations are performed in each mixed cell, and with measured data.

The results obtained by the "*urban*" and the "*urb_or_rur*" simulation in the large grid are very similar for Sperrstrasse and Allschwil (upper left and right-hand parts in Figure 4.12). The grid points corresponding to these two stations are both defined as urban area in the "*urb_or_rur*" simulation, but as 45 % or 56 % rural, respectively, in the "*urban*" simulation. Land use in the cells corresponding to Gempen and Liestal in "*urban*" corresponds to 85 % and 88 % of rural coverage, respectively, hence they are defined as rural in the method without land-use fractions.
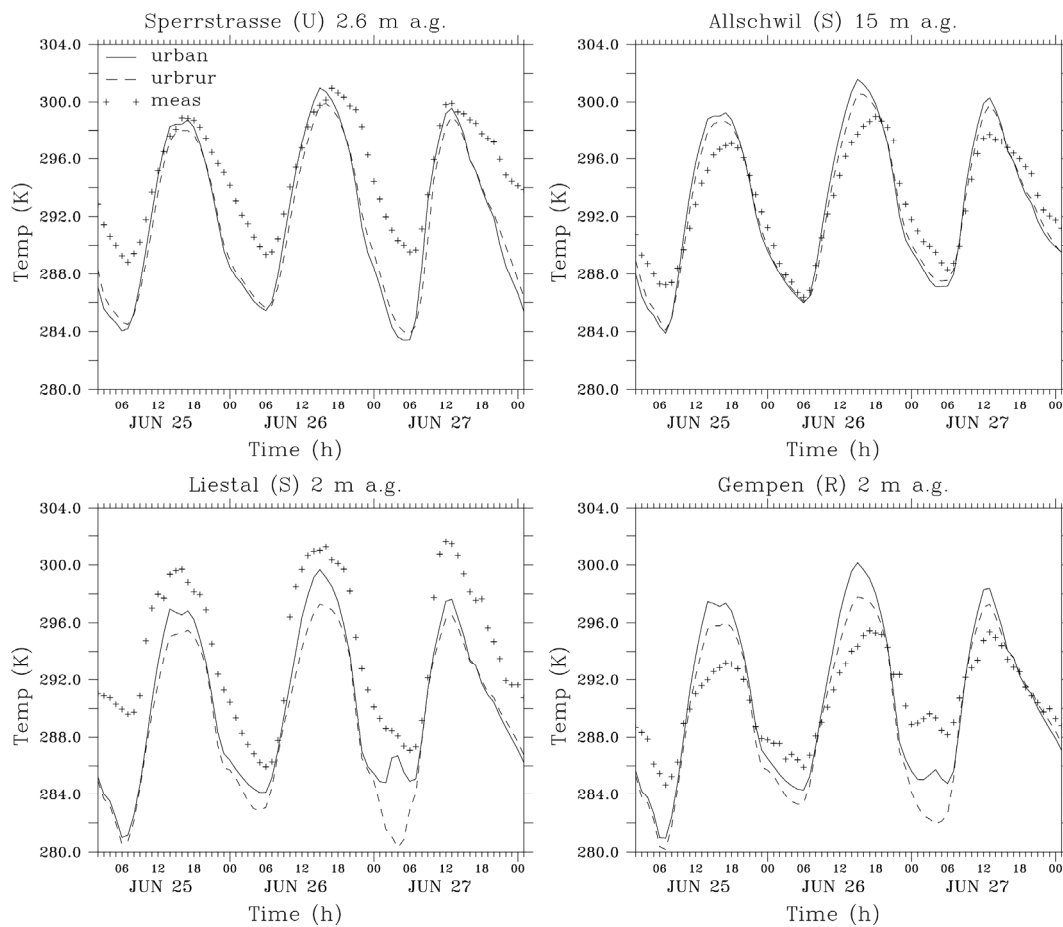
Figure 4.12. Temperatures as functions of time from 01 LT 25 June to 01 LT 28 June 2002 according to the "*urban*" (solid lines) and "*urb_or_rur*" (dashed lines) simulation in the large grid at Sperrstrasse (U), Allschwil (S), Liestal (S), and Gempen (R); observed values (crosses) are reported for comparison.

Neglecting the rural part of the calculation within an urban area, as in the two cells defined as urban (shown in the upper half of Figure 4.12), does not appear to have any impact on temperature results close to ground. To the contrary, neglecting the urban part of the calculation in cells containing a major part of rural coverage, and defined as rural in the "*urb_or_rur*" method, can have an impact on the simulated temperature distribution, as shown in the lower half of Figure 4.12. Temperatures calculated while allowing for land-use fractions are higher, particularly so during nighttime when the other method clearly underestimates the temperatures. The method disregarding land-use fractions is actually unable to reproduce weaker nighttime cooling of the

roughness sublayer (by heat release from urban surfaces) in rural grid cells that contain a few percent of urban coverage.

As a conclusion for simulations involving a horizontal resolution of 4 km, the positive impact of the inclusion of land-use fractions on temperature is significant, mainly for rural grid points containing a minor fraction of urban coverage. In other words, neglecting a minor part of rural coverage within an urban area appears to have no impact on temperature in the model, while neglecting a few percent of urban coverage at a predominantly rural grid point appears to lead to significant temperature bias.
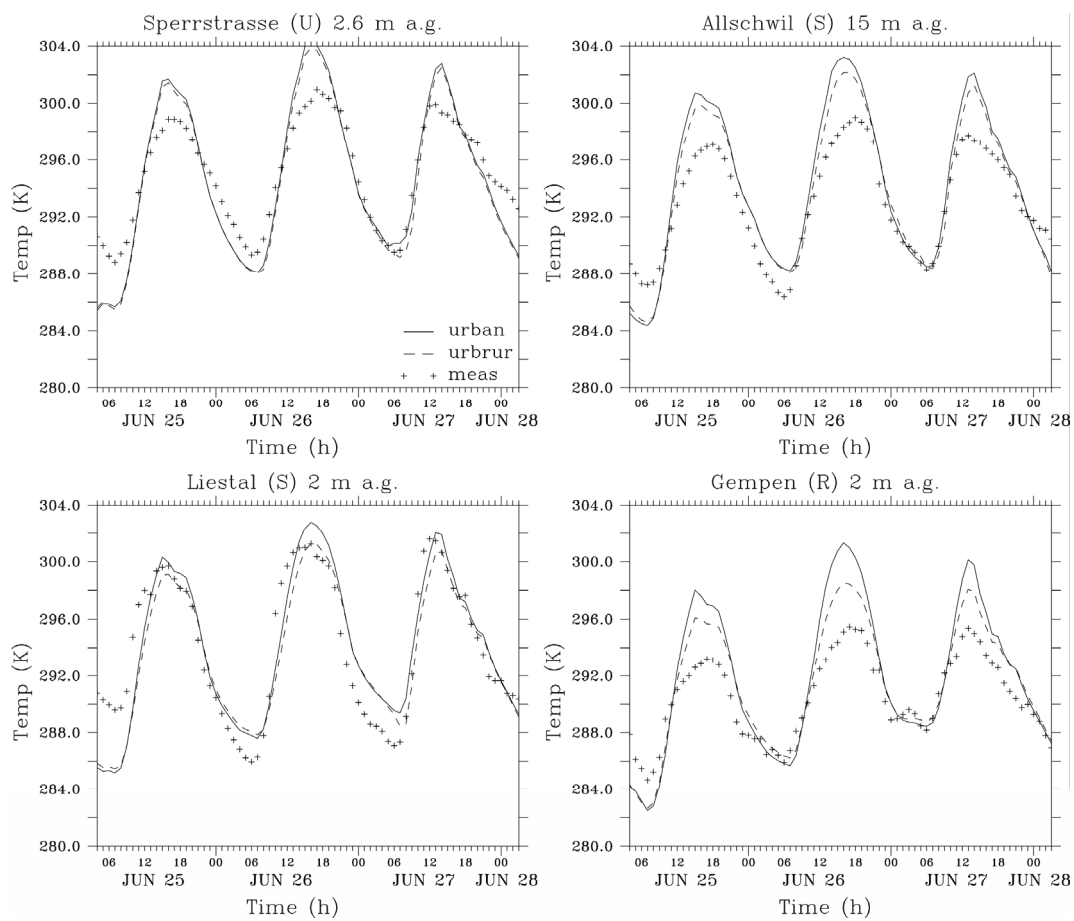

Figure 4.13. Temperatures as functions of time from 03 LT 25 June to 03 LT 28 June 2002 according to the "*urban*" (solid lines) and the "*urb_or_rur*" (dashed lines) simulation in the small grid at Sperrstrasse (U), Allschwil (S), Liestal (S), and Gempen (R); observed values (crosses) are reported for comparison.

The picture obtained in the high-resolution grid (1 km by 1 km) is slightly different (Figure 4.13). Due to finer resolution, the grid point corresponding to Liestal is now defined as urban. The two simulations now reveal rather small differences at this point, just as found for the Sperrstrasse and Allschwil sites which are also considered as urban in the method disregarding fractional land use. The last grid point shown in Figure 4.13, Gempen, is defined as rural (just as in the grid with 4 km resolution). Nevertheless, in the high-resolution grid the differences between the two simulations are much smaller than in the low-resolution grid, particularly so during nighttime. The results are in even better agreement in the method disregarding fractional land use during day time.

The flux-weighting technique appears not to have any positive impact on temperatures calculated with a finer horizontal resolution. This suggests that a finer grid is able to compensate for the neglect of urban coverage within rural areas. Therefore, decisions as to the choice of horizontal resolution and the method for flux calculations (with or withouit fractions) would depend on a number of factors such as:

- size of the domain: simulation over a large domain with very high resolution will take much more CPU time

- accuracy of land-use input data: nowadays, very accurate land-use data bases (with a resolution of 1 km or better) covering the entire planet are available on the Internet

- computing power, particularly when longer episodes (*eg*, one week) are to be simulated.

4.4.3. *Impact of horizontal resolution*

The horizontal resolution of the model grid has a determining impact on the quality of the results. High resolution will lead to more accurately calculated meteorological fields. This is due to the more precise input information on topography and land use. It was seen when comparing

the topography and definition of urban areas in the large grid with a resolution of 4 km (Figure 4.1) and in the small grid with a resolution of 1 km (Figure 4.3) that the latter contains more detailed information. Hence, the model will be able to account for specific local processes induced by topography or land use (*eg*, local wind systems in a small valley not seen by a 4-km resolution topography). Moreover, model results from a fine grid are more accurate due to a more precise spatial discretisation. There is a factor 16 between the numbers of model points at 1 km by 1 km and 4 km by 4 km resolution. Hence, a finer grid will yield more detailed meteorological field patterns.

Usually there are two sides to any problem. Choosing the highest available resolution (defined by that of the input data, as there is no point in having a model grid resolution higher than the resolution of the input data) is not always the best solution. Other elements have to be taken into account. First, the parameterisation and the assumption used to solve the governing equations of a mesoscale model are valid over a certain range of cell sizes, usually from 1 to 10 km. Secondly, resolution has to be adapted to domain topography. A complex terrain (one with sharp variations) needs a high resolution in order to account for these rapid changes of the surface. Lastly, increasing the resolution means an increase in the cost of CPU time used for the calculations. As mentioned above, the 1 km by 1 km resolution has 16 times more points than the 4 km by 4 km grid. Hence, simulations in a given domain will be longer by at least a factor of 16 in the 1 km by 1 km grid. The difference becomes even more important inasmuch as larger cells can be resolved with a lower time discretisation and still satisfy the CFL criteria (see Chapter 2). In other words, the finer the resolution, the more grid points are needed and the shorter the time step. It is of interest, therefore, to assess the impact of resolution on the simulation results, and hence see whether a higher resolution can produce results compensating the extra cost in

calculation time. This decision is a matter of personal appreciation, priorities (accuracy versus calculation time), and hardware (computing power).

For an evaluation of this point, a 4 km by 4 km grid was defined in the same small domain as the 1 km by 1 km grid. Three different sets of results could then be compared with each other and with data measured *in situ* (Figure 4.14): results obtained in the 1 km by 1 km grid, results obtained in the 4 km by 4 km grid, and results obtained with 1-km resolution but averaged to the 4-km grid. This last set of results is obtained by averaging the results for the 16 points in the fine grid that correspond to one point in the small domain with a 4-km resolution. Both simulations were run with the urban module and with the flux-weighting method (percentage of rural and urban land use in each cell).
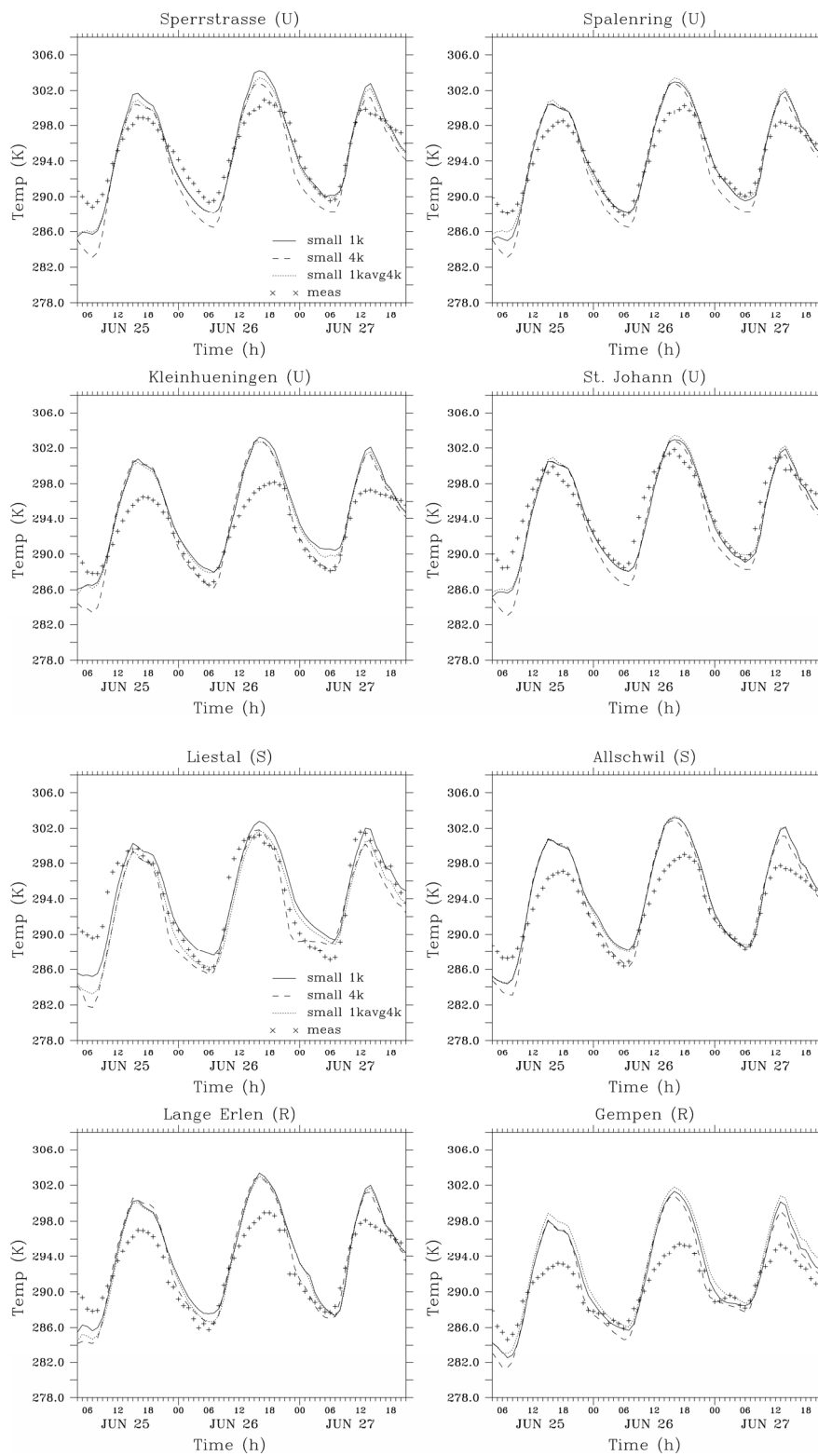
Figure 4.14. Temperatures as functions of time from 03 LT 25 June to 21 LT 27 June 2002 close to ground for 1-km resolution (solid lines), 4-km resolution (dashed lines), and with the 1-km-grid results averaged to the 4-km grid (dotted lines) of the small domain at four urban (U), two suburban (S), and two rural (R) measuring sites; observed values (crosses) reported for comparison.

The three sets reveal rather small differences. Still, temperatures calculated in the 4-km-resolution grid are lower by 1-2 K during nighttime in the urban area, while the 1-km grid and its averages in a 4-km grid yield identical results and a better fit of data measured *in situ* (except for the Kleinhüningen station). The temperature differences vanish during daytime for all the stations shown in Figure 4.14, except for Liestal and Gempen. The percentages of rural and urban coverage in these two cells may undergo a strong modification by changing the horizontal resolution, as they are located in transition zones between urban and rural.
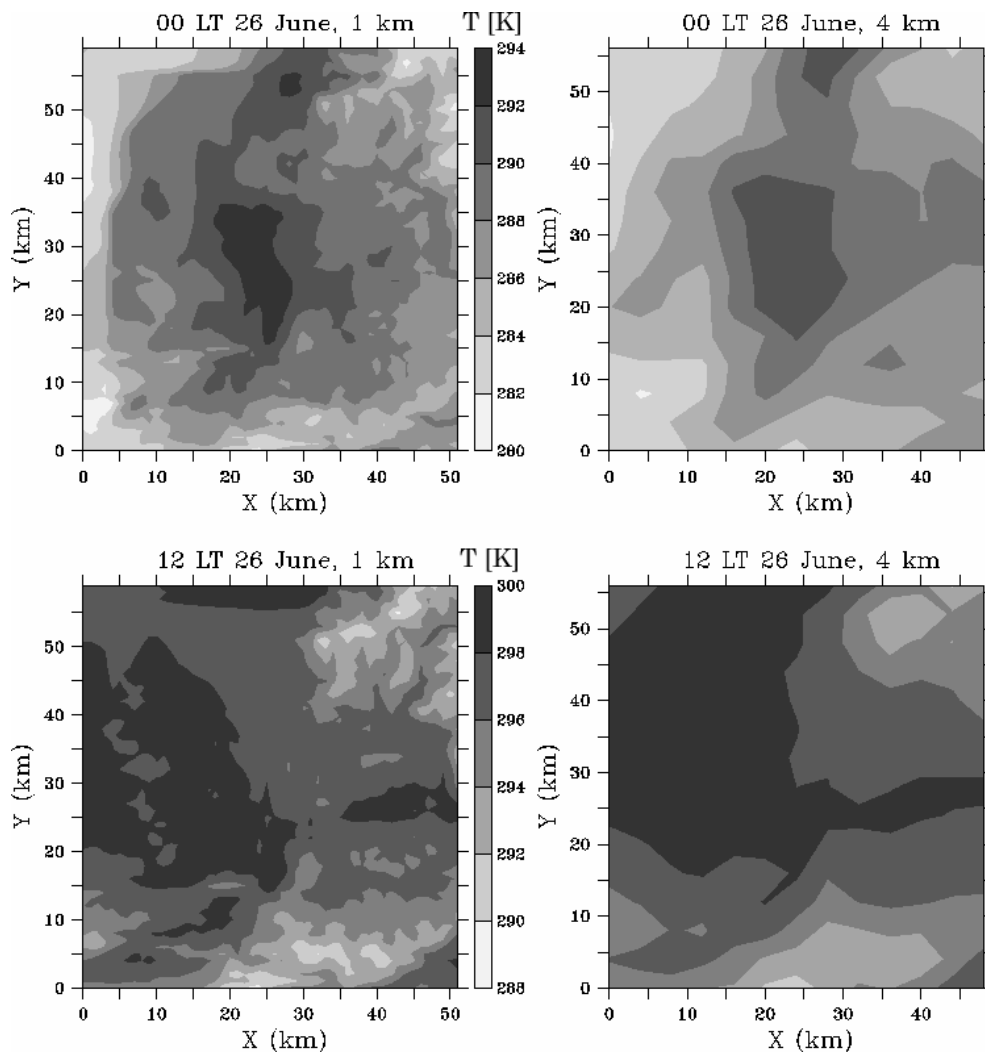

Figure 4.15. Temperature fields at 2.5 m a.g. according to simulations with 1-km (left) and 4-km (right) horizontal resolution over the small domain for 00 LT (top) and 12 LT 26 June 2002 (bottom).

Two-dimensional maps of the domain reveal the impact of horizontal resolution more clearly than a comparison of results for given points as shown above. Just as for the resolution of topography and land-use input, a model output having a higher resolution will produce more detailed meteorological fields (Figure 4.15).

As mentioned in the previous section, horizontal resolution and land-use definition (mixed cells versus entirely urban or entirely rural cells) are two input parameters that influence the model results. Statistical results (fractional bias and root-mean-square differences relative to measured data) for the 4-km grid in the small domain were compared with results for the 1-km grid simulation (Figure 4.16) in order to determine whether the method allowing for fractional land-use patterns can compensate for lower resolution. (Both simulations employ the method allowing for fractional land-use patterns.)
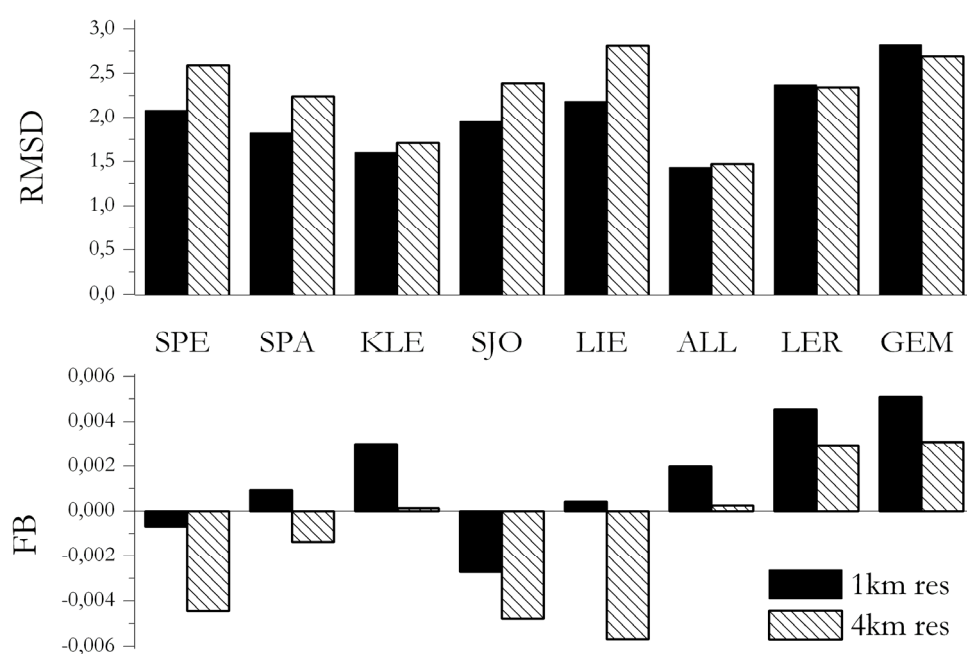

Figure 4.16. Fractional bias (FB) and root mean square difference (RMSD) to ground measurements from eight sites of 1 km resp. 4 km horizontal resolution temperature simulation with landuse fractioning.

The root-mean-square differences and the fractional bias tend to be lower for the 1-km-resolution grid in urban and suburban areas, while the 4-km resolution appears to perform better for rural areas (although RMSD against measured data are very similar between both simulations).

The same statistical parameters were calculated for the simulation with the two grid resolutions without land-use fractions ("*urb_or_rur*" method, Figure 4.17).
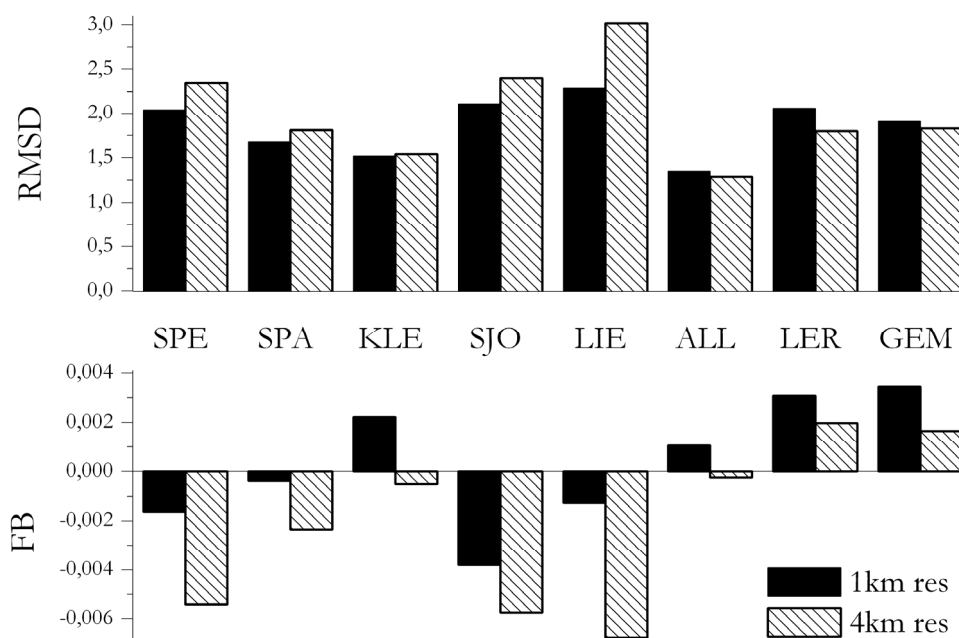

Figure 4.17. Fractional bias (FB) and root mean square difference (RMSD) to ground measurements from eight sites of 1 km resp. 4 km horizontal resolution temperature simulation without landuse fractioning.

For almost all stations (except Liestal), the statistical results of Figure 4.17 (without land-use fractions) are better than the results of simulations involving land-use fractions. Statistics, therefore, does not confirm the results obtained in the previous section, where it was found that neglecting the urban contribution in predominantly rural cells had a negative impact on temperature simulation.

Still, the overall differences between simulation and observations are reasonably low (between 1.29 and 3.02 K) for all stations. Thus, a change in horizontal resolution or the use of the land-coverage fractions will not dramatically influence model results at a given point, but will have an impact on the overall horizontal meteorological field pattern (see, *eg*, Figure 4.15).

4.4.4. *Turbulence*

Measurements of the turbulent activity are available mainly at the ground, and only in few stations. Sperrstrasse and Spalenring provide a profile reaching to 35 m a.g..
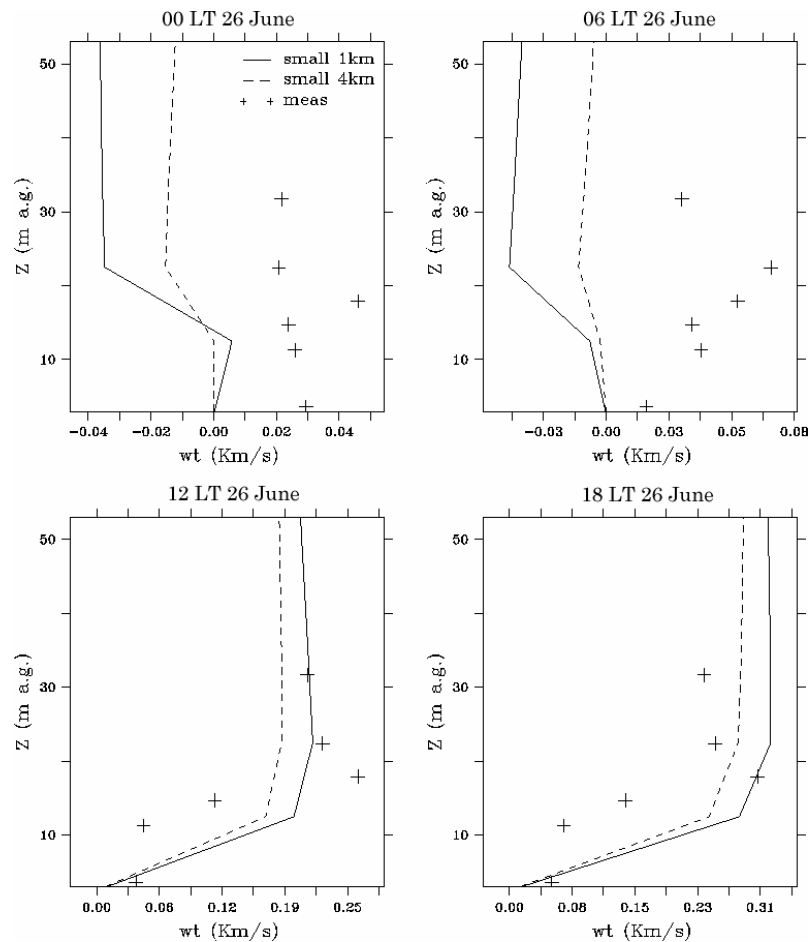

Figure 4.18. The profiles of turbulent vertical fluxes of sensible heat ($\overline{w'\theta'}$) simulated by the model in the small domain with 1-km resolution (solid lines) and with 4-km resolution (dashed lines, and data measured at the Sperrstrasse site within and above the street canyon (crosses), at 00 LT 26 June (top left), 06 LT 26 June (top right), 12 LT 26 June (bottom left), and 18 LT June 2002 (bottom right).

The turbulent vertical fluxes of sensible heat ($\overline{w'\theta'}$) simulated with "*urban*" are compared with measured data from Sperrstrasse in Figure 4.18.

The results show that the model with urban parameterisation is able to reproduce the vertical patterns of heat flux within and directly above the street canyon. Differences in shape arise from the vertical resolution of the model, which has no point between 12 and 22 m a.g., and hence is not able to capture vertical changes with the same accuracy as do measurements.

An impact of horizontal resolution on the vertical turbulent profiles within the surface layer appears to be present particularly during nighttime when the two sets of results (solid and dashed lines in Figure 4.18) differ most strongly.

It will be of interest to report the mixing heights calculated with the model in order to see whether the diurnal cycle can be recognised and the values are reasonable. The mixing height is defined as the altitude beyond which the vertical potential-temperature profile beomes inhomogenous. During daytime when turbulent mixing is active, the mixed layer is called the convective mixed layer. Its daytime development can be followed by plotting potential-temperature profiles at different times.

The simulated turbulent mixing heights are higher over urban areas, as seen out in Figure 4.19 and Figure 4.20. This is due to the fact that the urban boundary layer is warmer than its surroundings, causing turbulent eddies to reach higher altitudes above the Earth's surface.
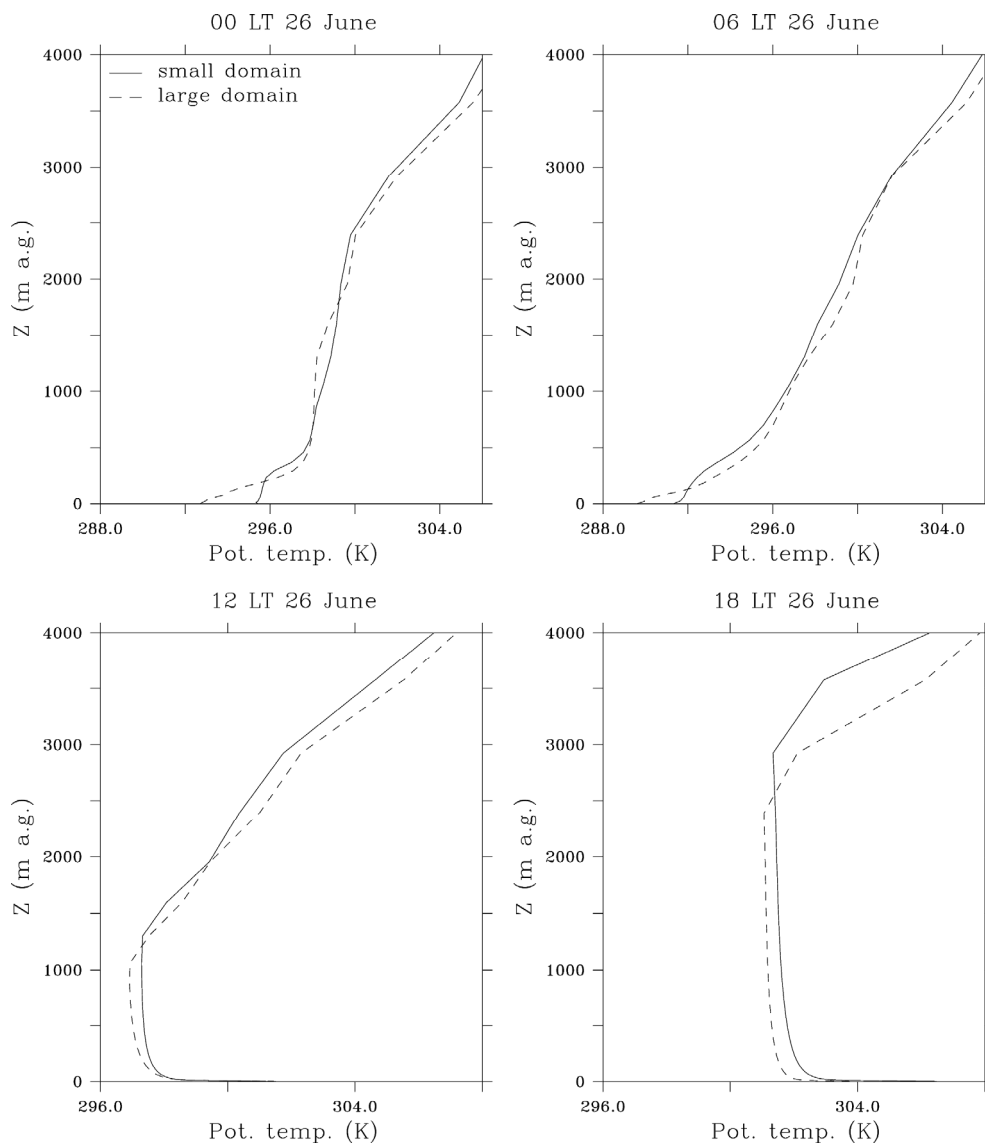
Figure 4.19. Development of the mixing layer in urban areas. The maximum mixing height is attained in late afternoon (bottom right), with about 2500 m a.g. for the simulation in the small domain and 3000 m a.g. for the simulation in the large domain.
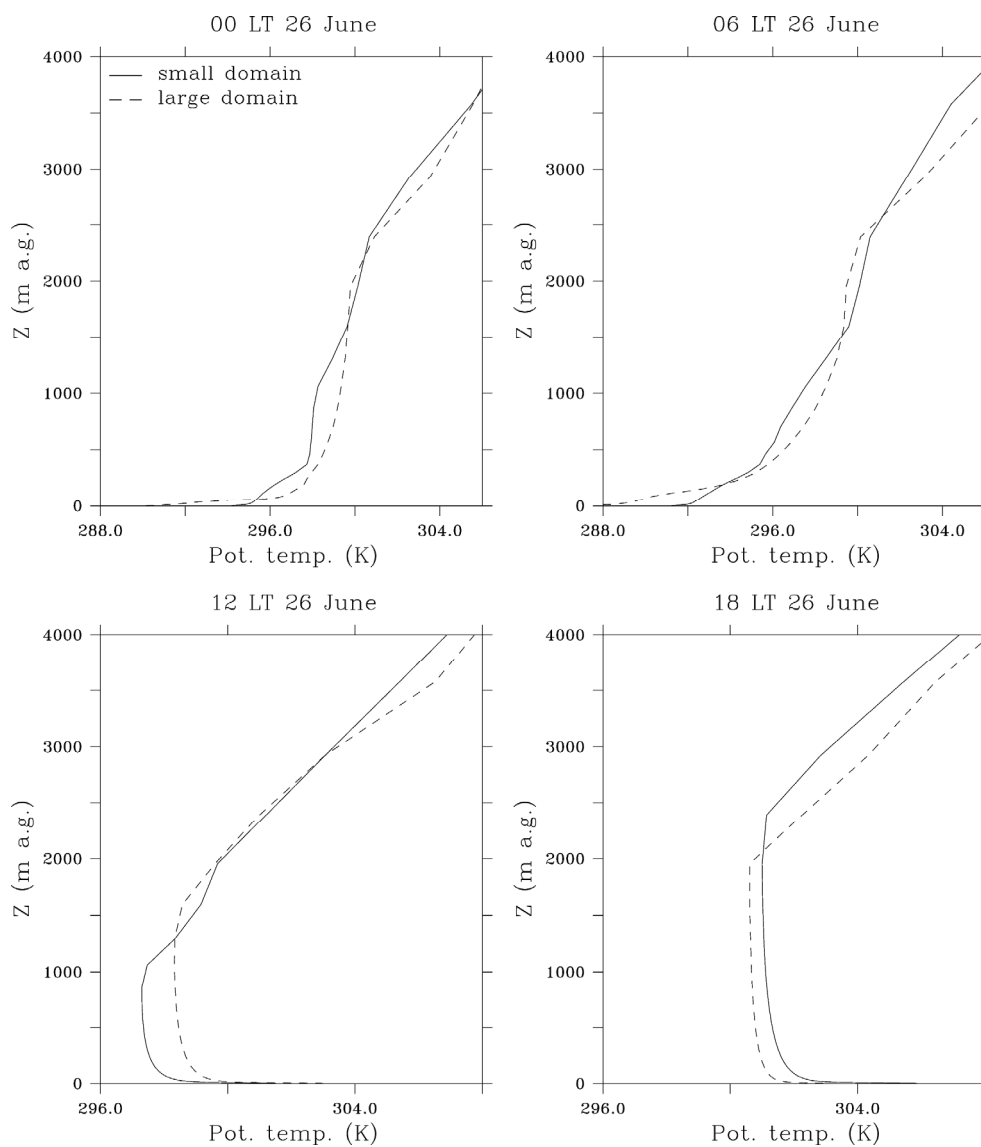
Figure 4.20. Development of the mixing layer in rural areas. The maximum mixing height is attained in late afternoon (bottom right), with about 2000 m a.g. for the simulation in the small domain and 2500 m a.g. for the simulation in the large domain.

The maximum mixing height is reached in the late afternoon when skies are cloudless. Solar activity heats up the ground during all this time, and accumulated heat and energy give rise to turbulent eddies of maximum size. Unfortunately, measured potential-temperature profiles are not available to validate the simulated mixing heights, but the pattern obtained by the model appears reasonable when confronted with theory (Stull, 1988) and with observations from other studies, and it is reasonable that the simulated convective mixed layer is thicker in urban

environments. Measurements made during May 2002 over the city of Hannover (Emeis *et al*, 2004), which can be compared to Basel in terms of climatology, gave a convective mixing-layer height of the order of 1000 m. This is less than the 2000 to 3000 m found here, but due to higher turbulent activity, the mixed layer will in general be higher on a warm mid-summer day than on a day of spring. Sodar data collected in northern Austria during the summers of 1997 and 1998 gave mixing-layer thicknesses of up to 2400 m (Baumann *et al*, 2001).

4.4.5. *On the utility of radiation forcing*

It has been mentioned in the description of the mesoscale model that a possibility exists to force the radiation in the model using experimental data. This should allow one to indirectly account for cloud episodes over the simulated domain. Some clouds did in fact develop over Basel during the afternoon on the fourth day of simulation (28 June). This is an opportunity to determine the impact of this option (added recently) on the simulated temperature distribution (Figure 4.21).
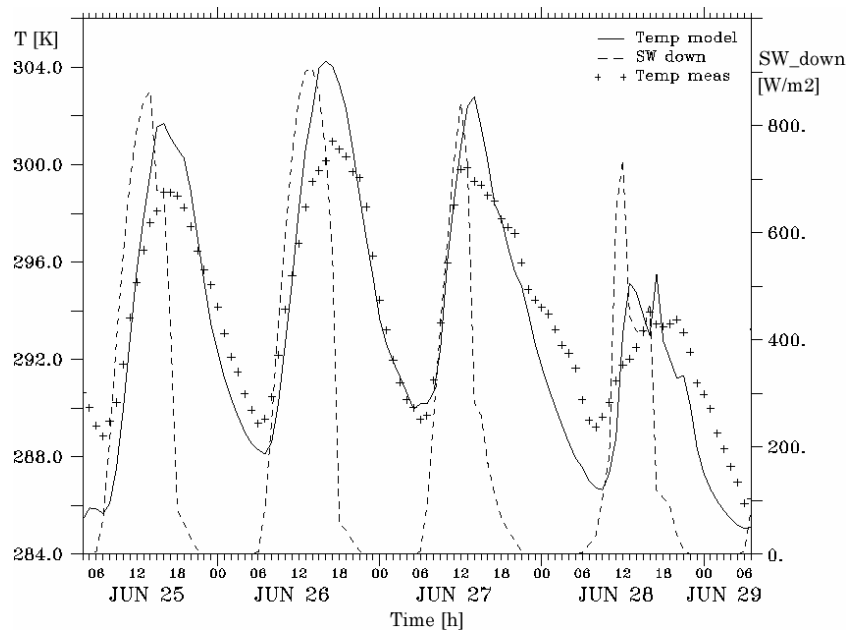

Figure 4.21. Temperatures calculated by the model (solid lines, left-hand scale) and the prescribed, incoming shortwave radiation (dashed lines, right-hand scale), set in relation to the temmperatures measured *in situ* (crosses, left-hand scale) at Sperrstrasse from 04 LT 25 June to 07 LT 29 June.

The strong decrease in measured temperatures occurring in the afternoon of 28 June is well reproduced by the model thanks to radiation forcing in the calculation. This example demonstrates the utility of such a forcing. However, it is not always possible to obtain the radiation input data needed. The method can be extremely useful when the simulated meteorological fields are used to feed a photochemical model for calculations of air pollutant concentrations. The intensity of photochemical reactions in the atmosphere is a function of the solar energy currently available. Therefore, neglecting clouds and the related decrease of incoming radiation can lead to overestimating the formation of pollutants (such as ozone) or their destruction.

4.5. Conclusions

The mesoscale model was applied to two nested grids over Basel and its surroundings. Several model versions have been tested varying the horizontal resolution, the parameterisation method for the urban area (using the new parameterisation scheme or the traditional method), and the use of land-use input data (fractions of rural and urban coverage within a given cell, or taking each cell as being entirely urban or entirely rural). The simulation results were compared with data measured at several observation sites located in urban, suburban, and rural areas, since validation of this model in three-dimensional simulations was one of the major objectives.

When comparing results obtained by simulations using the detailed parameterisation scheme were compared with results obtained by the traditional parameterisation method, it was seen that the new scheme is better able to account for the influence of a city on PBL flow. This constitutes confirmation of the results obtained in the one-dimensional validation performed in Chapter 3. The urban scheme can capture most of the urban-induced processes, such as the urban heat island. Still, simulated daytime temperatures estimated by the model often appear to be high. It

was seen when comparing them with measured temperatures that they increase faster than the observed values, and hence overestimate the maximum. Moreover, the changes in shape of the curve around the maximum are sharper (see, *eg*, Figure 4.14). This trend should be analysed and, if possible, corrected in the future. According to one possible explanation, the urban module overestimates heating from building elements near the ground; this had already been pointed out in the one dimensional validation.

No decisive general improvement of the results was obtained when using a technique implemented recently, where the heterogeneity of land coverage within given cells is taken into account by weighting the urban and rural flux calculation for each cell. Some improvement could be seen for transition zones where rapid changes in surface type can be accounted for by the use of land-use fractions.

The horizontal resolution has very little influence on any particular grid point, but the overall pattern of meteorological variables can be seen in more detail using a higher resolution. This should not be neglected when modelling the atmosphere over a complex terrain where the resolution needs to be high in order to account for small topographic features.

Lastly, radiation forcing recently implemented in the mesoscale model appears to improve model results (temperature, heat fluxes) when clouds develop in the domain during the simulation episode. In this way one can actually account for cloud shadowing and the associated decrease in incoming solar radiation in a simulation. This should be of great utility when the meteorological fields obtained as output are used to feed an air quality model, since the photochemical reactions occurring in the atmosphere are a function of available solar energy.

References

Baumann, K., and Piringer, M.: 2001, 'Two years of boundary layer measurements with a sodar – statistics and applications', *Phys. Chem. Earth* **26**, 205-211

Bornstein, R. D.: 1987, 'Mean diurnal circulation and thermodynamic evolution of urban boundary layers', *Modeling the Urban Boundary Layer*, Amer. Meteorol. Soc., Boston, 53-93

Christen, A.., Vogt, R., and Rotach, M. W.: 2003, 'Profile measurements of selected turbulence parameters over different urban surfaces', *Proceedings 4th International Conference on Urban Air Quality, Prague March 25-27 2003*, pp. 408-411

Dupont, S., Otte, T. L., and Ching, J. K. S.: 2004, 'Simulation of meteorological fields within and above urban and rural canopies with a mesoscale model (MM5)', *Boundary-Layer Meteorol.*, in press

Emeis, S., Münkel, C., Vogt, S., Müller, W. J., and Schäfer K.: 2004, 'Atmospheric boundary-layer structure from simultaneous SODAR, RASS, and ceilometer measurements', *Atmos. Environ.* **38**, 273-286

Fehrenbach, U.: 1999, *Analyse und Bewertung lokal- und regionalklimatisch wirksamer Faktoren in der Region Basel*, Diss. Phil.-Nat. Fak., Univ. Basel, ISBN 3-85977-245-7

Martilli, A., Clappier, A., and Rotach M. W.: 2002, 'An urban surface exchange parameterisation for mesoscale models', *Boundary-Layer Meteorol.* **104**, 261-304

Martilli, A.: 2003, 'A two-dimensional numerical study of the impact of a city on atmospheric circulation and pollutant dispersion in a coastal environment', *Boundary-Layer Meteorol.* **108**, 91-119

Martilli, A., Roulet, Y.-A., Junier, M., Kirchner, F., Rotach, M.W., and Clappier, A.: 2003, 'On the impact of urban exchange parameterisations on air quality simulations: the Athens case', *Atmos. Environ.* **37**, 4217-4231

Masson, V., Grimmond, C.S.B., and Oke, T.R.: 2002, 'Evaluation of the Town Energy Balance (TEB) scheme with direct measurements from dry districts in two cities', *J. Applied Meteorol.* **41**, 1011-1026

Oke, T. R.: 1973, 'City size and the urban heat island', *Atmos. Environ.* **7**, 769-779

Oke, T. R. : 1982, 'The energetic basis of the urban heat island', *Quart. J. Roy. Meteorol. Soc.* **108**, 1-24

Rotach, M. W., Christen, A., and Vogt, R.: 2003, 'Profiles of turbulence statistics in the urban roughness sublayer with special emphasis to dispersion modeling', *Proceedings, 5th International Conference on Urban Climate, September 1-5 2003,* Lodz, Poland

Roulet, Y.-A., Martilli, A., Rotach, M. W., and Clappier, A.: 2004, 'Validation of an urban surface exchange parameterization for mesoscale models – 1D case in a street canyon', *submitted to J. Applied Meteorol.*

Stull, R.B.: 1988, *An introduction to Boundary Layer Meteorology*, Kluwer Academic Publishers, 670 pp.

Vogt R., Christen A., and Rotach, M. W.: 2003, 'Vertical structure of sensible heat flux in an urban canopy layer', EGS-*AGU-EUG Joint Assembly April 6-11, 2003 Nice,* Abstract No: EAE03-A-12252

Chapter 5

Meteorological and air-quality modelling over the Mexico City basin

Abstract

The mesoscale meteorological model with urban parameterisation was used and validated in simulations of the atmosphere over the Mexico City basin. The period of simulation coincided with a typical ozone pollution episode during the dry season and consisted of 48 consecutive hours within a large measuring campaign designed to assess air quality in the basin. The simulated meteorological fields were passed to a Eulerian photochemical model in order to simulate the space and time distribution of the air pollutants during this episode and test emission reduction scenarios. Results obtained with the meteorological model (temperature, wind speed, and wind direction) were in good agreement with data recorded in the city during the episode. The model air-quality study led to a representation of space and time distribution of the air pollutants in harmony with the measured quantities. Prime consideration was given to the ozone plume, which in its development and motion is subject to the basin's specific meteorological conditions.

5.1. Introduction

The Mexico Megalopolis Metropolitan Area is one of the largest megacities in the world, being home to nearly 20 million inhabitants, covering 1500 km^2, and counting some 3.5 million motor vehicles (Molina *et al*, 2002). The city is surrounded by mountains that make air dispersion difficult. Its geographical location, at a high altitude (2240 m a.s.l.) and close to the equator, implies high solar radiation intensity that leads to rapid formation of lower-troposphere ozone enhanced by high NO_x emissions, associated with the high vehicle density in the city, and by high VOC emissions from combustion processes in industry and households. All these elements combined have made Mexico City one of the most highly polluted urban regions in the world.

Reacting to the progressive deterioration of air quality in the city and its surroundings, local authorities started several integrated assessment projects in order to understand the situation and reduce air pollution. One of them, the Mexico City Program, was initiated in 1999 as a case study of the "Integrated Program on Urban, Regional and Global Air Pollution"[1]. Data on air quality collected by systematic pollutant concentration monitoring constitute crucial information for this project. The Mexico City Program used data collected in the IMADA-AVER field experiment (Doran *et al*, 1998) conducted in the Mexico City basin from 22 February to 24 March 1997.

The main goals of the air quality study of this chapter were: in a first step, validate the meteorological model with the urban parameterisation applicable to the area of interest. In a

---

[1] The "Integrated Program on Urban, Regional and Global Air Pollution" was initiated at the Massachusetts Institue of Technology (MIT) in 1999. Its overall goal is to provide objective, balanced assessments of the causes and alternative cost-effective solutions to urban, regional and global air pollution problems through quality scientific, technological, social and economic analysis. Mexico City was selected for an initial case study toward this goal (http://eaps.mit.edu/megacities/).

second step, pass the simulated meteorological fields to a Eulerian photochemical model (TAPOM, described in Chapter 2) in order model air quality over the Mexico City basin. The simulated episode was selected to fall into the IMADA-AVER measuring campaign during which meteorological parameters and pollutant concentrations where measured at several observation sites in Mexico City and its surroundings. This provides an excellent opportunity for validating both the meteorological model and the photochemical model.

The photochemical application should yield a picture of the three-dimensional pollutant-transport situation over the region and track the development of the pollution plume formed over the city and its surroundings. Once the photochemical model has been validated for the test domain, it will then provide an opportunity for testing the impact of emission abatement strategies on ozone formation. It is beyond doubt that the control of photochemical pollution is not easy: While reduced emissions of primary pollutants (*eg*, NO_x or VOC) will produce a proportional reduction of pollution levels due to these species, the control of secondary pollutants (*eg*, O_3) is much more complex and highly nonlinear.
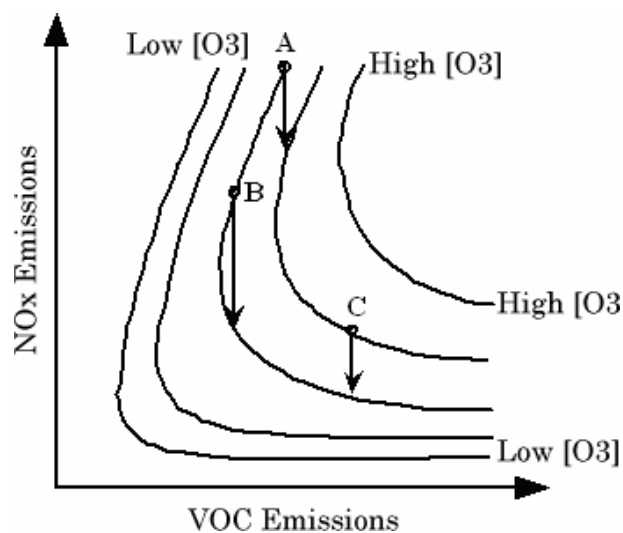

Figure 5.1. Ozone isopleths (lines of identical concentration) as functions of the NO_x and VOC emission levels.

The behaviour of secondary pollutants depends on their absolute and relative quantities and on the space and time distribution of precursor emissions (NO_x and VOC, in the case of O_3). This is well illustrated by a plot of ozone isopleths (lines of identical ozone concentration) as functions of the NO_x and VOC emission levels (Figure 5.1).

Assume a moderate initial ozone level (central curves in Figure 5.1). Depending on the position along the isopleth (that is, on the relative levels of the NO_x and VOC emissions), a reduction of NO_x emissions can have a completely different impact on the ozone concentration:

- in point A: NO_x emission reductions will increase the resulting ozone concentration

- in point B: NO_x emission reductions will have no effect on ozone concentration

- in point C: NO_x emission reductions will decrease the resulting ozone concentration.

Thus, applying specific measures designed to reduce emissions will not always satisfy the objective pursued. Therefore, the consequences of a particular emission abatement strategy should always be investigated before actions are taken. The different points defined within the above plot of isopleths correspond to different locations in the city. Point A would correspond to a downtown area where the relative NO_x emission levels are high relative to the VOC emission levels. This area is said to be VOC-sensitive, since ozone levels can only be reduced through VOC emission reduction. By the same principle, point C is defined as NO_x-sensitive.

A model study represents in fact the most appropriate tool for quantifying the impact of (hypothetical) measures taken to reduce pollution, *eg*, a reduction of vehicular emissions in the city, since the chemical and meteorological processes underlying the problems of air quality are highly nonlinear.

Section 5.2 of the present chapter constitutes a description of the meteorological model setup. Section 5.3 analyses the pollutant data available for validating the model. For this purpose, the concentrations of various pollutants observed at several stations within the simulated domain are studied. Together with measured meteorological parameters, the pollutant transport patterns emerging from this analysis provide information on the meteorological flow situation prevailing in the lower part of the PBL during the episode simulated. The meteorological model is validated in Section 5.4. The results of the air-quality simulation are presented in Section 5.5. In conclusion, the NO_x and VOC emission reduction scenarios are used to reveal NO_x and VOC-sensitive zones in Mexico City and its surroundings.

5.2. The model setup

Mexico City is located at an average elevation of about 2240 m above sea level in a basin at a subtropical latitude of 19°25' N. The basin is surrounded on three sides by mountain ranges rising to almost 5500 m a.s.l. (the volcano Popocatepetl). South-east from the city is a wide mountain pass, to the north the basin is open toward a plateau (Figure 5.2 and Figure 5.4).

A field campaign (IMADA-AVER, Doran *et al*, 1998) was conducted during the dry season between 24 February and 22 March 1997. During this period, the highest ozone concentrations were measured on 2 March. Since the focus of interest of any air quality modelling study should be the pollution peaks, the period from 01 LT 1 March to 01 LT 3 March 1997 was selected for the simulation.
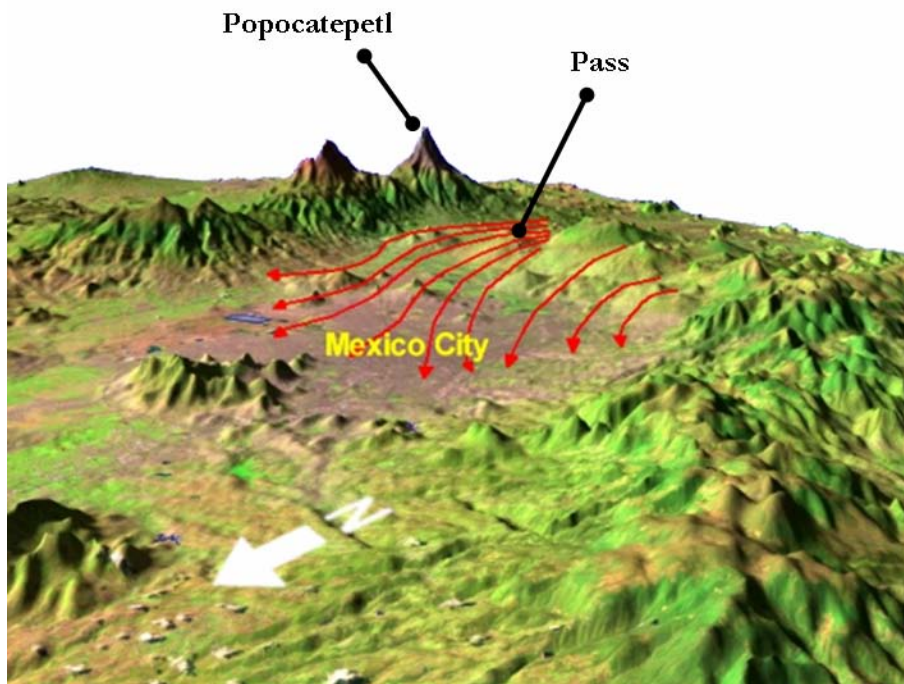
Figure 5.2. The Mexico City basin and its main topographic features.

5.2.1. *Domains for meteorological modelling*

A system of two nested grids was used for the meteorological simulation. The outer grid covered an area of 202.5 km by 279 km, and was divided into 45 by 62 cells with a 4.5-km horizontal resolution (Figure 5.4). It included the mountains surrounding the basin of Mexico City as well as the steep slope on the far side of the southern mountain range. A stretched, terrain-following mesh with 25 vertical layers was used which had thicknesses between 10 m near the Earth's surface and 1000 m at the top of the domain at an elevation of 14 km a.s.l.. The topography (GTOPO30, see Chapter 4) and the land cover were provided by the U. S. Geological Survey (http://www.usgs.gov./), both with a horizontal resolution of 1 km. As in Chapter 4, temperature and wind values were initialized and forced at the domain boundaries using the NCEP/NCAR Reanalysis data and the Four-Dimensional Data-Analysis (FDDA) technique described in Chapter 2. The synoptic winds reported for 1 and 2 March are typical of the winter

dry season over the plateau of Mexico City (Whiteman *et al*, 2000); they blow from the south-east (Figure 5.3).
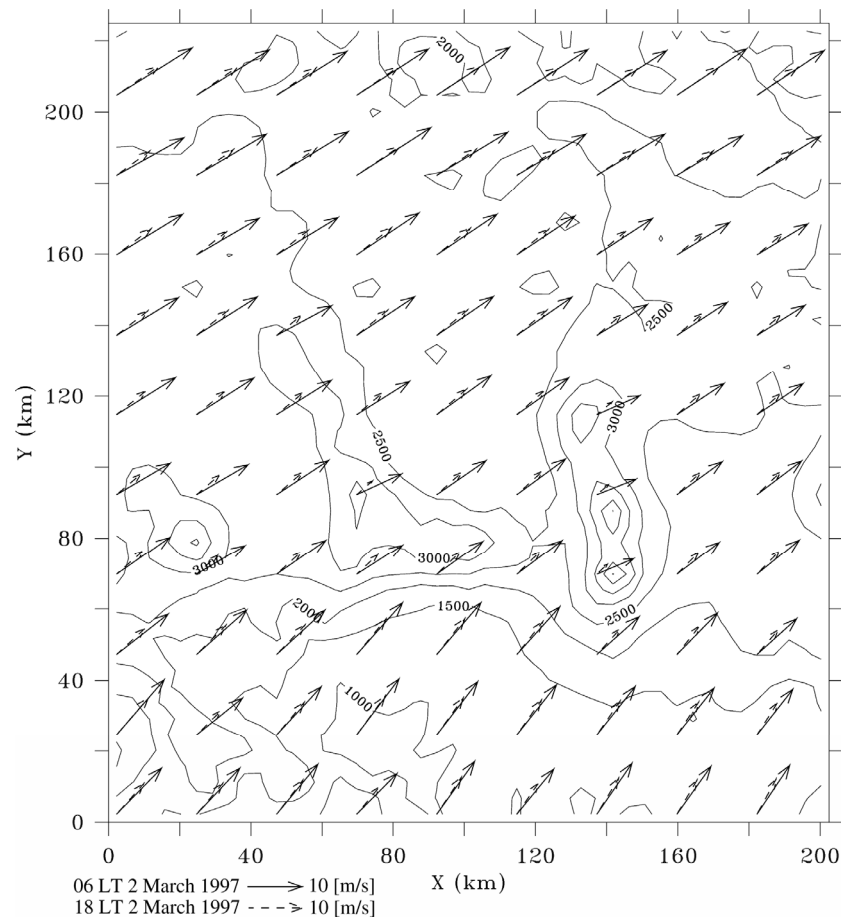

Figure 5.3. Synoptic wind at 5000 m a.g. given by the NCEP/NCAR Reanalysis data and interpolated over the Mexico Basin at 06 LT (solid arrows) and 18 LT (dotted arrows) 2 March 1997.

The inner grid encompassed the Mexico City basin and a minor part of the surrounding mountains. It had a horizontal resolution of 2.25 km by 2.25 km, and extended over a domain of 112.5 km by 101.25 km, which represents a grid of 50 by 45 cells (Figure 5.4). The terrain-following mesh had the same vertical resolution as the large grid. Results of the large meteorological grid were used to force the initial and boundary conditions for temperature and wind using the same FDDA technique as in the large grid.

The urban area within the small domain occupies 256 grid points (1230 km^2) representing 11 % of the total simulated area. The remainder is considered as rural with sandy-clay-loam soil characteristics (input data for the soil module: Tremback and Kessler, 1985, see the description given in Chapter 2). The initial soil moisture content was set to 0.21 (volume of water per volume of soil). No detailed data regarding the morphology and thermal properties of the buildings were available for Mexico City. In agreement with reported data and literature (Oke *et al*, 1992, 1999; Masson *et al*, 2002; Martilli *et al*, 2002), the city was represented by a single urban class with an average building height of 12 m and (for the fractional flux calculation described in Chapter 2) with 5 % of rural area within the city. The street width and the building width were set to 15 m and 30 m, respectively. Assuming this morphology, the roughness height needed for the traditional parameterisation method of urban areas (MOST, see Chapter 2) was set to 1 m. The thermal properties of the buildings are listed in Table 5.1.

Table 5.1. Shape and physical properties of urban elements in the model: K_s is the substrate thermal conductivity of the material, C_s is the specific heat of the material, T_{int} is the initial temperature of the material, ε is the emissivity of the surface, α is the albedo of the surface, and z_0 is the roughness length of the surface.

Surface	K_s [$m^2 s^{-1}$]	C_s [$J m^{-3} K^{-1}$]	T_{int} [$°K$]	ε [-]	α [-]	Z_0 [m]
Wall	0.57e-6	1.0e06	291	0.90	0.2	---
Roof	0.62e-6	1.0e06	291	0.90	0.2	0.01
Street	0.47e-6	1.74e06	290	0.95	0.2	0.01

5.2.2. Domain for air-quality modelling

The domain for air-quality modelling covering an area of 85.5 km by 90 km encompassed Mexico City as well as the southern and western mountain ranges. It was discretised in 19 by 20 grid cells with a 4.5-km horizontal resolution (Figure 5.4). A stretched terrain-following mesh was built up

(using the topography data from GTOPO30) with 12 vertical layers ranging in thickness from 30 m near the surface to 2000 m at the top of the domain at an elevation of 7500 m a.s.l. For the purposes of reducing the influence of the boundary conditions in the zone of interest, the domain was extended at the lateral boundaries with the large meteorological grid along the eastern, western, and northern boundary, while a dumping zone of 16 grid cells was added to the southern boundary. Counting the additional cells the domain then had a total dimension of 202.5 km by 225 km. For emissions input into the model, the 1998 official emissions inventory for the Mexico City Metropolitan Area (CAM, 2001) covering the domain of 85.5 km by 90 km as described above was used.
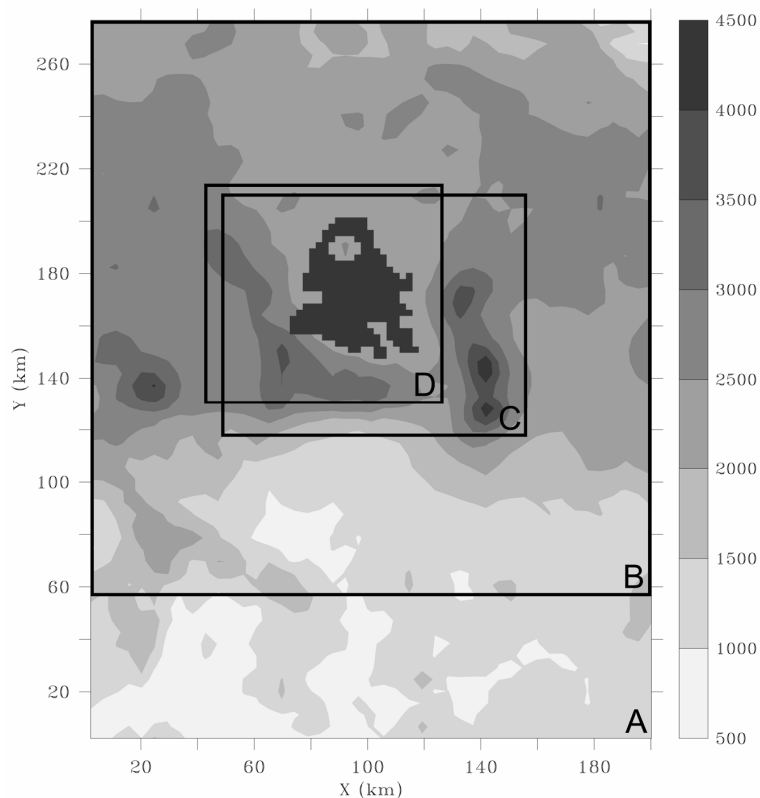
Figure 5.4. Topography of the Mexico City Basin and its surroundings, showing the Mexico City urban area (shaded) and the simulation grids: (A) The large meteorological grid of 45 by 62 cells with a 4.5-km horizontal resolution; (B) the full air-quality domain with extended boundaries containing 45 by 50 cells with a 4.5-km horizontal resolution; (C) the small nested grid for the meteorological simulation with a grid of 50 by 45 cells and a horizontal resolution of 2.25 km; (D) the emissions-inventory and air-quality simulation domain containing 19 by 20 cells with a 4.5-km resolution.

The initial and boundary conditions for the pollutant concentrations was provided by GEOS-CHEM (Bey *et al*, 2001), which is a three-dimensional global model for tropospheric chemistry driven by assimilated meteorological observations from the Goddard Earth Observing System (GEOS) of the NASA Data Assimilation Office (DAO). Table 5.2 shows the average concentrations used as the boundary conditions of the air-quality modelling domain.

Table 5.2. Time and space-averaged boundary conditions for the concentrations of the main pollutants considered by the photochemical model.

Chemical species	*Mixing ratio [ppm]*
NO	5.196e -4
O_3	3.154e -2
HNO_3	3.101e -4
HNO_4	2.927e -6
H_2O_2	1.356e -3
HCHO	4.257e -4
CO	7.111e -2
ALD	6.420e -5
KET	8.562e -4
ONIT	3.865e -6
N_2O_5	5.506e -7
OLT	3.792e -5
ISO	6.040e -5
CSL	7.397e -5

The meteorological fields needed as input for the photochemical model were provided after pre-processing (interpolation of the meteorological data into the photochemical model grid) by the mesoscale model simulation in the two nested grids described above. The photochemical model (TAPOM, see Chapter 2) solves equations for chemical transformations, horizontal transport by the mean wind, incoming solar radiation, and vertical diffusion in each cell. Output of the model are the concentrations of all pollutants considered in each cell of the domain.

5.3. Data analysis and meteorological description

Ozone data can be used to locate the pollution plume emitted by a city (*eg*, studies over Milan: Martilli *et al*, 2003, and over Athens: Clappier *et al*, 2000). Data indicating very low ozone concentrations during the night imply that the station is close to important sources of NO_x, since high NO_x concentrations will contribute to ozone destruction. High NO_x concentrations are also incompatible with high ozone concentrations during the day, hence such stations will again not show the highest ozone concentrations. Thus, stations signalling low ozone values generally are located in urban areas. Relatively high ozone levels during nighttime indicate that the measuring site is located a certain distance away from the NO_x emission sources. This is typical for stations outside the city. The highest ozone peak among sites in the city surroundings will be recorded when the pollution plume produced by the city reaches such a station. It follows that the ozone measuring stations will for the most part belong to one of three categories:

- stations representative for background pollution coming from outside the city, where the ozone data show almost no daily variation, ozone levels remain relatively high during the night and do not significantly increase during daytime

- stations located inside the city, where the ozone level is very low during nighttime and reaches the background level during daytime

- stations located in the city plume, where ozone measurements reveal relatively high concentrations (background concentrations) during the night and the highest ozone concentrations in the afternoon.

Viewed against this classical situation, the simulated episode of 2 March 1997 in Mexico City exhibited some special features. The low levels of ozone measured during the night at all observation sites (Figure 5.5) would place them into the second of the categories defined above (inside the city). On the other hand, some of these stations recorded a high, relatively sharp

ozone peak during the afternoon, and hence indicate that the city plume remains inside the city. This atypical situation is due, on one hand to the large spread of the urban area and on the other hand to specific features of the meteorological circulation.
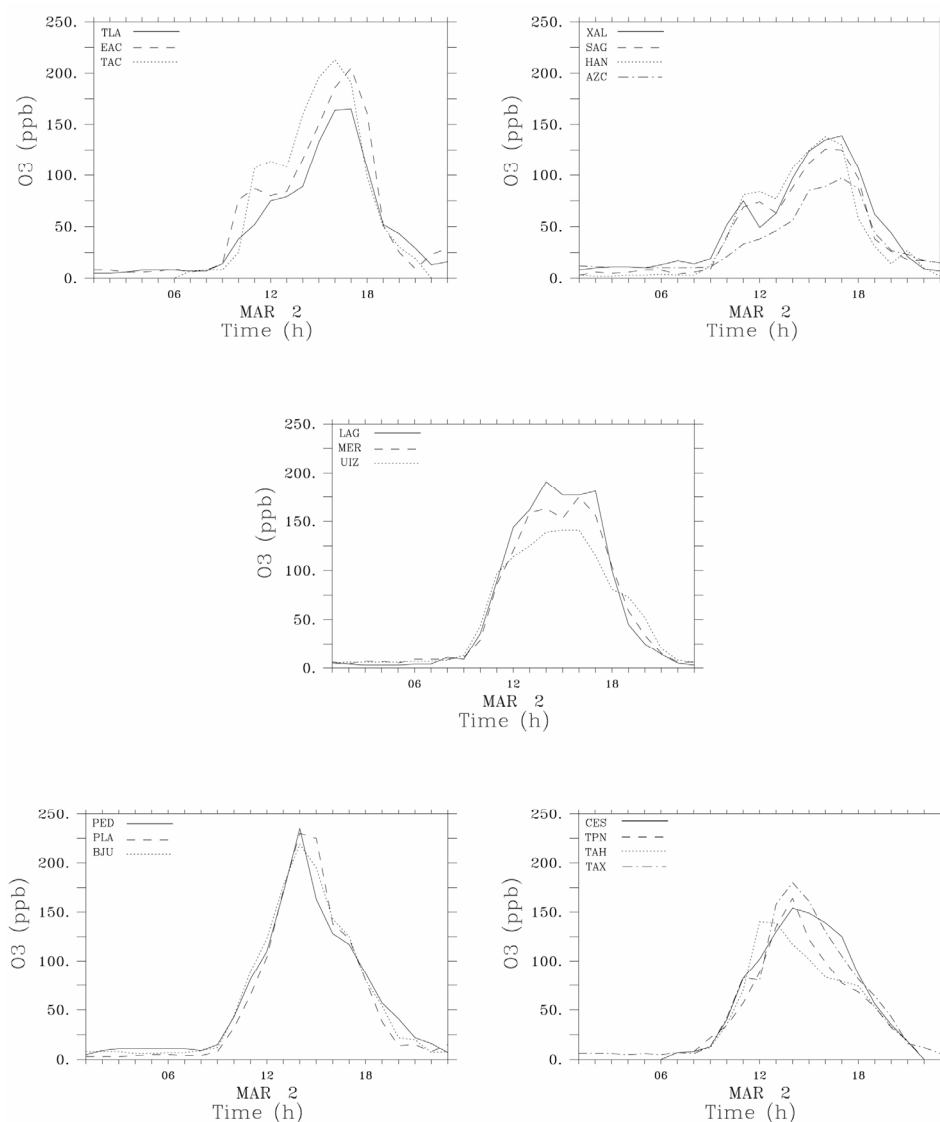

Figure 5.5. Ozone data recorded from 00 LT 2 March to 23 LT 2 March 1997, and arranged in five distinct groups differing in peak intensities and in the times at which the peaks occur (see location of the stations in Figure 5.6).

The ozone concentrations start to increase at every station at 09 LT. For the stations located in the southern part of the domain (PED, PLA, BJU, and CES, TPN, TAH, TAX, see the locations

indicated in Figure 5.6) the maximum ozone concentrations are reached at 13 LT. For the

stations located north of the city (TAC, EAC, TLA, and SAG, XAL, HAN, AZC) the ozone

maximum occurs around 16 LT. Moreover, higher ozone levels are recorded at the stations in the

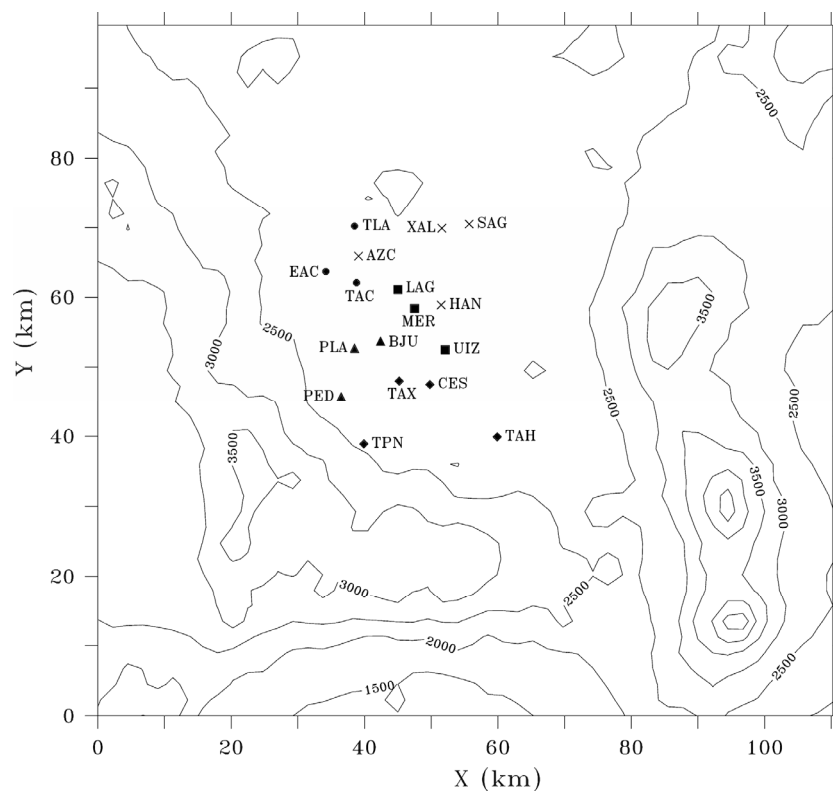eastern part of the domain (PED, PLA, BJU and TAC, EAC, TLA).

Figure 5.6. Locations of the air-quality measuring stations within the simulated domain. Different symbols are used to distinguish stations of the five groups differing in the ozone peak intensities and in the times at which the peaks occur.

A diagram where the ozone maxima of the stations are entered as functions of their time of

occurrence (Figure 5.7) can be used to reveal groups of measuring stations exhibiting similar

behaviour. In terms of these two criteria (O_{3max} and time of occurrence of the ozone peaks), five

groups of stations can be distinguished:

  - the southern stations, where the ozone maxima occur in the early afternoon; these can be

    further divided into two groups: PED, PLA, and BJU, which show the highest ozone

concentrations (between 230 to 240 ppb), and CES, TPN, TAH, and TAX, which show lower ozone concentrations (between 140 to 180 ppb)

- the northern stations, where the ozone peak occurs later in the afternoon; these can be further divided into two groups: TAC, EAC, and TLA, which show high ozone concentrations (between 160 to 210 ppb), and SAG, XAL, HAN, and AZC, which show lower ozone concentrations (between 100 to 140 ppb)

- the stations in the city centre (LAG, MER, and UIZ) lacking a distinct or sharp ozone peak.

Fast *et al* (1998) used the IMADA-AVER data for an analogous type of classification. They arrived at sets of stations slightly different from the ones presented above for part of the measuring sites.
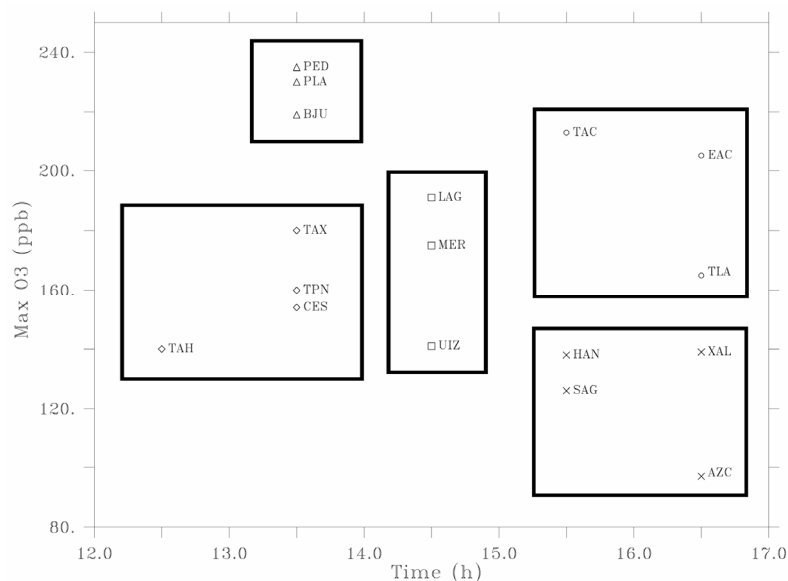

Figure 5.7. Daily ozone maxima as functions of their time of occurrence for all measuring sites within the Mexico City area (based on measurements made during 2 March 1997).

The above classification shows that at 13 LT, the urban plume is located along a line running from PLA in the east to TAH in the west, and that it moves towards the northern part of the domain during the afternoon (line running from EAC to SAG at 17 LT).

This plume behaviour can be explained in terms of meteorological circulation. On 2 March, the circulation is similar to that "influenced by thermally driven flow" as described by Bossert (1997). In such a situation, the synoptic scale winds are low while the winds thermally induced by the topography are predominant. The radiative cooling of the ground occurring at night induces downslope winds from the surrounding mountains that converge to a complex circulation within the basin. Over the city area the winds are very weak (around 1 m/s). Upslope easterly and northerly winds are generated from 9 LT to 13 LT due to differential heating of the ground in the western and southern part of the domain (close to EAC, TAC, PLA, and PED). At the same time upslope southerly winds are generated along the far side of the mountain range. Since that side of the mountains is steeper and longer (from 3000 m a.s.l. down to 1000 m a.s.l.) than the one on the Mexico basin side (from 3000 m a.s.l. to 2000 m a.s.l.), the slope winds generated on the southern side will become stronger than the winds inside the basin. Between 13 LT and 14 LT, the southerly wind start to blow over the pass on the south-east corner of the domain (Figure 5.2) and enter the basin. A wind convergence line is formed south of the city. This convergence then moves progressively to the northern part of the domain, since in the basin the southerly wind is stronger than the northerly wind. The location of the pollution plume emitted by the city is explained by the location of the wind convergence. The pollution plume actually is concentrated at the convergence line where the ozone maxima are formed.

5.4. Results of the meteorological modelling

The results from three different simulations in the small grid were compared with data from several observation sites in Mexico City. First the model was run with the urban parameterisation (Martilli, 2002) described in Chapter 2 and used in Chapters 3 and 4. In a second run denoted '*trad*', the traditional method with a roughness length of 1 m was used when accounting for the

presence of the city. Finally a simulation without urban area denoted '*rural*' was performed. When comparing the results obtained in these three simulations, it will be possible to:

- decide whether the new parameterisation is an improvement over the traditional method when large urban areas must be accounted for,

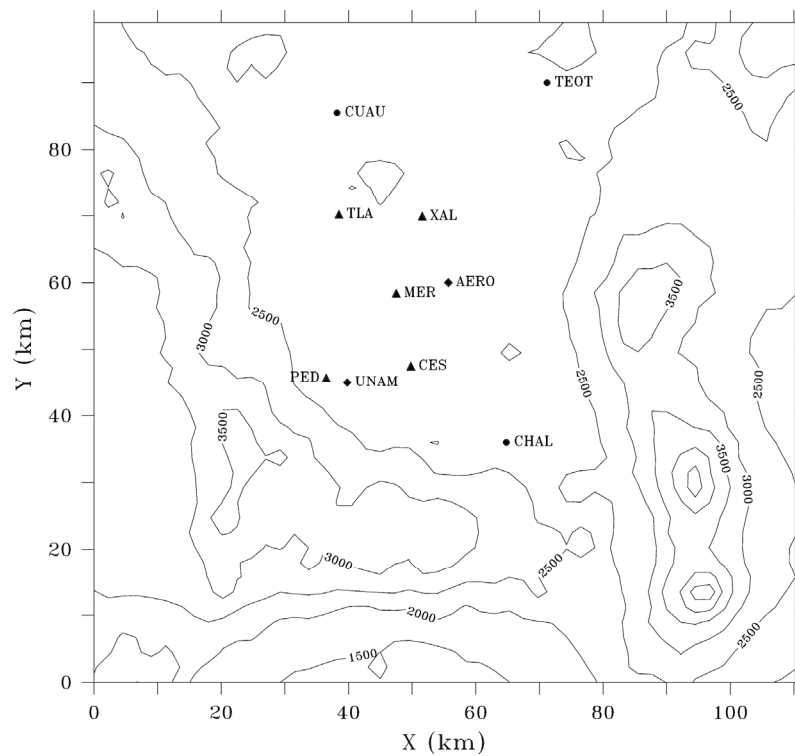- assess the impact of a city on the flow fields in the PBL.

Figure 5.8. Locations of the measuring sites used for validating the model: five ground observation sites providing wind, temperature, and air-pollutant concentration data (triangles), three wind profilers providing wind-speed and wind-direction profiles (circles), and two sounding balloons providing wind profiles (diamonds).

For the purposes of validating the model, one station was selected from each of the groups defined in Section 5.3 on the basis of ozone values. Ground data for wind speeds and temperatures were compared with model results applicable at the corresponding point. Moreover, vertical wind profiles (speed and direction) were available on an hourly-average basis at three

observation sites from radar wind-profiler[2] measurements, while two sounding balloons provided vertical wind and temperature data. (Temperature profiles are not available for UNAM.) The locations of all the measuring stations used for the validation are shown in Figure 5.8.

5.4.1. Temperature

The temperatures measured close to ground during the simulated episode were similar at the five observation sites used for validation (Figure 5.9). The daily extremes went from about 284 K at 06-07 LT to almost 302 K at 15-16 LT (depending on the station).

As expected, the three simulations produce different types of behaviour, particularly so during the night where both '*trad*' and '*rural*' overestimate the temperature decrease and deviate by more than 5 K from the measured data (at 00 LT 2 March), while '*urban*' produces better agreement with the measured data. During daytime, the three simulations yield rather similar results; the simulated maximum temperature constitutes an underestimate differing by 2 K (XAL) to less than 1 K (PED) from the measured data. The temperature data from station PED were the ones best reproduced by '*urban*', according to the root-mean-square differences between simulated and experimental values calculated for the entire episode (Figure 5.10).

---

[2] Radar (radio detection and ranging) transmits microwaves. By measuring the frequency (Doppler) shift in the signal, radial velocities can be found. In meteorology, radar applications were first developed for measuring turbulence within the PBL. Nowadays a wide range of atmospheric sounders exist for deployment and operational gathering of wind and other meteorological data (Stull, 1988).
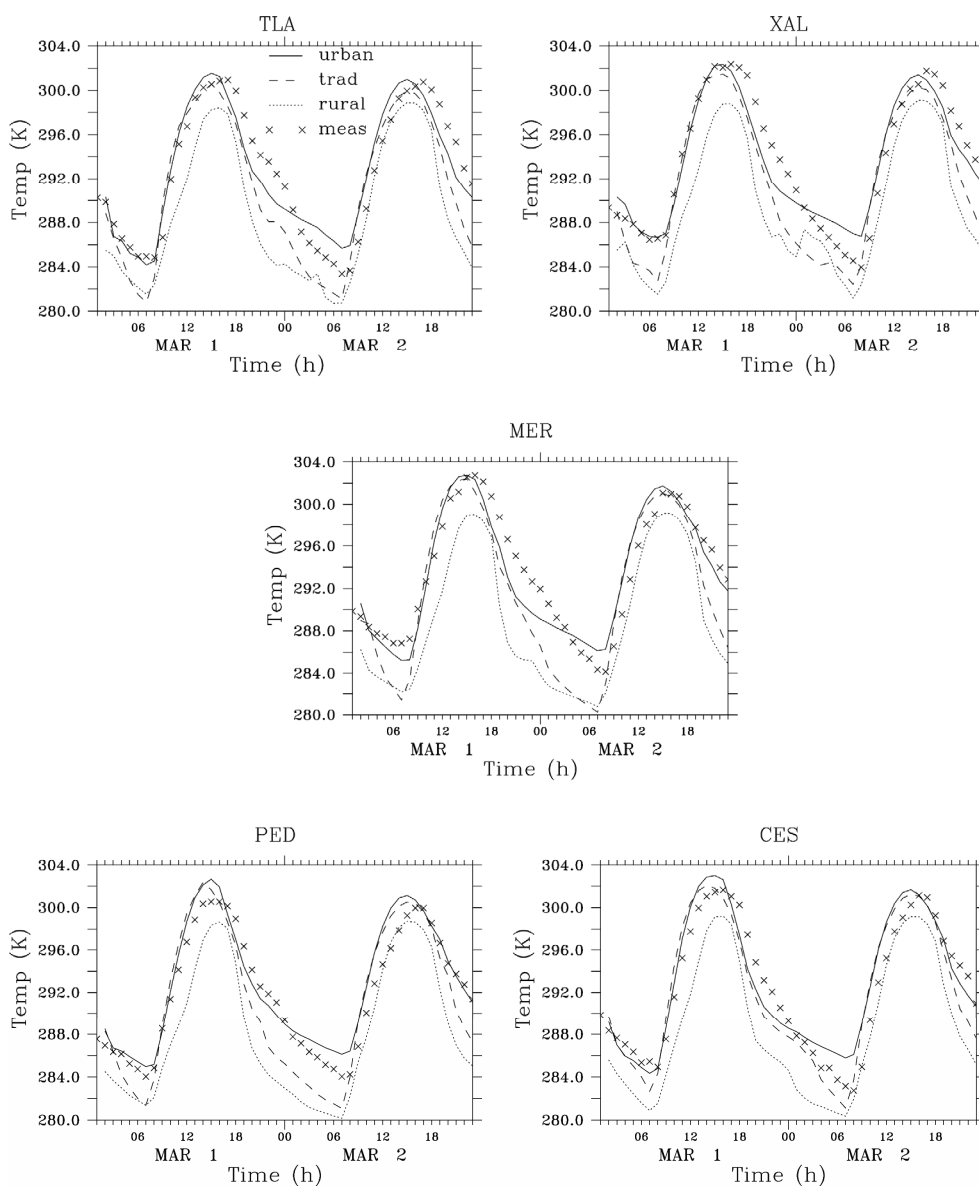
Figure 5.9. The temperature distributions close to ground as functions of time from 01 LT 1 March to 23 LT 2 March 1997 according to simulations '*urban*' (solid lines), '*trad*' (dashed lines), and '*rural*' (dotted lines) and according to the measurements (crosses) for five ground observation sites (the arrangement of the five representations shown in this figure reflects the mutual positions of the geographical locations of the stations indicated by triangles in Figure 5.8).
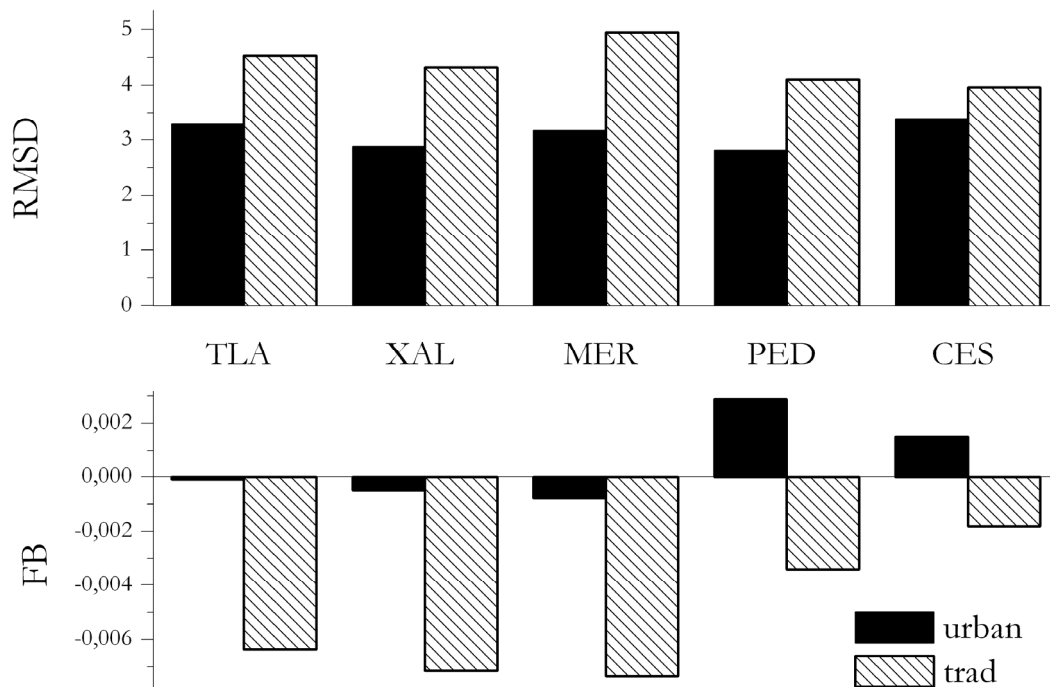
Figure 5.10. Fractional Bias (FB) and Root-Mean-Square Differences (RMSD) of the temperatures close to ground between '*urban*' and the measured data (black bars) and between '*trad*' and the measured data (hatched bars) for the entire episode (01 LT 1 March to 01 LT 3 March) (see the definitions of FB and RMSD in Chapter 3).

The temperature increase occurring after sunrise at all five measuring stations is well reproduced by '*urban*' and, to a certain extent, by '*trad*' as well.

The simulated vertical temperature profiles can be compared with data obtained from soundings at two locations (Airport and UNAM). At the Airport, soundings are available only for 1 March 1997 (Figure 5.11).
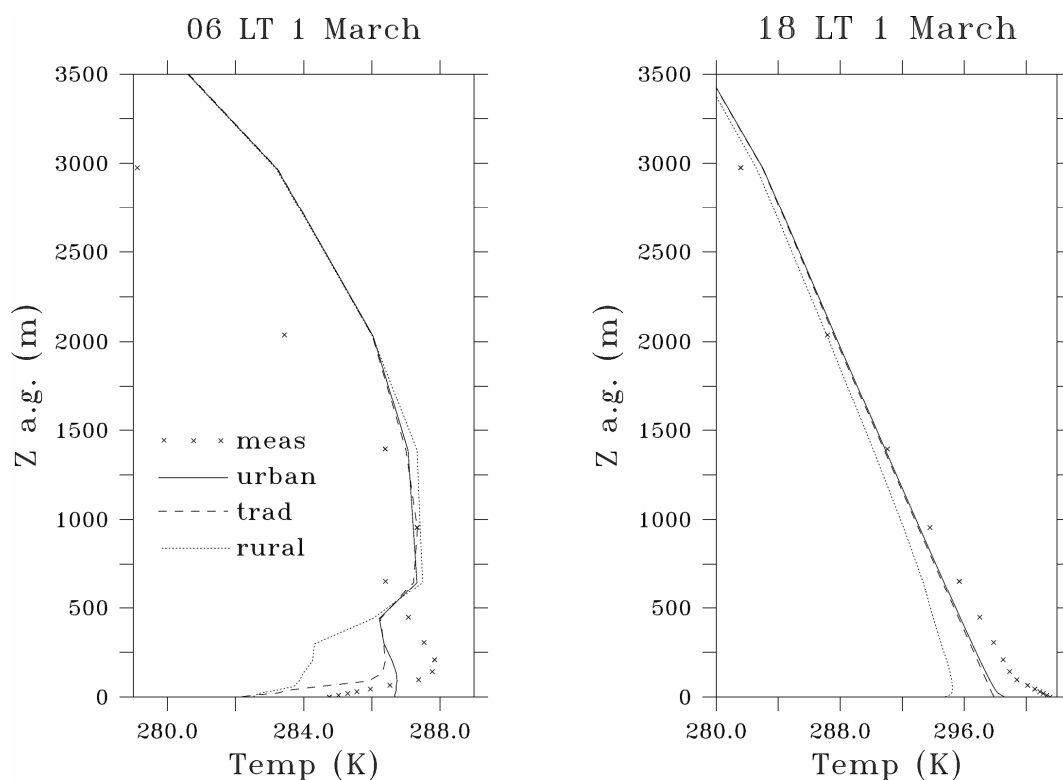
Figure 5.11. Vertical temperature profiles at the Airport according to the simulations '*urban*' (solid lines), '*trad*' (dashed lines), and '*rural*' (dotted lines) and according to sounding data (crosses) at 06 LT and 18 LT 1 March 1997.

The situation at 06 LT 1 March indicates a first temperature inversion layer within the first few hundred metres and a second inversion layer between 600 and 800 m a.g. according to measured data. In the '*rural*' and ' *trad*' simulations, these two inversion layers emerge from the calculated values, while '*urban*' yields a constant temperature profile (warmer than recorded data) up to 500 m a.g. but captures the second inversion layer. This discrepancy is caused by the fact that the Airport is located at the edge of the city in rural-dominated surroundings. The model, however, considers the corresponding cell as urban, and hence calculates a warmer temperature close to ground with the urban parameterisation (just as for the other grid points shown in Figure 5.9). At 18 LT 1 March, the temperatures computed by '*rural*' in the PBL are lower than recorded data, while '*urban*' and '*trad*' are closer to reality. The tendencies revealed at 06 LT are just the opposite,

since '*urban*' and '*trad*' provide a better fit of the observed temperatures than '*rural*'. Above 1500 m a.g. the three simulations yield similar results, all in agreement with the measured data.

Four soundings were launched from the observation site of UNAM on 2 March, at 08 LT, 11 LT, 16 LT, and 19 LT, respectively (Figure 5.12). The profile measured at 08 LT reveals a strong inversion layer between 100 m and 400 m a.g. corresponding to the warmer residual layer formed during nighttime above the surface layer. This inversion layer in not found in the three simulations, which compute constant temperature profiles up to 400 m a.g. In the second profile (11 LT), the air starts to become unstable, particularly close to ground where it is heated first by incoming solar radiation. The '*urban*' and '*trad*' simulations are both able to reproduce this sharp temperature gradient close to ground.
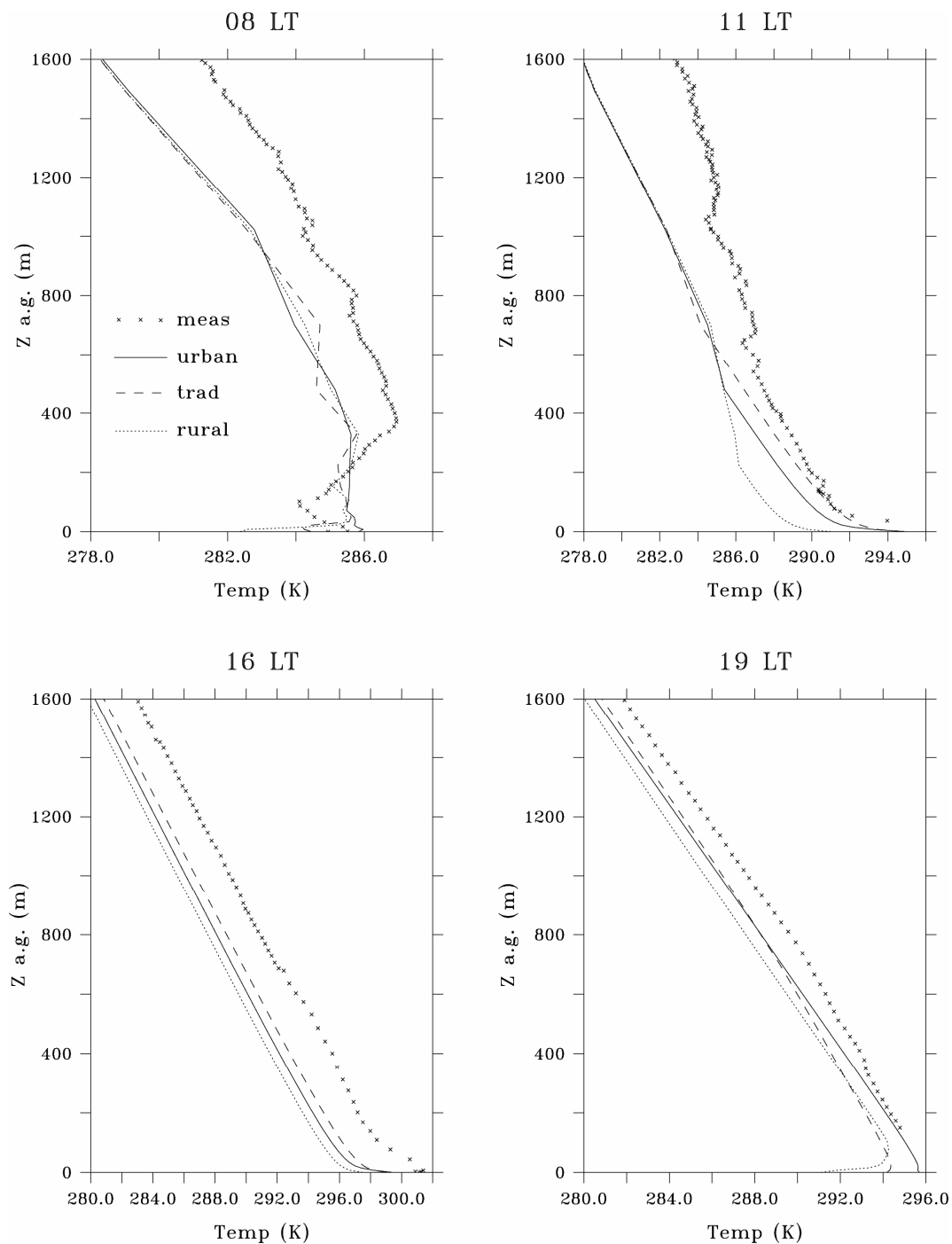
Figure 5.12. Vertical temperature profiles at the observation site of UNAM according to the simulations '*urban*' (solid lines), '*trad*' (dashed lines), and '*rural*' (dotted lines) and according to sounding data (crosses) at 06 LT (top left), 11 LT (top right), 16 LT (bottom left), and 19 LT (bottom right) 2 March 1997.

The sounding (16 LT) made in mid-afternoon when vertical turbulence and eddies are well developed, yields a profile with a constant gradient of -6 K/km (in harmony with the mean temperature decrease within the troposphere). This gradient is well reproduced by the model,

though with a shift of 2 K in absolute values. The last sounding (19 LT) still shows a rather constant gradient with temperatures decreasing with increasing height between 150 m and 1600 m a.g., which is also well captured by the model. No data were recorded over the first 100 m a.g., so that the differences in behaviour between '*rural*' and '*urban*' cannot be discussed. In the '*urban*' simulation, warmer temperatures are computed close to ground, while '*rural*' already starts to reveal the stable nightly profile existing within the first tens of meters.

The pattern of mixing heights developing during the day could not be assessed, since the sounding profiles stopped at 1600 m a.g. During afternoons, the PBL height exceeds this altitude reaching about 3000 m a.g. (Williams *et al*, 1995).

Considering the data and the results of simulations with respect to temperature, it can be seen from the comparison presented above that the model has been validated successfullly, both for ground results and for the vertical profiles.

5.4.2. Wind

The synoptic wind situation can be described as a southerly to south-easterly wind prevailing during the entire episode simulated, according to the NCEP/NCAR Reanalysis data used for the forcing (Figure 5.13). This feature is well reproduced by the model, according to results shown in the same figure which were obtained with simulated wind fields at 5000 m above ground for different times during the simulation.
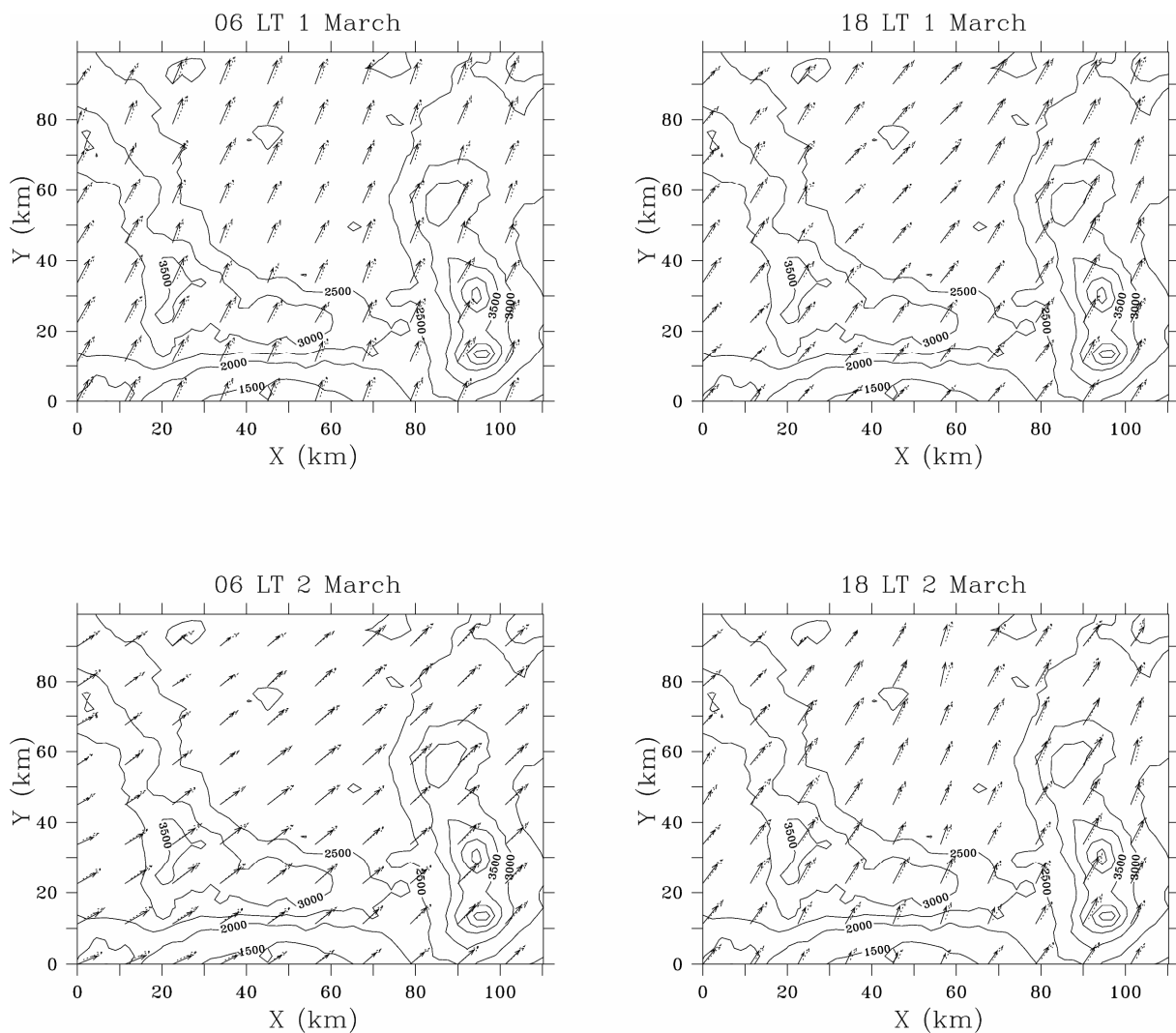
Figure 5.13. Wind fields at 5000 m above ground according to the '*urban*' simulation (solid lines) and to the forcing data (dotted lines) at 06 LT 1 March (top left), 18 LT 1 March (top right), 06 LT 2 March (bottom left), and 18 LT 2 March (bottom right).

The wind flows close to ground are influenced by topography (mechanically induced wind systems) and by differential soil heating (thermally induced wind systems), as described in Chapter 1. It follows that these wind patterns are rather different from the ones produced by the geostrophic wind as presented above, and they are much more complex (Figure 5.14), particularly under conditions where the geostrophic wind is weak, as in the present case. Results computed by '*urban*' were compared with data measured above five selected stations. The model produces data in good agreement with the measured data. Moreover, the wind patterns actually correspond

to what can be expected when considering the topography. Anabatic winds are in fact well developed over the entire domain during daytime, while at night a weak "chaotic" wind blows over the city, and a strong katabatic wind blowing toward the city is generated by the southern and eastern mountains. The simulated wind speeds are lower over the urban area, since the urban parameterisation was used.
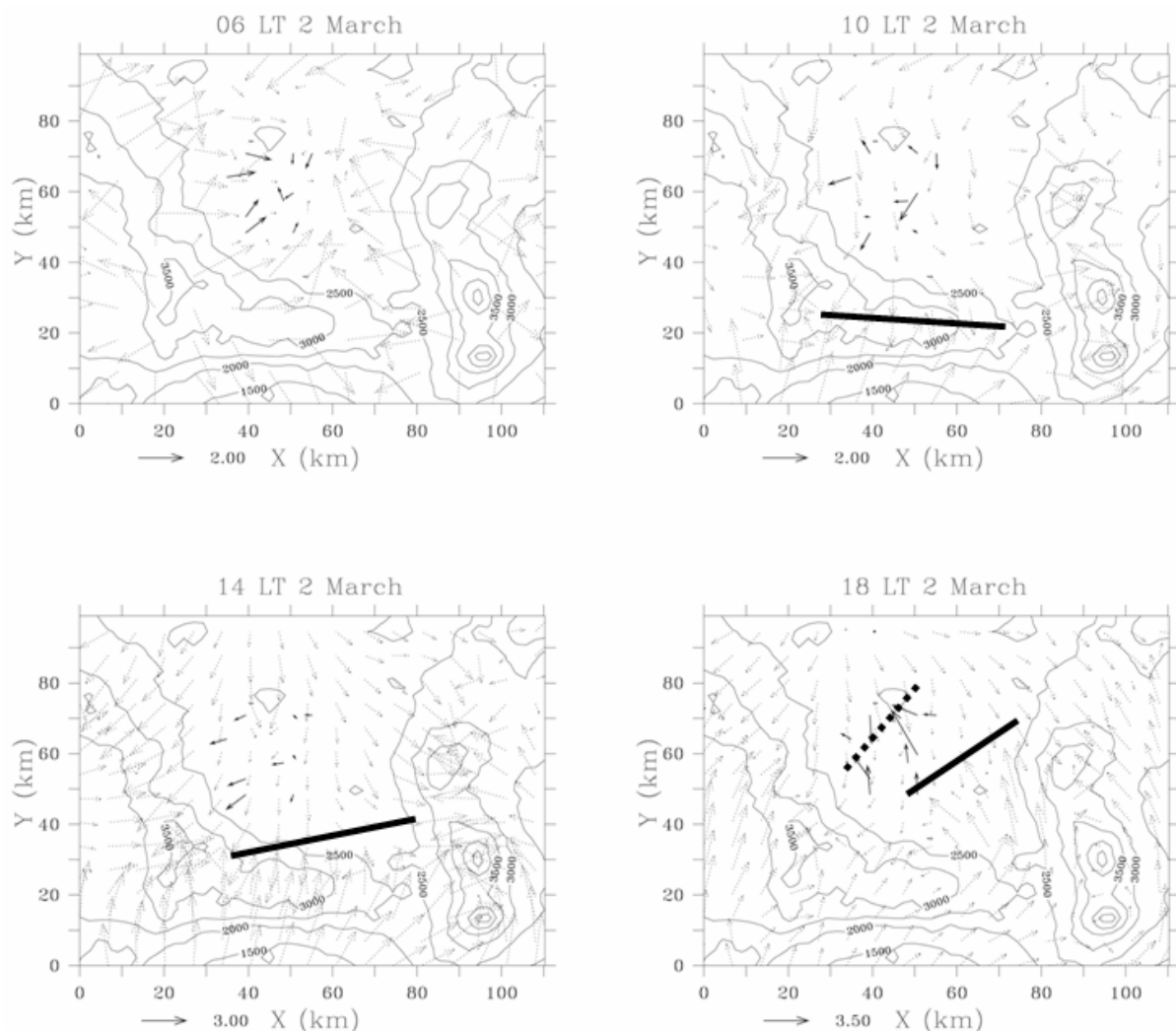

Figure 5.14. Wind fields close to ground according to the '*urban*' simulation (dotted lines) and according to the measurements made at five observation sites (solid lines) at 06 LT (top left), 10 LT (top right), 14 LT (bottom left), and 18 LT 2 March (bottom right). The heavy straight solid lines indicate convergence obtained by the model between the northerly flow and the southerly flow blowing over the southern mountain range or entering the basin across the pass south-east of the city, while the heavy dotted line shows the convergence deduced from measured wind data.

The convergence line revealed by the ozone data analysis in Section 5.3 is also detected by the model. The simulated wind fields close to ground actually reproduce the convergence lines (the heavy black lines in Figure 5.14) formed, on one hand by the northerly flow over the basin and on the other hand by the southerly flow blowing over the southern mountain range or entering the basin over the pass south-east of the city. The convergence line predicted by the model does not appear at exactly same place as that revealed by measured data, since it moves not as far north in the basin as observed. Still, the model is able to simulate the southerly flow entering the basin as well as the resulting convergence over the city, which undoubtedly is important for ozone plume formation, as demonstrated in Section 5.3 above with measured data and in Section 5.5 below with the air-quality simulation. The migration of the convergence line obtained by '*trad*' was the same as that obtained by '*urban*', while '*rural*' placed the convergence further south. This is due to the fact that the wind deceleration over the city is not taken into account in '*rural*'. Hence, the northerly wind turns out to be stronger in '*rural*' than in '*urban*', and pushes the convergence line southward.

One can see when looking at the wind-speed distribution close to ground over the entire episode simulated that the model underestimates the daily peaks of wind speed which occurred, both on 1 and 2 March in the late afternoon (Figure 5.15). During nighttime, the simulated wind speeds yield a better fit of the measured data. Since the impact of buildings on the flow fields in the surface layer is taken into account, simulated wind speeds generally are lower in '*urban*', and to a certain extent in '*trad*', than those computed by '*rural*'.
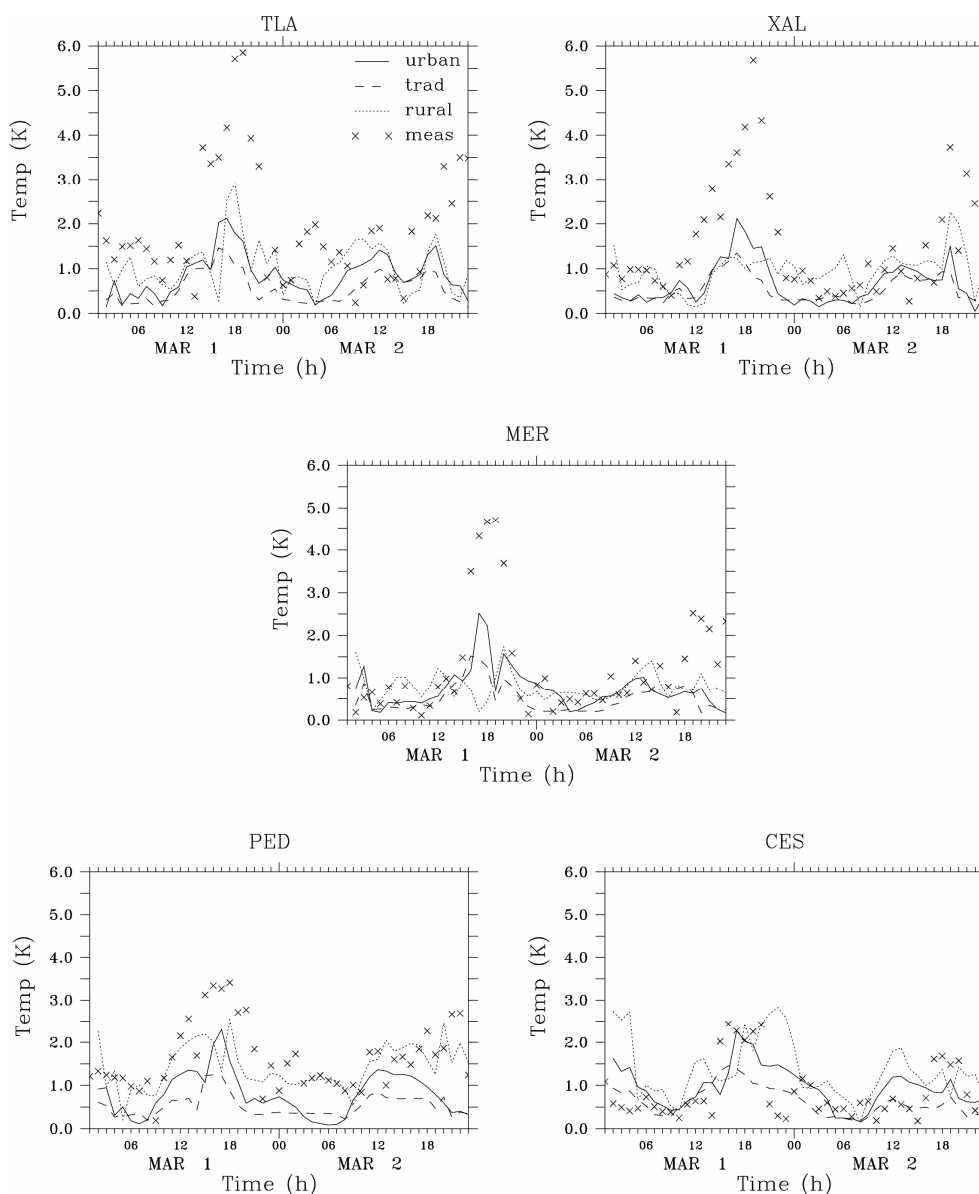
Figure 5.15. The wind-speed distributions close to ground as functions of time from 01 LT 1 March to 23 LT 2 March 1997 according to simulations '*urban*' (solid lines), '*trad*' (dashed lines), and '*rural*' (dotted lines) and according to the measurements (crosses) for five ground observation sites.

The distributions of wind speeds and wind directions along the vertical were compared with wind-profiler data recorded at three locations (see Figure 5.8) which, depending on the station and on the parameter observed, reached a maximum of 4000 m a.g. For the purposes of validating the model, the wind-profiler data from the observation site CUAU (see the location in Figure 5.8) were used. A comparison of profiles performed for the other two stations (CHAL and TEOT), which give results similar to those from CUAU, can be found in the Annexes.

Vertical wind-speed and wind-direction profiles were only compared for '*urban*' (Figure 5.16 and Figure 5.17), since the differences between the three simulations become very small with increasing height (the results are always similar above 1000 m a.g.). The small differences arising between the simulations close to ground (see the Annex) are due to the influence of the city on its surroundings (the station is located only a few kilometres away from the city limits).
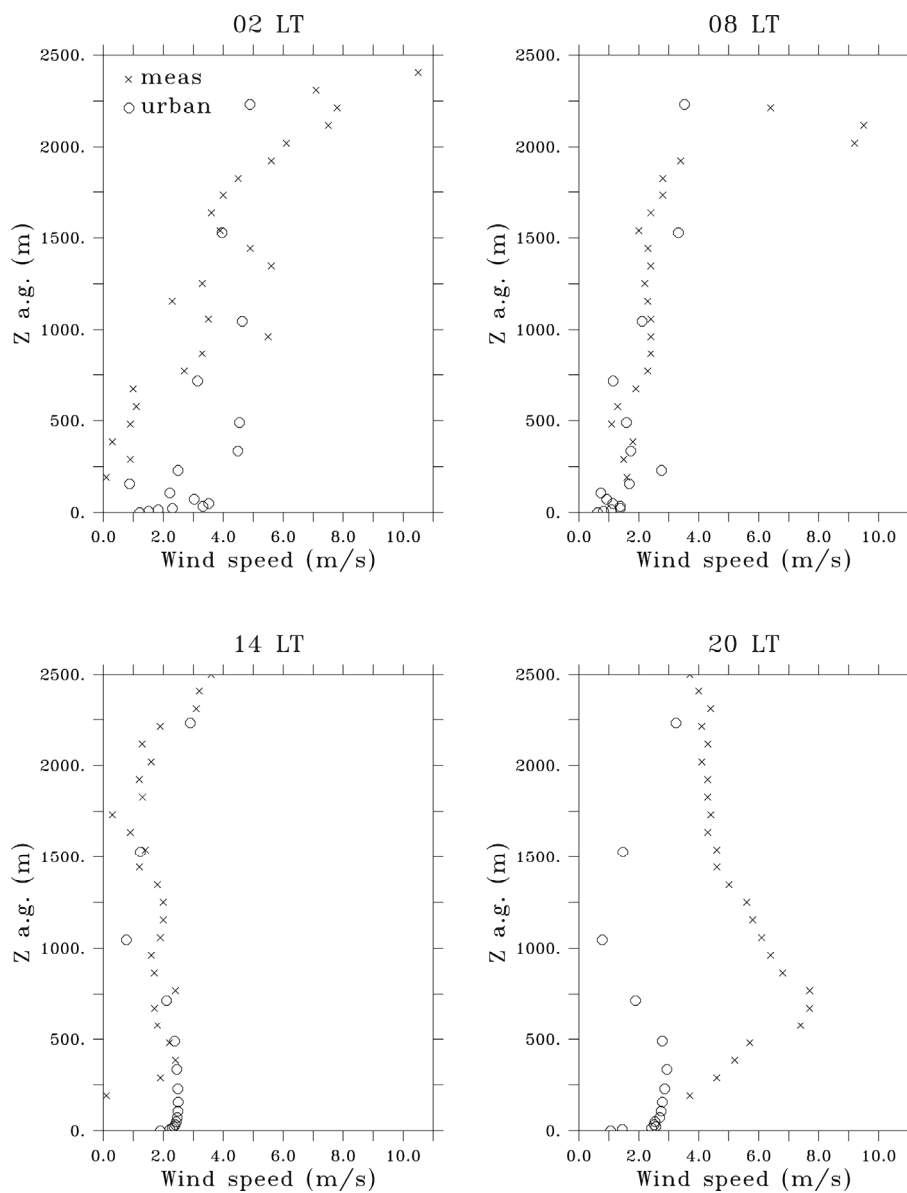

Figure 5.16. Vertical wind-speed distributions according to the simulation '*urban*' (circles) and according to the wind-profiler measurements at the station CUAU (crosses) at 2 LT (top left), 8 LT (top right), 14 LT (bottom left), and 20 LT (bottom right) 2 March 1997.

The vertical wind-speed distributions mesaured at night (*eg*, 02 LT) are very inhomogeneous, inasmuch as sharp variations occur over small vertical distances. Still, a trend for wind speeds to increase from 1 m/s close to ground to 10 m/s at 2500 m a.g. can be pointed out. The model reproduces the sharp speed variations close to ground, but the overall trend of wind speeds increasing with increasing height is underestimated, since the simulated wind speed at 2000 m above ground is of the order of only 6 m/s. Shortly after sunrise (08 LT) the "chaotic" nighttime profile with low wind speeds up to 1000 m a.g. is still present, both according to the measurements and according to the simulations. Above this height, the observed wind speeds increase very rapidly (from 2 to 8 m/s between 1000 and 1500 m a.g.), while the model computes a smaller wind-speed gradient in this layer and reaches wind speeds of 8 m/s, only at 4000 m a.g.

During the night and early in the morning, the wind direction changes from south-west close to ground to north-east at 1000 m a.g. and then to an east-south-easterly wind corresponding to the mean synoptic wind direction (Figure 5.3) above 1500 m a.g. The south-westerly wind close to ground corresponds to the downslope wind generated by nighttime radiation cooling along the mountain range west of the city which blows down the eastern slope towards the city (see the location of the station relative to the mountain range west of the city in Figure 5.8).

In the afternoon (14 LT), the measured wind speeds remain more or less constant from ground up to 1000 m a.g. (2 m/s), where they start to increase with a constant gradient. This layer of constant profile then coincides in height with the PBL, where turbulent mixing is responsible for homogenous conditions. In the model, this overall shape is computed, but the increase in wind speeds occurring above 1500 m a.g. is overestimated.
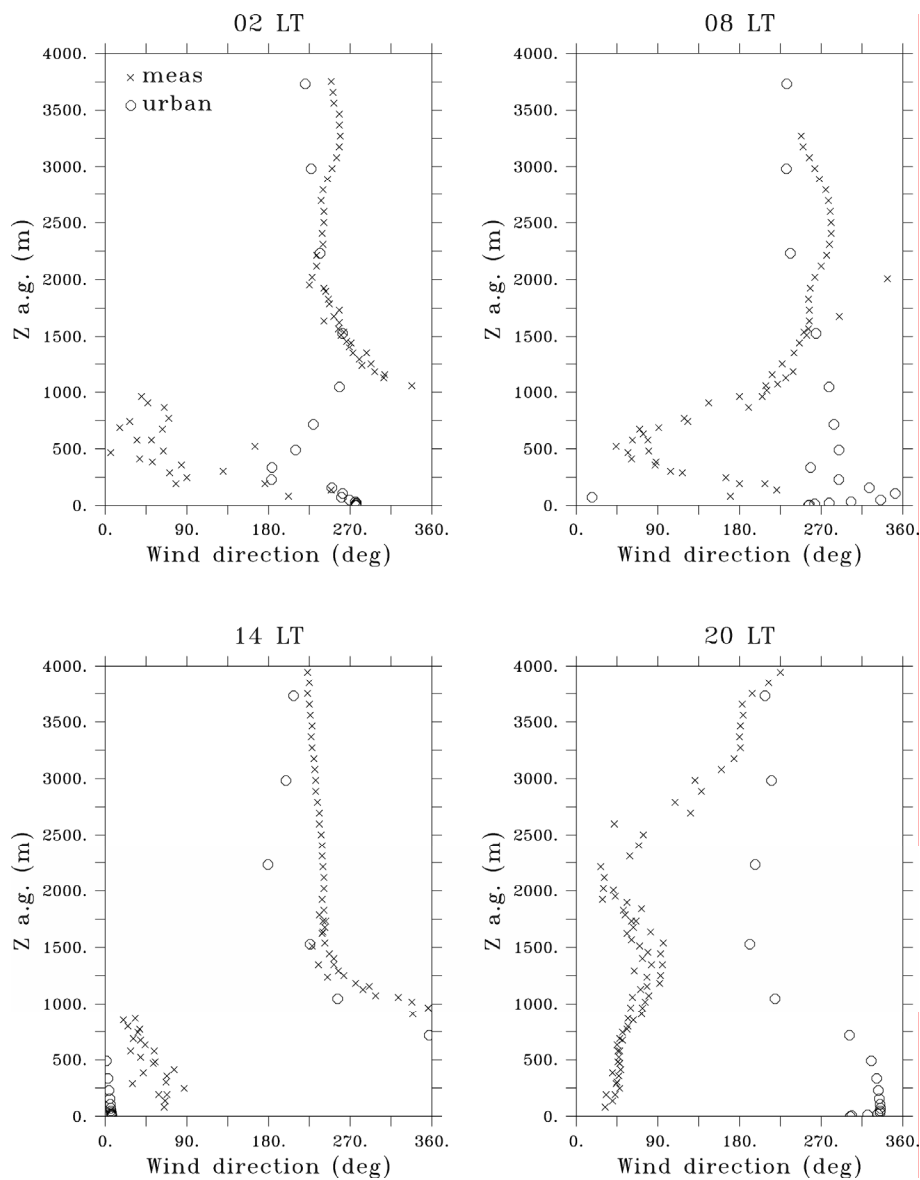
Figure 5.17. Vertical wind-direction distributions according to the simulation '*urban*' (circles) and according to the wind-profiler measurements at the station CUAU (crosses) at 2 LT (top left), 8 LT (top right), 14 LT (bottom left), and 20 LT (bottom right) 2 March 1997.

The observed wind directions are well reproduced along the entire profile. The wind blows from north-east from ground up to 1000 m a.g., which corresponds to the thermally induced daytime upslope wind from the basin towards the western mountain range. Above this height, the observed winds change to the synoptic wind direction (east-south-east), and so do the simulated winds.

Shortly after sunset (20 LT, sunset is at 19 LT for the simulated period), when the mixing height had just reached its maximum, the wind speeds are more or less constant up to 2000 m a.g., with values of 4 m/s from the measurements and of 2 m/s from the model. The measured direction is north-east up to the top of the PBL and then changes to the synoptic east-south-east wind. The simulated directions coincide with the synoptic wind direction, already at 1500 m a.g., which indicates that the model underestimates PBL height at that time.

The direction of the synoptic wind measured by the wind profiler is in good accord with the direction indicated by the data used for the forcing. This provides confirmation that the forcing data, which were interpolated from low resolution to the meteorological grid, represent the actual situation over the Mexico City basin during the period of interest.

5.5. Results of air-quality modelling

The Eulerian photochemical model was run over the Mexico City area (domain B defined in Figure 5.4) while using the meteorological fields simulated by '*urban*' as the inputs. However, only the portion corresponding to the emissions inventory (domain D) was used for visualising the results and validating the model against the the measured data. The photochemical results were compared with two runs using the meteorological fields from '*trad*' and from '*rural*', respectively, in order to determine the impact of the new urban parameterisation on air-quality modelling. One measuring station out of each group defined in Section 5.3 was used for the validation, just as done when validating the meteorological modelling.. These five stations were those chosen for the meteorological validation. For the purposes of validation, only the second day of the simulation was used (2 March), since the first day serves as initialisation period during which the model attains stability with respect to the pollutant concentrations.

5.5.1. Primary pollutants

The NO$_2$ concentrations recorded as functions of time during 2 March 1997 at each station, and those found by the simulations, are shown in Figure 5.18.
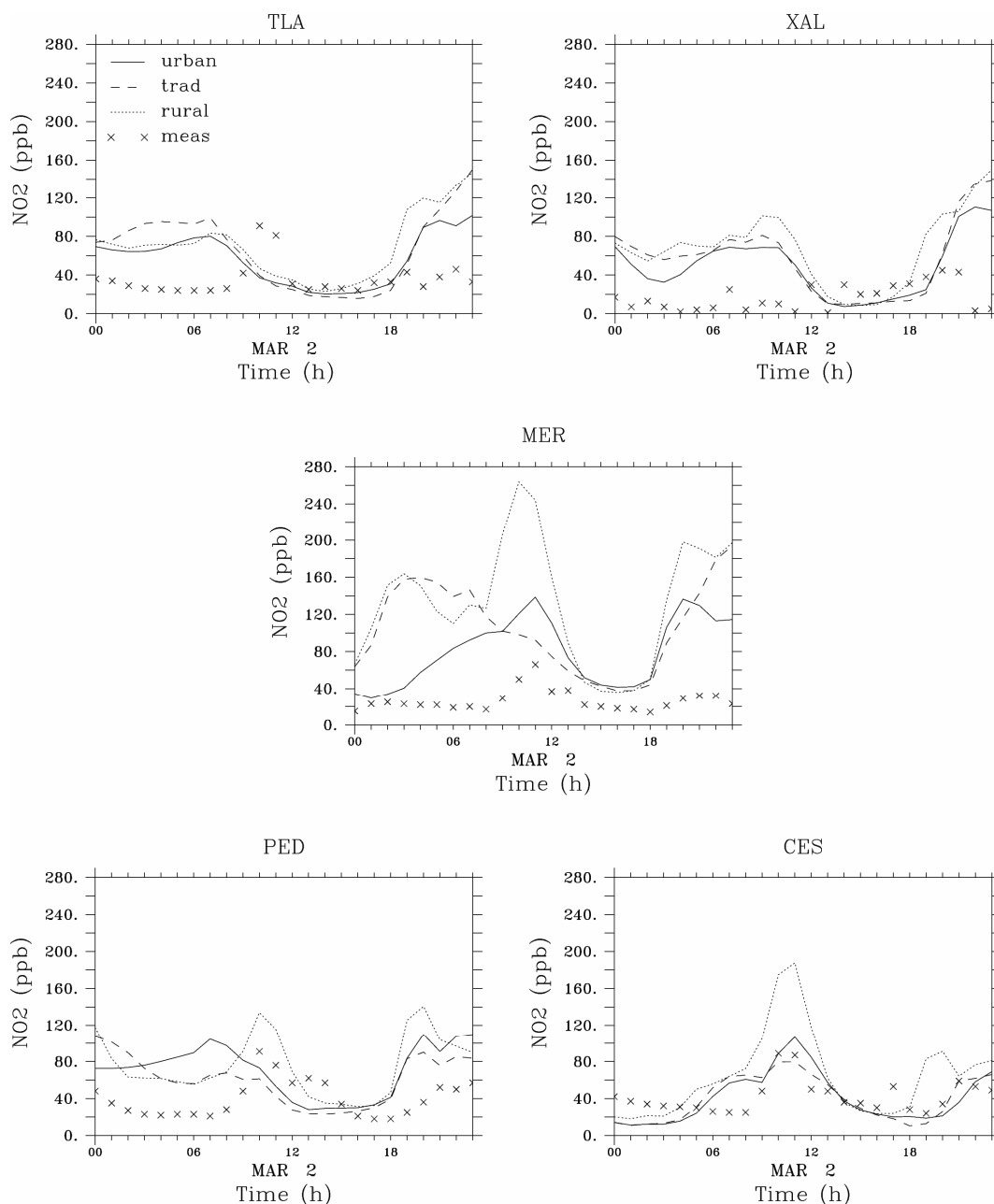

Figure 5.18. NO₂ concentrations [ppb] close to ground as functions of time from 00 LT 2 March to 23 LT 2 March 1997 according to the simulations '*urban*' (solid lines), '*trad*' (dashed lines), and '*rural*' (dotted lines) and according to the measurements (crosses) for five ground observation sites.

The background levels of NO_2 in the city are around 40 ppb. During peaks (10-11 LT, depending on the station), the concentrations double in all the stations except XAL, where almost no daily variations were measured. The model results overestimate the concentrations at all stations. It had been pointed out above that the model underestimates the mixing layer in late afternoon. The high values of the simulated NO_2 concentrations found at that time thus are to be seen in relation to this phenomenon. A thinner mixing layer implies a smaller volume of air within which the pollutants are vertically dispersed, and hence higher pollutant concentrations within this layer. Qualitatively, the daily pattern and in particularly the occurrence of peaks is reproduced.

The simulation of primary pollutants heavily relies on two kinds of input data. On one hand, on good quality of the emissions inventory, which is important for the amount of pollutants injected into the model, but which is not easy to guarantee. On the other hand, on the local meteorological input, which is crucial, since primary pollutants are very rapidly transformed. Thus, simulated concentrations at a given point highly depend on PBL height and on winds calculated for that point. It is very difficult, therefore, to obtain simulated primary pollutant concentrations that are consistent with the experimental conditions.

It is important in this context to evaluate the impact of urban parameterisation on the primary-pollutant simulation, since it operates through a simulation of the local meteorological conditions. In the present case, simulations according to the urban scheme produce model results involving lower peak values, which are more realistic in view of measured data. The fit of model results to measured data thus is improved, *eg*, in MER and CES.

The space distribution of NO_2 in the domain according to the '*urban*' simulation (Figure 5.19) reveals a diurnal cycle over the city where, due to a higher traffic activity (see the hourly evolution

for 2 March 1997 in the Annexes), the concentrations increase during the day. The surroundings remain free of NO_2, since emitted pollutants are chemically transformed before they reach the countryside or are vertically carried away by the turbulence. This pattern is typical of a primary pollutant emitted in a city (*eg*, see the studies over Milan: Martilli *et al*, 2003, and over Athens: Clappier *et al*, 2000).
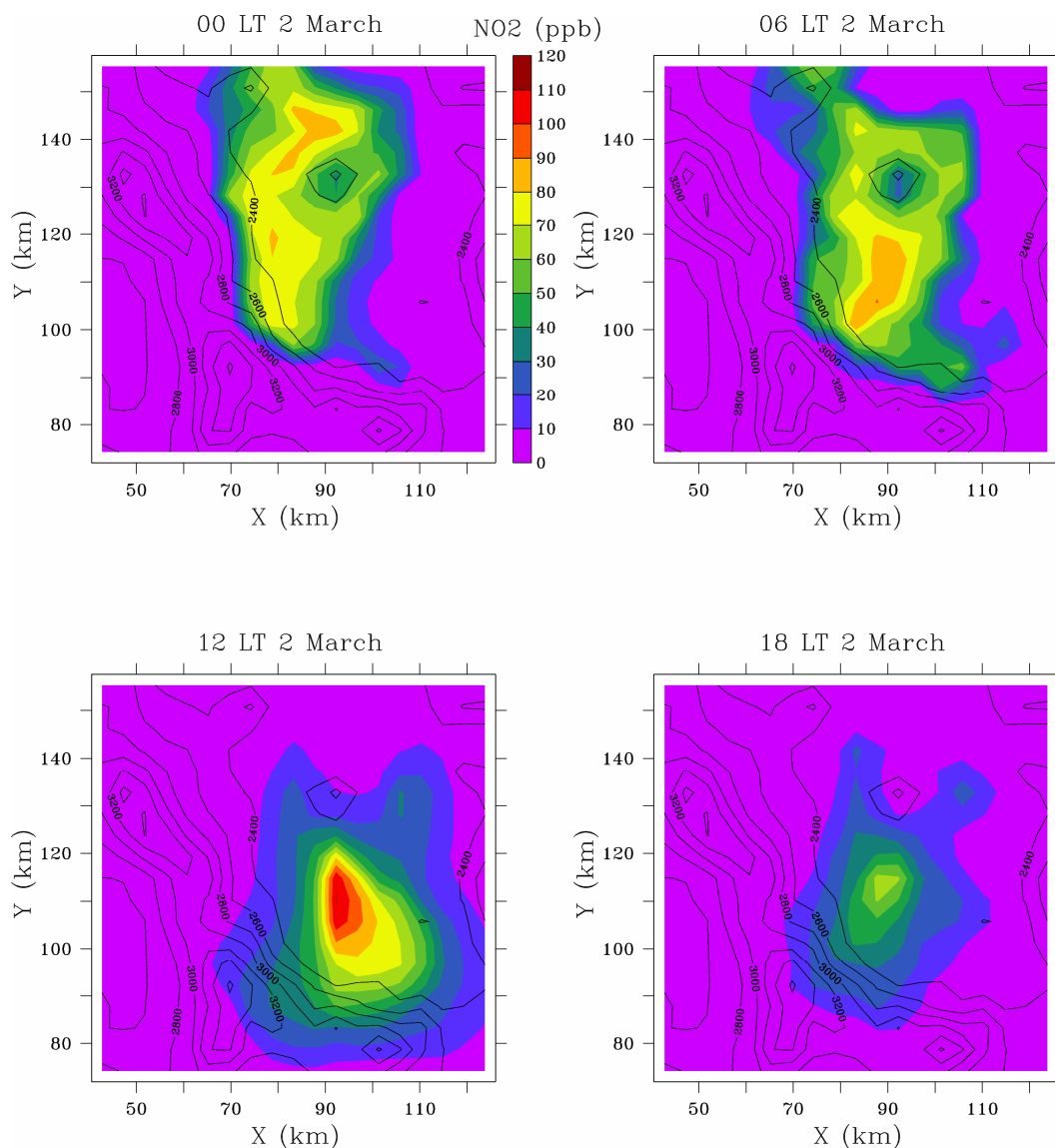

Figure 5.19. NO_2 concentrations [ppb] close to ground in the Mexico City Area at 00 LT (top left), 06 LT (top right), 12 LT (bottom left), and 18 LT 2 March 1997 (bottom right) according to a TAPOM simulation using the '*urban*'-simulated meteorological fields as input.

The plume is pushed northward during nighttime, and southward during daytime, which is in harmony with the wind fields produced by the model (Figure 5.14). Concerning vertical transport, the pollutants are subject to the effects of turbulence during daytime, as shown by a vertical profile of the NO_2 concentration along a north-south profile across the Mexico City Area (Figure 5.20).
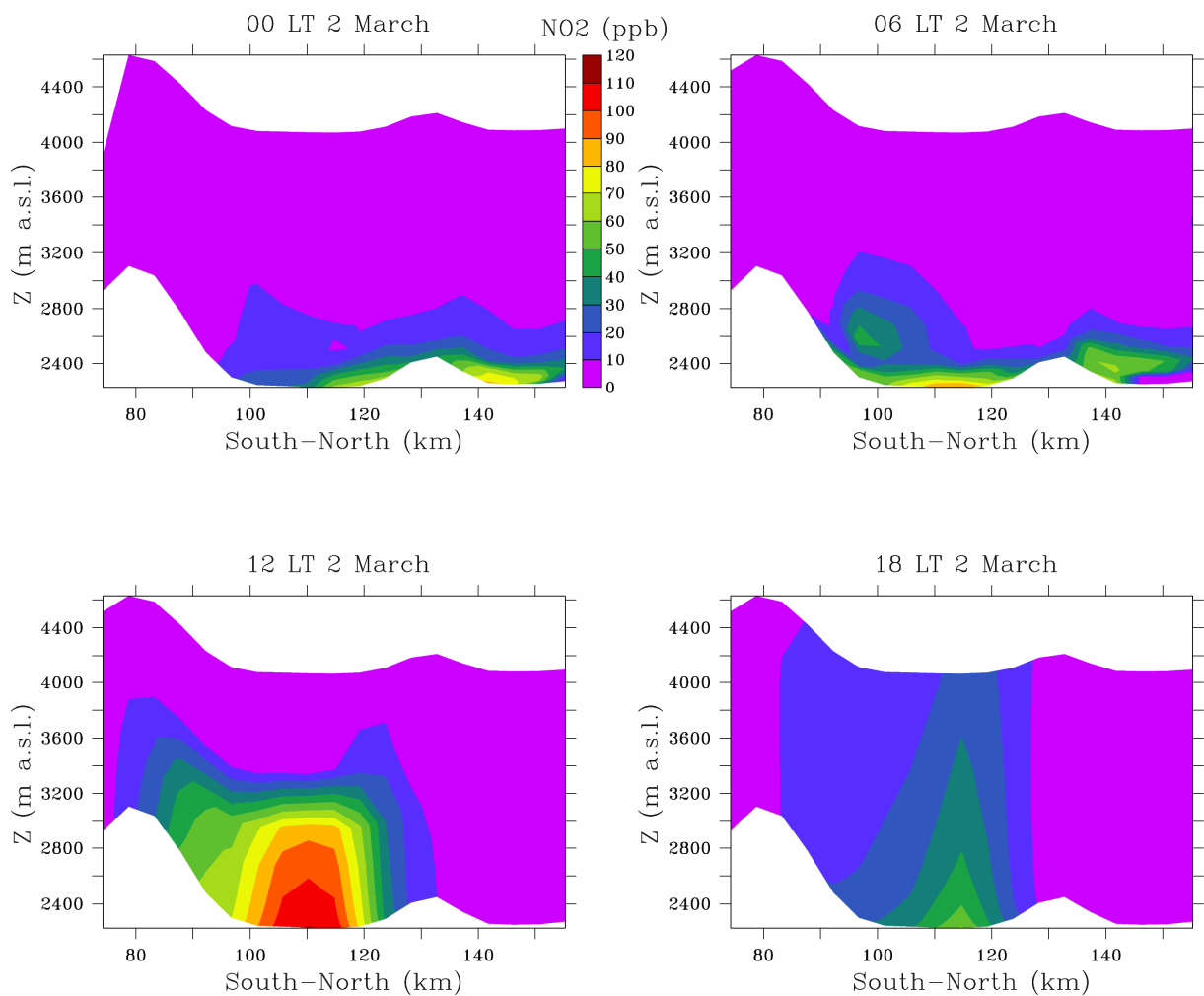

Figure 5.20. Vertical distribution of the NO₂ concentrations [ppb] in a south-north profile in relation to topography across the Mexico City area (from 100 to 120 km on the x-axis) at 00 LT (top left), 06 LT (top right), 12 LT (bottom left), and 18 LT 2 March 1997 (bottom right) according to a TAPOM simulation using the '*urban*'-simulated meteorological fields as input.

The concentrations of NO_2 above the city start to increase with increasing traffic emissions (06 LT). The incoming solar radiation initiates turbulence, which mixes the pollutants within the

PBL. Therefore, the concentrations are nearly constant up to 1000 m a.g. at 12 LT. During the afternoon, maximum turbulence intensity produces the maximum PBL height and, hence, the maximum air volume within which the pollutants can be dispersed. Moreover, the NO_2 in this layer is used for O_3 formation. Hence, the NO_2 concentration in the PBL decreases (18 LT). After sunset, the PBL collapses and shrinks to the nocturnal, stable boundary layer (a few tens of metres) within which the pollutants are trapped (00 LT). The values of 40 to 50 ppb found above this stable layer at 06 LT highlight the neutral residual layer within which the pollutants are trapped during the night after PBL decay.

5.5.2. Secondary pollutants

Contrary to what was found for the primary pollutants, the calculated ozone concentrations are very similar for all three simulations at the five stations selected (Figure 5.21), although differences exist between the wind fields according to different simulations.

The model underestimates the ozone peak at all the stations. It is able nevertheless to reproduce the typical daily cycle of the ozone concentrations including ozone production during the day (when solar radiation is available for the reaction) and destruction through NO_x and VOC during the night. The simulated ozone concentration peaks which occur at the stations at dissimilar times are smoother than measured peaks (Figure 5.21). These smoother simulated peaks are due to the weak winds prevailing during the episode simulated, and giving rise to air stagnation above the city.
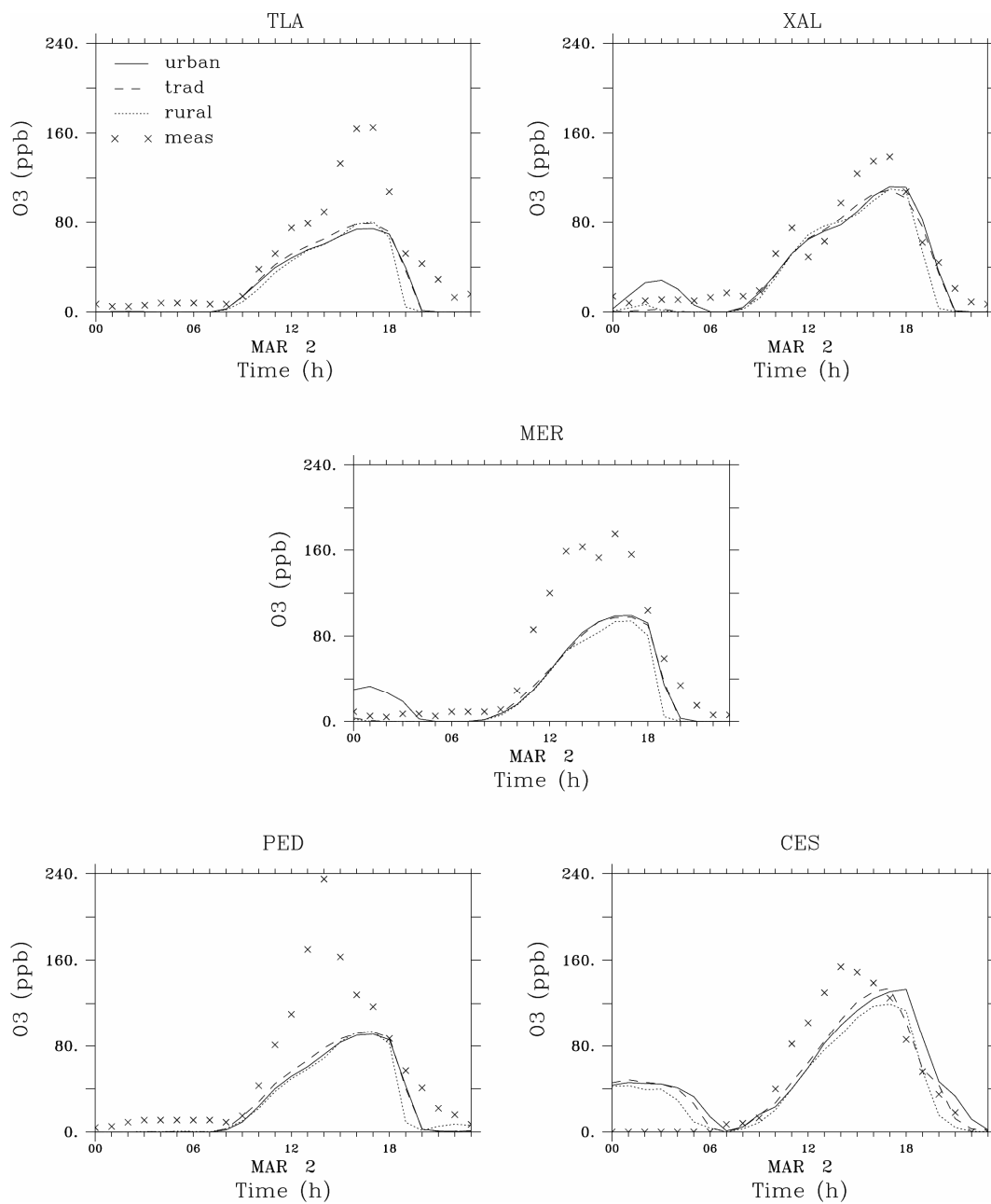
Figure 5.21. O₃ concentrations [ppb] close to ground as functions of time from 00 LT 2 March to 23 LT 2 March 1997 according to the simulations '*urban*' (solid lines), '*trad*' (dashed lines), and '*rural*' (dotted lines) and according to the measurements (crosses) for five ground observation sites.

Underestimating the peak at a given point can be interpreted in two ways. First, the model may not be able to produce enough ozone with the given quantity of precursors. This in turn can have two different reasons: either the chemical mechanism needs to be modified, or the emissions inventory does not reflect the real situation. West *et al* (1999) have shown that the emissions

inventory used in the present study underestimates the VOC emissions by a factor two. Secondly, the model may produce concentrations identical with those of the peak, but they do not occur at the same point. This would be due to the meteorological conditions prescribed to the photochemical model. Therefore, both the emissions inventory and the meteorological fields are crucial input data for a photochemical model.
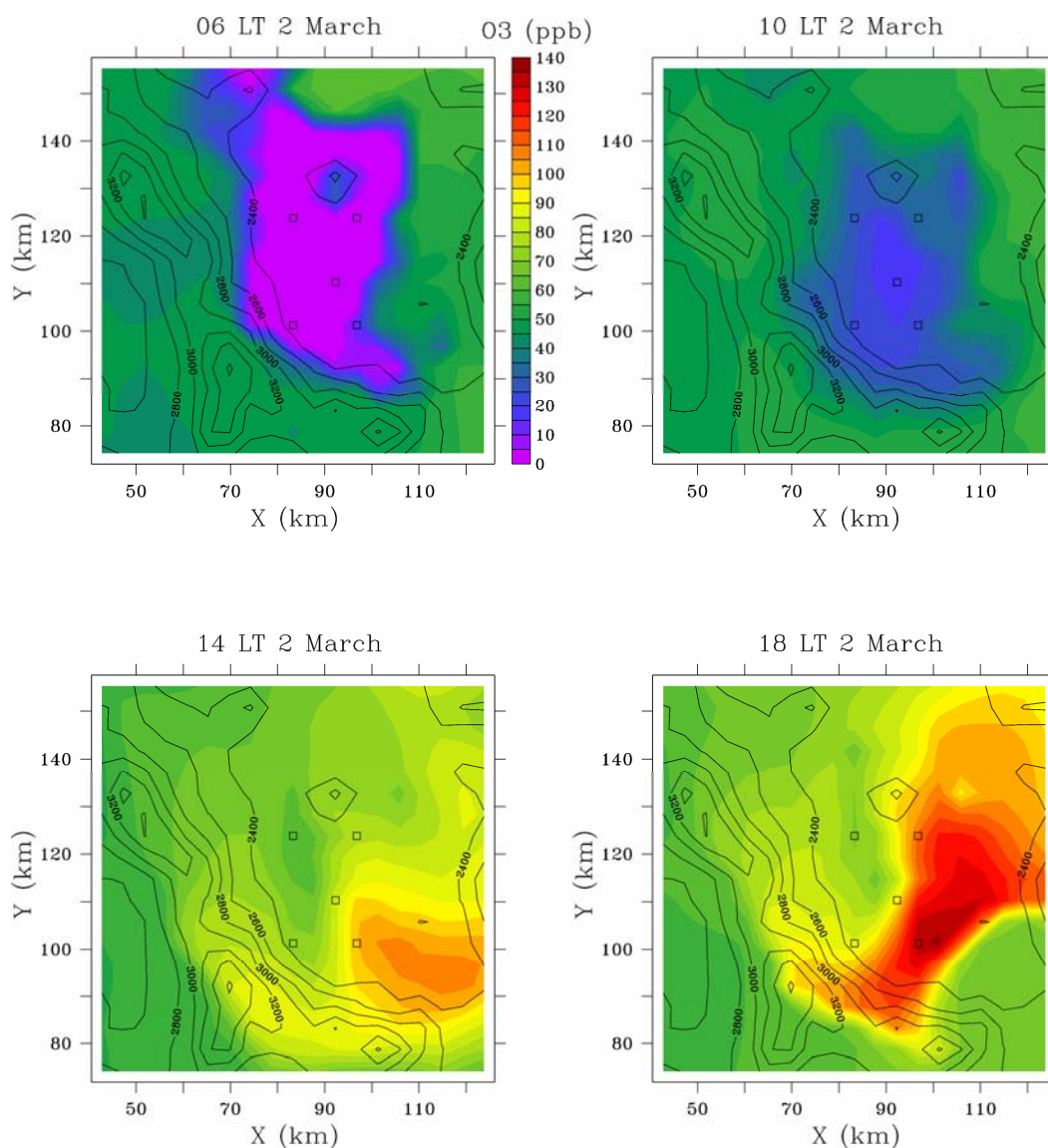

Figure 5.22. O$_3$ concentrations [ppb] close to ground in the Mexico City Area at 06 LT (top left), 10 LT (top right), 14 LT (bottom left), and 18 LT 2 March 1997 (bottom right) according to a TAPOM simulation using the '*urban*'-simulated meteorological fields as input. The measuring sites used for validation are indicated on the maps with squares.

The maximum ozone concentration of 140 ppb produced by the model occurs at 18 LT (Figure 5.22, see the hourly evolution on 2 March in the Annexes), while the maximum measured concentration amounts to almost 240 ppb (at the measuring site PED). However, this value of 240 ppb is not typical, since the maxima at all other stations are only about 150 to 180 ppb. Therefore, except for this exceptional value measured at PED, the model is able to produce ozone in similar quantities as observed in the domain.

Looking back at the ozone distributions found at each measuring site (Figure 5.21), we notice that the model results were best for the south-east station (CES). The space distributions measured at 14 LT and 18 LT 2 March (Figure 5.22) show that the ozone plume crosses this station, while the other observation points are located further north. Hence, at station CES the highest peak intensity is measured. This is in harmony with the data analysis (Section 5.3) and with the meteorological results (Section 5.4) in which a convergence line was detected. The model placed this convergence line south of its actual position (Figure 5.14), and so the location of the ozone plume. For this reason the simulated ozone concentrations are strongly underestimated at TLA, XAL, MER, and PED, since the maximum peak intensity (which is simulated further south than its actual position) is missed.

The vertical profiles across the domain (Figure 5.23) reveal the ozone consumption layer existing during the night (6 LT) and reaching 200 m a.g. over the city, where the ozone concentration falls to zero. Above this layer, the ozone concentration corresponds to the background level of the region (50 to 60 ppb), except for a zone south of the city where concentrations are lower. There, ozone is consumed by the NO_2 trapped in the residual layer, as explained above. Ozone production starts shortly after sunrise.
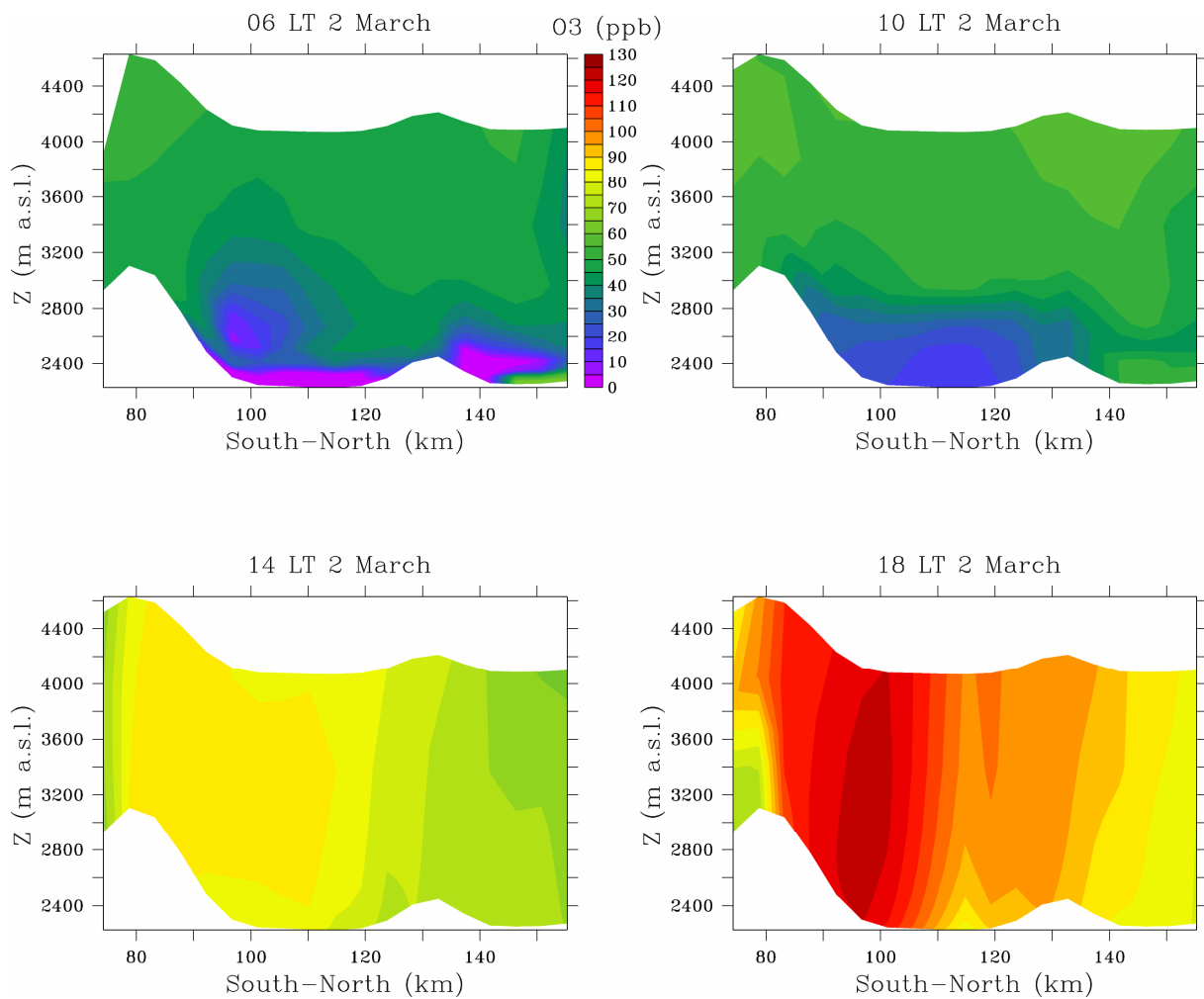
Figure 5.23. The vertical distributions of the O₃ concentrations [ppb] in a south-north profile in relation to topography across the Mexico City area (from 100 to 120 km on the x-axis) at 06 LT (top left), 10 LT (top right), 14 LT (bottom left), and 18 LT 2 March 1997 (bottom right) according to a TAPOM simulation using the '*urban*'-simulated meteorological fields as input.

At 10 LT, the concentration over the city is already about 30 ppb. The ongoing solar activity produces more ozone and more turbulence as well, which results in vertical transport of the pollutant, just as for NO₂. The convergence line discussed above, and its associated ozone maximum, appear diffusely in the profiles at 14 LT, and more distinctly at 18 LT, where ozone attains its maximum concentrations over the entire thickness of the PBL.

5.6. Emission reduction scenarios

The results of the photochemical model over the Mexico City area have been validated in the previous section. Hence, the model can now be used to test emission reduction scenarios. For this purpose, TAPOM was run, on one hand with a reduction of the NO_x emissions by 35 %, and on the other hand with a reduction of the VOC emissions by the same percentage. Both scenarios were tested with the '*urban*' meteorological fields and with the '*trad*' meteorological fields as inputs for TAPOM. The new simulated ozone concentrations were first analysed as such, then their relative impact on ozone abatement was evaluated in order to ascertain NO_x and VOC-sensitive zones.

5.6.1. NO_x emission reduction

Lower amounts of NO_x emitted all across the city, according to the model, lead to larger ozone concentrations over major part of the city area (Figure 5.24), with a maximum increase of 60 ppb occurring in centre city.

As a consequence, the ozone maximum reaches a value of 170 ppb in the domain at 18 LT (when the plume is well developed). Referring to the ozone isopleths shown in Figure 5.1, the entire city area thus corresponds to point A in the diagram, where a NO_x emission reduction leads to enhanced ozone production. This VOC-sensitive behaviour is typical of city centres (*eg*, Milan: Junier, 2004).
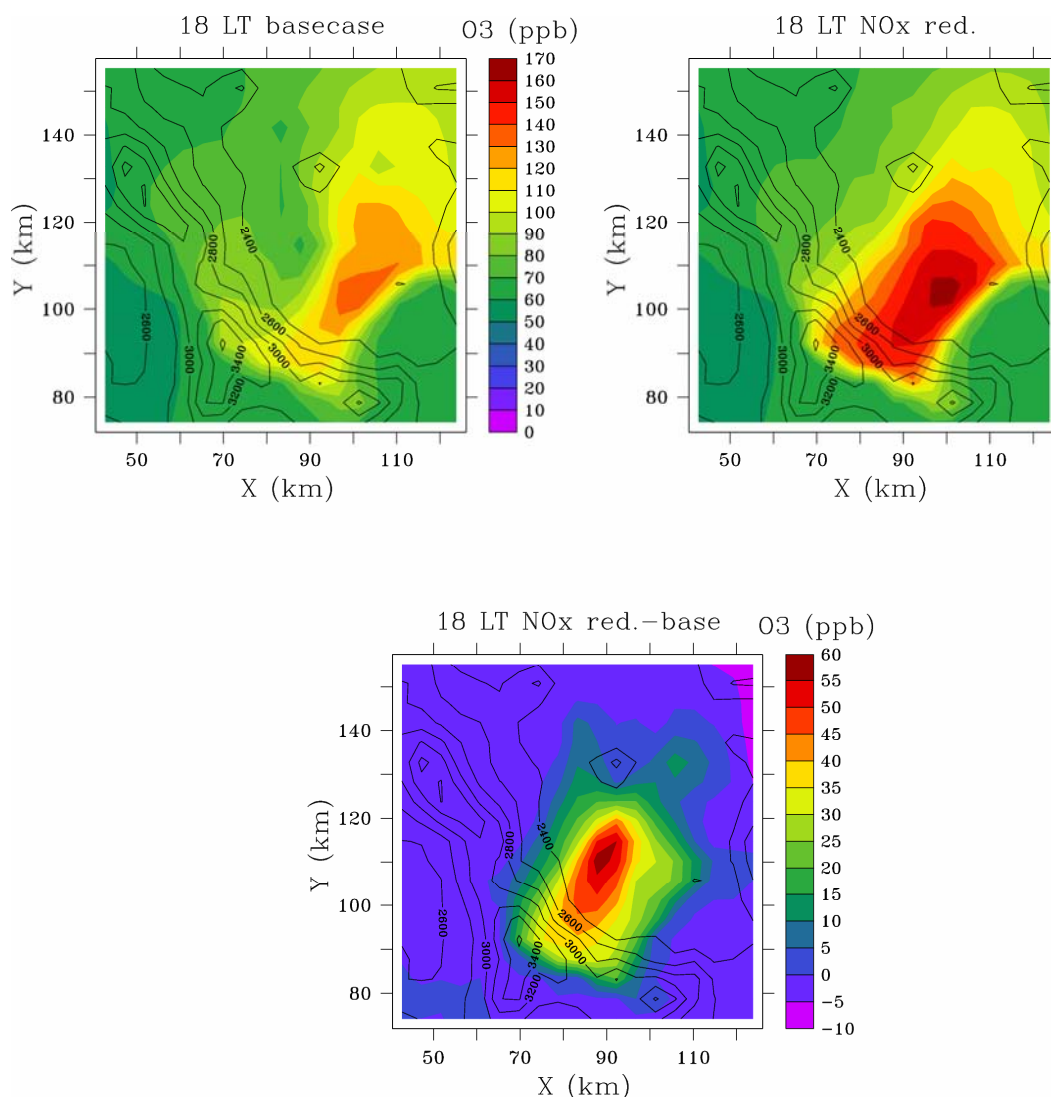
Figure 5.24. O$_3$ concentrations [ppb] close to ground in the Mexico City area at 18 LT according to a TAPOM simulation using the '*urban*'-simulated meteorological fields as input: base case for emission input according to the inventory (top left), NO$_x$ emissions lowered by 35 % (top right), and ozone concentration differences [ppb] between the two simulations (bottom). Positive values indicate that a reduction of NO$_x$ emissions has led to more ozone.

5.6.2. *VOC emission reduction*

The VOC reduction scenario produces more encouraging results, since in this scenario the ozone concentrations are lowered by 20 to 50 ppb over the entire city area (Figure 5.25). This result confirms that the entire city is a VOC-sensitive area, where ozone concentrations can only be reduced by a reduction of the VOC emissions.
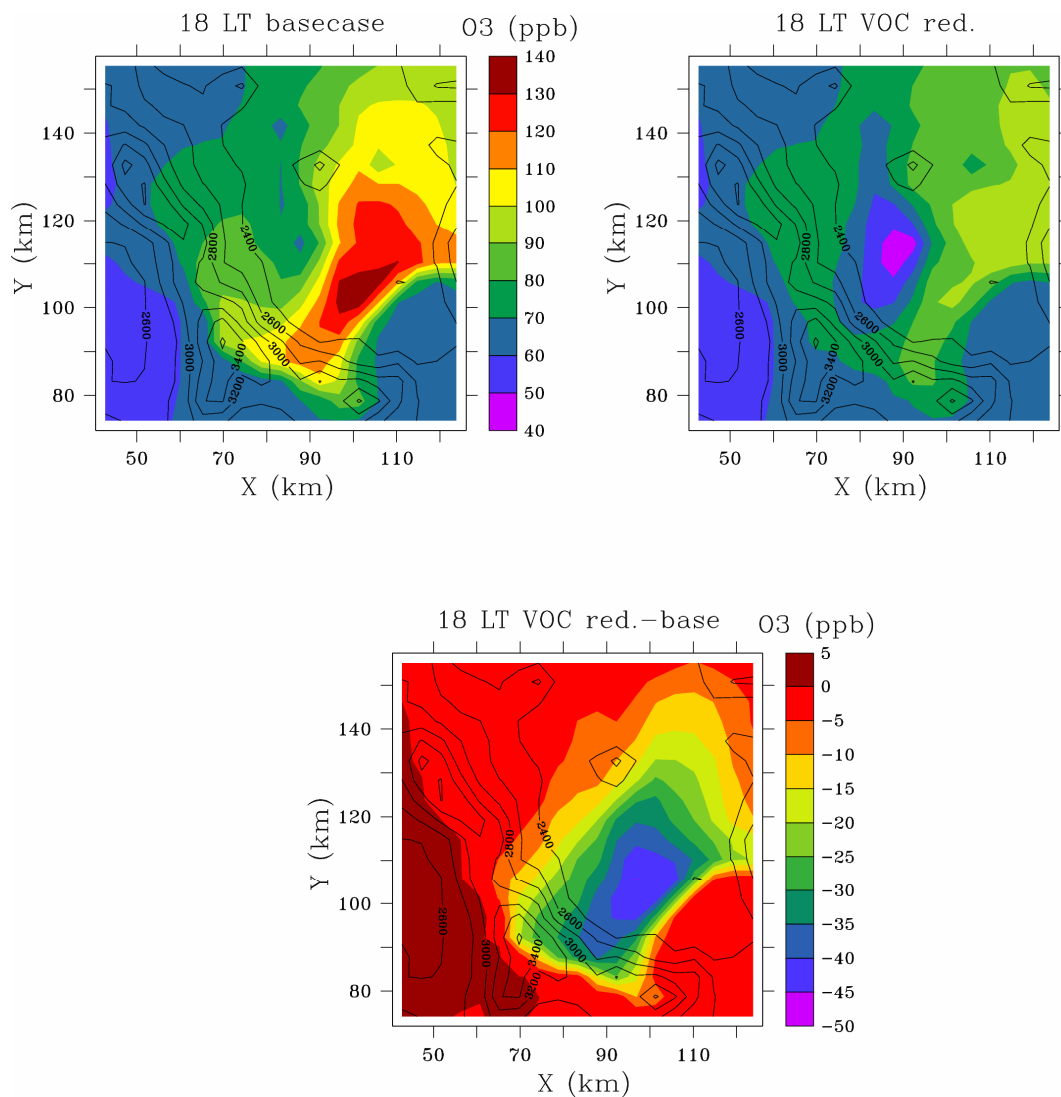
Figure 5.25. O₃ concentrations [ppb] close to ground in the Mexico City Area at 18 LT according to a TAPOM simulation using the '*urban*'-simulated meteorological fields as input: base case for emission input according to the inventory (top left), VOC emissions lowered by 35 % (top right), and ozone concentration differences [ppb] between the two simulations (bottom). Negative values indicate that a reduction of VOC emissions has led to less ozone.

Finally, the ozone concentration differences between the simulations with a NO$_x$ reduction scenario and the simulations with a VOC reduction scenario were calculated in order to obtain maps for the VOC and NO$_x$-sensitive zones (Figure 5.26).
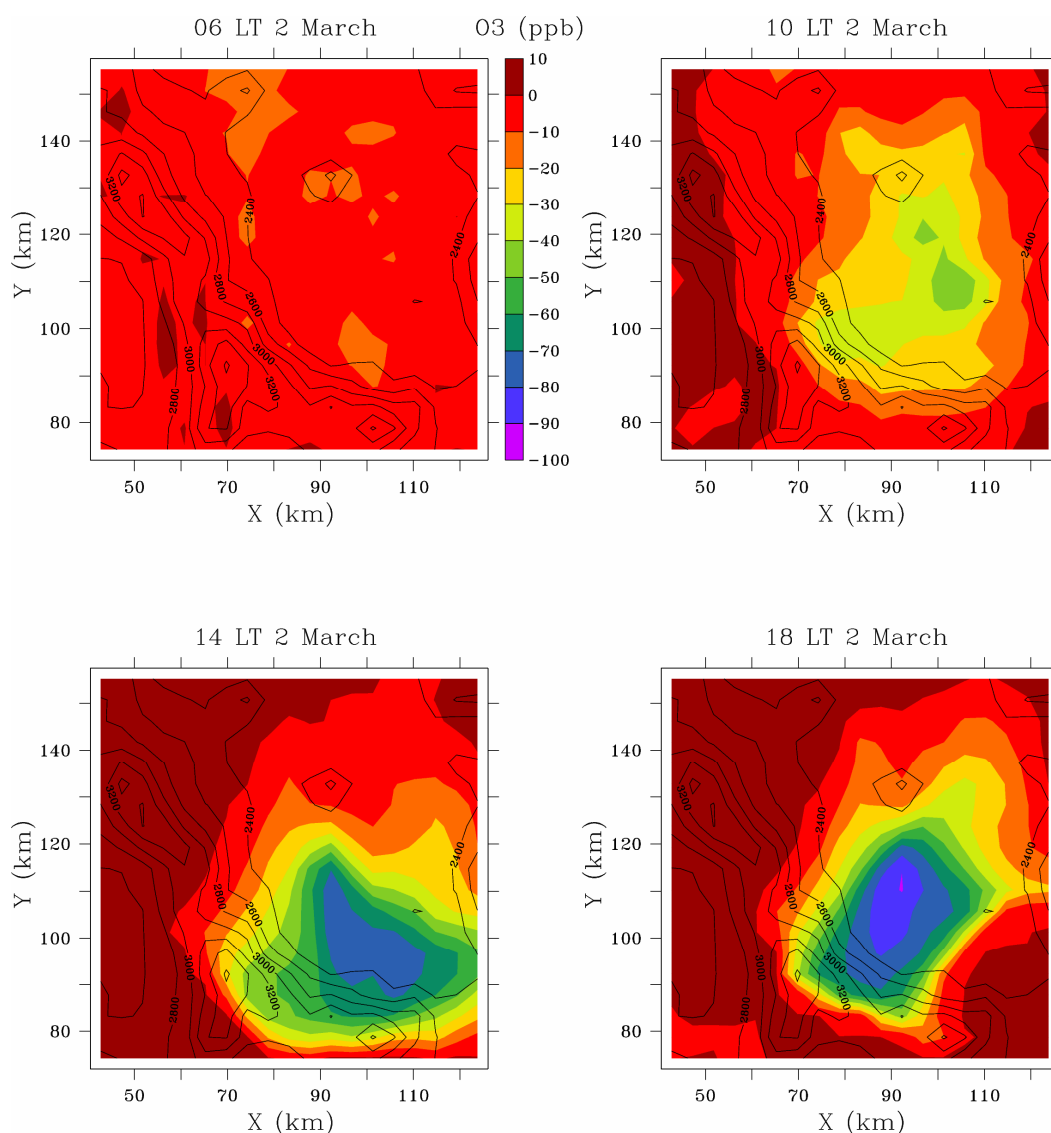
Figure 5.26. Differences in O₃ concentrations [ppb] close to ground between the VOC and NOₓ reduction scenario in the Mexico City area at 06 LT (top left), 10 LT (top right), 14 LT (bottom left), and 18 LT 2 March 1997 (bottom right) according to a TAPOM simulation using the '*urban*'-simulated meteorological fields as input. Negative values indicate that a reduction of VOC emissions has led to lower ozone concentrations than a reduction of NOₓ emissions.

The entire city area is highly VOC-sensitive during daytime, since a reduction of the VOC emissions by one third leads to an ozone reduction of the same order of magnitude. The city surroundings are indifferent to NOₓ emission reductions during nighttime (just as the city area), but turn into a slightly NOₓ-sensitive area during daytime. A one-third NOₓ emission reduction will in fact lead to an ozone concentration reduction of the order of 10 % in the city surroundings.

As already shown, the urban parameterisation scheme improves the results of the photochemical model, especially what primary pollutants concern. Nevertheless, the shape of the ozone plume is also modified. Hence, emissions reduction scenarios should not produce the same results for '*urban*' and for '*trad*'. The ozone plume calculated by '*urban*' is indeed larger in horizontal space as the plume obtained by '*trad*' at 18 LT (Figure 5.27). This is probably due to the weaker wind above the city calculated by the urban module.
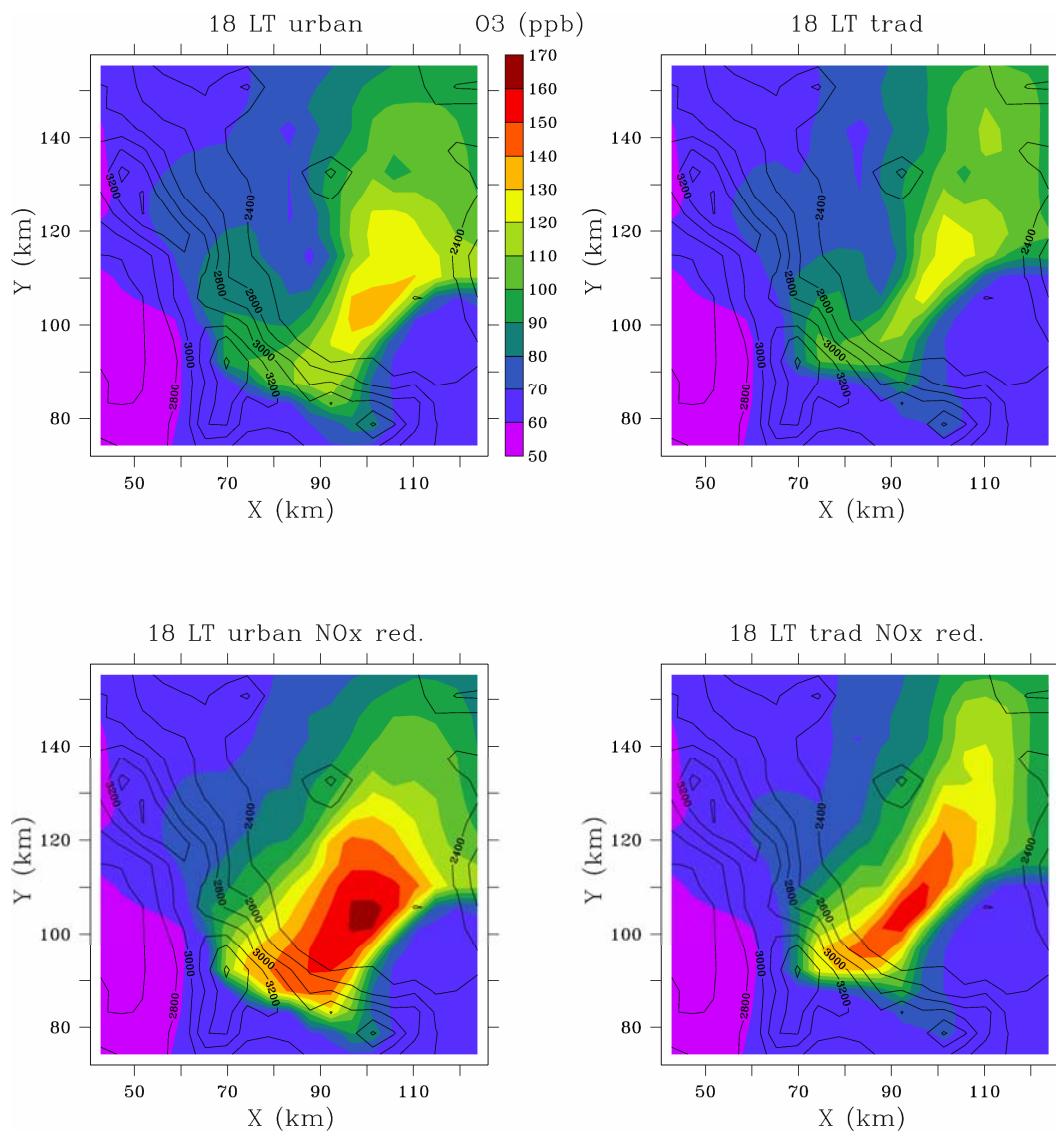

Figure 5.27. O$_3$ concentration [ppb] near ground in the Mexico City Area at 18 LT according to TAPOM simulation with the '*urban*' (top left) and the '*trad*' (top right) simulated meteorological fields as input, and the same situation with a NO$_x$ emissions reduction by 35% with '*urban*' (bottom left) and '*trad*' (bottom right).

Similar to the basecase simulation, the NO_x reduction scenario produces more ozone, covering a more extended area, over the city with '*urban*' than with '*trad*' (bottom of Figure 5.27). The differences between the traditional method and the urban scheme occurs therefore not only for primary pollutants (as seen by comparison with point measurements), but also for the pattern of the ozone plume.

5.7. Conclusions

The mesoscale model with the urban parameterisation scheme was applied to the atmosphere over the large Mexico City Metropolitan Area. This simulation was tested against a simulation with the traditional method for urban modelling, and against a simulation not accounting for the urban area. The comparison of the model results with measured data showed that the mesoscale simulation over the Mexico City basin was improved when the new scheme was used, particularly so with respect to the temperatures within the city.

The validated model was used to feed a Eulerian photochemical model which in turn was used to perform an air-quality study over the highly polluted Mexico City area. The episode simulated was a 48-h period during an intense measuring campaign that took place in the 1997 dry season (February-March). The analysis of the results focused on primary pollutants (NO_2) and on the formation and transport of secondary pollutants (O_3) in the atmosphere. The model results yield values of ozone production over the area studied that are in agreement with observed concentrations. The specific features of the domain (large urban expanse and complex topography of the surroundings) lead to the development of ozone concentration peaks in the pollutant plume over the city, in contrast to many other cases where ozone is found downwind over the surrounding rural area. Weak winds during the episode are also responsible for plume stagnation. The model reproduces the ozone plume over the city, but not in exactly the same

place as indicated by direct measurements. This is due to simulated meteorological fields underestimating the southerly wind entering the basin during daytime. Nevertheless, the levels of ozone production simulated by the model are in agreement with the measured data, according to a comparison made at a measuring point situated within the simulated plume.

The use of urban paramerisation has an impact on air-quality modelling for primary pollutants. The module modifies the meteorological fields directly above the city, where the primary pollutants are emitted. Therefore, an increase in the quality of meteorological input will lead to improved modelling of the primary pollutants. The impact of urban parameterisation on secondary pollutants is minor at any given local site, but the overall plume pattern is found to be strongly modified, as revealed with an analysis of the abatement strategies.

By tests of abatement strategies, VOC and NO_x-sensitive areas have been highlighted within the domain. As expected, the entire city area is VOC-sensitive during daytime, and more or less indifferent during nighttime (just as the rest of the domain), while the city surroundings become slightly NO_x-sensitive during daytime.

In future work on the Mexico City case study, the meteorological calculations should be improved. This can be done, on one hand by improving the input data for the urban module, in particular the morphological data characterising buildings and streets, and on the other hand by fine-tuning the model so as to increase the accuracy of the wind convergence representation. This in turn should lead to an improved primary and secondary pollutant simulation. Attention should also be given to the emissions inventory, which is a major source of uncertainties in air-quality modelling.

Acknowledgments

References

Bey I., Jacob, D. J., Yantosca, R. M., Logan, J. A., Field, B., Fiore, A. M., Li, Q., Liu, H., Mickley, L. J., and Schultz, M.: 2001, 'Global modeling of tropospheric chemistry with assimilated meteorology: Model description and evaluation', *J. Geophys. Res.* **106**, 23073-23096

Bossert, J. E.: 1997, 'An investigation of flow regimes affecting the Mexico city region', *J. Applied Meteorol.* **36**, 119-140

CAM (Comisión Ambiental Metropolitana): 2001, '*Inventario de emisiones a la atmósfera, Zona Metropolitana de Valle México, 1998*'

Clappier, A., Martilli, A., Grossi, P., Thunis, P., Pasi, F., Krueger. B. C., Calpini, B., Graziani, P., and van den Bergh, H.: 2000, 'Effect of sea breeze on air pollution in the Greater Athens Area. Part I: Numerical simulations and field observations', *J. Applied Meteorol.* **39**, 546-562

Doran, J. C., Abbott, S., Archuleta, J., Bian, X., Chow, J., Coulter, R. L., de Wekker, S. F. J., Edgerton, S., Elliott, S., Fernandez, A., Fast, J. D., Hubbe, J. M., King, C., Langley, D., Leach, J., Lee, J. T., Martin, T. J., Martinez, D., Martinez, J. L., Mercado, G., Mora, V., Mulhearn, M., Pena, J. L., Petty, R., Porch, W., Russell, C., Salas, R., Shannon, J. D., Shaw, W. J., Sosa, G., Tellier, L., Templeman, B., Watson, J. G., White, R., Whiteman, C. D., and Wolfe, D.: 1998, 'The IMADA-AVER boundary layer experiment in the Mexico City area', *Bull. Am. Meteorol. Soc.* **79**, 2497-2508

Fast, J. D., and Zhong, S.: 1998, 'Meteorological factors associated with the inhomogeneous ozone concentrations within the Mexico City basin', *J. Geophys. Res.* **103**, 18927-18946

Martilli, A., Clappier, A., and Rotach, M. W.: 2002, 'An urban surface exchange parameterisation for mesoscale models', *Boundary-Layer Meteorol.* **104**, 261-304

Martilli, A., Neftel, A., Favaro, G., Kirchner, F., Sillman, S., and Clappier, A.: 2002, 'Simulation of the ozone formation in the northern part of the Po Valley', *J. Geophys. Res.* **107**(D22), 8195

Masson, V., Grimmond, C. S. B., and Oke, T. R.: 2002, 'Evaluation of the Town Energy Balance (TEB) scheme with direct measurements from dry districts in two cities', *J. Applied Meteorol.* **41**, 1011-1026

Molina, L. T. and Molina, M. J. (Ed.): 2002, '*Air quality in the Mexico megacity, an integrated assessment*', Kluwer Academic Publishers, 384 pp.

Oke, T. R., Spronken-Smith, R. A., Jáuregui, E., and Grimmond, C. S. B: 1999, 'The energy balance of central Mexico City during dry season', *Atmos. Environ.* **33**, 3919-3930

Oke, T. R., Zeuner, G., and Jáuregui, E.: 1992, 'The surface energy balance in Mexico City', *Atmos. Environ.* **26B**, 433-444

Tremback, C. J., and Kessler, R.: 1985, 'A surface temperature and moisture parameterisation for use in mesoscale numerical models', *Proceedings of the 7th Conference on Numerical Weather Prediction*, Montreal, Quebec, Canada, June 17-20

Whiteman, C. D., Zhong, S., Bian, X., Fast, J. D., and Doran, J. C.: 2000, 'Boundary layer evolution and regional-scale diurnal circulations over the Mexico Basin and Mexican plateau', *J. Geophys. Res.* **105**, 10081-10102

Williams, M. D., Brown, M. J., Cruz, X., Sosa, G., and Streit, G.: 1995, 'Development and testing of meteorology and air dispersion models for Mexico City', *Atmos. Env.* **29**, 2929-2960

Chapter 6

Conclusions and prospects

The increasing stress placed on our environment by economic development and continuing population growth threatens the sustainability of our world society and of the Earth's ressources for future generations. Preserving the quality of the air we breathe is among the problems to be solved for ensuring a sustainable development. Since the 1850s and the industrial revolution, the quantity of pollutants released each year to the atmosphere has grown exponentially, with negative consequences for our natural environment, our health, and our heritage. By now, global strategies and measures are needed to reduce air pollution. All the processes involved, *eg*, the meteorological phenomena and chemical reactions in the troposphere, are highly complex and nonlinear, so that it is very difficult to develop efficient abatement strategies on the side of pollutant emissions. The impact of scenarios concerning the reduction of primary pollutants on the distribution of ozone in the lower troposphere which has been demonstrated in Chapter 5 of this work for the case of Mexico City is a good illustration of this nonlinearity. Thus, according to the working model, a hypothesised reduction of nitrogen oxide emissions in the city actually produced an increase in ozone concentrations in the area studied. Therefore, the development of integrated strategies in air-pollution control in the first place presupposes a thorough understanding of all the elements involved. It is in this sense that numerical models represent a highly appropriate tool for understanding the situation, as they are able to simulate the formation and motion of the pollutant plume and test the impact of emission reduction scenarios on

pollutant concentrations in a given area of interest. An operational utilisation of these models for daily air pollution forecasts has now become feasible through fast progress in computer technology. Over recent decades, this technological revolution has catalysed the development of numerous meteorological mesoscale models in conjunction with Eulerian photochemical models.

Since primary pollutants are principally released in urban zones and ever more people live in these areas of concentrated human activity, it will be of interest to include into the models the physical impact of city features on the meteorological fields and, hence, on air quality. The presence of buildings actually modifies the flow fields by friction and drag from walls and roofs. The energy budget is also affected by radiation trapping within the street canyons and heat storage in the materials during daytime, and by heat release during nighttime.

In the present work, a mesoscale meteorological model was used which included a detailed parameterisation for inclusion of the urban effects mentioned above. In the traditional method, Monin-Obukhov Similarity Theory (MOST) was used to represent urban areas in a mesoscale model and calculate fluxes near the ground, just as in the case of rural land coverage, but with modified roughness lengths and thermal properties. In the new scheme developed in the present work, the city is represented as a combination of urban classes in which the building elements (street, roof, wall) are considered separately with regards to their morphological parameters (height, width, etc.) and their thermal parameters (heat capacity, thermal diffusivity, etc.).

In a first step, the urban module was validated off-line with a one-dimensional simulation within and above a street canyon in the city of Basel/Switzerland. The results of the simulation were compared with data obtained by measurements made on a meteorological tower within and above the canyon. These data were obtained in June and July 2002 during the Intense

Observation Period (IOP) of the Basel UrBan Boundary Layer Experiment (BUBBLE). The simulation using the new scheme was tested against the traditional urban parameterisation. Comparison showed that the vertical profiles of the meteorological variables and turbulent fluxes obtained with the urban module yield a better fit of measured data than simulations with a traditional parameterisation. More particularly, typical phenomena due to the presence of an urban area such as the deceleration of the flow field in the urban canopy often were well captured by the new parameterisation. Moreover, the observed vertical profiles often showed gradients at roof height (due to the formation of a shear layer) which in general were captured by the urban parameterisation, while the traditional method, because of the assumptions underlying MOST, was not able to reproduce these features. At this point, some weaknesses still exist in this parameterisation, and further development of the scheme is planned, as will be outlined in the outlook concluding the present chapter.

In a second step, the mesoscale model with detailed urban parameterisation was applied over a three-dimensional domain covering the city of Basel and its surroundings. A modification of the mesoscale model was introduced in this work with the aim of allowing the model to take into account the latent heat flux from vegetation within urban areas (in an earlier version of the model, a grid cell was regarded as either rural or urban, while in the new version, mixed cells are included as well). This modification turned out to have little impact in the city centre of Basel, but improved the simulation results in suburban areas where the heterogeneity of surface coverage is high. Prior to drawing more definite conclusions, however, this new model version should be evaluated for large cities containing important vegetation areas where the impact of the mixed-flux calculation might be more significant.

The importance of horizontal resolution on the simulated meteorological fields was also evaluated. It was found that the degree of horizontal resolution had very little influence at any particular grid point, but the overall pattern of meteorological variables obtained with a finer resolution included more details and features of interest. This should not be neglected when a complex terrain is subject to modelling, where accuracy of the resolution needs to be high in order to capture small topographic features.

The two parameters mentioned above (mixed-flux calculation and horizontal resolution) were also evaluated with respect to their relative importance. The horizontal resolution was found to be more important for the quality of the results than the inclusion of fractional land use within given cells. This conclusion should not be taken to imply that a finer resolution is always to be preferred, since this will only be true when the simulated domain presents a complex topography with sharp variations. Then a fine resolution would be needed to account for small topographic features (*eg*, valleys, hills, etc.). For a flat terrain, lower resolution will suffice. The interest of choosing the lowest practical resolution is that of a gain in CPU time.

The mesoscale model that was used here does not account for the presence of clouds in the humidity or radiation budget. Any clouds present during the episode simulated would produce a drop in temperature and incident solar radiation not detected by the model. Solar radiation can be prescribed to the model (instead of being calculated by the model itself) in order to "indirectly" account for the effects of cloud shadow. This modification was introduced into the model during the present work. Its impact was tested during the episode simulated over Basel, since a cloud episode actually occurred on the day of the episode. The temperature trends obtained by this modified simulation did reproduce the cooling due to cloud shadow. Thus, the modification produced a much better fit of measured temperatures by the model.

The results of the simulation using the detailed urban parameterisation were also compared with results obtained from a simulation using the traditional method of inclusion of urban areas. It was seen that the new scheme is able to account for the influence of a city on PBL flow in a rather more accurate way. This represents confirmation of the results obtained by the one-dimensional validation. The urban scheme can capture most of the urban-induced processes, such as the urban heat island. Still, the mesoscale model does require some further improvement, inasmuch as in its present form, some discrepancies between model results and measured data were revealed, particularly so in daytime temperature trends The simulated temperatures increased more rapidly than the observed values, so that the daily maximum was overestimated.

The final part of this work concerned air-quality modelling using the results of the mesoscale model with urban parameterisation to feed a Eulerian photochemical model. As mentioned above, an accurate meteorological modelling over urban areas is crucial for success in air-quality modelling. The complete modelling tool (meteorology with the mesoscale model and air quality with TAPOM) was applied to a case study over the Mexico City Metropolitan Area. Its wide expanse, its geographical position near the equator and at a high elevation, the specific meteorological conditions created by the surrounding mountains, its huge population (20 million inhabitants) and the large number of vehicles (3.5 millions) make it one of the most highly polluted areas in the world. It was a major objective of the present study to validate the mesoscale model over the Mexico City basin and use the simulated meteorological fields as input to air-quality modelling.

The results of the meteorological simulation were in good agreement with measured temperatures and winds close to ground and also with vertical profiles. The model was able to

reproduce the specific patterns of flow circulation, although not always with the same flow intensities as those measured. The model did capture the typical wind convergence developing over the city between the southerly winds blowing over the mountain ridge south of the city and the northerly winds descending from the Mexico plateau, but its simulated position was further south than the observed position. This convergence is crucial for the ozone plume developing over the city. Thus, the simulation results can be used by the photochemical model.

The simulated NO_2 peak concentrations occurring in the morning and in the evening during maximum traffic density were qualitatively correct in the model trends, but the actual values were higher than the measured values at all measuring stations. This overestimate arose from the fact that in the meteorological simulation, mixing-layer height during the day was underestimated. This implies that the estimates for the resulting mixed-air volume above the city are low, and thus the estimated primary-pollutant concentrations were high. The emissions inventory represents another potential error source, but this could not be evaluated.

Simulation of the ozone plume produced concentrations similar to those measured (a peak of 140 ppb in the simulation, peaks of 160-180 ppb from the measurements), but simulated migration of the plume was slightly different from that deduced from observations. This discrepancy has the same origin as that in the wind convergence line mentioned above. Consequently, the maximum simulated ozone concentrations also occurred further south than those observed.

The overall picture of the meteorological and photochemical situation over Mexico City was fairly well reproduced by the simulation, hence it was possible using the same model to evaluate the impact of emission reduction strategies. Hypothesised reductions of the emissions of NO_x and VOC by 35 % were tested. The entire city area was found to be VOC-sensitive during

daytime, since a simulated reduction of NO_x emissions actually induced an increase of the ozone peak of the order of 30 ppb. This is a situation typical of city centres, as it was also revealed in studies of the atmosphere over Milan and Athens for instance. The surroundings of Mexico City were found to be slightly NO_x-sensitive during daytime.

The pollutant concentrations simulated using the meteorological fields from the traditional urban parameterisation method as input were compared with results from the simulation using the new urban scheme, also for the secondary pollutants. Urban paramerisation has an impact on air-quality modelling for primary pollutants. The module modifies the meteorological fields directly above the city where the primary pollutants are emitted. As expected, therefore, an improved quality of the meteorological input had a positive impact on the modelling of these pollutants. The impact produced by the new urban scheme on secondary pollutants was minor for given local points, but the plume's general pattern was found to be strongly different: The meteorological fields found with the aid of the urban parameterisation produced a simulated ozone plume that was more extended in space than that found with the traditional method. This was mainly due to the fact that the wind speeds calculated by '*urban*' were smaller.

By implementing the detailed urban parameterisation in the mesoscale model, it was possible to improve the quality of the meteorological simulation in almost all applications tested within this work. Still, the mesoscale model and the urban scheme will require some further improvements. In the urban module, the possible addition of a countergradient contribution to the calculation of diffusion coefficients is of interest. In the same perspective, a parameterisation allowing for shear stresses arising from flow channelling in the street canyon should be introduced into the model. The impact of each surface type (street, wall, and roof) on the sensible heat fluxes should be investigated further. Surface water runoff, the evaporation of water pools on building roofs and

in streets and the different anthropogenic heat sources (smokestacks, air conditioning) should also be examined in future parameterisation development.

An effort should finally be made to identify the processes producing the most significant impact on air-pollutant concentrations. Such an analysis would serve the purpose of simplifying the model and the urban scheme while retaining only the most relevant processes and input parameters. The intended application of this simplified model would be an integrated operational tool that can be used for day-to-day air pollution forecasts. Thus, the next challenge to be taken up by our group at EPFL will be that of implementing the urban scheme in the operational meteorological and air-quality model of the Swiss Meteorological Insitute that is used for daily forecasting.

The improvements of the model, therefore, go in two directions. On one hand we try to be more precise and complete in the parameterisation and spatial resolution, by improving the current scheme and adding new parameterised processes; on the other hand, an effort of simplification is needed for day-to-day applications.

Appendix A

Vertical distribution of wind speed and wind direction according to the measured data from a wind profiler at Chalco (CHAL) and Teotihuacan (TEOT) for 2 March 1997, and according to the simulation with '*urban*' at the corresponding grid point.
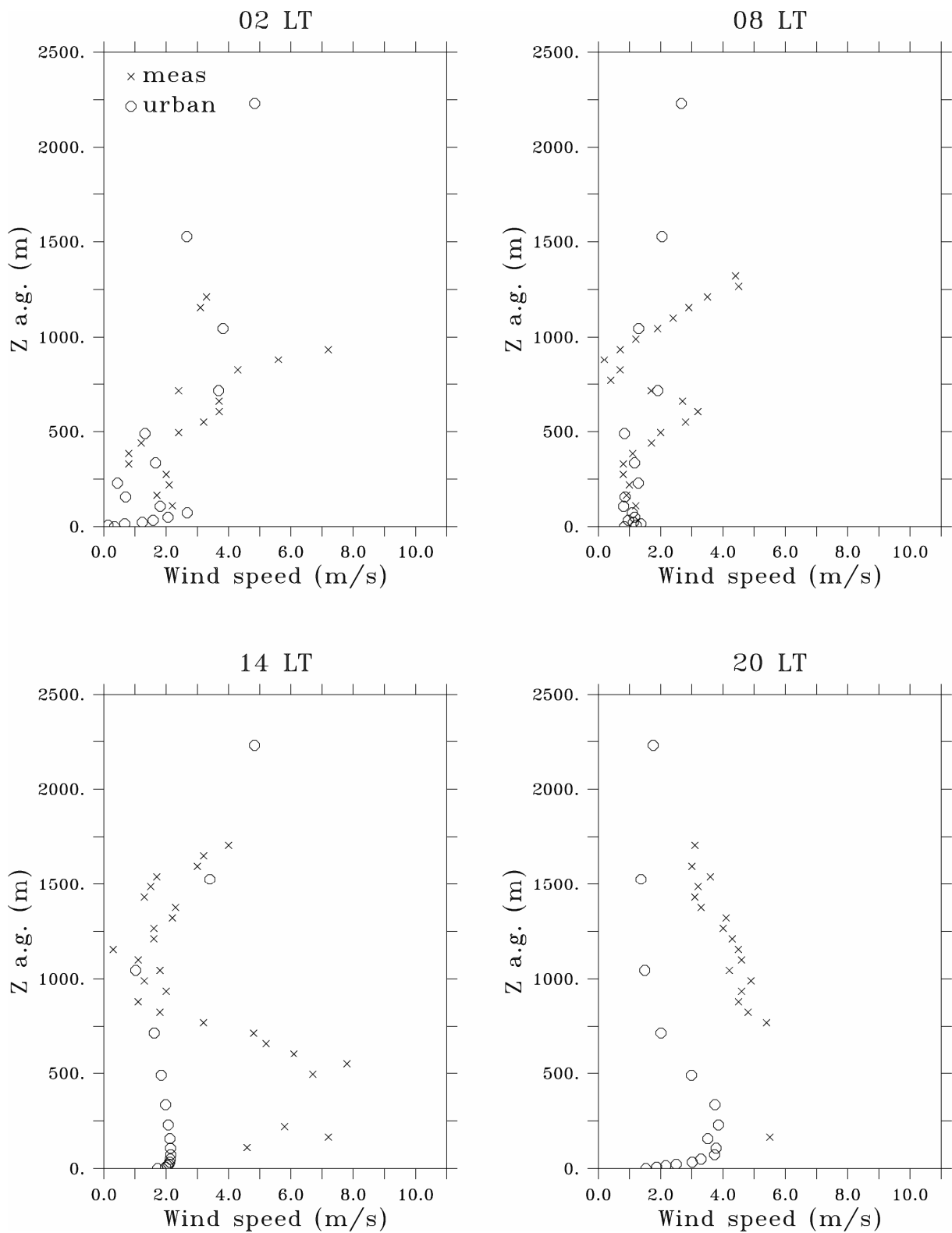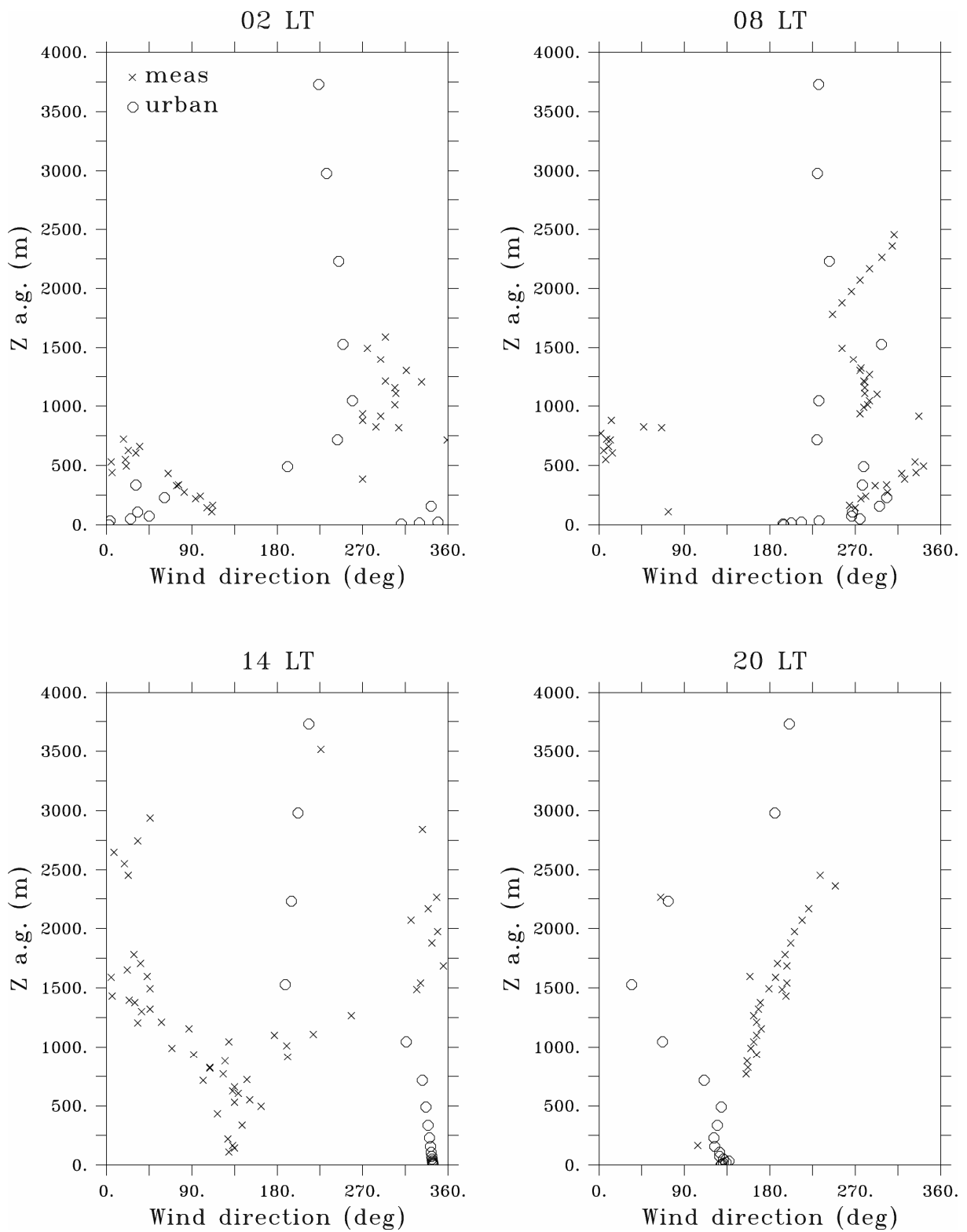
Figure A.1. Vertical wind speed distribution according to the simulation '*urban*' (circle) and to the wind profiler measured data at the station CHAL (cross) at 2 LT (top left), 8 LT (top right), 14 LT (bottom left) and 20 LT (bottom right) 2 March 1997.
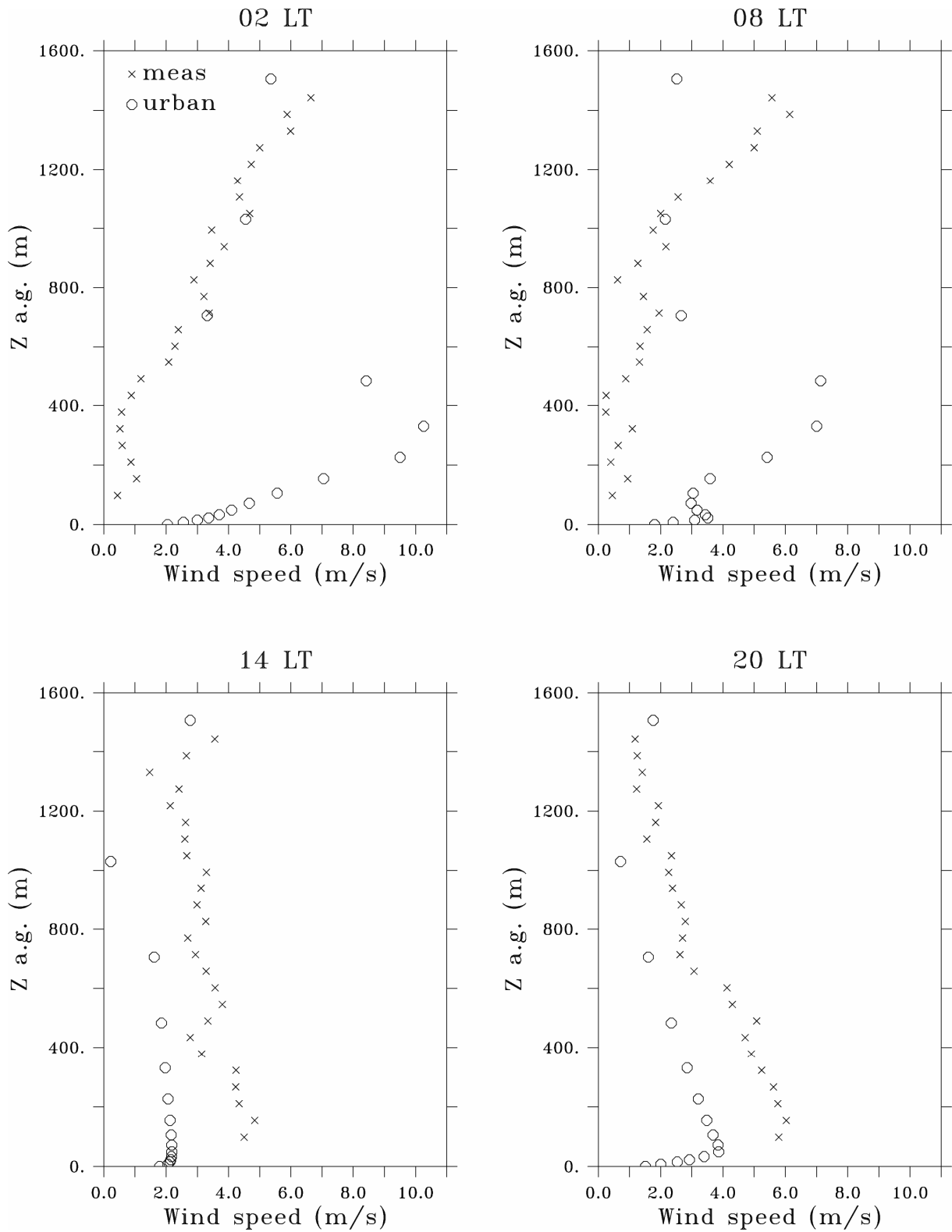
Figure A.2. Vertical wind direction distribution according to the simulation '*urban*' (circle) and to the wind profiler measured data at the station CHAL (cross) at 2 LT (top left), 8 LT (top right), 14 LT (bottom left) and 20 LT (bottom right) 2 March 1997.
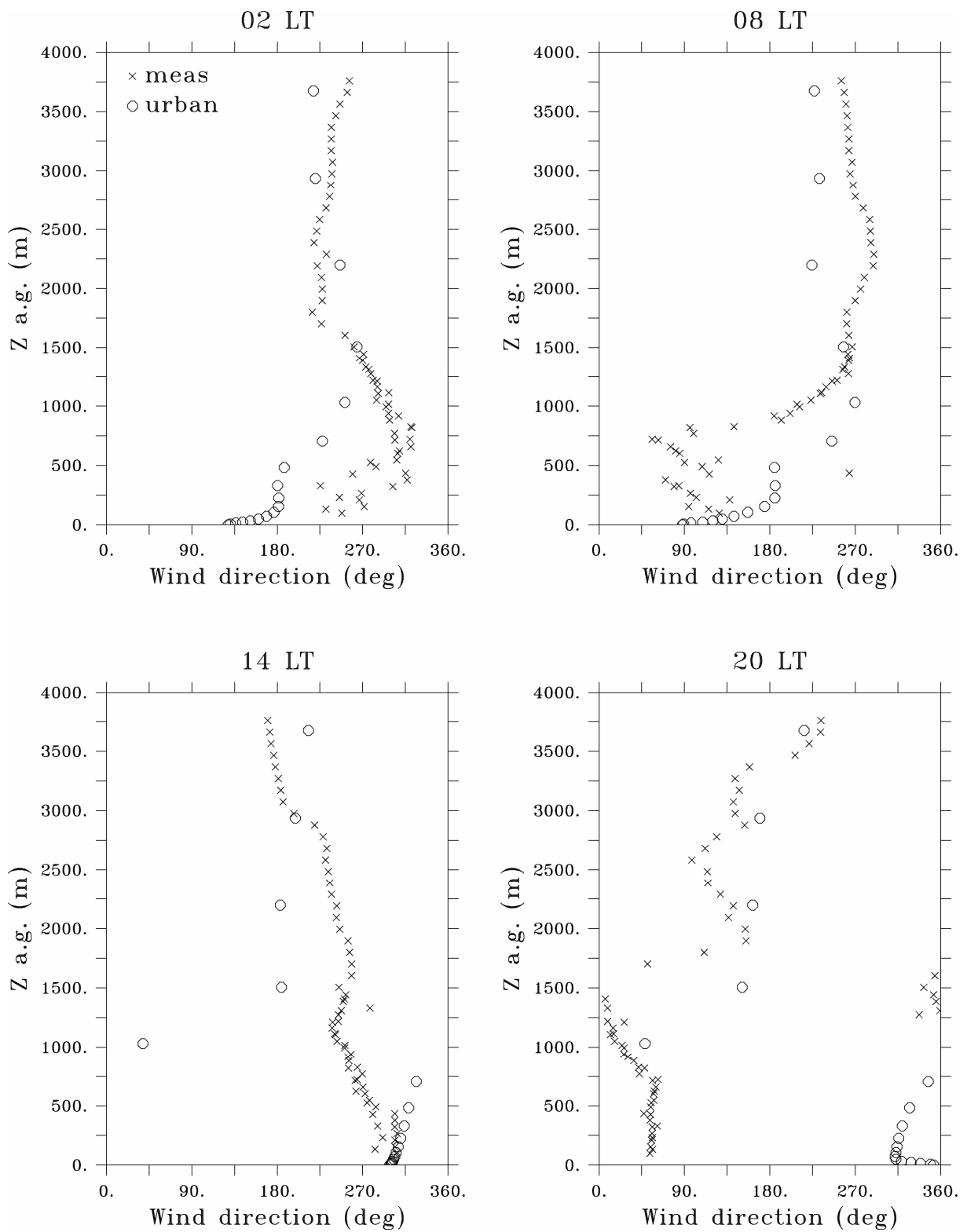
Figure A.3. Vertical wind speed distribution according to the simulation '*urban*' (circle) and to the wind profiler measured data at the station TEOT (cross) at 2 LT (top left), 8 LT (top right), 14 LT (bottom left) and 20 LT (bottom right) 2 March 1997.

Figure A.4. Vertical wind direction distribution according to the simulation '*urban*' (circle) and to the wind

profiler measured data at the station TEOT (cross) at 2 LT (top left), 8 LT (top right), 14 LT (bottom left)

and 20 LT (bottom right) 2 March 1997.

Appendix B

Hourly evolution of the NO_2 and O_3 concentrations [ppb] near ground in the Mexico City Area from 00 LT to 23 LT 2 March 1997 according to TAPOM simulation with the '*urban*' simulated meteorological fields as input, and representation of the corresponding wind field according to the '*urban*' simulation.
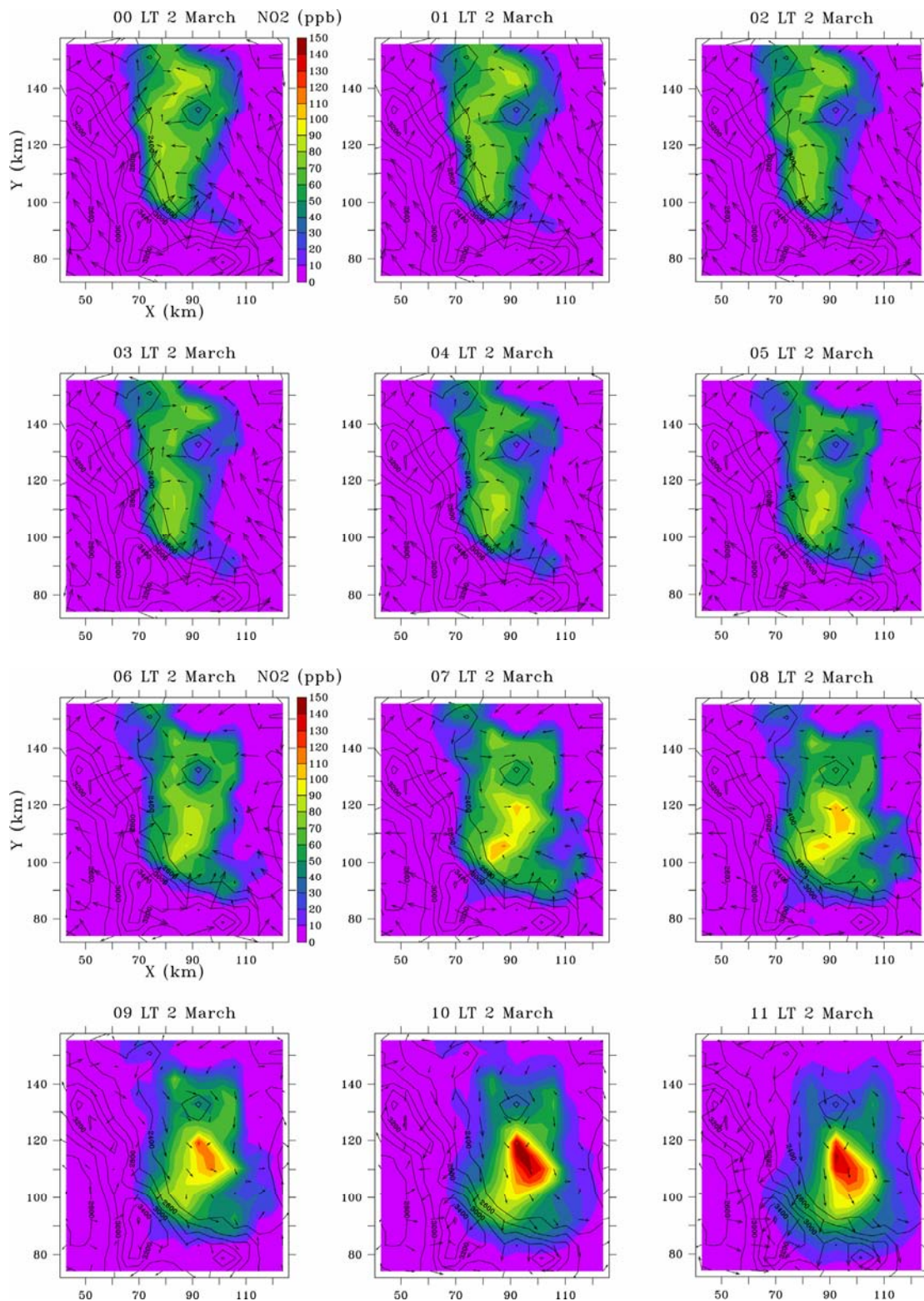
Figure B.1. NO₂ concentration [ppb] near ground in the Mexico City Area from 00 LT to 11 LT 2 March 1997 according to TAPOM simulation with the '*urban*' simulated meteorological fields as input, and representation of the wind fields according to the '*urban*' simulation.
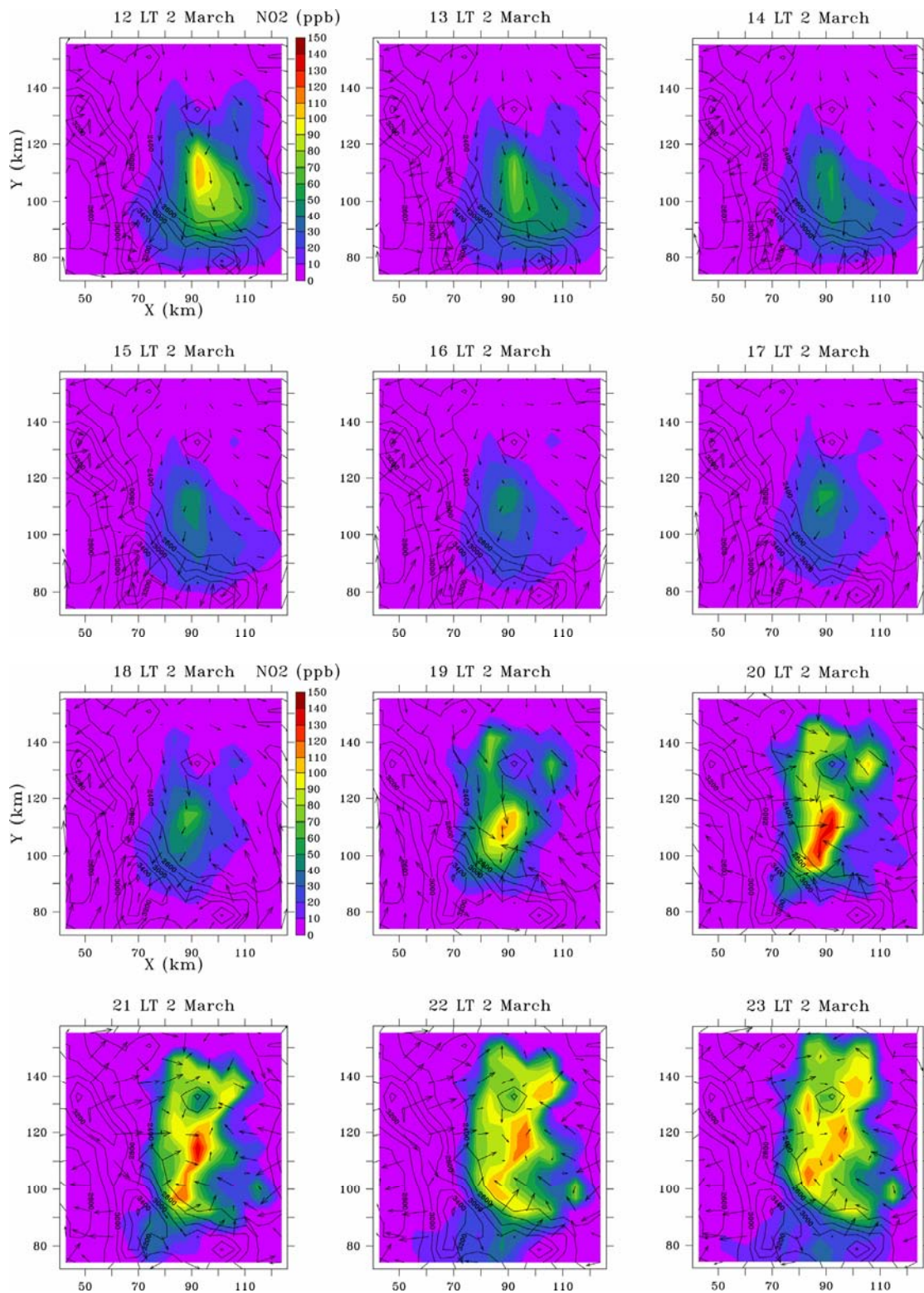
Figure B.2. NO$_2$ concentration [ppb] near ground in the Mexico City Area from 12 LT to 23 LT 2 March 1997 according to TAPOM simulation with the '*urban*' simulated meteorological fields as input, and representation of the wind fields according to the '*urban*' simulation.
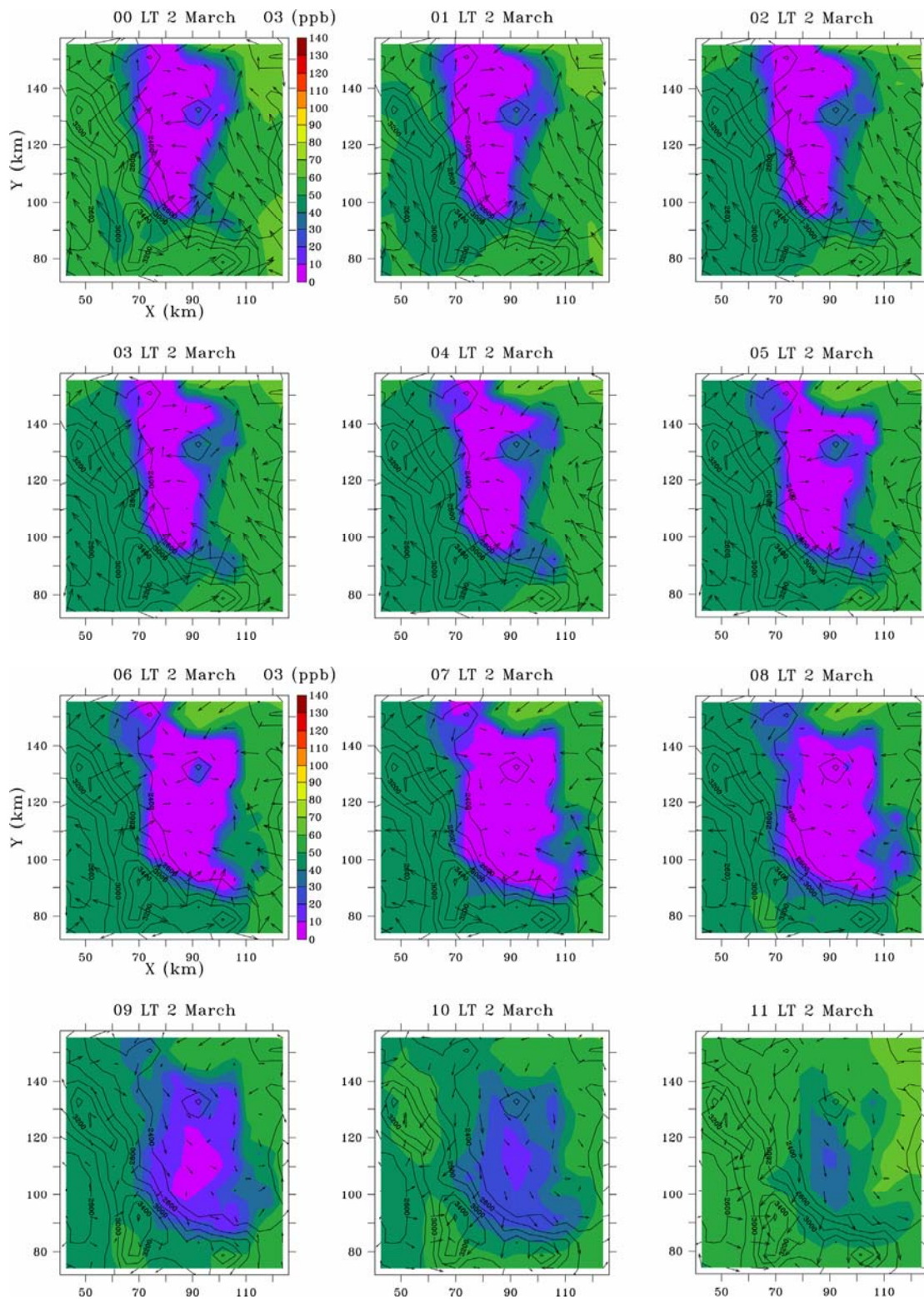
Figure B.3. O₃ concentration [ppb] near ground in the Mexico City Area from 00 LT to 11 LT 2 March 1997 according to TAPOM simulation with the '*urban*' simulated meteorological fields as input, and representation of the wind fields according to the '*urban*' simulation.
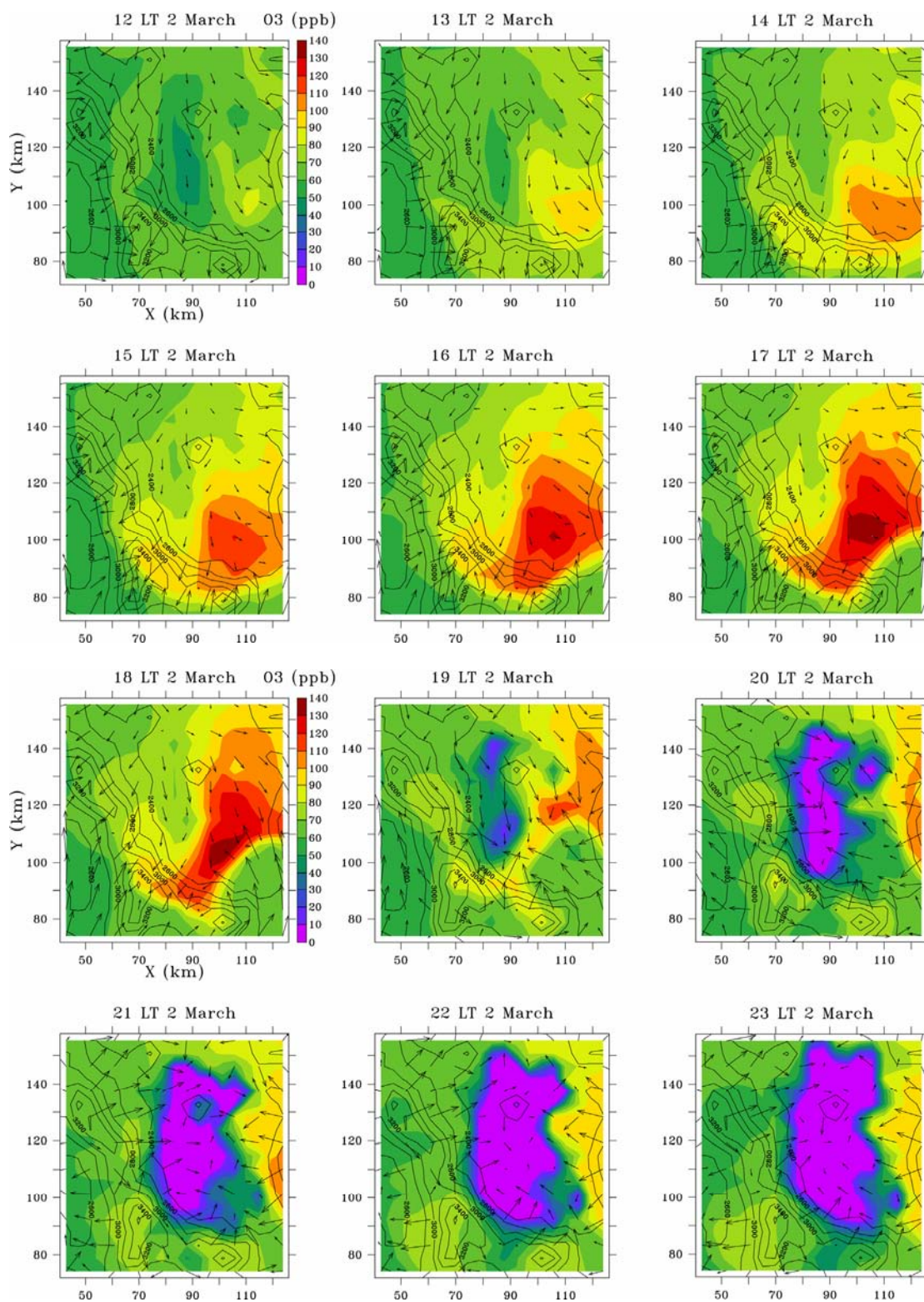
Figure B.4. O₃ concentration [ppb] near ground in the Mexico City Area from 12 LT to 23 LT 2 March 1997 according to TAPOM simulation with the '*urban*' simulated meteorological fields as input, and representation of the wind fields according to the '*urban*' simulation.
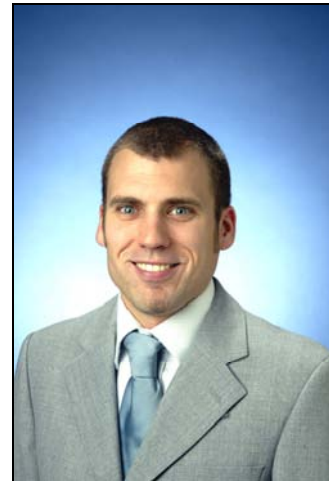
Yves-Alain Roulet
Born on 1ˢᵗ October 1973
Swiss citizen
MSc in natural sciences ETHZ
PhD in technical sciences EPFL

Education

2000-2004	Ph.D. in mesoscale atmospheric modelling, Swiss Federal Institute of Technology in Lausanne, Air Pollution Laboratory
1999-2003	Masters in management and finance, Business School (HEC) Lausanne University
1993-1998	MSc in natural sciences, Swiss Federal Institute of Technology in Zurich
1989-1992	Upper secondary education at the Gymnase cantonal vaudois de Burier/La Tour-de-Peilz (VD). Maturité Fédérale scientifique.

Work experience

1999-2004	Swiss Federal Institute of Technology (EPFL), Lausanne, Air Pollution Laboratory
Research assistant in the modelling group, applied environmental project on air quality management for the Canton of Obwalden, mesoscale meteorological modelling for an international research project on urban meteorology, teaching to graduate and under-graduate EPFL students, correction of examinations and supervision of diploma thesis, in charge of the purchase of IT equipment for the Laboratory
2000-	Swiss Institute for Business Cycle Research in Zurich (KOF)
Translation of documents (letters, technical reports) from German into French
1996-1997	World Meteorological Organization (WMO), Geneva
Trainee, preparation of documents for an international conference on water resources in Asia and Pacific Islands
1996-1997	Swiss national weather services (MeteoSwiss), Zurich
Trainee, research project on the quality of precipitation forecasts in Switzerland

Computer skills

- Programming experience: Excellent skills in Fortran 77, basic knowledge of C, HTML and Java
- Operating systems: Very good knowledge of UNIX, Windows and Mac
- Networks: UNIX environment, configuration of network PC's for professional needs

Language skills

- French: mother-tongue
- English: fluent
- German and Swiss German: fluent

Hobbies, interests

- Sports: football (captain and member of the committee of the Lausanne University Club), jogging, cycling, trekking
- Other: gastronomy, œnology (wine-appreciation course)

Publications

Roulet Y.-A., Kirchner, F., Junier, M., Martilli, A., Clappier, A., Jiménez, R., Calpini, B. and van den Bergh, H.: 2000, '*Modellierung der Auswirkungen einer Tunneleröffnung auf der Luftqualität im Kanton Obwalden*', Project report, 32 pp

Kirchner F., Couach, O., Junier, M., Kuebler, J., Martilli, A., Roulet, Y.-A, Sathya, V., Clappier, A. and van den Bergh, H.: 2000, 'Application of the Chemical Mechanism Adaptation Programme CHEMATA for the design of Chemical Mechanisms', *Contribution to the Project CMD, May 2000*

Sathya, V., Couach, O., Junier, M., Kuebler, J., Martilli, A., Roulet, Y.-A and van den Bergh, H.: 2000, 'An ozone budget system for precise evaluation of the role of local emissions in uncertainty analysis with photochemical grid models', *Eurotrac Symposium 2000, Garmish-Partenkirchen, March 2000*

Junier M., Clappier, A., Roulet, Y.-A., van den Bergh, H., Cuvelier, C. and Thunis, P.: 2001, 'Numerical Simulation of the Links between Air Pollution, Aerosols and Solar Radiation', *Proceedings from the EUROTRAC-2 Symposium 2000, Garmish-Partenkirchen, March 2000*

Sathya V., Russell, A. G, Clappier, A., Junier, M., Martilli, A., Kirchner, F., Couach, O., Kuebler, J., Roulet, Y.-A., Perego, S., Maignan, M., van den Bergh, H.: 2001, 'An Ozone Budget System for Quantifying the Role of Emissions in Defining Exposure', *Proceedings from the EUROTRAC-2 Symposium 2000, Springer-Verlag Berlin, Heidelberg*

Roulet Y.-A.: 2002, 'Integration of urban effects in a mesoscale dynamical model over the region of Basel (Switzerland) as a part of the BUBBLE experiment', *Proceedings of the Fourth Symposium on the Urban Environment, Norfolk, Virginia (USA), 20-24 mai 2002*

Kirchner F., Junier, M., Roulet, Y.-A., Clappier, A., van den Bergh, H.: 2002, 'The Influence of New Kinetic Data and of Species Lumping on the Model Results', *Proceedings from the EUROTRAC-2 Symposium 2002, Margraf Verlag, Weikersheim 2002*

Martilli A., Roulet, Y.-A., Junier, M., Kirchner, F., Rotach, M. W. and Clappier, A.: 2003, 'On the impact of urban exchange parameterisations on air quality simulations: the Athens case', *Atmos. Environ.* **37**, 4217-4231

Roulet Y.-A., Martilli, A., Rotach, M. W. and Clappier, A.: 2003, 'Modelling of urban effects over the city of Basel (Switzerland) as a part of the BUBBLE project', *Proceedings of the Fifth International Conference on Urban Climate, Lodz, Poland, 1-5 septembre 2003*

Roulet Y.-A., Kirchner, F., Jimenez, R. and Clappier, A.: 2003, '*Modellierung der Auswirkungen einer Tunneleröffnung auf der Luftqualität im Kanton Obwalden, Teil II*', Project report, 33 pp

Rotach M.W. *et al*: 2004, 'BUBBLE – a Mayor Effort in Urban Boundary Layer Meteorology', *Submitted to J. of App. Meteorol., March 2004*

Roulet Y.-A., Martilli, A., Rotach, M. W. and Clappier, A.: 2004, 'Validation of an urban surface exchange parameterization for mesoscale models –1D case in a street canyon', *Submitted to J. of App. Meteorol., April 2004, 1ˢᵗ review on 15ᵗʰ June 2004*

Conferences

Roulet Y.-A.: 'Outils pour la simulation et le contrôle de la qualité de l'air', *Journées Scientifiques du Département de Génie Rural de l'EPFL*, 7-8 septembre 2000, Gruyères/FR, Suisse

Roulet Y.-A.: 'Modellierung des Auswirkungen einer Tunneleröffnung auf der Luftqualität im Kanton Obwalden', *Présentation aux membres du gouvernement cantonal et aux chefs de services concernés*, 4 mars 2001, Sarnen, Obwalden, Suisse

Roulet Y.-A.: 'Le préprocesseur des données météorologiques', *First TAPOM Meeting*, 27 septembre 2001, EPFL, Lausanne, Suisse

Roulet Y.-A.: 'Integration of urban effects in a mesoscale dynamical model over the region of Basel (Switzerland) as a part of the BUBBLE experiment', *Fourth Symposium on the Urban Environment*, 20-24 mai 2002, Norfolk, Virginia (USA)

Roulet Y.-A.: 'Introduction of an urban module into Numerical Weather Prediction models', *FUMAPEX Kick-off Meeting*, 27-29 november 2002, Copenhague, Danemark

Roulet Y.-A., Martilli, A., Rotach, M. W. and Clappier, A.: 'Modelling of urban effects over the city of Basel (Switzerland) as a part of the BUBBLE project', *Fifth International Conference on Urban Climate*, 1-5 septembre 2003, Lodz, Poland